OPTOACOUSTIC SPECTROMETRY FOR SMALL SOLID AND LIQUID SAMPLES

by

Bromley Charles Beadle, B.Sc., A.R.C.S., Grad.R.I.C.

A Thesis submitted for the Degree of

DOCTOR OF PHILOSOPHY

of the University of London

September 1978

Chemistry Department,

Imperial College of Science and Technology,

London, SW7.

ADDENDA

Page 56, line 9; "tha" should read "the"

Page 63; Equation 3.1. should read

" $P_{abs\lambda} = P_{0\lambda} \left[1 - \exp(-2.3\varepsilon_{\lambda} cl)\right]$ "

Equation 3.2. should read

" $P_{oas\lambda} = P_{0\lambda} \left| 1 - \exp(-2.3\varepsilon cl)\right] \beta$ "

Page 86, line 16; "has" should read "had"

Page 110, line 3; "i.e." should read "However"

Page 113, line 7; "arrangment" should read "arrangement"

Page 176, line 15; "prepartion" should read "preparation"

Page 176, line 18; "charactarised" should read "characterised"

Page 202, line 16; "0.39 Pa W^{-1} and 0.43 Pa W^{-1}"

should read "39 Pa W^{-1} and 43 Pa W^{-1}"

Page 206; reference 37 should read

"Hayes, H. V. and Cram, E. R., ...".

Page 150; Figs. 5.22C and 5.22D should read 5.22A and 5.22B respectively.

ABSTRACT

The design and performance characteristics of both single-beam and double-beam optoacoustic spectrometers are reported. The double-beam spectrometer provides for automatic correction of the spectra obtained for the variation in output energy of the source with wavelength.

A wide variety of sample types have been examined, including those of inorganic, biochemical, phytochemical and geochemical origin, in both the ultraviolet-visible and near-infrared regions.

The utility of optoacoustic spectrometry has been extended via phase analysis of the resultant signal to provide information concerning the spectra of samples composed of distinct layers.

ACKNOWLEDGEMENTS

The work presented in this thesis was undertaken in the Chemistry Department of the Imperial College of Science and Technology between October 1975 and September 1978. Except where due reference is made it is entirely original and no part has been submitted for any other degree.

I would like to thank my supervisors, Dr. M.J.Adams and Dr. G.F.Kirkbright, for their advice and encouragement throughout the course of this work. I would also like to thank my fellow researchers in the OAS research group for many useful discussions and suggestions.

I am indebted to the Laboratory of the Government Chemist for the provision of a Studentship, and the Paul Instrument Fund Committee for much of the apparatus employed in the research.

Finally, I would like to thank my wife Mary for her invaluable assistance in the preparation of this thesis.

B. C. Beadle.

CONTENTS

CHAPTER ONE

INTRODUCTION

1.1 The Absorption Of Electromagnetic Radiation.

The dual nature of electromagnetic radiation allows phenomena associated with light and its interaction with matter to be considered by one of the two classical postulates; as a wave or particle (the Corpuscular Theory). The optical phenomena of reflection, diffraction, interference, refraction and scattering can best be described on the basis of the wavelike nature of radiation (1) whereas the processes of emission and absorption of radiation by atoms or molecules are best considered in terms of the particle theory, (2,3). The link between these wavelike and particle natures is given by the Planck equation,

$$\Delta E = h\nu = \frac{h c}{\lambda} = h c \bar{\nu} \qquad \ldots 1.1$$

and the relationship developed by De Broglie expressing the wavelength of a 'particle' in terms of its mass (m) and velocity (v),

$$\lambda = \frac{h}{m v} \qquad \ldots 1.2$$

where ΔE is the energy change in the elementary system that results when a photon of energy $h\nu$ has been absorbed or emitted, ν , λ and $\bar{\nu}$ are the frequency, wavelength and wavenumber respectively of the wave motion associated with the radiation, and h and c are Planck's constant and the velocity of light in vacuo respectively.

The electromagnetic spectrum, together with the most common types of regional atomic or molecular transition, is given in Fig. 1.1. This thesis is concerned with electronic and vibrational transitions and these are to be discussed further.

Electronic excitation of a molecule (4) involves the promotion of an electron from a ground-state orbital to an excited-state orbital with a corresponding increase in the molecular energy, changes in molecular symmetry and, occasionally changes in multiplicity (net

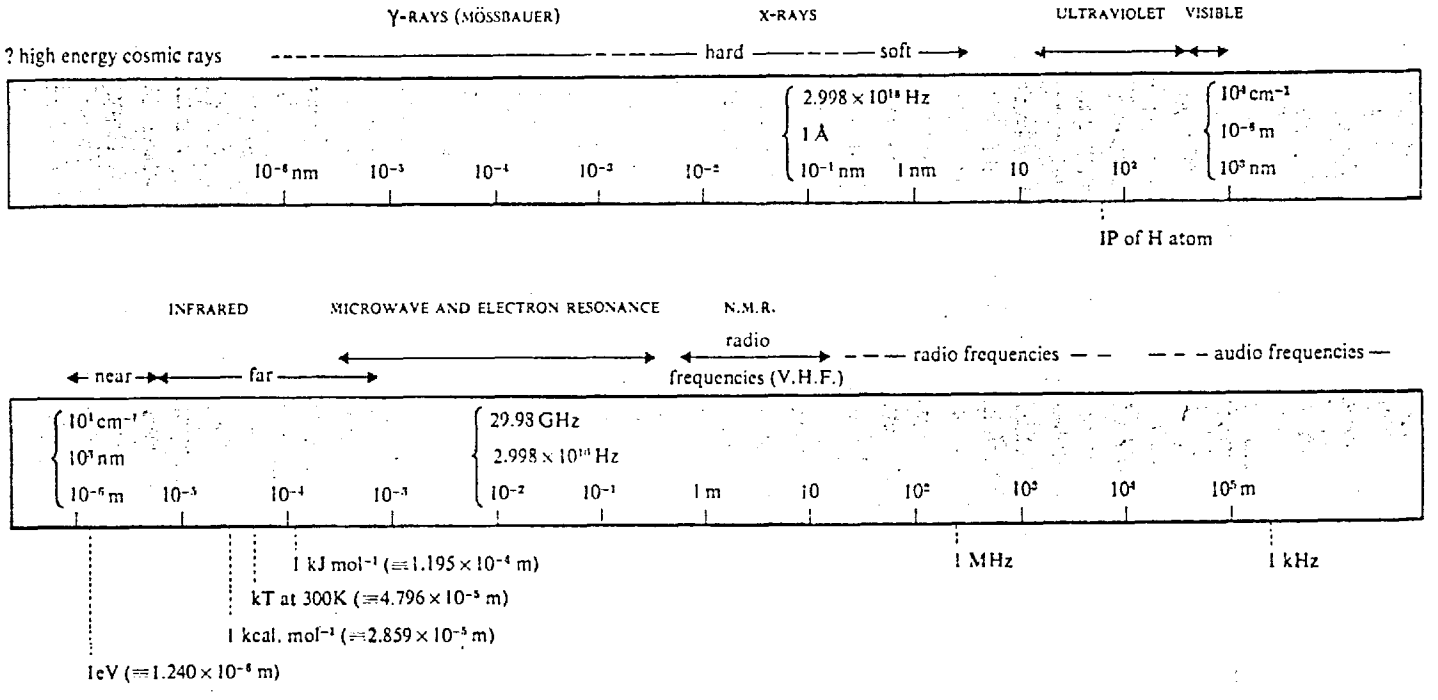

Fig. 1.1 The Electromagnetic Spectrum. (2)

electron spin). A Jablonski diagram (Fig. 1.2.) can be used to schematically represent the electronic energy levels of a hypothetical molecule. Superimposed on each electronic level are vibrational levels (and rotational levels on these), which correspond to vibrationally excited states for each specific electronic configuration (5). A relatively simple molecular system we may consider for discussion is that of an organic molecule in a liquid solution at room temperature (6). The majority of electronic transitions originate from the ground vibrational level of the ground electronic state and absorption of radiation by the molecule may result in the direct excitation of an electron to an excited vibrational level of an upper state electronic orbital. Radiationless transitions between excited vibrational levels within a given electronic state occur very rapidly compared to the time required for the electronic transition (Fig. 1.3). Therefore, any excess vibrational energy is quickly lost as the molecule returns to the ground vibrational level of the particular electronic state involved. Similarly, radiationless transitions between higher-energy excited singlet electronic states and the first excited state occur very rapidly. For this reason, nearly all electronic processes can be explained by considering only the ground state and the first singlet and triplet excited states (7). In the Jablonski diagram, each excited singlet state is shown with a companion triplet state at a lower energy level. This is an extension of Hund's rule from atomic spectroscopy, which states that the electronic configuration with the greatest number of unpaired electrons is the most stable configuration (8).

There are five basic intramolecular processes by which excitation energy can be dissipated: vibrational relaxation; internal conversion; fluorescence; intersystem crossing and phosphorescence. A

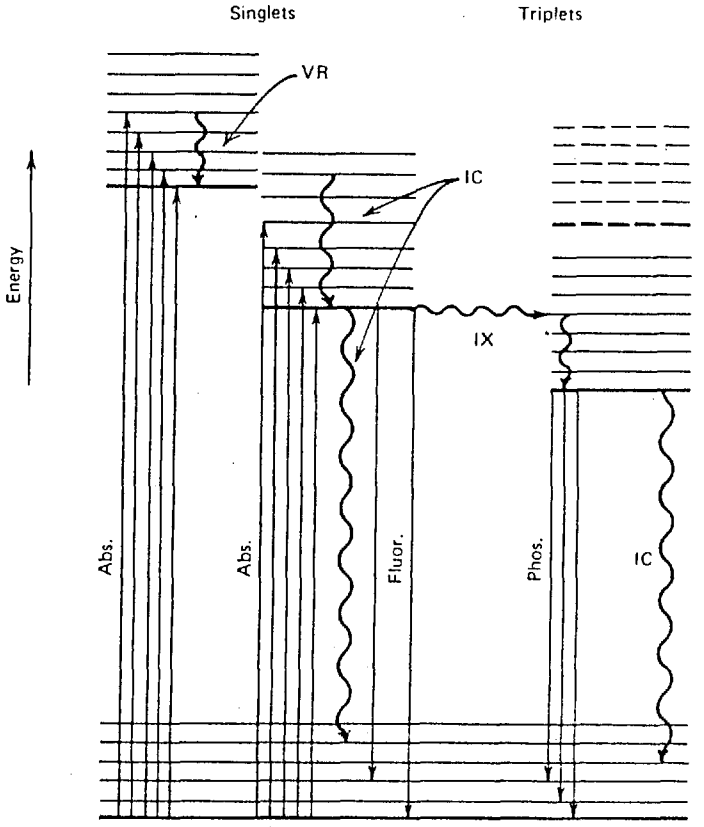

Fig. 1.2. Electronic energy level diagram (Jablonski diagram) for a hypothetical molecule showing absorption (Abs.), vibrational relaxation (VR), fluorescence (Fluor.), internal conversion (IX), and phosphorescence (Phos.). (7)

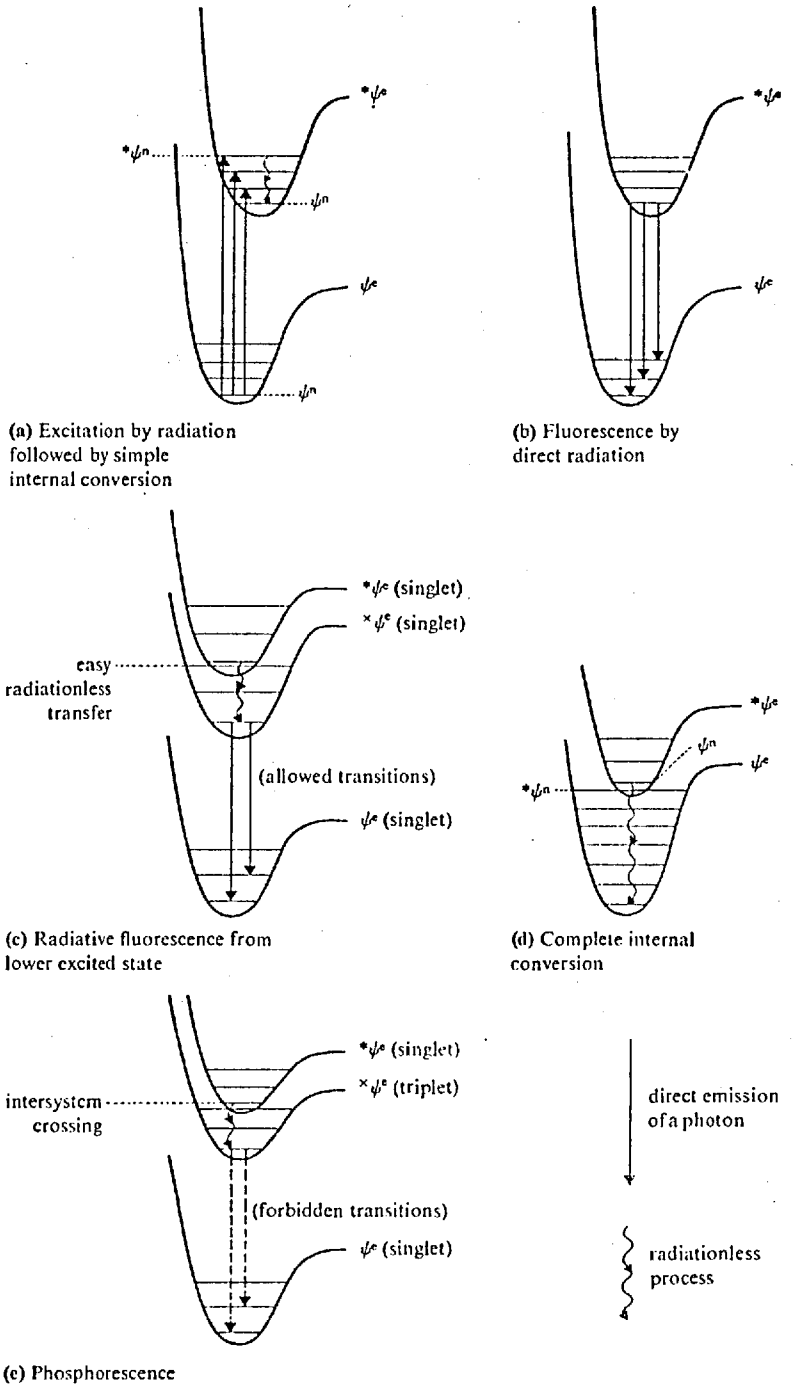

Fig. 1.3 Energy loss from excited molecular states. (2)

molecule at an excited vibrational level may lose this excess vibrational energy either by the emission of infrared radiation or by the transfer of energy to its surroundings (7). In the gas phase where molecule-molecule collisions are infrequent, infrared emission is observed. In the liquid or solid phase, such collisions are so frequent that all excess vibrational energy is lost to the surrounding media in 10^{-13} to 10^{-11}s and radiationless transitions between vibrational levels are more common.

The collective nonradiational processes by which an electronically excited molecule can return to its ground state are referred to as internal conversion (IC). These processes comprise the dominant routes of excited-state deactivation. Fluorescence is the direct radiational deactivation of an excited singlet electronic state (6). Photon emission occurs from the ground vibrational level of the excited electronic state to any of the vibrational levels of the ground electronic state. An additional process for the depopulation of the excited singlet state is the spin-forbidden conversion from the excited singlet to its companion, but lower energy, triplet state. This process, called intersystem crossing (ISC), is a vibrationally coupled process of the same general type as internal conversion and involves the reversal of electron spin (5). However, ISC proceeds at a rate roughly comparable to fluorescence deactivation due to the small energy difference between the singlet and triplet levels, which favours a vibrationally coupled crossover. Following intersystem crossover radiationless relaxation occurs resulting in population of the ground vibrational level of the excited triplet state. Phosphorescence is the direct radiative deactivation of the excited triplet state to the ground state (4). The spin-forbidden nature of the triplet-singlet transition and the smaller energy separation between the triplet level and the

ground singlet level combine to make nonradiative internal conversion processes the dominant modes of deactivation of the triplet state.

Vibrational excitation of a molecule (9) involves the production of a dipole moment in the system by inducing a stretching or vibrational mode. The energy of these oscillations can be predicted from the mechanical theory of harmonic oscillators, i.e. Hooke's Law, and such transitions are characteristic of absorption processes in the infrared region. The frequency, ν, of two adjacent atoms, approximating to point masses m_1 and m_2, executing a simple harmonic motion about an equilibrium point on the bond joining them is given by Equation 1.3,

$$\nu = \frac{1}{2\pi} \cdot \sqrt{\frac{k\,(m_1 + m_2)}{m_1 m_2}} \qquad \ldots 1.3$$

where k is the restoring force per unit displacement from the equilibrium point; the force constant. The frequency is the greater the smaller the mass of the vibrating nuclei and the greater the force constant. The force constant is determined by the electron density within a chemical bond. For large amplitude oscillations, vibrational modes at harmonics (overtones) of the fundamental frequency may be observed (10). In addition, polyatomic molecules may show combinational modes (11) due to the interaction of separate molecular vibrations. Raman activity is observed for a molecular system where its electrical polarisability changes during the motion and is complementary to conventional vibrational absorption studies (2).

In the gas phase, studied by high resolution spectroscopy, the vibrational and rotational levels may be observed superimposed on electronic levels, and similarly rotational levels on the vibrational levels (4). In the condensed phase, where molecule-molecule interactions are far more frequent, the net effect is to broaden the sharp absorption bands corresponding to the multiplicity of discrete

energy levels available for excitation into broad, rather featureless, bands.

1.2. Molecular Absorption Spectrometry.

The absorption of radiant energy incident upon a sample is commonly measured by detecting the transmitted radiation (9). Alternatively for opaque samples, diffuse reflectance spectroscopy (13) may be employed to measure the unabsorbed radiation reflected from the sample surface. Quantitative analysis by these techniques depends upon the Beer-Lambert law for absorption studies (14) and, in general, the Kubelka-Munk theory for diffuse reflectance (15).

1.2.1. Beer-Lambert Law.

When incident radiation of radiant flux P_o traverses a sample, the radiation is reduced in power by the losses indicated in Fig. 1.4. If the absorption process is considered, then for monochromatic radiation the power of the transmitted radiation (P) is given by,

$$P = P_o \, 10^{-\varepsilon b c} \qquad \ldots 1.4$$

where ε is the extinction coefficient (a constant for a sample under fixed experimental conditions), b is the sample path length and c is the concentration of the absorbing substance. This is expressed more commonly as,

$$A = \log \frac{P_o}{P} = \varepsilon b c \qquad \ldots 1.5$$

where A is the absorbance. Beer's law is additive for multicomponent mixtures providing there is no interaction between the absorbing species. Deviations from Beer's law may be due to both chemical and instrumental causes. These include a change in the chemical species

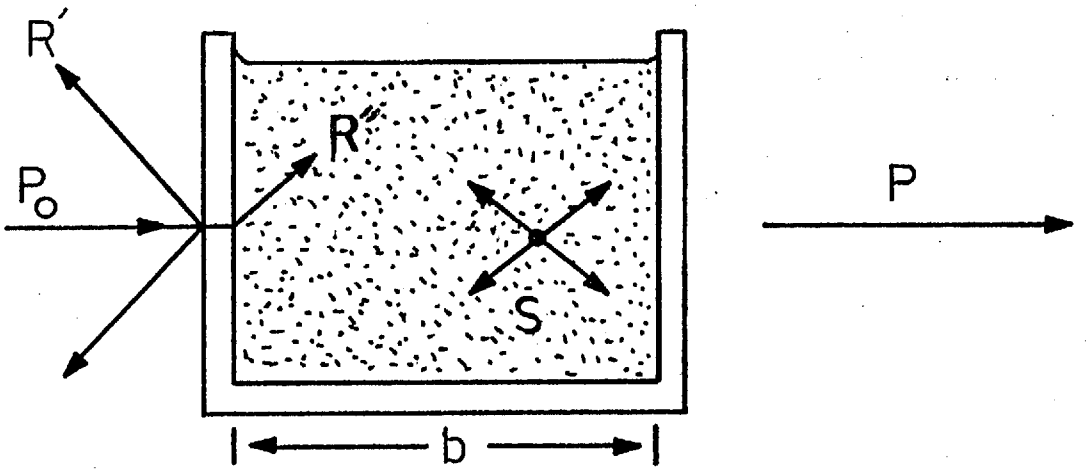

P_o – incident radiation beam.

P – emergent radiation beam.

R′ – reflection at the interfaces of the sample container.

R″ – refraction at the sample container interfaces.

S – scattering processes due to particles in the sample (including Rayleigh and Raman scattering by the sample molecules themselves).

Fig. 1.4 Incident radiation impinging on a system whose optical path length is b .

present due to concentration, temperature, solvent and photochemical effects. Luminescence processes and nonmonochromatic incident radiation may also produce deviations from the predicted linearity.

1.2.2. The Kubelka-Munk Theory.

The most generally accepted theory concerning diffuse reflectance and the transparency of light-scattering and light-absorbing layers has been developed by Kubelka and Munk (13). Development of the theory for an infinitely thick opaque layer yields the Kubelka-Munk equation (16), which may be expressed as,

$$\frac{(1 - R'_{\infty})^2}{2R'_{\infty}} = \frac{k}{s} \qquad \ldots 1.6$$

where R'_{∞} is the absolute reflectance of the layer of infinite thickness, k the molar absorption coefficient and s is the specular scattering coefficient. However, rather than determining R'_{∞}, it is more convenient in practice to determine the relative diffuse reflectance, R_{∞}, which is measured against a standard material, e.g. magnesium oxide or barium sulphate. Thus,

$$R_{\infty} = \frac{R'_{\infty}\ (\text{sample})}{R'_{\infty}\ (\text{standard})} \qquad \ldots 1.7$$

As the absolute reflectance of the standards available never exceeds 0.99 (13), it is essential to specify which standard is used. The Kubelka-Munk equation then assumes the form (15),

$$F(R_{\infty}) = \frac{(1 - R_{\infty})^2}{2R_{\infty}} = \frac{k}{s} \qquad \ldots 1.8$$

Thus a linear relationship should be observed between $F(R_{\infty})$ and the absorption coefficient when s is constant within the wavelength region examined. The scattering coefficient can be made independent of wavelength by using a sample particle size greater than the wavelength

of the incident radiation.

When the reflectance of a sample diluted with a non or low-absorbing powder is measured against the pure powder, k may be replaced by the product $2.303\epsilon C$, where ϵ is the extinction coefficient and C the molar concentration (13). The Kubelka-Munk equation can then be written as,

$$F(R_\infty) = \frac{(1 - R_\infty)^2}{2R_\infty} = \frac{C}{k'} \quad \ldots 1.9$$

where k' is a constant equal to $s/2.303\epsilon$. At sufficiently high dilutions, the regular reflection from the sample approximates that from the standard and is thus cancelled out in a comparison measurement.

A straight-line relationship between $F(R_\infty)$ and C is only observed when examining weakly absorbing substances and only when the particle size of the sample is relatively small, i.e., approximately 1μm in diameter (17). Deviations from linearity are also observed for any significant departure from the infinite thickness of absorbent assumed in the theory. These cases, where the theory does not hold, have been explained by Kortüm (15) by the postulate that reflected radiation consists of both regular (mirror) reflection and diffuse reflection. The deviations from the above equation occur when the regular reflection interferes with the measurement of the diffuse reflection.

1.3. The Optoacoustic Effect.

An alternative method of measuring the radiant energy absorbed by a sample is to detect the heat produced by radiationless deactivation of the excited electronic and vibrational energy levels in the sample. The temperature variation due to this heat production

mechanism is the basis for the optoacoustic effect (12). This arises when radiation, interrupted at a suitable frequency, is incident upon an absorbing species in a constant-volume cell. The periodic temperature variation induced in the sample produces a pressure change in the cell filler gas of the same period as the incident radiation. Thus by placing a pressure transducer (microphone) in the cell, the amplitude of the pressure variation can be monitored; this being dependent upon the radiant energy absorbed.

1.3.1. Historical Development Of The Optoacoustic Effect.

The original observation of the optoacoustic effect can be attributed to Bell (18). He demonstrated that when a rapidly interrupted beam of sunlight was incident on thin discs of certain substances in an enclosed volume, an audible sound was produced. This work prompted a series of experiments to be conducted independently by a number of scientists.

Röntgen (19), working on the absorption of heat rays by gases, demonstrated the effect with ammonia. He concluded that the heating and expansion of the gas, together with the subsequent cooling and contraction, were the causes of the acoustic signal. Similar work with gases and vapours was conducted by Tyndall (20). He showed that strongly absorbing gases were more effective at sound production and that the sound was produced by incident energy beyond the red-end of the visible spectral region. The lack of a convenient sound detector defeated Tyndall's attempts to develop a methane gas analyser for use in mines.

It was observed by these and other workers (21,22) that the frequency of the sound produced was identical with that of the modulation of the radiation source.

Bell continued his researches with solids (23), increasing the number of samples with which he could obtain an optoacoustic signal. He demonstrated that the effect could be observed with visible radiation as well as infrared, and also noted that the intensity of sound produced by a substance varied depending on which part of the spectrum was incident upon it. His explanation for the production of sounds from solids was by a process of cyclic desorption and readsorption of gas from the surface to produce the pressure fluctuations. He also studied a number of liquids, but obtained much weaker signals.

The historical development of the optoacoustic effect proceeded from this work with the advance of gaseous detectors and, solid sample radiation monitors.

Gases.

The foundation for the practical application of the optoacoustic effect to the qualitative and quantitative analysis of gas mixtures was laid by the work of Veingerov (24 - 27). He studied the infrared radiation absorbed by gaseous samples from a Nernst filament source using a moving coil microphone to monitor the amplitude of the acoustic signal. A 0.2% (by volume) mixture of carbon dioxide in a non-absorbing gas could be detected at atmospheric pressure. Mixtures of absorbing gases were analysed by placing a cell containing all but one of the components of the gas mixture between the sample cell and Nernst filament; this served as an optical filter. The accuracy and sensitivity of the analysis was limited by the poor response of the microphone transducer and the background signals produced by the absorption of radiation by the cell walls.

In 1943, Luft (28) reported an optoacoustic gas analyser which used a reference cell to compensate for absorption by the cell walls. The reference cell contained only that component of the mixture

in the sample to be analysed. Instruments using this arrangement were able to detect a few ppm of carbon dioxide or other strongly absorbing gases in air, and are still in use today (29).

The infrared absorption spectra of gases and vapours were measured by Veingerov (30) using a monochromator with his previously reported experimental arrangement. The use of the optoacoustic effect as a detector of infrared radiation proved to be of considerable interest, and a number of attempts were made to improve the sensitivity and reliability of this type of technique by developing the theoretical aspects and more suitable cells and pressure transducers (31 - 33). Multiple pass instruments (34) were investigated to increase the sensitivity of the technique.

Laser source optoacoustic spectrometry (LOAS) has recently been employed to measure very low gas concentrations, as the sensitivity of the technique is improved with increasing source power. The main difficulty with LOAS is the necessity for a good coincidence between the absorption bands of analyte gases with known laser emission lines. The sensitivity of this technique is sufficient to detect 0.01 ppm methane in a nitrogen atmosphere (35).

Solids.

Soon after Bell's initial work, Hayes et al (37) patented an optoacoustic detector using a finely divided charcoal receiving element for the incident radiation. A condenser microphone was employed to monitor the pressure change produced in a later paper by Hayes (38). The detector consisted of a finely divided gas occluding substance confined in an hermetically sealed chamber, one side of which was a thin metal diaphragm forming part of the condenser receiver. The radiation receiving element was 'fluff', the carbonised pappus of a flower. To operate the detector, the magnitude of the voltage change

across the microphone transducer was measured on removing a shutter before the detector to expose it to the incident radiation. Hall (39) proposed the use of an A.C. bridge to measure the change in capacitance of the microphone. This overcame the $^{1}/_{f}$ noise and drift problems associated with direct amplification of the microphone signal for continuously modulated radiation of frequency 1 - 3 Hz.

In 1946, Golay et al (40) investigated the Hayes detector, but decided to use optical detection of the pressure variation due to the insensitivity of the microphone transducer then employed. It was shown experimentally that Bell's suggestion that occluded gases in solid samples were responsible for the acoustic signal was erroneous. In fact, the purpose of the receiving material was to heat the gas, after absorption of incident radiation. A more convenient and reproducible black antimony film was used to replace the 'fluff' as the metal film has a lower specific heat and is easier to fabricate. The optical monitoring system consisted of antimony coated on a colloidion film with a nearby parallel glass window. The distortion of the film was detected by observing the shift in a system of interference fringes formed by reflection of light from the film and adjacent glass plate.

It is of historical interest to note that this work was conducted to develop a detector array system for monitoring the infrared emission from aircraft to control searchlight operations. However, radar was simultaneously developed and employed due to the limitations imposed by weather conditions on the Golay cell.

The theoretical aspects of pneumatic detectors were discussed by Golay (41) as a foundation for improvement of this type of system. An optical lever arrangement consisting of a light source incident upon a colloidion membrane, with a photocell detector was

used (42) instead of the interferometric system. Helium was tried as a filler gas instead of air, but this reduced the sensitivity of the detector. In 1949, Golay (43) redesigned the detector in its present form as a detector for infrared radiation in spectrophotometers. Xenon was chosen as the filler gas due to its low thermal conductivity.

A number of non-selective, infrared detectors were reported using receiving elements of carbonised duck-down (44) or a layer of black pigment (45,46). This type of detector was improved (47) and used by Houghton et al (48) to show that the optoacoustic effect could be obtained with solid films. This work was not further developed, however, and the analytical implications were ignored.

In 1973, Parker (49) noted that a background signal was obtained during experiments on gases using an optoacoustic cell, and showed that this was due to absorption of the incident light by the cell window. He attempted to produce a theoretical model for this observation. Kerr (50) used the technique to measure absorption by thin films at laser wavelengths, and produced a method of absolute calibration for his instrument.

In recent years the technique has been revived for the examination of solid samples and optoacoustic spectrometry is now a rapidly expanding field of study in the ultraviolet, visible and infrared regions. Harshbarger and Robin (51) published a review of the optoacoustic effect in 1973, in which they discussed the use of the optoacoustic technique to obtain information concerning photochemical gaseous reactions and the absorption spectra of solids and amorphous gels. Rosencwaig (52) has reported the optoacoustic spectra of a number of solids and biological materials, which agree closely with their conventional optical absorption spectra.

It should be noted that as well as obtaining spectral information, the optoacoustic effect has been used in the gas phase to investigate the rate of energy transfer between the vibrational and translational degrees of freedom of gas molecules. This was suggested by Gorelic (53) and practically developed by Slobodskaya (54) for the measurement of the excited states in the 2.7, 4.3 and 14.8 μm carbon dioxide bands. Several workers have since improved the technique and measured vibrational relaxation times in a number of gases (55 - 57).

CHAPTER TWO

INSTRUMENTATION FOR OPTICAL ABSORPTION SPECTROMETRY

2.1. Introduction.

The 'optical' region of the electromagnetic spectrum (Fig. 1.1) can be seen to extend from a wavelength of approximately 10^{-4}m (100μm) in the far-infrared to ca. 10^{-7}m (100nm) in the far-ultraviolet. An instrument for measuring the absorption of radiation in this wavelength interval will consist of certain essential components. A schematic diagram of a spectrometer capable of measuring molecular absorption spectra in the ultraviolet, visible and infrared regions is shown in Fig. 2.1. In fact, limitations on instrument design are imposed below 200nm and above ca. 10μm as it is necessary to evacuate the spectrometer to prevent the absorption of radiation by oxygen and water vapour respectively (58). In the infrared region, it is necessary to use an interferometric system at wavelengths greater than ca. 40 μm due to the low intrinsic source intensity and lack of suitable optical materials to manufacture dispersing elements (59).

The basic requirements of an optical spectrometer are:

i) A source of radiant energy.

ii) A dispersive device for the isolation of the desired spectral band of radiant energy.

iii) An absorption cell for sample containment.

iv) A detector.

v) Electronics system for signal detection, amplification and readout.

The necessary components to construct a spectrometer will be selected by both the spectral region of operation and the application for the instrument. The general aim of the equipment is to provide a wide free spectral range and a means of isolating a restricted band of wavelengths. By restricting the radiant energy incident upon the sample to a range of frequencies that can be absorbed by the species of interest, the percentage change in response for a given concentration

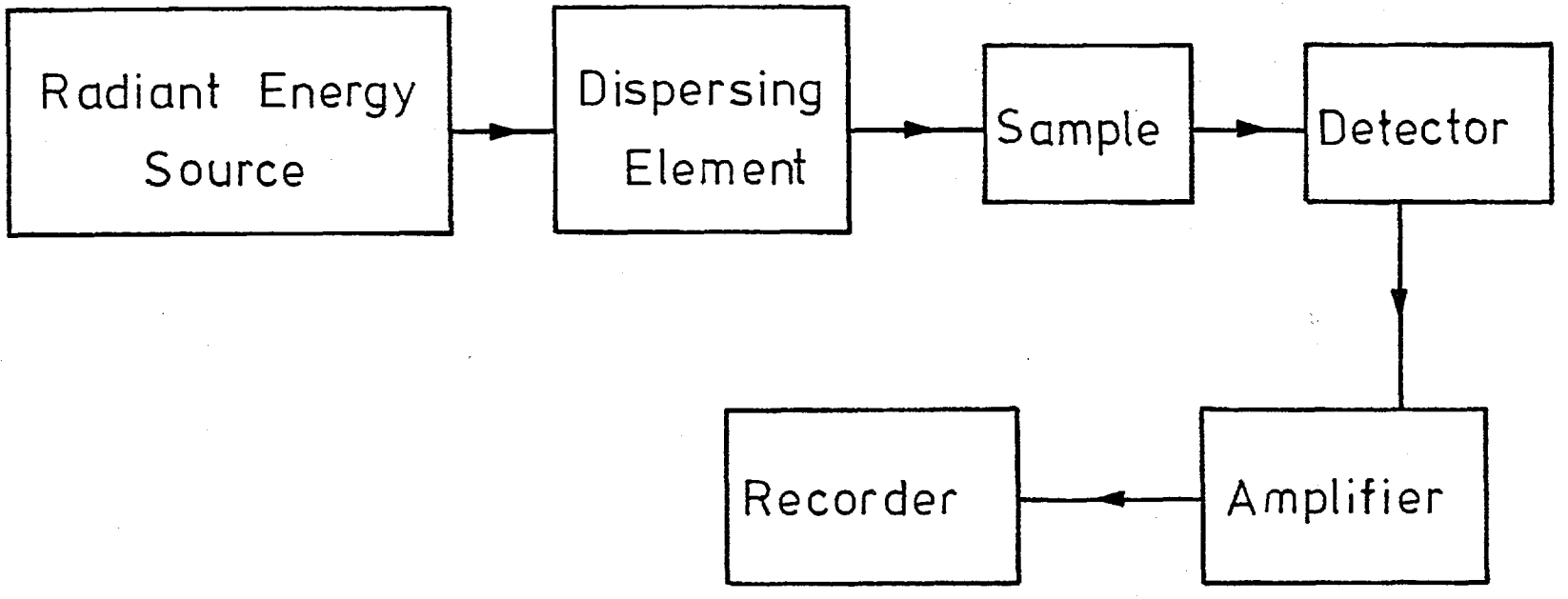

Fig. 2.1 Essential components of an optical spectrometer.

becomes greater and the technique analytically more specific (9).

2.2. Sources.

The function of the radiant source is to provide radiation of sufficient intensity for measurement in the spectral region of interest. The emission of a source may be described as being line or continuum in nature(60); though there is no sharp distinction between the classifications. The term continuum is applied to both true continua (incandescence) and to those sources where many closely spaced lines or bands are emitted over a wide wavelength range (the rare gas arcs).

The simplest and most common form of continuum source is the tungsten filament lamp (61). This emits the major portion of its energy in the near-infrared region. The operating temperature of the lamp can be increased to decrease the wavelength of the energy maximum, but the useful lifetime of the lamp may be reduced. The radiation emitted from this source has a spectral distribution similar to that of an ideal black-body emitter (62). The limitations of the lamp are that it cannot be used above an intensity set by the melting point of the filament and its emission is limited to the transmission region of the quartz envelope (0.2 - 3 μm , approximately). For a continuum radiation source in the infrared region, a Nernst glower (63) may be employed. This is an electrically heated filament made of a mixture of rare-earth oxides. At wavelengths above 10μm , more energy may be obtained from a heated silicon-carbide strip or rod, i.e., a Globar (64). In the far-infrared region (>150μm), a high pressure mercury arc lamp contained in a quartz envelope may be employed as a source of black-body radiation (59). Above about 2.7 μm the quartz envelope is opaque and is itself an emitter of black-body radiation, but above

approximately 150 μm the envelope transmits the arc radiation.

In the ultraviolet region, an alternative form of continuum source is that employing the extensive, diffuse band emission of hydrogen and deuterium discharge lamps (58). These are low-pressure lamps that produce a far more intense continuum than does a tungsten filament between approximately 170 and 400 nm , with a peak emission wavelength at about 230 nm.

To overcome the limitations of incandescent sources it is necessary to employ a gas plasma or electric discharge to obtain higher intensities. Xenon arcs or mercury discharge lamps are employed in the visible and near-ultraviolet regions (5). These provide a high radiant flux of continuum radiation plus additional intense radiation at the wavelengths characteristic of the xenon or mercury emission spectrum.

Spectral line emission sources are produced generally by atomic emission processes (60). Excitation energy may be supplied by the absorption of radiation, by kinetic energy transformation from inelastic collisions with electrons or atoms, by energy transfer processes involving excited species, or by thermal excitation; usually a complex combination of the other mechanisms. The traditional line emission sources of this type are flames, arcs, sparks and glow discharges (hollow cathode lamps).

The relatively low temperatures attained within flames ensure that only the resonance lines of alkali metals and alkaline earths will be excited. The principal use of the flame is in flame emission spectrochemical analysis for these analytes (65) and atomic absorption spectroscopy where high excited state populations are not required (66). The arc source can be used to produce sufficiently high temperatures to excite the neutral spectra of atoms and molecules,

and often many ion lines (60). The plasma jet (67), a development of the high current arc, can be used to achieve an even higher operating temperature. Sparks may be employed to excite several degrees of ionisation in the atoms of the electrode material or of the carrier gas between the electrodes (60).

These sources are more commonly employed in emission spectrometry rather than for absorption measurements. However, glow discharges are used as a source for absorption work. The positive column of a glow, or electrodeless discharge, can be used to produce molecular, atomic and ionic spectra by excitation of gases or vapours at pressures of a few torr (66). The hollow cathode lamp (67) makes use of the cathode glow to produce an intense, fairly compact, source. Material from the cathode walls is spluttered into the discharge by collisions from the filler gas ions so that metals and salts as well as gases can be made to emit. Electrodeless discharges, sustained by radiofrequency or microwave generators, are useful for producing high purity spectra (66). Electrode contamination is avoided by placing the lamp, containing the gas or solid with appropriate filler gas, in an induction coil or resonant cavity.

Lasers (62) provide a source of radiation that has the unique properties of being extremely coherent and available in a very narrow bandwidth. In addition, the output of a laser can be of very high energy and concentrated into a very small area. Although a wide variety of lasers have been developed, covering the spectral region from the near-ultraviolet to far-infrared (68), these have been of limited use in analytical spectrometry as the only spectral lines emitted are those characteristic of the lasing media. However, lasers, tunable over a limited spectral range, are now available in the visible and near-infrared regions using fluorescent organic dyes (69), and in the

infrared region by the use of semiconductor diode emission (70). The applications of these tunable lasers to spectroscopy are not widespread at present due to their high cost and the limited free spectral range of each emitting dye or diode.

2.3 Dispersing Devices.

These can be classified under three general headings, i.e., filters, prisms and diffraction gratings.

Filters can be further sub-divided into those that function by selective absorption of unwanted wavelengths, e.g., gelatin, liquid and tinted glass filters, (71) or those that depend upon constructive and destructive interference of radiation for their transmission characteristics, i.e., interference filters (1). Although filters are limited to single-wavelength applications, they can be employed in dedicated instruments (72).

A prism (66,71) can be used to disperse a polychromatic beam of radiation into a spectrum. Its action depends upon the variation of the index of refraction of the prism material with wavelength. Prisms are limited in application, as they need to be constructed of materials which have a high dispersion and transmittance in the spectral region of interest.

Diffraction gratings (62,73) can be used over a wide range of wavelengths as they can be designed to function by front-surface reflectance, rather than by transmission which would be analogous to the prism. Replica gratings are actually employed in many commercial monochromators as they can be mass-produced at reasonable cost from master gratings, which have individually ruled lines (grooves). Each groove can function as a centre for scattering the light rays reaching it. However, the grating will introduce phase differences into a

wavefront incident upon it (for non-normal angles of incidence), since each part of the wavefront will have travelled a different distance during reflection by the grating. Constructive combination of the wavefront will occur when different parts are in phase, i.e., when their net path difference is equal to an integral multiple of a wavelength (λ). Thus,

$$n \lambda = 2 d \sin \theta \qquad \ldots 2.1$$

where n is the order of interference, d is the distance between adjacent grooves and θ is the angle of diffraction. The angular dispersion is given by rearrangement and differentiation of this expression with respect to λ .

$$\frac{d\theta}{d\lambda} = \frac{n}{d \cos \theta} \qquad \ldots 2.2$$

The resolving power of a grating is given by (1),

$$R = \frac{\lambda}{\Delta\lambda} = n N \qquad \ldots 2.3$$

where N is the total number of grooves on the grating. Thus a high dispersion may be obtained by using a very finely ruled grating. Alternatively it may be obtained with a few lines but at a high order (and blaze angle) - an echelon. A grating may be blazed for a desired wavelength by a special angle (echelette) of the groove. This concentrates the bulk of the diffracted intensity in one of the orders of the spectrum. Blazing the grating also has the effect of causing a variation in reflected intensity with wavelength within an order. The theoretical efficiency of the grating, as derived from scalar wave theory (73), will be greater than 0.5 in the wavelength range,

$$\left(\frac{2}{2n+1}\right)\lambda_b < \lambda < \left(\frac{2}{2n-1}\right)\lambda_b \qquad \ldots 2.4$$

where λ_b is the blaze wavelength in the first order, and n is the order in which the grating is used. Thus the wavelength response of the grating is such that its efficiency is more rapidly attenuated for wavelengths that are less than the blaze angle than for those that are greater.

Although a grating can be blazed to obtain most of the reflected energy in a particular order, there will still be a certain amount of radiation transmitted simultaneously at half the required wavelength in the second-order, a third the required wavelength in the third-order, etc., when operating in a first-order mode. Thus blocking filters are required to remove overlapping spectral orders (66). When a large number of these are required to isolate the required spectral region, then a double (prism-grating) monochromator arrangement may be employed (61).

2.4. Absorption Cells.

The position of the sample cell in instruments designed either for ultraviolet-visible or infrared operation is seen to differ (9). In the former case, the cell is placed after the dispersing device since luminescence and photochemical processes may otherwise interfere with the measurement. The actual dimensions of the cell depend upon the physical state of the sample and the intensity of the absorption bands to be measured. In the ultraviolet and visible regions, for solution samples, path lengths of 1cm are standard. For the mid-infrared region liquid cells of 0.005 - 0.1 cm thick are employed, whilst gas cells 10 - 100 cm long are used (63). In the near-infrared region where even lower band intensities are encountered, corresponding cell path lengths may be up to a hundred times as great as those for the fundamental region (74).

Although gases and liquids may be examined directly, it is often necessary to dissolve solids to examine them by transmission spectrometry. However, not all substances can be dissolved in reasonable concentration in a solvent which is nonabsorbing in the regions of interest. Attenuated total reflectance (9) may be used to yield spectra from thin films or surfaces of materials that can be placed in contact with an optical surface.

The technique of diffuse reflectance spectroscopy (16) permits the study of the absorption spectra of not only solid materials but also of substances embedded or absorbed on to solid surfaces. The most common means of collecting the diffuse radiation reflected by a sample is the integrating sphere (15). This consists of a spherical chamber whose inner walls are coated with a matt, highly reflecting material that can reflect on to the detector the diffuse radiation from the sample as efficiently as possible in the wavelength region of interest. The sample and detector are usually designed to form part of the sphere wall. For less rigorous applications, a hemispherical or circumferential mirror system has been employed for the study of roughly textured samples such as textiles or powders of large particle size (13).

In all these cases, additional specialised cell designs exist for work at both low and high temperatures (9,13,63).

2.5. Detectors.

All detectors used in spectrometers function by converting the incident radiation into an electrical signal which can be extracted, amplified and recorded. Detectors can be classified into two main groups according to the mechanism of this conversion (73):

i) Photon detectors.

ii) Thermal detectors.

(i) Photon detectors record the absorption of the number of quanta of radiation incident at the detector causing excitation and emission of an electron. This is detected by either directly recording the number of events taking place in the detector (pulse, photon, counting), or by integrating the charge released during a given time (rate measurement); the overall measurement being the rate of arrival of photons. The photomultiplier tube (66) is an example of this form of detector, consisting of a photoemissive device with an inherent amplification stage utilising the photoelectrons produced by the absorption of photons. The working spectral range of photomultiplier tubes is controlled by the nature of the photocathode and the window material of the device. They are most efficient operating in the ultraviolet-visible region of the spectrum, although their ultraviolet response (<200nm) may be extended by the use of suitable scintillators (58). A photo-ionisation detector may be employed in the vacuum ultraviolet (<200 nm) (62); the ion current between two electrodes due to ionisation of the filler gas by absorbed radiation being the measured quantity. In the near-infrared region, photoconductive detectors employing semiconductor devices such as lead sulphide are commonly employed (74). These detectors can function for lower energy, incident, photons than photoemissive detectors as they rely on exciting electrons from a crystal lattice to a conduction band to act as current carriers rather than emitting them from the material surface. The requirement for the incident photon to have enough energy to produce a photoelectric event places a long wavelength limit on these devices in a similar manner to the photomultiplier tube systems.

(ii) The thermal detector functions by detecting the heating effect produced in a suitably absorbing material due to the incident

radiation energy. The output signal from an ideal (black-body) thermal detector will depend only on the energy of the radiant power absorbed and not its spectral distribution. These detectors are used principally in the medium and far-infrared regions (63). The thermocouple is widely in use at present in the mid-infrared with the Golay cell employed in the far-infrared region (75). Bolometers (19) and pyroelectric detectors (76) may also be employed.

The operating principle of the bolometer is the change of electrical resistance of a material due to the temperature change caused by the absorbed radiation. The semiconductor thermistor device is the most common form of bolometer. The pyroelectric detector is based on a cystal structure possessing a permanent electric dipole moment. The field produced by this is neutralised by surface charges attracted to the crystal faces. Temperature changes, induced by coating the crystal with a thin black layer to absorb incident radiation, will cause a change in permanent dipole moment. If the crystal material is an insulator an electric field appears due to the relatively long time required for rearrangement of surface charges. Thus for illumination of the detector by modulated radiation, a resultant signal can be detected with a pair of electrodes bonded normal to the polar axis of the crystal.

2.5.1. Pneumatic Detectors.

The Golay detector (42) employs an optical lever to monitor the expansion of a gas in a sealed chamber due to the heating effect produced by the incident radiation at an absorbing surface. The Golay cell (Fig. 2.2) consists of a chamber containing a gas of low thermal conductivity, usually xenon, with a window, A ; radiation passing through the window reaches a thin absorbing film, B , of low thermal capacity and high conductivity; the temperature

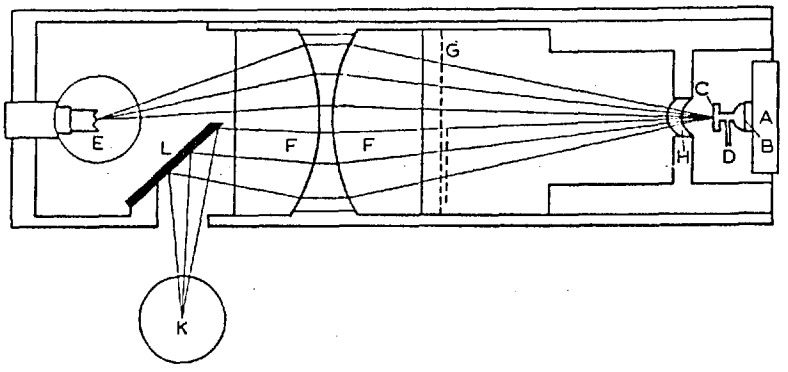

Fig. 2.2 The Golay Cell. (63)

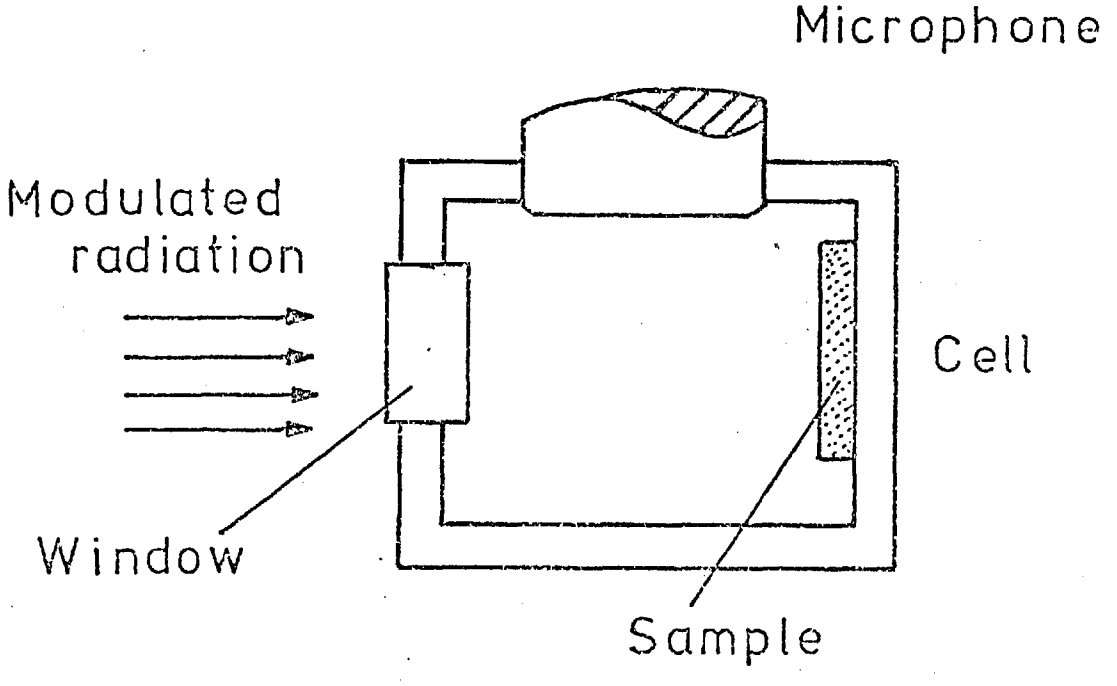

Fig. 2.3 The Optoacoustic Cell.

of which monitors the energy flux of incident radiation. Gas in contact with the film is heated by conduction and the mirror membrane, C , sealing the opposite face of the gas chamber suffers some distortion. To prevent room temperature changes from affecting the detector a fine leak, D , connects the detector chamber to a ballast reservoir of gas on the other side of the membrane. Thus the incident radiation must be modulated (ca. 10 Hz) as steady or very low frequency modulated radiation at the detector produces no pressure difference between either side of the membrane.

An optical system is employed to convert and amplify the movement of the membrane into an electrical signal. Light from the lamp, E , passes through a condenser, F, F , then through a line grid, G , and is concentrated on the mirror membrane. A lens, H , between the line grid and the mirror membrane, focuses the beam so that, in the absence of any deformation, an image of one part of the line grid is superimposed on another part of the same grid. If the image of a gap between lines coincides with a gap in the grid, light will be transmitted and may be detected by photocell, K , after reflection from mirror, L . Deformation of the mirror membrane causes a corresponding change in the intensity of light reaching the photocell.

The Golay cell is a non-selective detector and the receiving membrane is of unblackened aluminium or gold for far-infrared studies. It is so thin that with blackening of the absorbing surface it exhibits a flat spectral (energy) response from the visible to the far-infrared and microwave regions. At short wavelengths the sensitivity falls when the wavelength is comparable to the film thickness and at long wavelengths when the wavelength approaches the diameter of the receiving element.

The principle of operation of an optoacoustic cell (Fig. 2.3) is similar to that of the Golay cell. Incident radiation is absorbed by a sample leading to the expansion of the filler gas in the cell due to the heat flow from the sample. With a black material as the sample, this cell functions as a wide band detector of radiation similar to the Golay cell. However, by placing a substance that has differing absorption characteristics with wavelength in the cell, a detector that responds to specific bands of wavelengths is created. Conversely, by recording the amplitude of the pressure change versus wavelength, an absorption spectrum of the sample can be recorded.

The incident radiation on the cell is modulated as before, but at higher frequencies (20 Hz - 20 kHz). This enables a sensitive microphone transducer to be employed to monitor the amplitude of the periodic pressure change produced in the cell. It is interesting to note that the cell design, upon which Golay based his work, employed a microphone transducer (38). The principal reason for the change to an optical lever arrangement was the absence of sensitive microphone transducers (40).

The condenser microphone (77) now available commercially is highly sensitive and in addition has operating characteristics of high stability, flat response over a wide frequency range and very low internal noise. The operating principle of the condenser microphone (78) is that of a parallel plate capacitor, where the charge is kept constant. The voltage across the plates is then proportional to the distance between the plates. The back plate is kept fixed and the front plate is a thin metallic diaphragm which can respond to incident sound pressure waves. Thus the sound varies the voltage across the plates, and gives an audio output signal. The charge on the plates is kept constant by polarising the plates via a large resistor (Fig. 2.4)

Fig. 2.4 Schematic diagram of a capacitor microphone.

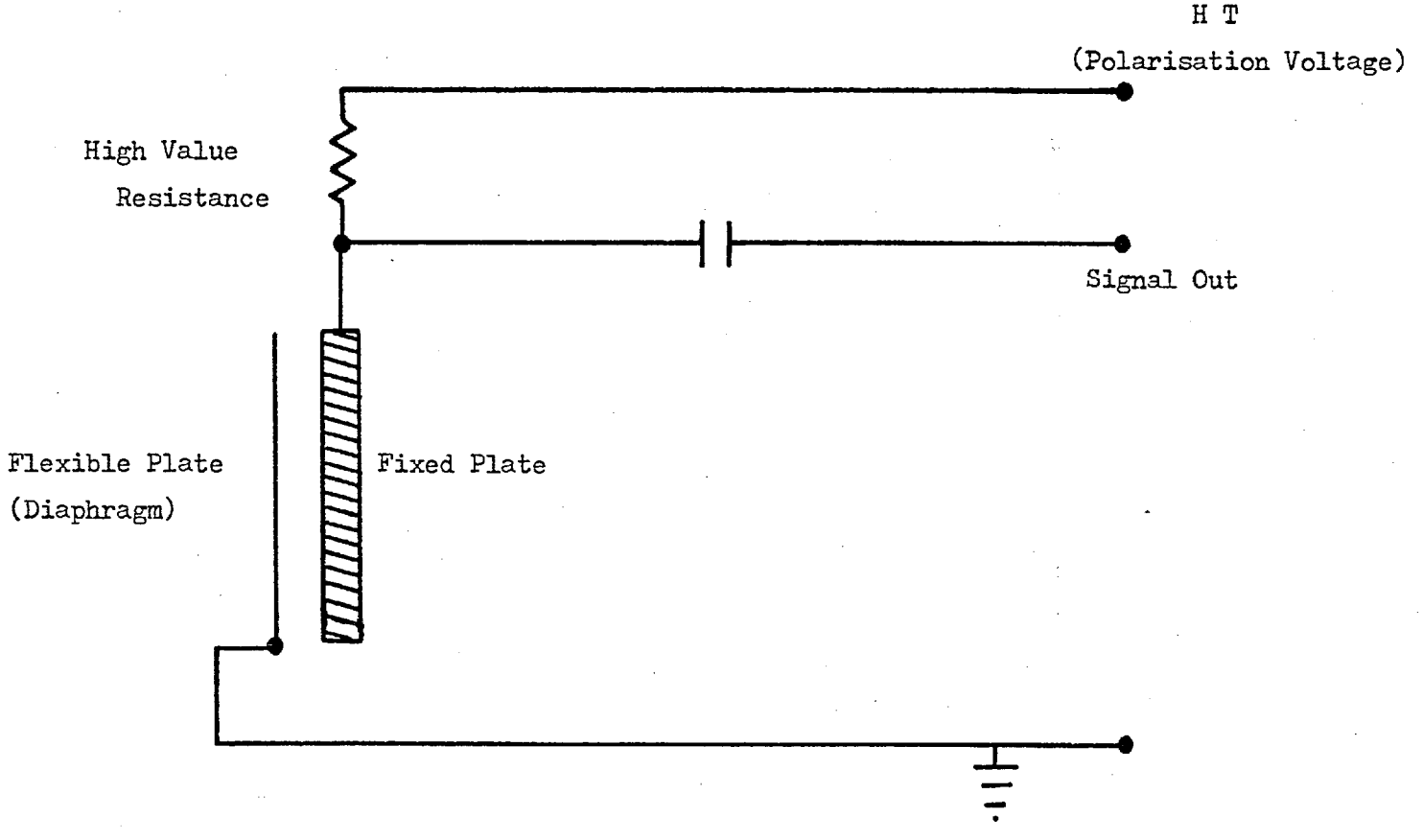

Fig. 2.5 Equivalent circuit of a Brüel and Kjaer microphone and preamplifier.

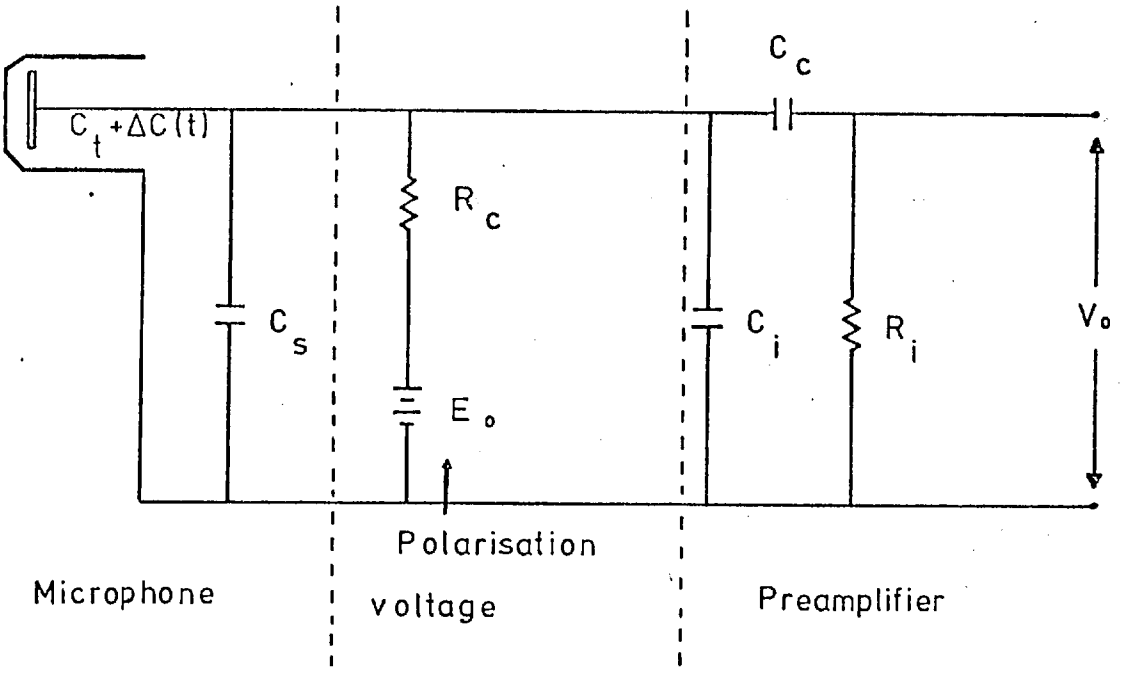

Fig. 2.6 Simplified circuit of a Brüel and Kjaer microphone and preamplifier.

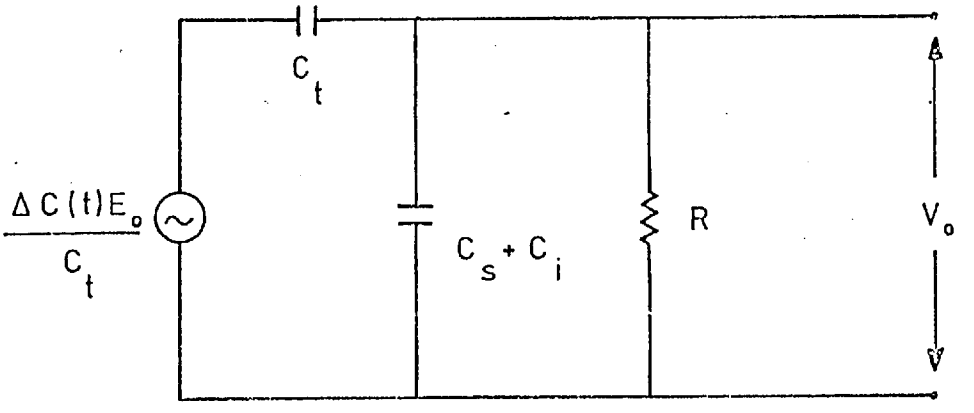

and the signal voltage is extracted via an isolating capacitor. Although the condenser microphone has a high output level, its source is a small capacitance. Thus it has a high source impedence value at audio frequencies and may suffer from stray fields picked up by the cable connecting it to its amplifier and from a deterioration in frequency response along the cable. So the preamplifier has to be built close to the signal source.

An equivalent circuit diagram (Fig. 2.5) and its simplification (Fig. 2.6) of a typical microphone and preamplifier system (78) are shown. The overall sensitivity (S) of this system can be described (77) by the expression :

$$S = \frac{\Delta C\,(t)}{C \cdot \Delta p\,(t)} \cdot E_o \cdot \frac{j w R C}{1 + j w R C} \quad \ldots 2.5$$

where $\Delta C\,(t)$ is the variation in capacitance due to sound pressure, $\Delta p\,(t)$ is the sound pressure variation with time, E_o is the polarisation voltage. C is given by,

$$C = C_t + C_s + C_i \quad \ldots 2.6$$

where C_t is the microphone capacitance, C_s is the stray capacitance and C_i is the input capacitance of the preamplifier.The coupling capacitance (C_c) is much greater than C_i and is thus neglected in the simplified circuit.

R is given by,

$$R = \frac{R_i \cdot R_c}{R_i + R_c} \quad \ldots 2.7$$

where R_i is the input resistance of the preamplifier and R_c is the charging circuit resistance. As

$$\Delta p\,(t) \propto \Delta C\,(t)$$

then

$$S \propto \frac{E_o}{C} \cdot \frac{j w R C}{1 + j w R C} \quad \ldots 2.8$$

Two basic cases can be considered from this expression for microphone sensitivity. The high frequency response, when $w R C \gg 1$, is given by

$$S \propto \frac{E_o}{C} \quad \ldots 2.9$$

Thus the sensitivity is proportional to the polarisation voltage but inversely proportional to the total capacitance. If any capacitance additional to that of the transducer is allowed to load the transducer, the overall sensitivity will be reduced. Hence the usual close proximity of microphone and preamplifier to avoid the total circuit capacitance exceeding that of the transducer.

At low frequencies, when $w R C \ll 1$, then

$$S \propto \frac{E_o}{C} \cdot j w R C \quad \ldots 2.10$$

This expression is frequency dependent, and associated with the transition to frequency dependence of sensitivity a cut-off frequency (f_c) can be defined (78) when $w R C = 1$ and the sensitivity is reduced by 3dB. Then,

$$f_c = \frac{1}{2\pi R C} \quad \ldots 2.11$$

The input resistance of the preamplifier must be very large at low frequencies; the lower frequency limit being typically of the order of 2 Hz (77).

2.6. Electronic Measurement Methods.

The output of the detector is normally measured as a function of wavelength, time or analyte concentration. This output is either in the form of an analogue (current, voltage or resistance) or digital (count rate) signal (79,80). In the simplest form, many spectroscopic detectors produce DC signals which are amplified by DC amplifiers for display on meters or potentiometric chart recorders. Although the problems of offset and drift associated with DC amplifiers may be overcome by the use of chopper stabilised operational amplifiers (81), the presence of 1/f noise in the signal seriously restricts the extent to which the signal-to-noise ratio can be improved by low-pass filtering. Thus, it is often desirable to modulate the signal to transform the signal information from DC to an AC frequency high enough to avoid drift and 1/f problems (9). The AC signal can then be amplified by an AC amplifier and converted back into DC, by a demodulator or rectifier, suitable for feeding to a readout device. The simplest form of modulation is that imposed on the signal between the detector and amplifier (80). However, the drift and DC errors present in the detector signal are also modulated and then amplified. This can be overcome by modulating the radiation incident on the detector.

AC amplifiers can be classified under two headings; namely asynchronous and synchronous detection of the AC input for conversion to DC. All AC amplifiers contain an initial amplification stage which is then fed to the detection stage (82). An asynchronous detector is essentially a type of full-wave rectifier. The DC output of the detector is proportional to the amplitude of the AC input to the detector; the DC component being extracted by low-pass filtering. The main problem with this arrangement is that a noise offset will be

produced at the detector output due to rectification of the noise input. This problem is completely eliminated by the synchronous detector (83). This is also known as phase sensitive detection, an AC amplifier with a synchronous detector being referred to as a lock-in amplifier (81).

2.6.1. Phase Sensitive Detectors.

The phase sensitive detector (p.s.d.) can be simply represented by a two-position switch which alternatively gates either the signal or the inverted signal into a low-pass filter (Fig. 2.7). The effect of this is that when the AC signal and reference input have the same frequency and are in-phase, the lock-in output gives the average amplitude of the signal. A phase difference between the signal and reference affects the output value. In particular a phase shift of 90^{o} brings the output to zero, whilst a phase shift of 180^{o} results in a full value but negative output. To counteract any such phase shifts caused in an experiment, a phase-shift facility is usually included in a lock-in system. When the signal and reference inputs are not at the same frequency, then the average value of the switch output is zero, provided a sufficiently long time is taken to establish the average. The lock-in amplifier has the effect of filtering out voltage fluctuations which are not at the reference frequency. Thus it rejects noise, responds only to signals coherent with the reference voltage and produces a DC output. That is, it acts as a filter and linear rectifier.

The p.s.d. can be thought of as a multiplier circuit, the output of which (v_o) is the product of the signal input (v_i) and the reference input (v_r); that is

$$v_o = v_i \cdot v_r \qquad \ldots 2.12$$

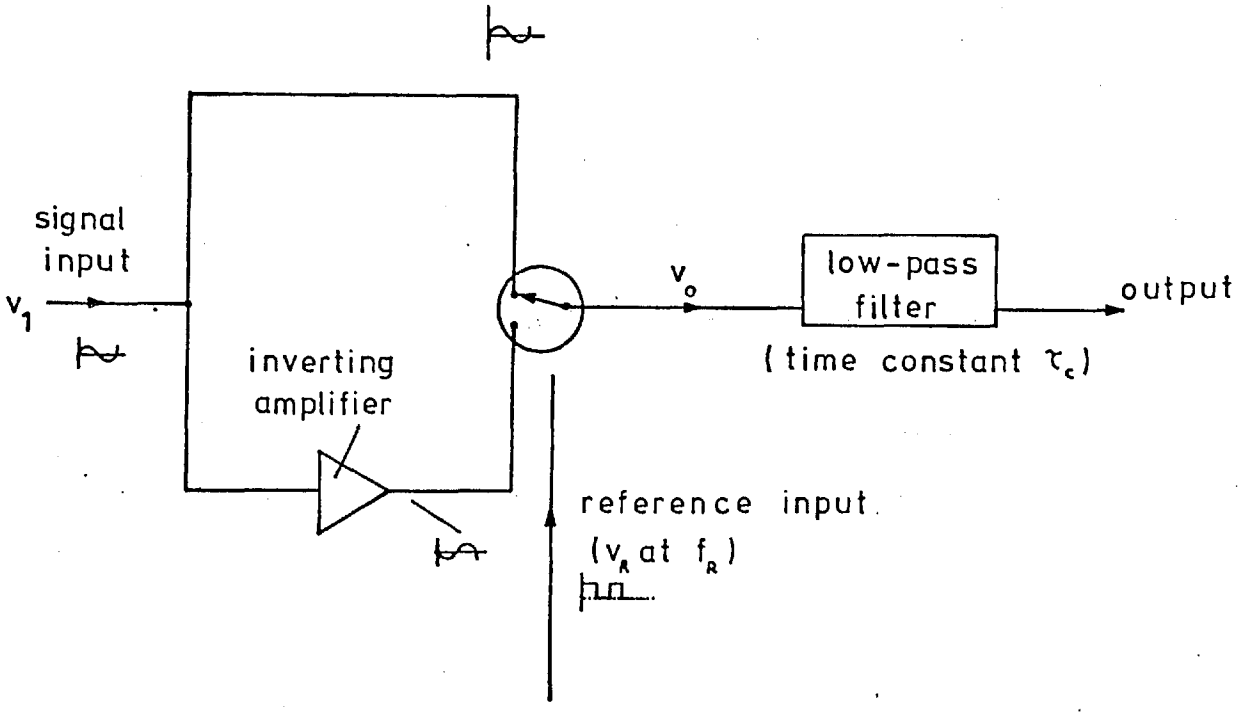

Fig. 2.7 Schematic diagram of a phase-sensitive detector.

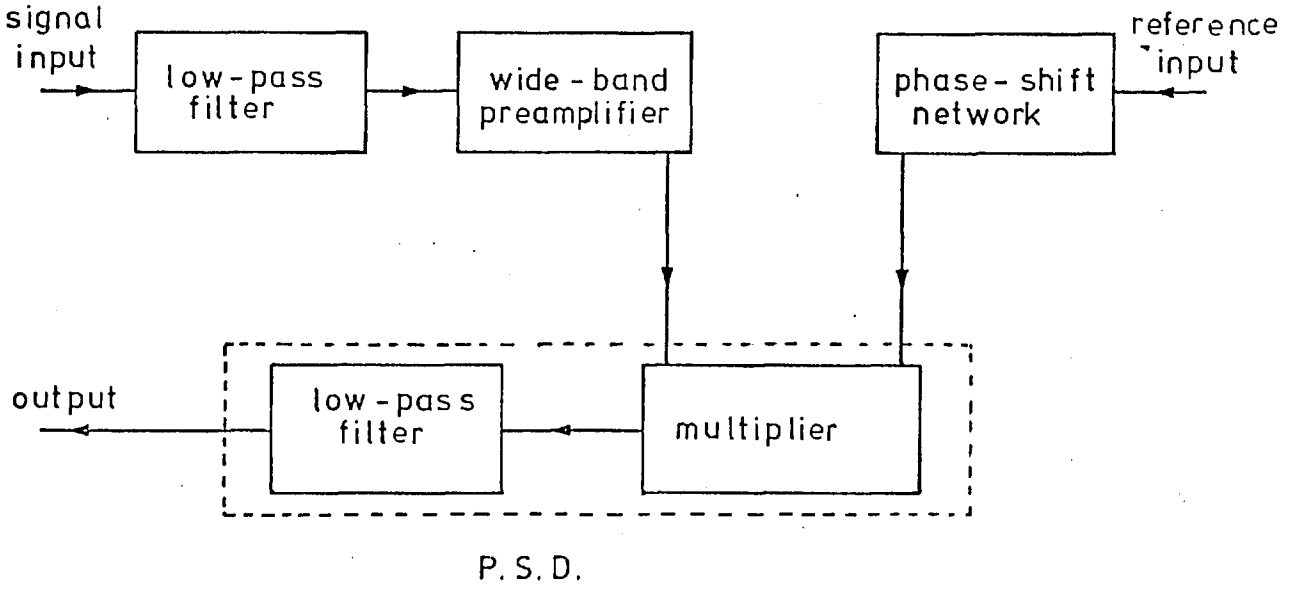

Fig. 2.8 Schematic diagram of a lock-in amplifier.

The reference signal obtained from the light-chopper is a square wave of period T_r. This waveform can be described as a superposition of sinusoidal components. The dominant component is at the fundamental angular frequency $w_r = 2\pi/T_r$. All odd harmonics of this frequency are also present in the reference signal and the amplitude of these terms is inversely proportional to the harmonic number. For simplicity, only the effect of the fundamental component is considered, to demonstrate the behaviour of the multiplier, and so

$$v_r = V_r \cos w_r t \quad \ldots 2.13$$

where $w_r = 2\pi f_r$ and f_r is the reference frequency. The signal input to the multiplier, that is the p.s.d., consists normally of the synchronous signal to be measured accompanied by random or discrete frequency asynchronous signals; that is noise. Since both signal and noise can be described in terms of a superposition of sinusoidal components, a typical component (either signal or noise) of the signal channel input is considered, described by

$$v_i = V_i \cos w_i t \quad \ldots 2.14$$

The multiplier output signal (v_o) is therefore given by

$$v_o = v_i v_r = V_i V_r \cos w_i t \cos w_r t \quad \ldots 2.15$$

Normally V_r is held constant at unity so that

$$v_o = V_i \cos w_i t \cos w_r t \quad \ldots 2.16$$

If the component v_i is an asynchronous or noise component then

$$w_i = 2\pi f_i \neq w_r = 2\pi f_r$$

and

$$v_o = \tfrac{1}{2}V_i\left[\cos 2\pi t(f_i - f_r) + \cos 2\pi f\, t(f_i + f_r)\right] \qquad 2.17$$

The noise frequency ($f_i = f_n$) can assume any value where the noise spectral density is not zero. If the low-pass filter has a cut-off frequency (f_c) which is significantly lower than the reference frequency, then the term containing ($f_n + f_r$) will be strongly suppressed and the only noise components which get through the low-pass filter unattenuated are those having frequencies where $|f_n - f_r| < f_c$. That is, the lock-in amplifier is a bandpass filter which only permits frequencies near f_r to appear at the output.

When $f_i = f_r$, as in the case with the signal of interest, then the output is a DC voltage which is proportional to the signal amplitude and which depends upon the phase difference between the inputs. That is, if v_i is a signal of the form

$$v_i = V_i \cos (w_r t + \varphi) \qquad \ldots 2.18$$

then

$$v_o = V_i \cos (w_r t + \varphi) \cos w_r t \qquad \ldots 2.19$$

$$= V_i\left[\cos^2 w_r t \cos \varphi + \sin w_r t \cos w_r t \sin \varphi\right] \quad . 2.20$$

$$= \tfrac{1}{2}V_i\left[\cos(2w_r t + \varphi) + \cos \varphi\right] \qquad \ldots 2.21$$

and the filtered (averaged) output voltage is

$$\overline{v_o} = \tfrac{1}{2}V_i \cos \varphi \qquad \ldots 2.22$$

The improvement in the signal-to-noise ratio depends on the bandwidth of the filter and the distribution of noise. The bandwidth can be shown to be $B = 1/(\pi \tau_c)$, where τ_c is the time constant of the output low-pass filter, and is centred about the reference frequency f_r (82). The effective φ of the filter is

$$\varphi = f_r/B = \pi \tau_c f_r \simeq 3 \tau_c f_r$$

Typically for the extraction of optoacoustic signals, where f_r = 30Hz and τ_c = 3s then, φ is 270. This is an order of magnitude better than the typical maximum usable φ of a passive tuned filter. A lock-in filter will also automatically track signal frequency changes since the reference frequency is changing simultaneously. The signal-to-noise improvement through this filter is proportional to (input noise bandwidth / output noise bandwidth)$^{1/2}$. It is the automatic frequency-tracking feature which allows the lock-in filter to operate with such a narrow bandwidth and hence be so effective in signal recovery.

A commercial lock-in amplifier consists of refinements to this basic system, which are indicated in Fig. 2.8 (83). It is useful to include a low-pass filter on the signal input to the lock-in amplifier due to the latter's ability to detect harmonics of the reference frequency in the signal to be measured.

2.6.2. The Boxcar Integrator.

The boxcar integrator (80,82) is used when it is desired to measure a small 'time slice' of a repetitive transient signal. It consists basically of an electrically gated DC amplifier followed by a low-pass filter or integrator. The amplifier is gated ''on'' for an adjustable interval of time (the gate width) each time a trigger pulse is received. A delay time between the trigger pulse and the gate may be selected.

A boxcar system can be used in either the fixed delay mode or the sweep delay mode. In the fixed delay mode, a constant delay time allows one particular time slice of the signal to be studied, e.g., the fluorescence emission in a pulsed excitation system (80). In the sweep delay mode, the delay time is increased from a low initial value, thereby scanning the gate interval through the period

of a repetitive signal. The output of the gated amplifier is then low-pass filtered and recorded as a function of the delay time, resulting in a plot of the signal waveform. This allows fast, repetitive waveforms to be extracted from a great deal of random noise without undue distortion of the signal waveform. This is achieved because the effective time resolution of the system is determined by the gate width, whereas the effective noise bandwidth is determined by the time constant of the low-pass filter.

A general disadvantage of a boxcar system in this mode is that all the waveform information falling outside the gate interval is wasted. The overall efficiency of the system becomes very low when short gate widths and long sweep times are used, as is required for the measurement of fast, noisy waveforms.

2.6.3. The Multichannel Signal Averager.

The poor efficiency of the boxcar system for measuring fast, noisy waveforms is overcome in a multichannel signal averager (80,82). This system may be viewed as an array of sequentially gated boxcar integrators, each one of which is assigned to a unique time segment of the signal waveform and is gated ''on'' only during that time segment. Each time segment is averaged over many repetitions of the signal waveform and so none of the signal information is wasted. Random noises are averaged towards zero as the number of repetitions is increased. For N responses the noise voltage is in effect reduced by $\sqrt{N}$ (for Gaussian random noise; the noise voltage reduces less rapidly for non-Gaussian noise) (82).

It should be noted that an overall feature of all signal processing systems for enhancing the signal-to-noise ratio is that they all trade measurement time for a reduction in noise. The assumption

that has to be valid for these systems to function is that the noise is not correlated with the signal.

CHAPTER THREE

PRELIMINARY STUDIES OF THE OPTOACOUSTIC EFFECT

3.1. Introduction.

The optoacoustic effect may be demonstrated (85) with simple apparatus such as shown in Fig. 3.1. When radiation in the visible and near-infrared region of the spectrum from a low power quartz-iodine, tungsten lamp is incident on a suitable absorbing material, e.g., carbon black, contained in a closed system, the energy absorbed by the sample is converted into heat, provided that the material does not luminesce or degrade photochemically. By modulating the incident radiation with a rotating sector, the heat produced in the sample is also modulated at the same frequency. In a closed system of constant volume, this heating effect produces a periodic increase in pressure which follows the modulation frequency of the incident radiation. At modulation frequencies between 30Hz and 20kHz , this varying pressure produces an audio-frequency, acoustic signal the amplitude of which may be measured with a simple microphone transducer. With gaseous samples, this periodic pressure change is detected directly in the gas, whereas with solid and liquid samples the optoacoustic signal is detected indirectly by monitoring the periodic pressure change in the gaseous environment surrounding the sample; the gas becomes heated intermittently at the modulation frequency by heat transfer at the sample-gas interface. Despite the indirect nature of the detection for solid samples, some of the strongest optoacoustic signals have resulted from the observation of the effect with solids. Indeed, in Bell's original work (23) using the sun as the source, distinctly audible signals were detected for various samples using the unaided ear as the detector. It is apparent with the simple apparatus in Fig. 3.1 that the amplitude of the signal is directly proportional to the intensity of the source (86). In addition, the amplitude of the signal is inversely proportional

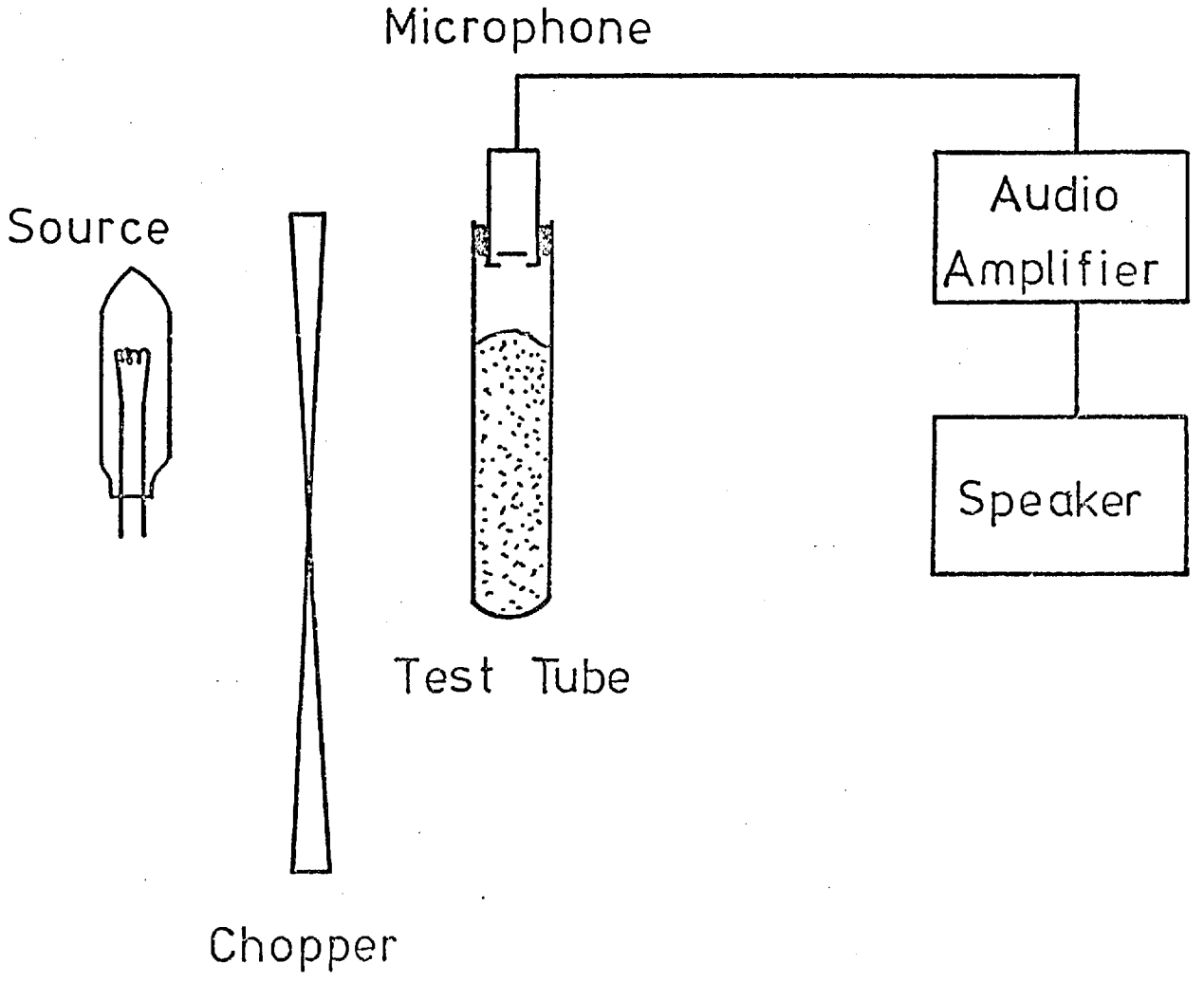

Fig. 3.1 Apparatus for demonstration of the optoacoustic effect.

to the modulation frequency, as at high operating frequencies the radiant energy supplied to the sample per open chopper period decreases resulting in less heat energy per pulse being available after degradation to produce the pressure change. It is also observed that the amplitude of the optoacoustic signal is greatest for samples of large surface area, e.g., fine powders, where more efficient heat transfer to the surrounding gaseous atmosphere is possible.

The optoacoustic effect can only be observed when the incident radiation is absorbed by the sample. Thus, by varying the wavelength of the radiation incident upon the sample, the amplitude of the optoacoustic signal observed at a given wavelength will provide a measure of the ability of the sample to absorb the incident radiation, i.e., the absorption spectrum of the sample will be obtained. The optoacoustic power spectrum obtained by measurement of the signal amplitude versus the wavelength of the incident radiation should, therefore, resemble the absorption spectrum of the sample and be complementary to the reflectance spectrum. The use of optoacoustic spectrometry for the examination of solid samples should have a number of advantages over conventional optical absorption or diffuse reflectance spectrometry. These advantages include the following:

1) In contrast to optical absorption or reflectance spectroscopy, where the response of the photometric detector, i.e., a photomultiplier or photocell, employed is proportional to the photon flux; in the optoacoustic effect the microphone response is proportional to the optical power absorbed by the sample, i.e., radiometric detection (87) in which the detector response is proportional to both the photon flux and the individual photon energy (frequency). A photon at 200 nm can therefore result in twice as much heat energy after absorption, and therefore a proportional intermittent increase in

pressure monitored by the microphone, as a photon at 400 nm . Thus it is a power spectrum that is monitored. This effect could be advantageous in the ultraviolet region, where difficulties can arise in absorption or reflectance spectroscopy if a rapid decrease in output intensity from the continuum source occurs at wavelengths of less than 300 nm . Conversely, this effect could be disadvantageous in the infrared region.

2) It has been shown by Kreuzer (35) that for an optoacoustic spectrometer employing a laser source, the absorption of 10^{-9}W of optical power by a gaseous sample can give a signal-to-noise ratio of greater than unity in the optoacoustic signal. With a suitable continuum source and a monochromator of large aperture, used with a half-spectral bandpass of 10 nm , a power of 10^{-3}W should be obtainable for sample illumination at all wavelengths in the visible and near-ultraviolet region. The detection of materials with high absorptivities at low concentrations, or as very small samples, should therefore be possible. Alternatively, satisfactory spectra should be measurable for materials with very low absorptivities. A low absorptivity may arise as a result of the low oscillator strength of the transitions involved or as a result of the high specular reflectance of the sample surface. Thus it can be expected that the technique should permit a higher detection sensitivity for fine powders and crystalline samples than is attained in reflectance or absorption spectroscopy and that spectra should be obtained only when very small amounts of samples are available.

3) Although radiation must be absorbed by the sample in order to obtain an optoacoustic signal, there is no need to detect radiation transmitted by the sample, unlike conventional absorption spectrometry. As only absorbed energy is detected, no problems should arise from scattered source radiation, unlike reflectance spectroscopy,

as an acoustic rather than an optical transducer is employed. The difficulties encountered in diffuse reflectance spectrometry (16) owing to the variation in the relative contributions to the signal of specular and diffuse reflectance components as the particle size varies should not be observed in optoacoustic spectrometry. The disadvantage encountered with fine powders of weakly absorbing species in diffuse reflectance spectroscopy (15), that only a small diffusely reflected component appears in the spectrum owing to failure of the incident radiation to penetrate tha sample, should be offset in optoacoustic spectrometry by the ability to detect weak absorption effects and an increase in signal amplitude resulting from improved heat transfer efficiency between the sample and its gaseous environment as the particle size is reduced. For strongly absorbing powder samples, the latter effect should result in very strong optoacoustic signals for samples of very small particle size. In general, the freedom from problems with scattered light should make optoacoustic spectrometry suitable for the examination of turbid or highly scattering samples, e.g., hard and soft biological tissues.

4) For small samples, high absolute sensitivity should result without resort to the microscope illumination and viewing optics required in the examination of such samples by optical absorption or reflectance spectroscopy (88). Although the optical arrangement used to illuminate the sample is still important, owing to the need to ensure maximum energy absorption from the source, the requirement of wide solid-angle viewing of the sample by the detector should not be as important in optoacoustic spectrometry as in optical spectroscopy. In a sample cell of constant volume, it is necessary only to arrange to minimise the volume of gas in the cell in order to create the maximum pressure change for a given temperature rise, and then to

monitor this pressure change efficiently.

5) The technique should provide valuable information in the study of fluorescent or phosphorescent materials. In these instances, part of the absorbed energy is re-emitted radiatively and is not degraded into thermal energy by radiationless transitions as with most absorbing species (4). Hence, in the optoacoustic spectrometric power spectra of such materials, the absorption bands that normally give rise to fluorescence or phosphorescence will be attenuated relative to those absorption bands at which radiationless transitions are responsible for de-excitation of the excited state. The technique should therefore prove complementary to spectrofluorimetry and phosphorimetry in the study of luminescence phenomena and for quantum efficiency measurements, φ , as the complementary radiationless loss ($1 - \varphi$) is measured.

6) As the observation of optoacoustic signals for solid samples depends on the transfer to the surrounding gaseous environment of energy released after absorption of radiation, optoacoustic spectrometry may prove useful in studies of heat transfer efficiency at solid-gas interfaces and in thermal conductivity measurements.

A single-beam spectrometer was constructed to study the optoacoustic spectra of solid samples and evaluate some of the potential advantages of the technique indicated above.

3.2. Instrumentation.

A schematic diagram of the single-beam optoacoustic spectrometer assembly constructed for this work is shown in Fig. 3.2. A 1kW high-pressure, xenon-arc continuum source (Oriel Corp., Stamford, Conn., U.S.A.,Model 6269) was employed. An air-cooled housing was used for source operation. This was fitted with an ultraviolet-grade fused silica

double-element condensing lens assembly and a spherical rear reflector. This optical arrangement provided for f/1.0 collection efficiency for radiation from the arc lamp.

The source radiation was focused through the blades of a rotating chopper (Brookdeal Electronics Ltd., Bracknell, Berks., Model 9749) on to the entrance slit of a grating monochromator. The frequency of the chopper was variable between 1Hz and 100Hz with a three blade sector or 1Hz and 1kHz with a thirty blade sector; the former sector being required for stable operation at low frequencies. The chopper generated a 3.5V square-wave reference signal for the detector electronics by means of a light-emitting diode/phototransistor assembly.

A 200mm, f/4 monochromator (Metrospec, Diffraction Gratings and Optics Ltd., Chobham, Surrey) fitted with a plane grating (50 x 50 mm , 1200 lines mm^{-1}) blazed at 300nm , interchangeable slits and a wavelength scanning motor was mounted on the optical rail of the system. The reciprocal linear dispersion obtained at the exit slit of the monochromator was 4nm mm^{-1}. The slit assembly consisted of five fixed slits ruled on a single ultraviolet-transmitting quartz plate giving half-spectral bandpass values of 1, 2, 5, 10 and 20 nm. The symmetrical Czerny-Turner optical configuration (73) permitted four possible arrangements for entrance and exit beams, either in-line, parallel or at right angles, by the use of interchangeable mirror and slit mounts. The radiation emerging from the exit slit was refocused by using a front-surfaced concave mirror (50mm in diameter, 200mm focal length) and directed into the optoacoustic cell.

The cell (Fig. 3.4) was constructed from stainless steel and had an internal volume of about $5cm^3$. An entrance window was provided by use of a silica disc (25mm in diameter and 2mm thick)

Fig. 3.2 Schematic diagram of the single-beam optoacoustic spectrometer.

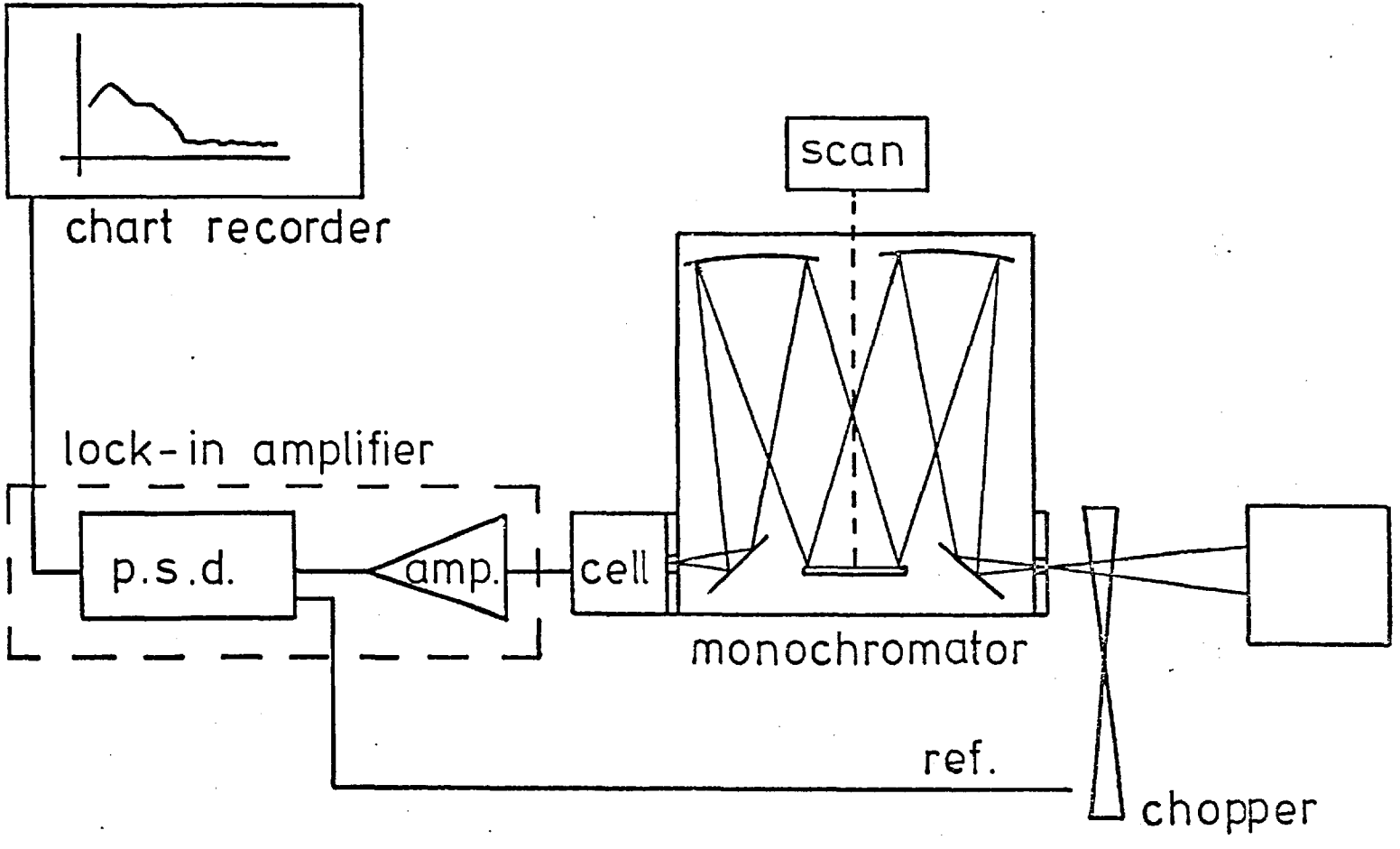

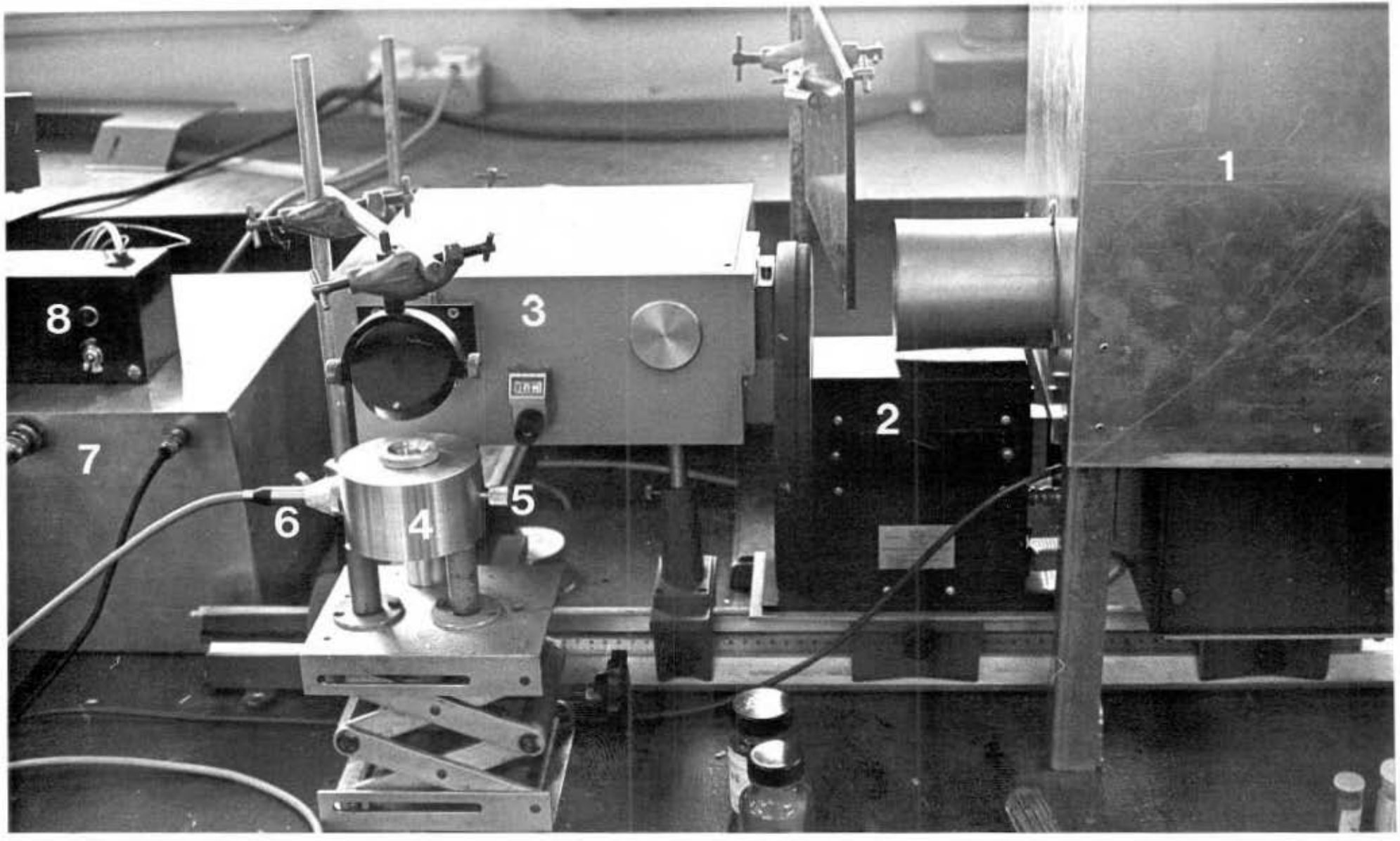

Fig. 3.3

Key to Fig. 3.3

1. Xenon arc source enclosed in a housing providing for ozone extraction.
2. Variable-speed rotating sector.
3. Monochromator.
4. Optoacoustic cell.
5. Pressure release valve.
6. Microphone preamplifier.
7. Power supply for microphone transducer.
8. Control unit for wavelength scanning motor.

Fig. 3.4 The Optoacoustic Cell.

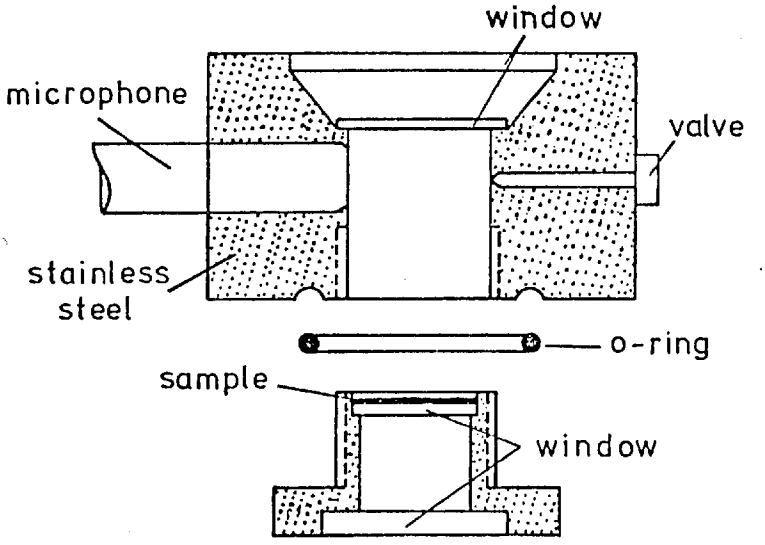

mounted on the cell with epoxy resin. The sample plate was also a similar silica disc (20mm in diameter and 1mm thick) sealed into a threaded stainless steel tube. This sample unit could be screwed into the cell, against a rubber O-ring, to form a pressure-tight system. The optoacoustic signal was monitored by using a $\frac{1}{2}$in diameter capacitor microphone as a transducer (Type 4166, Bruel and Kjaer Ltd., Hounslow, Middlesex.) and positioning it in the cell adjacent to the sample tray and entrance window. In order to prevent damage to the microphone diaphragm when inserting the sample unit, and to allow gases other than air to be admitted to the cell if required, a pressure release valve was provided opposite to the microphone diaphragm. The microphone was sealed into the cell so that the diaphragm formed part of the cell wall. The polarisation voltage to the microphone was provided by a 200V dry-cell power supply, the associated preamplifier being powered from a 28V tapping from the same supply. The microphone had a rated sensitivity of $5mV\mu bar^{-1}$ at this polarisation voltage. The internal cell walls were polished to reduce background absorption and stainless steel was employed in order to provide low thermal conductivity.

The optoacoustic signal from the microphone transducer was taken directly to a sensitive lock-in amplifier (Princeton Applied Research Corp., Princeton, New Jersey, U.S.A., Model 186) which utilised the reference signal generated at the variable-speed chopper to extract the signal waveform and present this as a DC potential to a potentiometric chart recorder (Servoscribe, Model RE511, Smiths Industries Ltd.). Optoacoustic spectra were then obtained by recording the output of the lock-in amplifier versus the wavelengths of the incident radiation at the sample cell during wavelength scanning of the monochromator.

3.3. A Simple Theoretical Model for the Prediction of the Magnitude of Optoacoustic Signals.

The optoacoustic effect can be observed only after the absorption of radiation by the sample. For a simple system, for example, a single absorbing particle or thin absorbing layer of homogeneous composition, the power absorbed can readily be calculated from the classical relationships that govern the absorption of electromagnetic radiation by matter. In order to obtain an estimate of the optoacoustic signal power, it is then necessary to quantify the fraction of this absorbed radiation that is lost by the excited state in its return to the ground state by radiationless transitions. Thus,

$$\begin{array}{c}\text{Optoacoustic signal} \\ \text{power}\end{array} = \begin{array}{c}\text{Power absorbed} \\ \text{from source}\end{array} \times \begin{array}{c}\text{Efficiency of} \\ \text{radiationless conversion}\end{array}$$

For a simple absorbing layer of thickness l of a species of molar absorptivity ϵ and concentration c in the sample matrix, the power absorbed at wavelength λ, $P_{abs\lambda}$, is given by the Beer-Lambert law as

$$\begin{aligned} P_{abs\,\lambda} &= \left[P_{o\,\lambda} - P_{o\,\lambda} \exp\left(-2.3\,\epsilon_{\lambda} c\, l\right)\right] \\ &= \left[P_{o\,\lambda}\left(1 - \exp\left(-2.3\,\epsilon_{\lambda} c\, l\right)\right)\right] \end{aligned} \qquad \ldots 3.1$$

where $P_{o\,\lambda}$ is the power of the incident radiation at wavelength λ.

The optoacoustic signal power, $P_{oas\,\lambda}$, is then obtained by multiplying $P_{abs\,\lambda}$ by an efficiency factor, β, which is a measure of the conversion efficiency of absorbed power to heat by radiationless processes, i.e.,

$$P_{oas\,\lambda} = \left[P_{o\,\lambda}\left(1 - \exp\left(-2.3\,\epsilon\, c\, l\right)\right)\right] \beta \qquad \ldots 3.2$$

For low absorption conditions, where the power absorbed is small, the higher terms in the expansion of $1 - \exp\left(-2.3\,\epsilon\, c\, l\right)$ can be

neglected, and so equation 3.2 can be written as

$$P_{oas\,\lambda} = P_{o\lambda}(2.3\,\epsilon c\,l)\,\beta \qquad \ldots 3.3$$

From this expression, it is evident that the optoacoustic signal under ideal conditions is directly proportional to the available power of the source at a given wavelength, the molar absorptivity of the absorbing species at this wavelength (ϵ) and the concentration, path length and power conversion efficiency.

It can be seen that if the optoacoustic signal is plotted against wavelength for an excitation source, the output power of which does not vary with wavelength, the spectrum obtained will give a direct measure of the variation of ϵ with wavelength, i.e., the absorption spectrum will be obtained.

It is also apparent from Equation 3.3 that for weakly absorbing species the amplitude of the optoacoustic signal will be directly proportional to the concentration of the absorbing species, so that linear calibration graphs can be expected. In addition, the direct proportionality between $P_{oas\,\lambda}$ and the absorption path length, l, will affect the manner in which the amplitude of the signal varies for strong and weakly absorbing species with sample thickness or particle size, for powdered samples.

For absorbing species that luminesce by fluorescence or phosphorescence, where a fraction of the absorbed energy is lost by radiative transitions rather than radiationless internal conversion and collisions, the optoacoustic signal power expected may be written as

$$P_{oas\,\lambda} = P_{o\,\lambda}(2.3\,\epsilon c\,l)\,(1-\varphi) \qquad \ldots 3.4$$

where φ is the luminescence quantum efficiency, which is complementary to β .

In a real experimental system, a number of factors relating to the instrument arrangement employed and to the characteristics of the sample will lead to modification of the ideal expression of Equation 3.3. Thus, for the continuum source used in optoacoustic spectrometry, the power incident upon the sample, $P_{o\lambda}$, is given by

$$P_{o\lambda} = I_{o\lambda} w H T_{\lambda} s \Omega/4\pi \quad \ldots 3.5$$

where $I_{o\lambda}$ (W cm^{-2} mm^{-1}) is the spectral irradiance of the source, w (cm) is the monochromator slit width, H is the slit height, s (nm) is the spectral band width employed, T is the transmittance of the monochromator at wavelength λ and Ω (sr) is the solid angle for sample illumination available from the particular source and monochromator assembly (5).

Thus the optoacoustic signal power becomes

$$P_{oas} = I_{o\lambda} w H T_{\lambda} s \frac{\Omega}{4} (2.3 \varepsilon c l)\beta \quad \ldots 3.6$$

In contrast to fluorescence or reflectance spectroscopy, in which the re-emitted or reflected optical power received at the radiation detector is further dependent on the optical viewing geometry (solid angle), in optoacoustic spectrometry, in the ideal case, all of the absorbed power that appears as kinetic energy after radiationless de-excitation is available to cause an increase in pressure in the cell and to generate the optoacoustic signal at the microphone transducer. In practice, however, a power transfer efficiency from sample to transducer of unity is difficult to achieve owing to loss of energy at the cell walls. For a real experimental system, therefore, it is necessary to introduce an additional power transfer efficiency factor into Equation 3.6 in order to account for this loss and for any loss in efficiency at the transducer.

For solid samples, the optoacoustic signal power may be expected to vary with particle size, for two reasons:

a) when the particle size (or surface area) varies, the power absorbed will vary owing to changes in the reflectivity of the sample (15).

b) as the particle size (surface area) varies, the efficiency of power transfer to the surrounding gas may vary.

The power transfer at the solid-gas interface may also be influenced by the thermal conductivity of the sample and the filler gas; this would then also be expected to affect the manner in which the observed optoacoustic signal varies with sample characteristics. The amplitude of the signal would also be expected to be inversely proportional to the heat capacity of the filler gas.

The initial studies undertaken on optoacoustic spectrometry were concerned with an investigation of the predicted variation in optoacoustic signal strength with the sample and instrument characteristics outlined above.

3.4. Results and Discussion.

In order to evaluate the performance characteristics of the optoacoustic spectrometer, and the fundamental instrument and sample parameters that govern the analytical application of the optoacoustic effect to solid samples, it was necessary initially to choose a standard sample of well defined absorption characteristics. Carbon black (granular charcoal; Hopkin and Williams, Chadwell Heath, Essex.) was chosen for this purpose, as it is readily obtainable, can be employed as a black-body reference absorber of constant absorptivity throughout the ultraviolet-visible regions and is a strong absorber for which optoacoustic signals are readily obtainable. This material was used to demonstrate the relationships between the optoacoustic signals obtained and the instrument and sample parameters.

Fig. 3.5

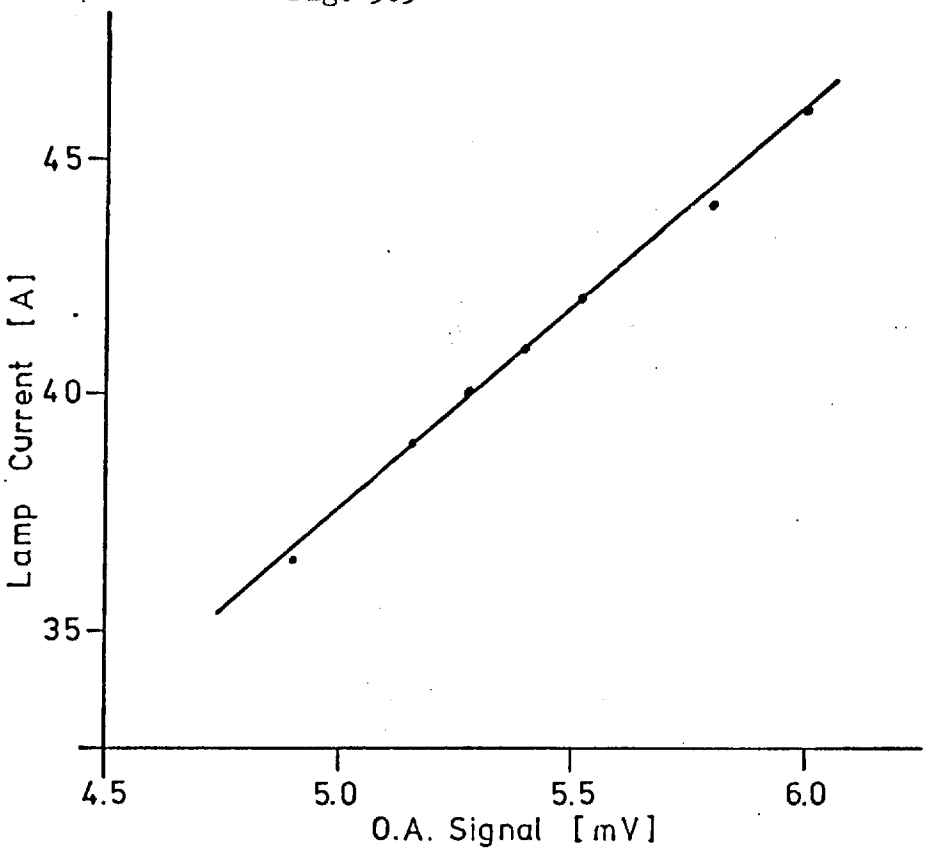
45
40
35
Lamp Current [A]
4.5
5.0
5.5
6.0
O.A. Signal [mV]

Fig. 3.6

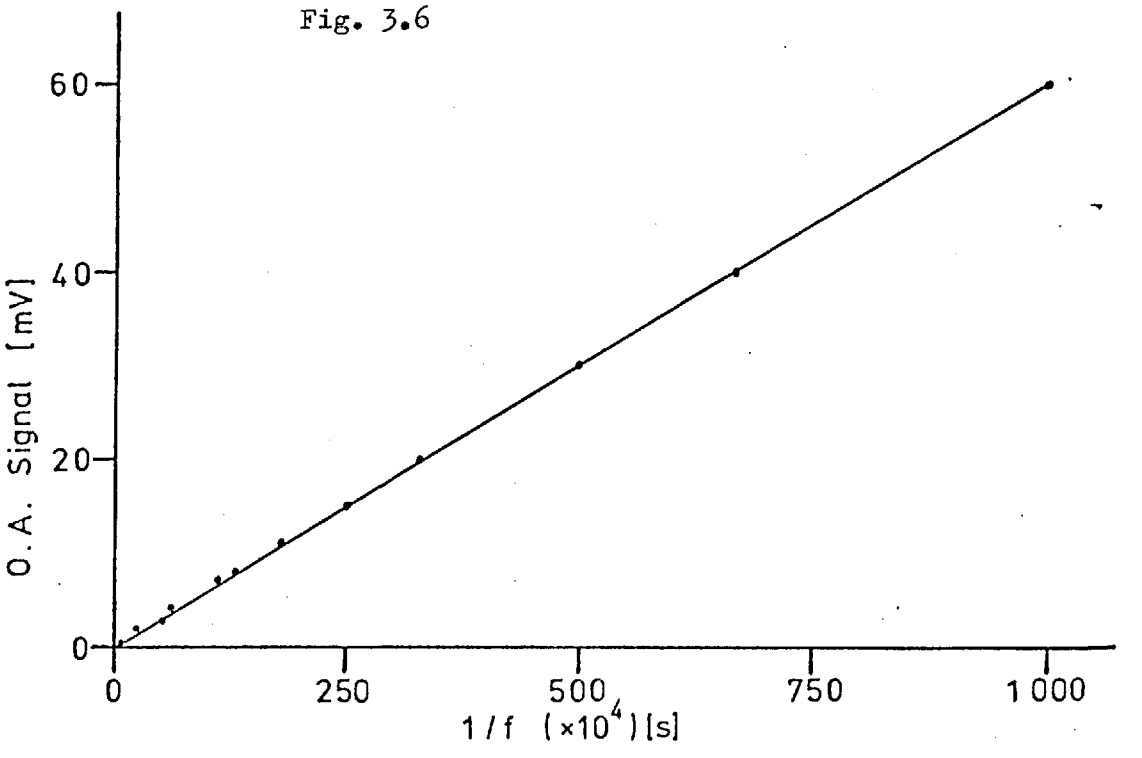
60
40
20
0
O.A. Signal [mV]
0
250
500
750
1 000
1 / f (×10⁴) [s]

3.4.1. Effect of Source Power and Modulation Frequency.

The predicted proportionality between the amplitude of the optoacoustic (O.A.) signal and the incident source power was readily confirmed using a carbon black sample by varying the operating current of a constant voltage supply to the xenon source. The results illustrated in Fig. 3.5 were obtained utilising a modulation frequency of 75Hz and 'white-light' illumination, i.e., by operation of the monochromator grating in the zero order mode.

The variation of the amplitude of the optoacoustic signal with the source modulation frequency was studied for carbon black, of particle size less than 76μm, for white-light illumination over the frequency range 10Hz - 1kHz. The variation of the optoacoustic signal amplitude with modulation frequency was an inverse proportionality as expected. Thus a graph of the signal amplitude versus the reciprocal of the frequency is linear (Fig. 3.6). This relationship follows from the direct proportionality obtained between signal amplitude and source power. Thus, as the modulation frequency increases, the power per pulse available for absorption by the sample decreases. All further studies reported in this chapter were conducted at modulation frequencies of less than 200Hz in order to maintain an adequate signal amplitude and to optimise the signal-to-noise ratio.

3.4.2. Effect of Nature of Filler Gas Used in Sample Cell.

As optoacoustic signals for solid samples are obtained indirectly by monitoring the periodic pressure change in the gaseous environment surrounding the sample in the constant-volume cell, it might be expected that the amplitude of the optoacoustic signals observed would depend on the physical properties of the gas in the sample cell. The particular properties of interest are the heat

Table 3.I

CELL FILLER GAS	SIGNAL AMPLITUDE (rms mV)
Helium	28.4
Argon	25.0
Nitrogen	21.2
Carbon Dioxide	17.5

Table 3.II (89)

GAS	C_v ($JK^{-1} mol^{-1}$)	k ($W m^{-1}K^{-1}$)
Helium	12.48	0.150
Argon	12.58	0.017
Nitrogen	20.70	0.025
Carbon Dioxide	28.27	0.016

capacity of the filler gas at constant volume (C_v) and its thermal conductivity. The effect of using different filler gases on the optoacoustic signal amplitude for carbon black with white-light illumination was therefore investigated. The results presented in Table 3.I were obtained for a carbon black sample in a closed sample cell that contained helium, argon, nitrogen or carbon dioxide at atmospheric pressure. The corresponding heat capacity and thermal conductivity values for these gases are shown in Table 3.II. It might be expected that the use of a filler gas of high thermal conductivity would lead to efficient heat transfer at the sample-gas interface and that this would be beneficial to the amplitude of the optoacoustic signal but that correspondingly greater energy losses to the cell walls might then offset this effect. At the low source modulation frequencies employed in this work, the results obtained indicate that the rate of heat transfer at the sample-gas interface does not limit the amplitude of the optoacoustic signal observed; with the stainless-steel cell employed, no relationship is observed between the thermal conductivity of the filler gas and the amplitude of the signals obtained. However, an apparent correlation can be seen between the heat capacity of the filler gas and the optoacoustic signal amplitude; as the heat capacity of the gas increases, the amplitude of the optoacoustic signal decreases. This results from the fact that, under otherwise constant conditions, the energy absorbed by the sample can produce only a small change in temperature and pressure (and therefore a small signal amplitude) in the constant volume of gas in the cell when a gas of large heat capacity is employed. It is apparent that no significant practical advantage or significantly higher sensitivity would accrue from the use of filler gases other than air with the sample cell and detector assembly used in this work. However, for air or water sensitive samples

Fig. 3.7 Carbon

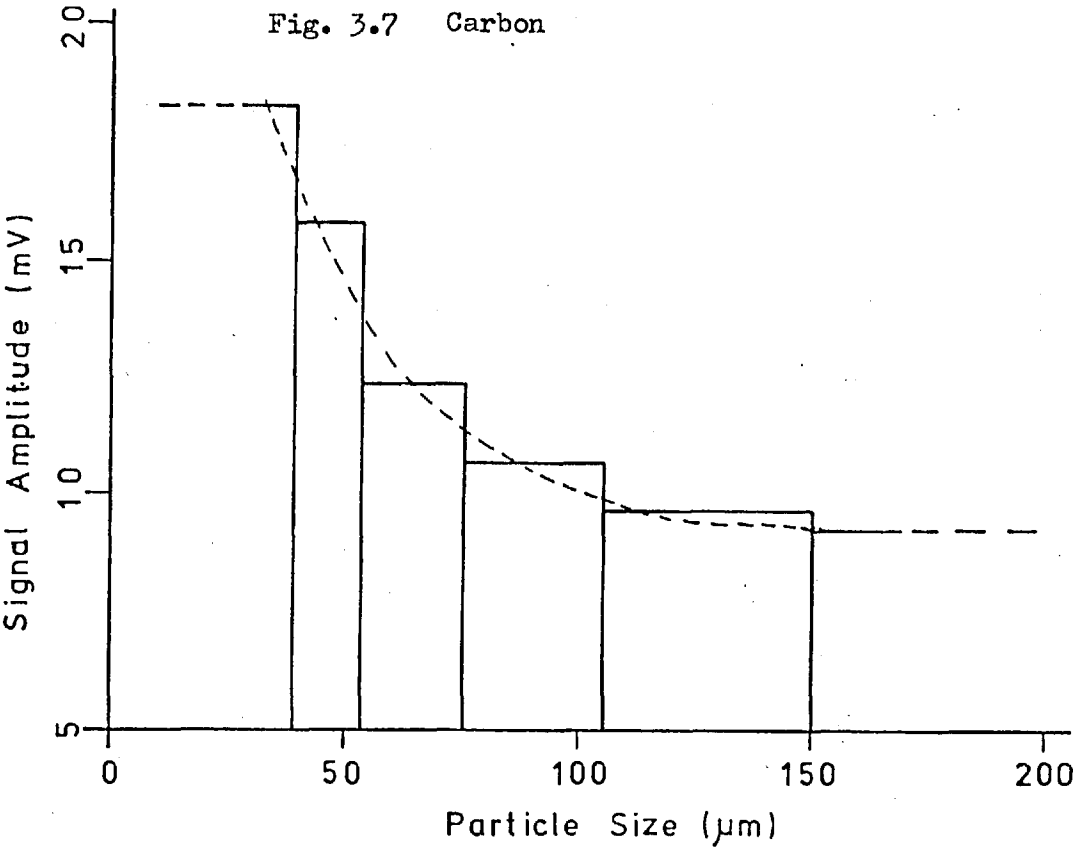

Fig. 3.8 Copper(II)Sulphate

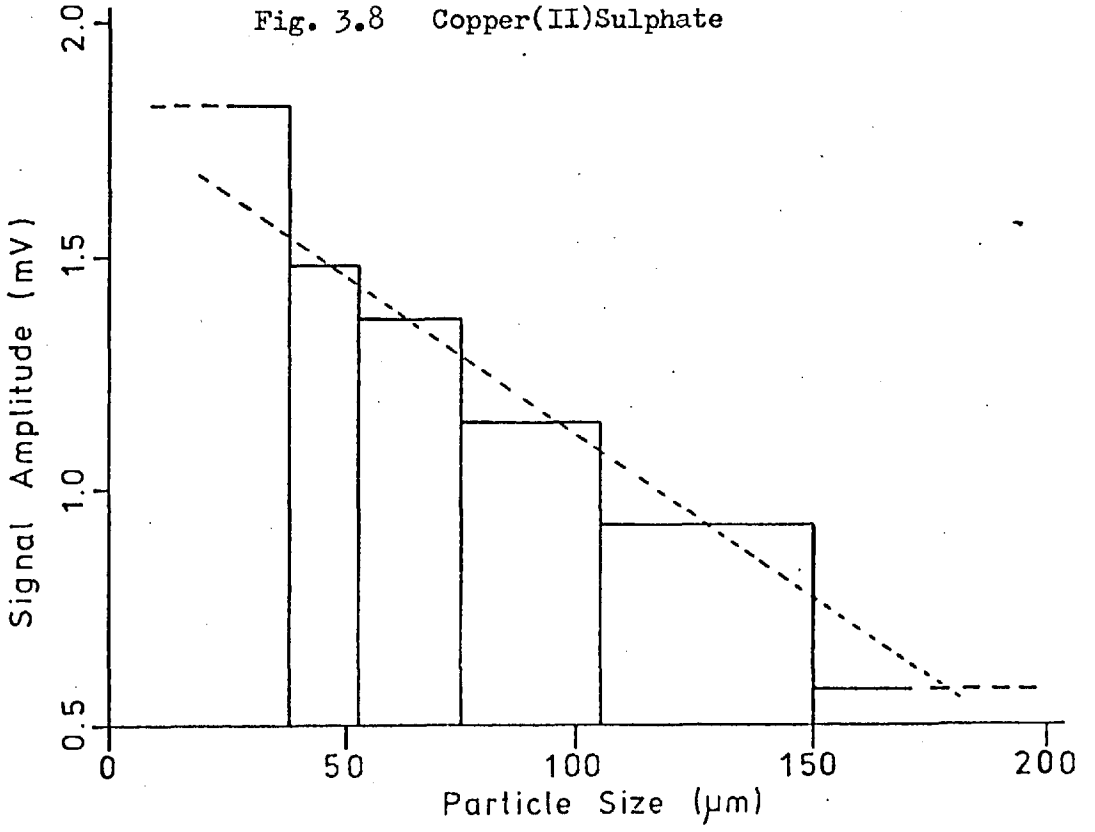

inert filler gases may be employed.

3.4.3. Effect of Particle Size of Sample.

The effect of the particle size of the sample for a strongly absorbing material was investigated, utilising samples of carbon black and a source modulation frequency of 75Hz for white-light illumination of the sample. Fig. 3.7 shows the signal amplitudes measured for a series of particle size ranges obtained with a set of standard test sieves. It is clear that the amplitude of the optoacoustic signal increases as the particle size of the sample decreases. This effect is not a mass effect, as the sample mass increases as the particle size increases. As the surface area increases, the power absorbed, which alone gives rise to the optoacoustic signal, thus also increases. The implication is that as the particle size decreases the absorbed power increases, owing to an increase in the mean effective absorbing path length (l in Equation 3.3). The power transfer efficiency at the solid-gas interface increases also as the particle size decreases.

The variation of the amplitude of the optoacoustic signal with particle size was also investigated for a weakly absorbing species. Crystalline hydrated copper(II)sulphate was employed in these experiments using the same particle size ranges as those of the carbon black samples. Fig. 3.8 shows the signal amplitudes obtained for these samples under the same experimental conditions used for the carbon black. The signal amplitude is again seen to increase as the particle size decreases, although the effect observed is not as pronounced as with carbon black.

It is apparent that for powdered samples, control of particle size will be important in quantitative applications of optoacoustic spectrometry. The effect on the analytical signal of variation in particle size, however, is less complex than that encountered in diffuse

reflectance spectroscopy (16). In the latter technique it has commonly been observed that either an increase or decrease in the magnitude of the observed reflectance at different wavelengths may be obtained, depending on whether the sample is a weak or strong absorber. The complicating factor is that both the diffuse reflectance component of the measured intensity and the specular reflectance component may vary independently with particle size and the molecular absorptivity for the species studied at different wavelengths; the measured reflectance, however, indicates only the observed net effect for both of these components. Thus the effect of particle size and sample absorptivity in optoacoustic spectrometry is fundamentally simpler to interpret owing to the fact that it is only the portion of the incident radiation that is absorbed that gives rise to the optoacoustic signal; no complications arise from the specular reflected radiation, which is not measured.

3.4.4. Effect of Amount of Sample and Concentration of the Absorbing Species.

The variation of signal amplitude with the sample size has been investigated (86) for a carbon black sample of particle size less than 76μm. The carbon powder was spread uniformly on to a 7mm diameter disc of double-sided clear adhesive tape. The mass of the sample was determined by weighing the adhesive tape with and without the powder sample. The optoacoustic signal was measured for this sample and for successively decreased masses of sample obtained by removing sections of the 7mm disc of tape and re-weighing. A linear relationship was obtained for the variation in signal amplitude with sample mass; as the sample mass and surface area decrease, the power absorbed from the incident beam of radiation becomes less so that the optoacoustic

signal amplitude is decreased. The minimum detectable mass of sample for carbon black, based on an estimation of the signal-to-noise ratio observed for the small background signal produced by the cell, was about 10μg. The effect of the concentration of the absorbing species has been investigated (85) for a strong absorber using milligram samples of mixtures of carbon black in magnesium oxide of particle size less than 76μm. A graph of the amplitude of the optoacoustic signal versus the concentration of carbon black in magnesium oxide, covering the range 0 - 100%, was linear at low concentrations, but deviated towards the concentration axis at high concentrations.

A further study of this concentration effect was made using undispersed radiation at a modulation frequency of 75Hz. For a mixture of carbon black of particle sizes in the range 45 - 53μm in unsieved magnesium oxide (A.R., Fisons, Loughborough, Leics.), a curved calibration graph was obtained (Fig. 3.9a). A microscopic examination (x220) of these samples revealed that the average particle size of the magnesium oxide was much larger than that of the carbon; the carbon particles being embedded in the larger magnesium oxide particles. The initial part of the calibration graph of Fig. 3.9a, therefore corresponds to carbon particles coating the magnesium oxide particles until saturation is reached. The latter part of the graph then corresponds to an increase in the mass of carbon black, producing a corresponding increase in the surface area of the absorbing species. A sieve analysis (Fig. 3.10), i.e., percentage weight composition versus particle size, of the magnesium oxide, showed that it consisted of a range of particle sizes distributed evenly about ca. 90μm.

The calibration graph for a mixture of carbon black of particle sizes in the range 150 - 250μm in unsieved magnesium oxide (Fig. 3.9b) further demonstrated this effect. Although the graph showed

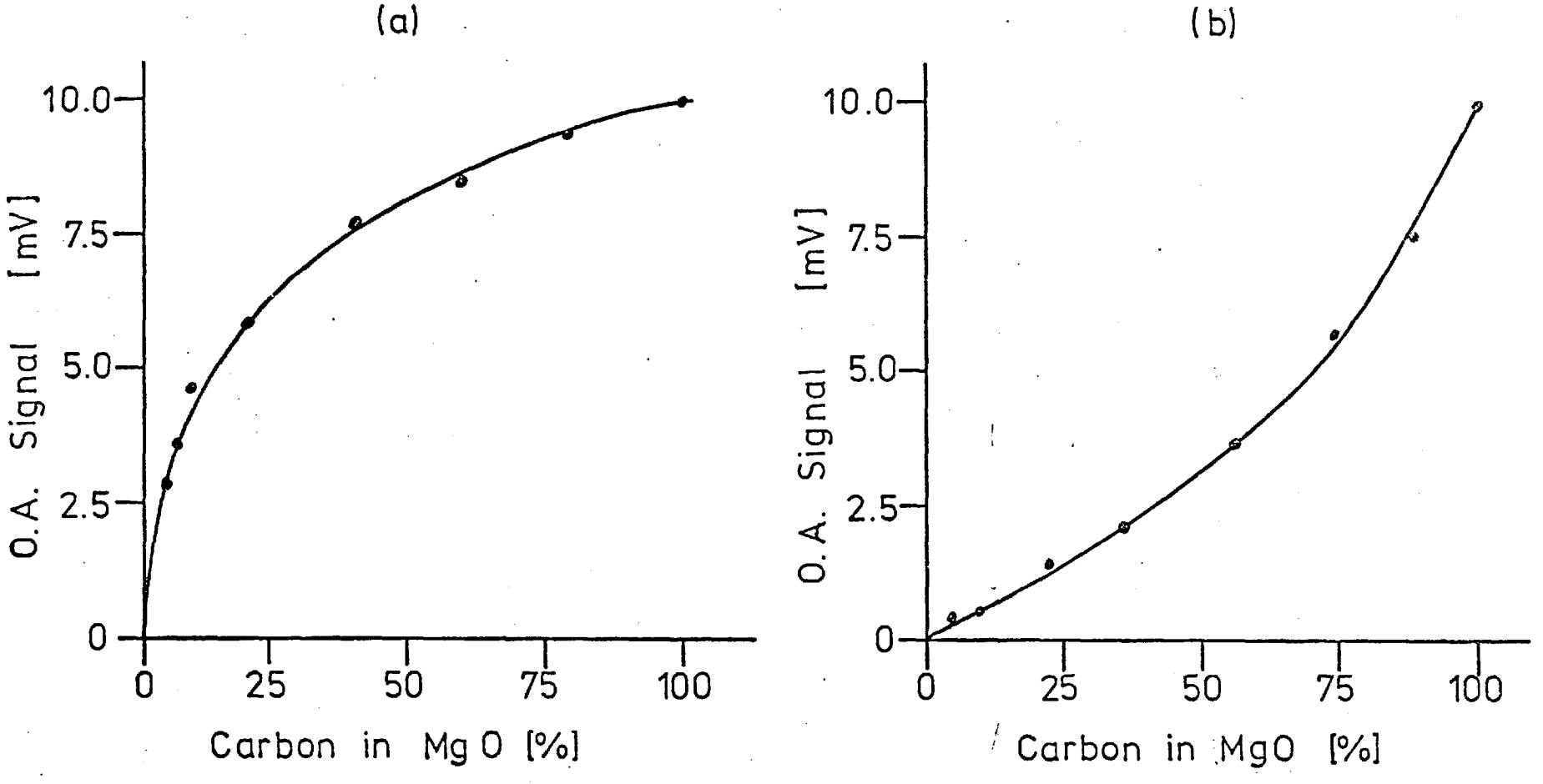
(a)
10.0
7.5
5.0
2.5
0
O.A. Signal [mV]
0
25
50
75
100
Carbon in Mg O [%]
(b)
10.0
7.5
5.0
2.5
0
O.A. Signal [mV]
0
25
50
75
100
Carbon in MgO [%]

Fig. 3.9

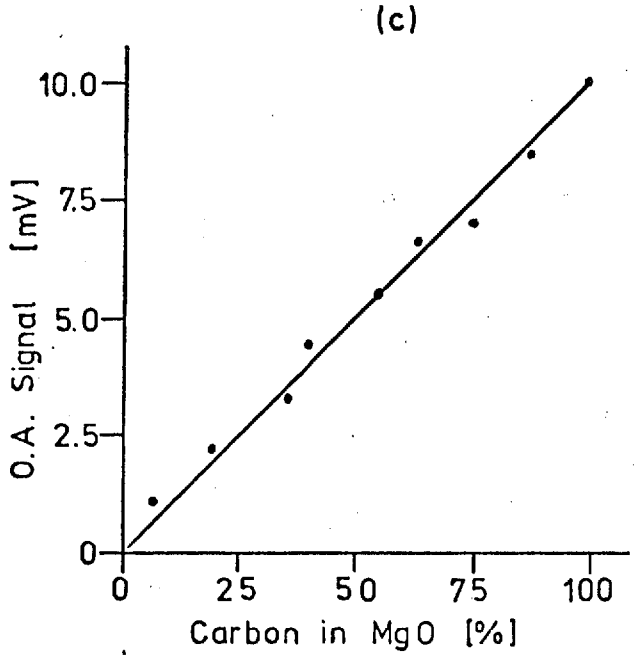

Fig. 3.9

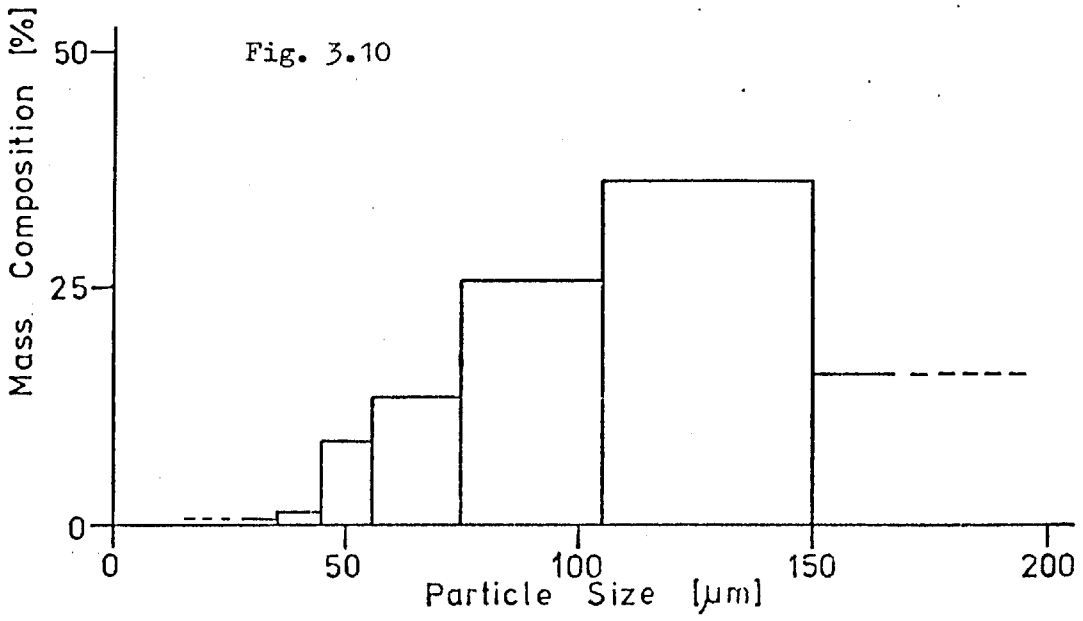

Fig. 3.10

greater linearity, an increase in slope was observed for higher concentrations of carbon. A microscopic examination of these samples confirmed that at low carbon concentrations the carbon particles were being coated by magnesium oxide. The most linear calibration graph (Fig. 3.9c) was obtained when the particle size of the carbon and magnesium oxide were closely matched; both were sieved to give a particle size range of 150 - 250μm. In this case, an homogeneous mixture means that the only effect observed is that of increasing concentration of the absorbing species.

3.5. Ultraviolet and Visible Optoacoustic Spectra.

3.5.1. Optoacoustic Spectrum of Carbon Black.

It has been shown (51,86) that the optoacoustic spectrum of carbon black is identical to the power spectrum of the source employed, measured with a thermocouple detector. The optoacoustic spectrum of particulate carbon black (<76μm) obtained with a 1kW xenon source and a spectral band pass of 10nm is shown in Fig. 3.11. The radiation incident upon the sample was modulated at a frequency of 75Hz. The carbon black is thus suitable for use as a reference absorption material, whose optoacoustic spectrum can be used to correct the observed spectra of other samples for the variation of source power with wavelength. This correction procedure for the optoacoustic spectra can be effected either manually, as with the spectra described in this chapter with the single-beam spectrometer, or automatically in a double-beam spectrometer in which the carbon black absorber is incorporated into the reference beam.

3.5.2. Preliminary Optoacoustic Spectra.

It has been demonstrated (85) that 'real' spectra are obtained by optoacoustic spectrometry, which give information relating to the

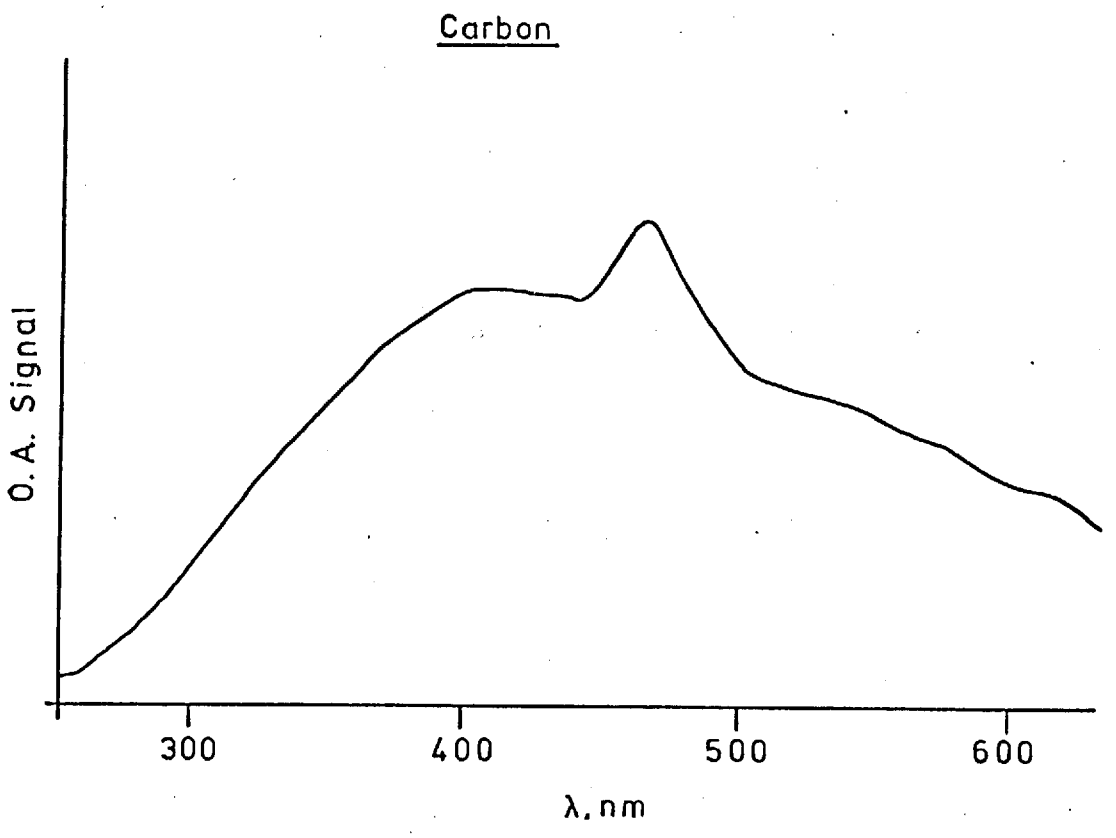

Fig. 3.11

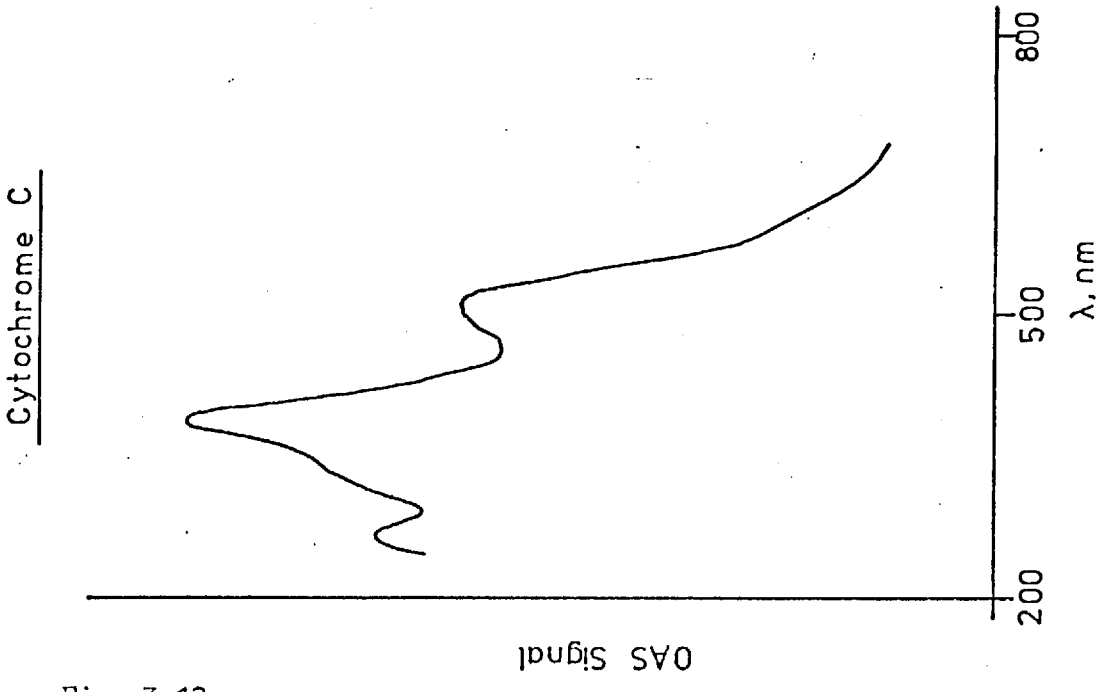

Fig. 3.12

molecular absorption characteristics of samples. The spectra were manually corrected for variation in output power of the source with wavelength using the optoacoustic spectrum of carbon black as reference. The optoacoustic spectra of samples of highly reflecting blue and red artists' gummed paper were measured and compared with the corresponding reflectance spectra. These were clearly identical. Although the highly reflecting nature of the paper gave rise to relatively weak absorption, and some degradation in the signal-to-noise ratio was observed in the reflectance spectra, the optoacoustic signal for these samples was readily measured. The optoacoustic spectrum of a 1 + 9 (m/m) mixture of cadmium sulphide and magnesium oxide was also measured (85,86). Cadmium sulphide is a direct-band semiconductor whose band edge occurs at 2.4 eV (90). The band edge measured from the optoacoustic spectrum occured at 500nm, which corresponds to 2.48 eV ; this value was thus in fair agreement with the literature and with a previous value obtained by optoacoustic spectrometry by Rosencwaig (91). The sample size taken for the optoacoustic measurements was 1mg, whereas the attachment for the spectrophotometer employed to obtain the reflectance spectrometer required a sample size of about 750mg.

The samples, the characterisation and determination of which by optoacoustic spectrometry has been examined in the work presented in this chapter, can be classified as being biochemical, inorganic, or phytochemical in origin. The optoacoustic spectra of all types of sample were determined in the wavelength region 250 - 700nm and normalised manually by reference to a carbon black (less than 76μm particle size) spectrum obtained on the same day. Unless otherwise stated, all the spectra were obtained using a monochromator half-spectral band pass of 10nm. Solution spectrometric studies were conducted by using a Perkin - Elmer, Model 124, double-beam spectrophotometer with a half-spectral

band pass of 2nm.

3.5.3. Optoacoustic Spectrometric Studies with Biochemical Samples.

The biochemical samples examined by use of optoacoustic spectrometry were all haemoproteins; iron porphyrins. The samples were chosen because of their importance in biochemical systems and their characteristic ultraviolet and visible region absorption spectra (92, 93). In neutral or alkaline solutions, metal-free porphyrins show intense absorption at about 400nm (the Soret or γ band) and four weaker absorption bands extending into the visible region of the spectrum. These four bands appear to be connected with the two free charges in tautomeric equilibrium on the pyrrole nitrogen atoms and protonation of the porphyrin or complexation with a positive ion reduces the four bands to two, the α and β bands. The Soret band is always present in haemoprotein spectra and is very intense; it is attributed to an allowed $\pi - \pi^*$ transition in a region remote from the metal atom. The α band (550 - 610nm) and the β band (520 - 550nm) are due to electronic transitions associated with charge-transfer interaction of metal orbitals with ligand states.

The optoacoustic spectra of the biochemical compounds, cytochrome c , peroxidase and catalase, clearly show these spectral features (Figs. 3.12 - 3.14). The cytochrome C and peroxidase (0.1mg samples) were examined as fine powders (C.F.Boehringer and Soehne GmbH,, Maanheim, Germany). The catalase sample was obtained as a 2% suspension of the crystalline catalase in aqueous ammonium sulphate solution (Boehringer and Soehne). A 20μl aliquot of this suspension was applied to the silica sample plate, dried in air and then examined. The optoacoustic spectra observed from these species in the wavelength region 250 - 700nm are shown in Figs. 3.12 - 3.14. These spectra agree well with the reported spectra of these extracts (92). The solution spectra

Fig. 3.14

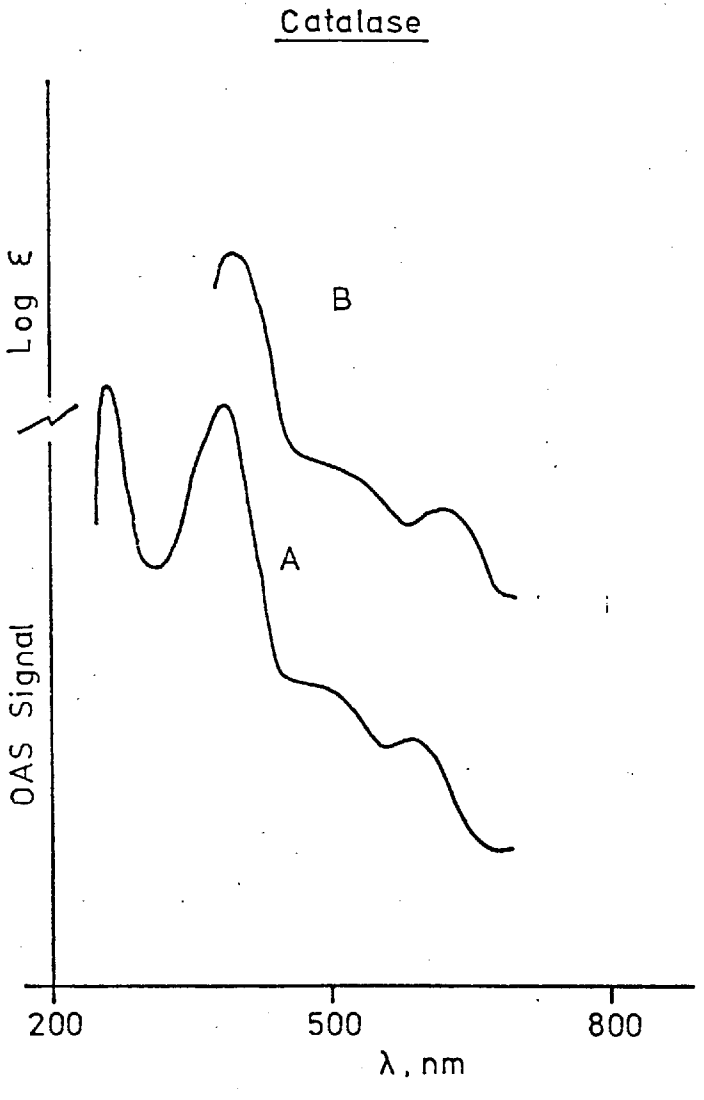

Fig. 3.13

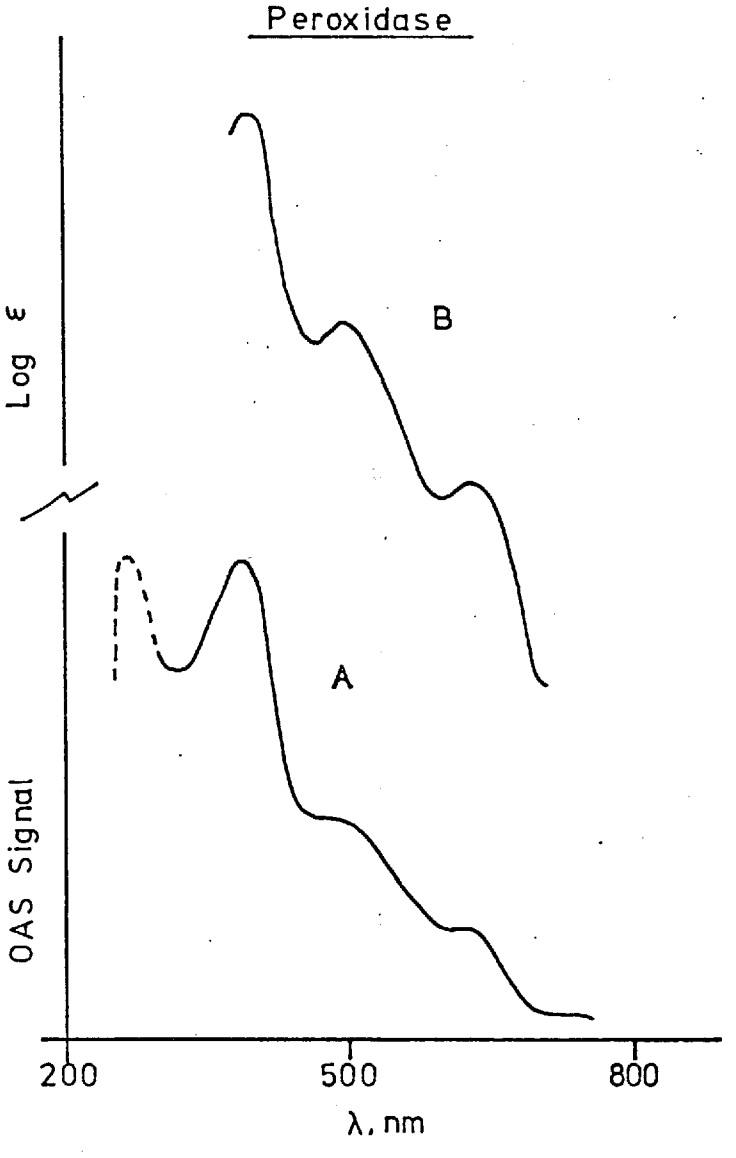

are shown for comparison with the optoacoustic spectra of catalase and peroxidase. Where comparisons are possible, these optoacoustic spectra agree with those reported by Rosencwaig (94). The simple sample preparation and the ability to examine microlitre samples without the need for refined sample handling, sample destruction and dissolution or microscopic illumination and viewing techniques should make optoacoustic spectrometry a valuable tool for the study of samples of biochemical origin.

3.5.4. Optoacoustic Spectrometric Studies Using Inorganic Samples.

Many inorganic species for which an analysis or identification is required may only be available in small amounts and solvent-solute interaction can cause large changes in the solution spectrum of the species to be identified. In such instances the spectra are obtained in a variety of solvents (93). In order to illustrate the advantages of optoacoustic spectrometry with such samples the spectra of several organometallic compounds have been examined. In all instances the optoacoustic spectra were obtained with less than 0.1mg of the solid sample and agree well with the corresponding electronic absorption spectra obtained in solution. Figs. 3.15A and 3.15B show the optoacoustic spectra obtained for ferrocene and nickelocene, respectively. The samples were in the form of fine crystalline powders. A comprehensive investigation of the electronic spectroscopy and a theoretical treatment of the spectra for these species has been undertaken by Scott and Becker (95).

Air — or water — sensitive compounds are frequently encountered in inorganic chemistry and for such unstable materials solution absorption spectrometry and conventional reflectance spectrometry may not provide the spectral data required for an identification. Because of the sealed, constant-volume optoacoustic cell employed in this work these compounds

Fig. 3.15 A, Ferrocene
B, Nickelocene

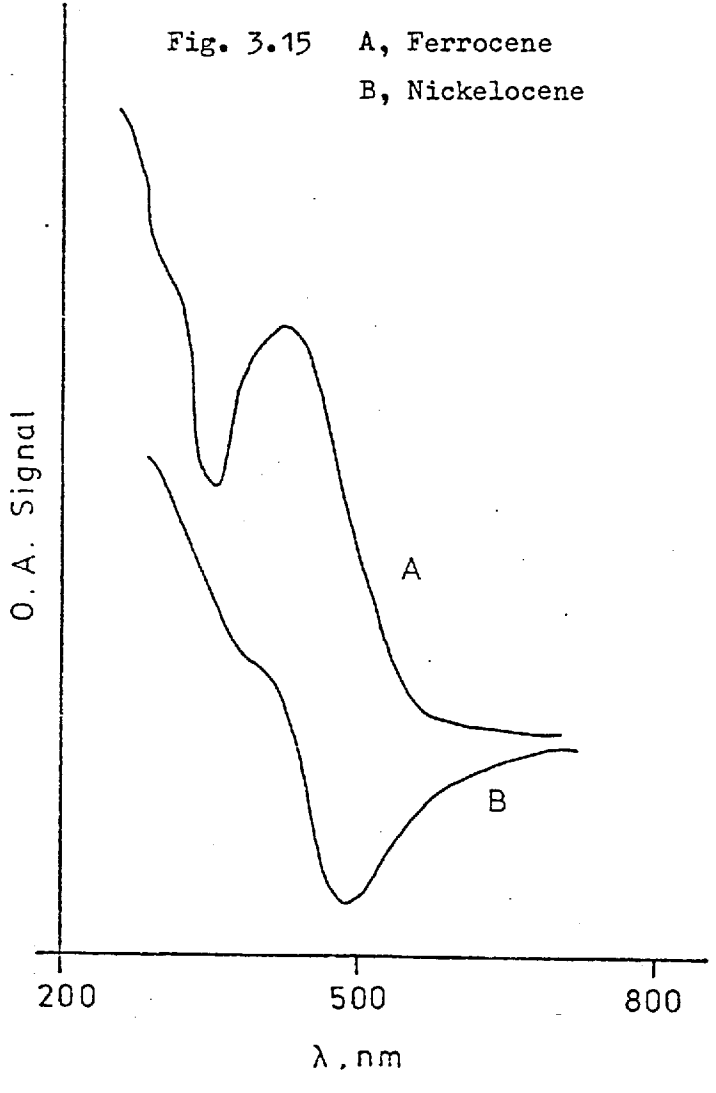

Fig. 3.16 Potassium Peroxochromate

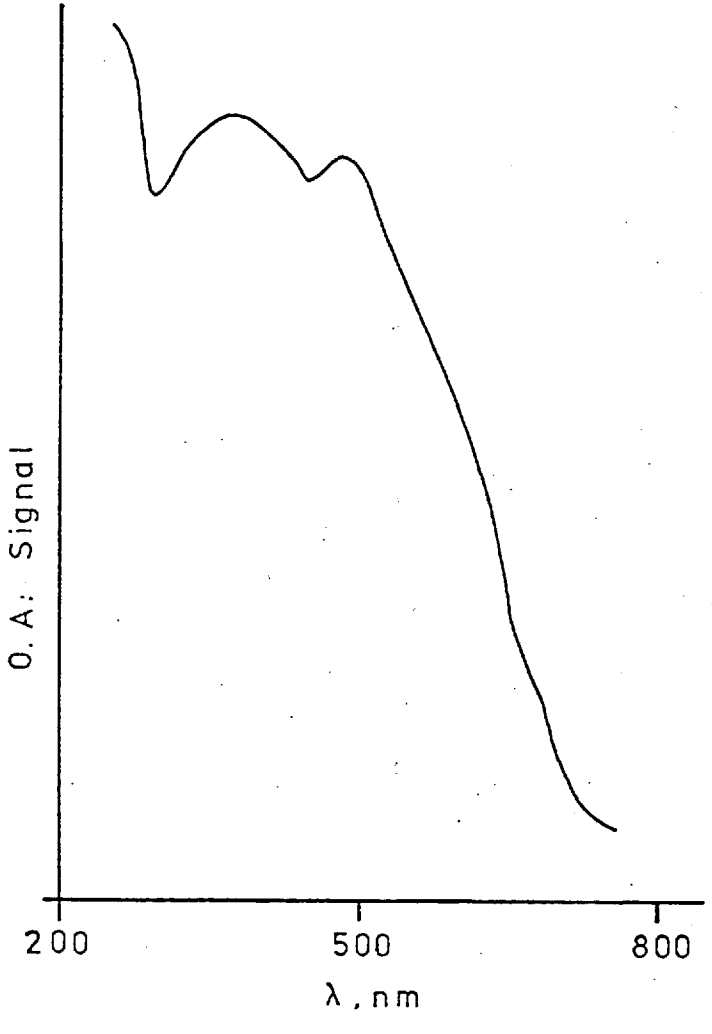

can be examined in an inert atmosphere without decomposition or purging of the optical path. Potassium peroxochromate is water—sensitive and in solution, at room temperature, readily decomposes to the chromate. It was prepared by the oxidation of a solution of chromium(IV)oxide in aqueous potassium hydroxide using an excess of 20-volume hydrogen peroxide, as described by Brauer (96). The resulting solution was filtered in a glove box under an atmosphere of dry nitrogen and the residue washed with 95% ethanol until the washings were colourless. The red crystalline potassium peroxochromate obtained was then dried under nitrogen and mounted in the optoacoustic cell without further treatment. The sample cell therefore was operated with a nitrogen atmosphere. For a solution of this salt in cold hydrogen peroxide McGarvey (97) observed a broad absorption band at about 500nm and Swalen and Ibers (98) reported the presence of two absorption peaks at 592 and 555nm. Employing reflectance spectroscopy, Anysas and Companion (99) examined the solid-state spectrum of crystalline potassium peroxochromate and identified absorption maxima at 248, 370 and 490nm, and a weak absorption shoulder at 620nm. The optoacoustic spectrum of potassium peroxochromate is shown in Fig. 3.16, although with this instrument assembly and using a spectral band pass of 10nm the weak shoulder is not apparent; however, the absorption peaks at 370 and 490nm are resolved.

3.5.5. Optoacoustic Spectrometric Studies with Phytochemical Samples.

In recent years the analysis of plant tissue has become a developing and distinct field of research and several texts have been devoted to phytochemical methods of analysis (100). Because of the complexity of plant tissue, separation techniques have been widely used in order to permit identification of the constituents present. Many of the compounds present in the sample are relatively major analytes, e.g., chlorophylls, and can readily be separated from the parent tissue

and identified. Other compounds, such as the terpenoids, may be present only in small amounts and their determination requires complex chemical pre-treatment of the plant tissue. Following extraction of the analyte from its matrix, many species are identified by ultraviolet and visible range solution spectrometry. The range of solvents used for spectrometric analysis of this nature is often large as the differing polarities of the species make the use of a single solvent impossible. Further, as solvent-solute interaction may alter the spectrum of a component, evaluation of spectra in a variety of solvents is frequently necessary in order to achieve identification (93). For example, carotenoids exhibit characteristic absorption bands in the wavelength region 400 - 500nm and conclusive identification of the particular terpenoid by solution spectrometry requires the spectra to be obtained in at least two solvents (100).

While data concerning solvent mixtures for chromatographic separation of plant components and dissolution of the sample for spectrometry is readily available; the in-vivo spectra of many plant constituents have received comparatively little attention. Indeed, because of the non-homogeneous nature of plant material, the problems of obtaining significant transmission or reflectance spectra are severe.

To demonstrate the value of optoacoustic spectrometry in the study of in-vivo plant materials, the ultraviolet-visible spectra obtained from fresh samples of spinach leaf were examined; the major absorbing components are the chlorophylls. The chlorophylls are similar to the haemoproteins discussed previously, i.e., they contain a porphyrin ring, this being chelated to magnesium at the ring centre. Although at least five chlorophylls have been identified, only two, chlorophyll a and b, occur in higher plants (101). The extract of chlorophyll in acetone obtained from samples of spinach leaf was examined in the

wavelength region 300 - 700nm by conventional solution spectrometry and the spectrum obtained is shown in Fig. 3.17. The absorption maxima at about 450 and 650nm are characteristic of chlorophyll spectra.

When a 10mm diameter section of leaf was cut from the spinach sample and examined by optoacoustic spectrometry the spectrum shown in Fig. 3.18A was obtained. By use of this method, negligible chlorophyll absorption was obtained; indeed, the leaf specimen showed a very low absorption signal throughout the visible spectral region. A second sample of spinach leaf tissue was crushed in a pestle and mortar and a smear applied to the silica sample plate, as described for the biochemical samples, and the optoacoustic spectrum obtained from this sample is shown in Fig. 3.18B. In this instance the characteristic visible absorption spectrum was obtained and the chlorophyll absorption bands are evident. It was also observed that the spectrum shown in Fig. 3.18B was obtained from a sample of spinach leaf from the surface of which the cuticle layer has been removed. It can be seen that if the difference spectrum from Figs. 3.18A and 3.18B is plotted, as in Fig. 3.19, the result is similar to the spectrum of the chlorophyll extract solution.

This difference in the optoacoustic spectra obtained from a whole-leaf sample and a homogenised sample can be explained by considering the structure of the leaf (102). In the whole-leaf sample the cuticle (surface layer) is transparent to the incident (and reflected) radiation in the visible region of the spectrum. The waxy cuticle then presents a thermal barrier to heat diffusion from the absorbing chloroplasts, contained below the surface in the sub-epidermal parenchyma cells, to the surrounding atmosphere. This effect suppresses observation of the optoacoustic spectrum of chlorophyll so that the spectrum of the surface layer can be obtained with only a minimum of interference from that of the substrate. This 'layer effect' presents an important difference

Fig. 3.18

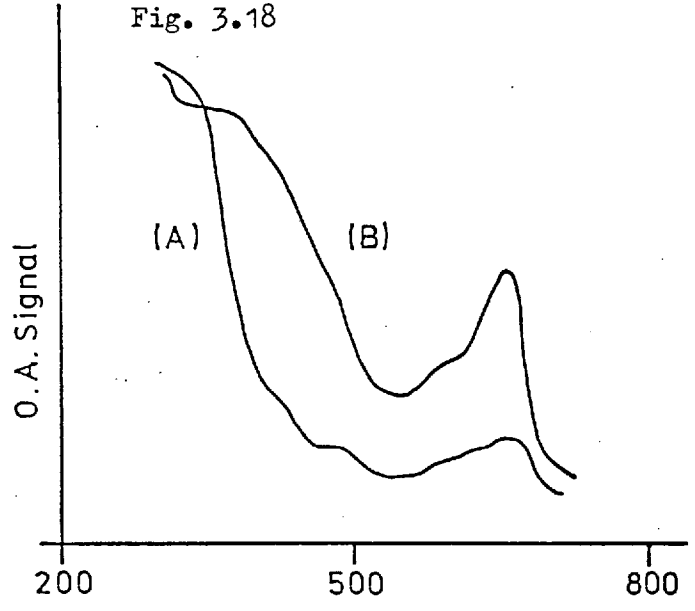

Fig. 3.19

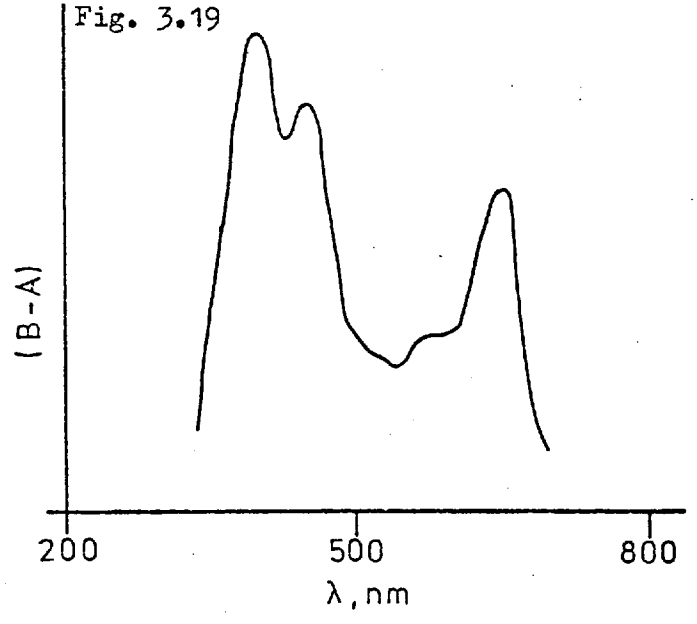

Fig. 3.17

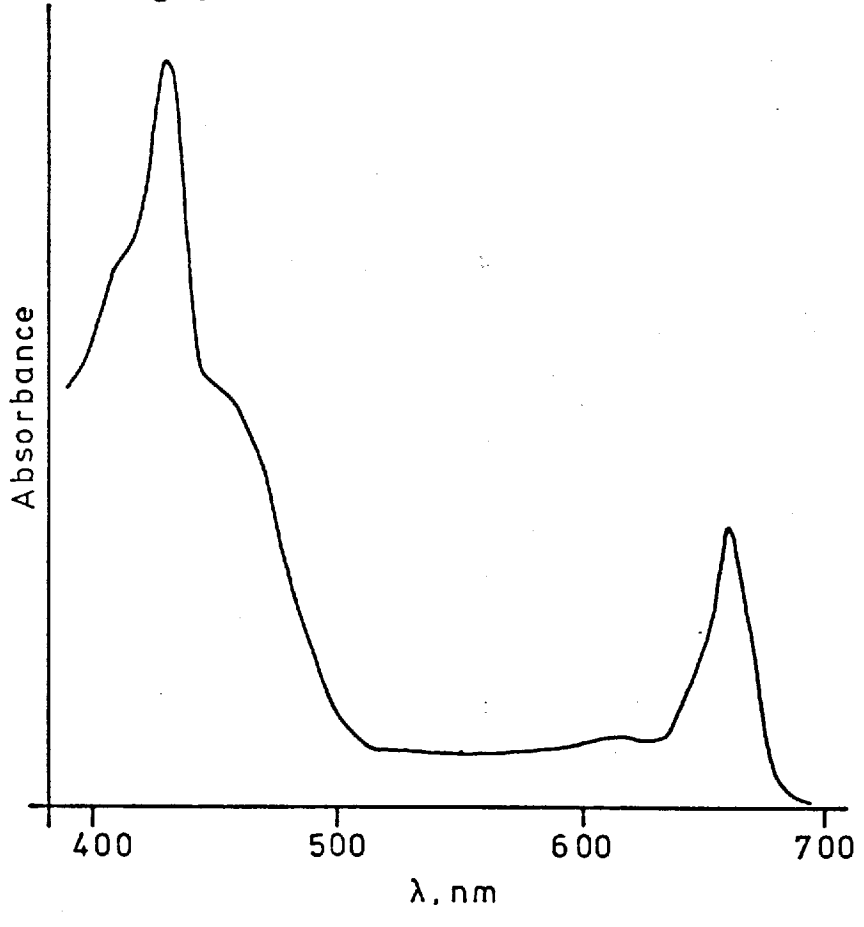

between optoacoustic spectrometry and optical absorption or transmission spectroscopy.

The predicted variations in optoacoustic signal amplitude, with sample and instrumental characteristics, from Equation 3.6, were seen to agree well with the results obtained initially. However, to explain the above layer effect it is necessary to further develop the theoretical treatment of the optoacoustic effect.

CHAPTER FOUR

THEORETICAL TREATMENT OF THE OPTOACOUSTIC EFFECT FOR SOLIDS

4.1. Introduction.

In the previous chapter of this thesis a simple theoretical treatment of the production of the optoacoustic signal was outlined in relation to the light absorption properties of the solid sample. Many of the factors controlling the amplitude of the measured signal were introduced and it was demonstrated that a graph of the amplitude of the measured optoacoustic signal versus the wavelength of the incident radiation is related to the electronic absorption spectrum of the sample in the ultraviolet-visible region. However, the layer effect, observed with the spinach leaf samples requires the theoretical treatment to be developed further.

The absorption of radiant energy by the sample is followed by its conversion into kinetic energy, and heat transfer through the sample to the solid-gas interface is then necessary for the production of the optoacoustic signal. The thermal characteristics of the sample, in particular the thermal diffusivity, may be expected to affect, therefore, the nature of the signal observed. Thermal diffusivity is the ratio of the thermal conductivity to the specific heat and density of a material and has dimensions characteristic of a diffusion coefficient: $(\text{length})^2 \times (\text{time})^{-1}$. Although it is a derived quantity, the thermal diffusivity of a material is of direct importance in heat-flow studies as it determines the rate of transient heat propagation through a sample. Because of its controlling effect and common occurence in heat-flow problems its determination is often necessary and a knowledge of thermal diffusivity of a substance can be used to calculate thermal conductivity data. An extensive review of this property of materials has been presented by Touloukian et al (103). A number of methods for its determination are discussed, as are data relating to a wide variety of materials.

It is the intention, in this chapter, to extend the simple

theoretical treatment of the optoacoustic effect that has been presented and discuss how this treatment can be applied to gain spectral data from non-homogeneous solid samples.

4.2. Theoretical Model.

The relatively simple case for an optoacoustic system in which a periodic temperature wave, derived from the absorption of modulated electromagnetic radiation, diffuses through a solid sample and into the surrounding gaseous atmosphere contained within an optoacoustic cell is considered. The theoretical solution is applied to the determination of the relative phase and magnitude of the observed optoacoustic signal. Although only a relatively simple mathematical treatment is presented, this is sufficient to provide for a better understanding of the optoacoustic effect and its analytical implications.

4.2.1. Periodic Heat Flow in One Dimension.

Initially, a solid sample of thickness d and which has the surface temperature at $x = 0$ varying in a periodic, sinusoidal manner is considered (Fig. 4.1a). This represents a solid sample being irradiated by a modulated source from the rear; the front surface of the sample being contained in a constant volume cell (Fig. 4.1b). If the diameter of the sample is very much greater than its thickness then the heat flow can be assumed to be in one direction only from $x = 0$ to $x = d$; edge effects and radial heat flow may be neglected (104). The temperature, T, at any time, t , and at any distance, x , in the solid can be determined as follows.

The Fourier equation for steady-state conditions of heat flow in an isotropic medium (103), when the thermal properties of the material are independent of temperature, but the temperature varies with time, t , can be stated as (105):

Fig. 4.1

(a) Semi-infinite solid

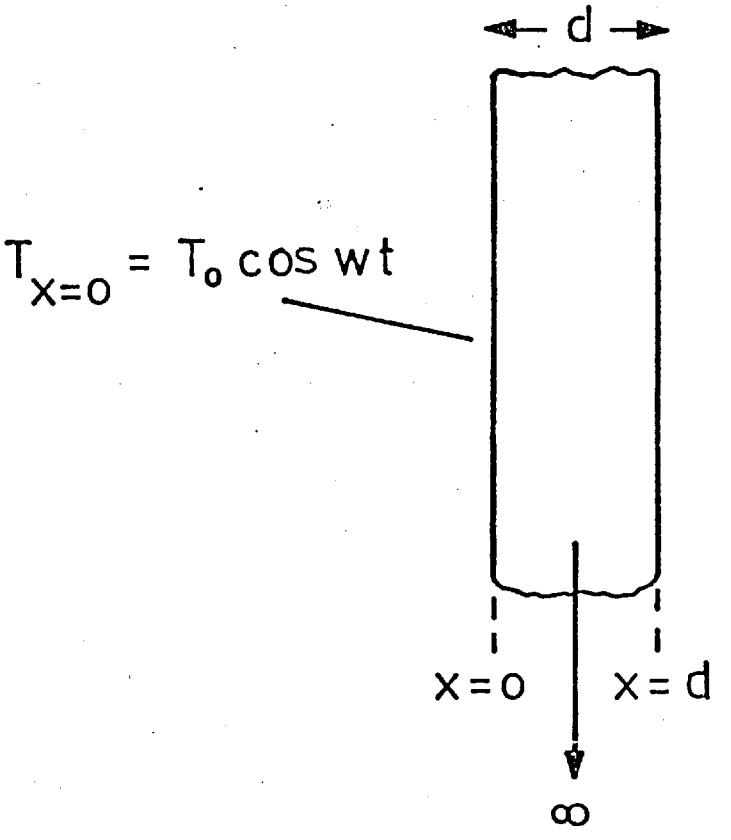

(b) OAS - back surface illumination

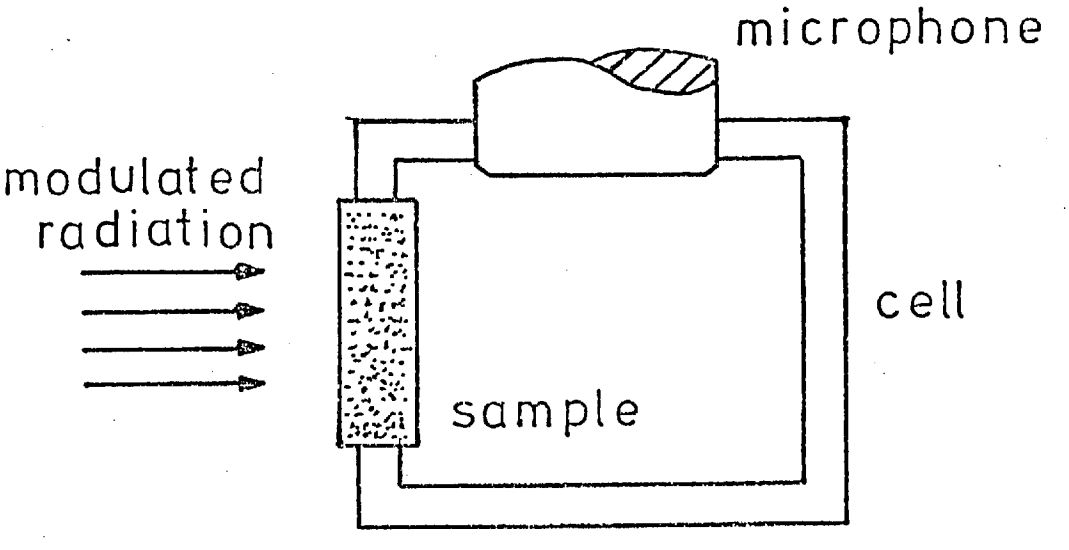

$$\frac{\partial T}{\partial t} = \alpha \cdot \nabla^2 T \qquad \ldots 4.1$$

where α is the thermal diffusivity of the sample and is defined as

$$\alpha = \frac{k}{\rho \cdot c_p} \qquad \ldots 4.2$$

and k is the thermal conductivity of the solid, ρ the density and c_p the specific heat.

The one-dimensional, non-steady conduction equation is

$$\frac{\partial T}{\partial t} = \alpha \cdot \frac{\partial^2 T}{\partial x^2} \qquad \ldots 4.3$$

In order to solve this equation, it is necessary to apply boundary conditions for the surface temperature. This temperature can be expressed as

$$T = T_o \cdot \cos w t \qquad \text{at } x = 0 \qquad \ldots 4.4$$

where w is the modulation frequency (rad. s^{-1}). Ingersoll et al (105) have discussed particular solutions of Equation 4.3 and the solution which fits Equation 4.4 is given by,

$$T = T_o \exp\left[-x \left(\frac{w}{2\alpha}\right)^{1/2}\right] \sin\left[w t - x \left(\frac{w}{2\alpha}\right)^{1/2}\right] \qquad 4.5$$

It should be noted that this solution does ignore the initial warming period resulting from the originally cold sample suddenly being subjected to a periodic surface temperature variation (104). Equation 4.5 can be re-stated as

$$T = T_o \cdot \exp(-b x) \cdot \cos(w t - b x) \qquad \ldots 4.6$$

where

$$b = \left(\frac{w}{2\alpha}\right)^{1/2} \qquad \ldots 4.7$$

i.e., the temperature distribution through the thickness of the sample corresponds in form to an exponentially damped sine wave.

A comparison of Equations 4.6 and 4.4 shows that at some

distance, x , in from the surface, the temperature oscillation is of similar period to that at the surface but of smaller amplitude, decreasing exponentially with increasing x, i.e.,

$$T = T_o . \exp(-b\,x) \qquad \ldots 4.8$$

Equation 4.6 also shows that the maximum of the temperature wave at x occurs at a time later than the corresponding maximum at the surface and this phase lag, $\Delta\theta$, is given by

$$\Delta\theta = -b\,x \qquad \ldots 4.9$$

or by a time delay, Δt , given by

$$\Delta t = \frac{b\,x\,p}{2\pi} \qquad \ldots 4.10$$

or

$$\Delta t = \frac{x}{2}\left(\frac{p}{\pi\alpha}\right)^{1/2} \qquad \ldots 4.11$$

where p is the period of modulation of the temperature oscillation produced by the incident radiation.

Equation 4.6 involves two dimensionless quantities, w t and b x . Fig. 4.2 shows a graph of T/T_o versus w t for values of b x of $0, \pi/4$ and $\pi/2$. As b x increases the curves show progressive lag in phase and attenuation in amplitude. In Fig. 4.3, T/T_o is plotted against b x for values of w t of $0, \pi/4, 3\pi/8$ and $\pi/2$, and the temperature variation with depth at different times is clear.

It should be noted that a similar derivation may be obtained by making an analogy with the theory of electrical transmission lines (106). It can be shown that a direct analogy can be made with the case for a 'submarine cable' with zero inductance and leakance. The theory of the steady periodic behaviour of such a line is well known and may be usefully employed in this case.

Fig. 4.2

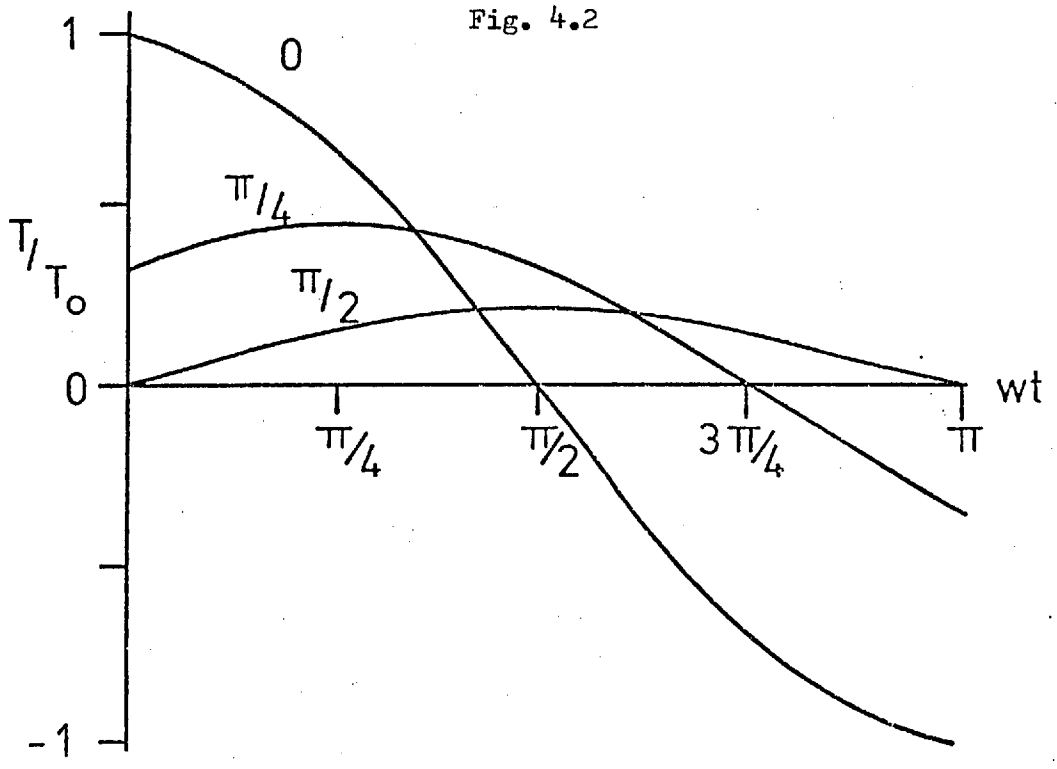

Fig. 4.3

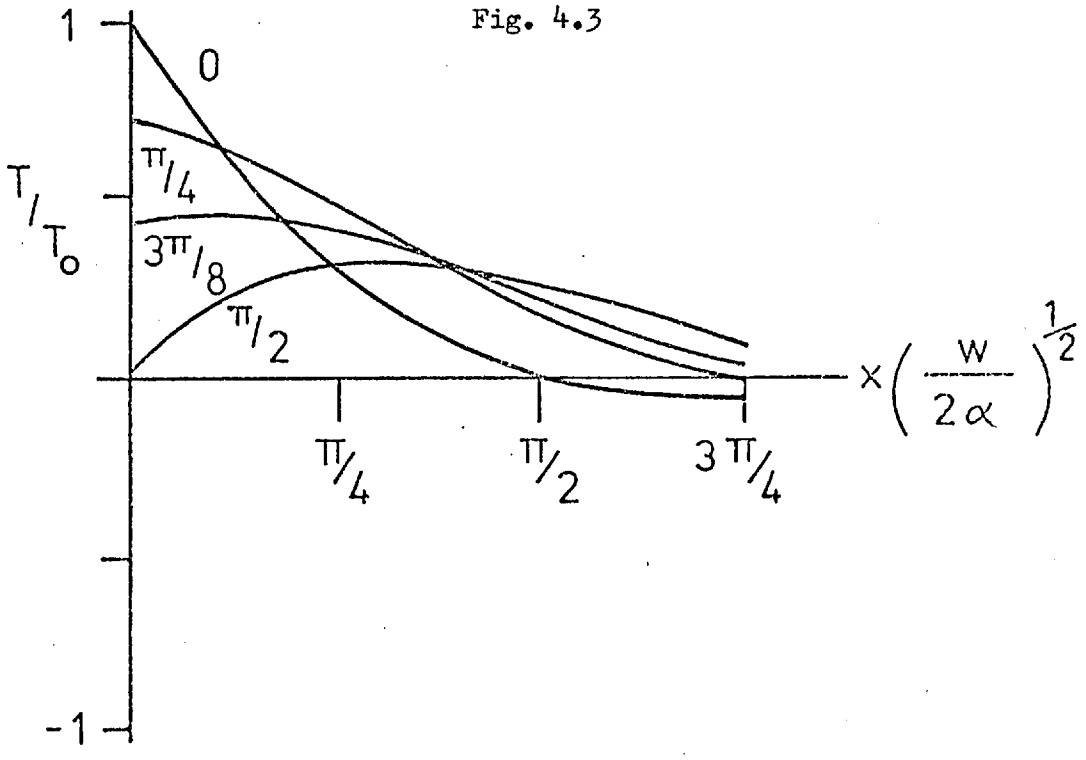

4.2.2. Optoacoustic Spectrometry and One Dimensional Heat Flow.

The equations derived above can be applied to optoacoustic studies. The periodic temperature variation at the front of the sample, $x = 0$ can be achieved by irradiation with modulated electromagnetic radiation and the temperature variation at the other surface, $x = d$, monitored by the optoacoustic effect in a closed cell, as is shown in Fig. 4.1(b).

The radiation incident at the sample surface is assumed to vary in a sinusoidal manner and can be represented as a function of time by

$$I(t) = I_o \cdot \cos w t \quad \ldots 4.12$$

where I_o is the incident radiant flux ($W\ cm^{-2}$)

The total radiation absorbed by the sample at a depth, x, is given by the Beer's law relationship and the heat generated at x by

$$F = \frac{a \cdot I_o}{w} \cdot \exp -(a\ x_1) \cdot \cos w t \quad \ldots 4.13$$

where a is the absorption coefficient and x_1 the optical absorption depth. It can be seen that a term for the efficiency of radiationless conversion is lacking from this expression for the sake of simplicity. The appearance of w in the denominator of Equation 4.13 provides for the conversion of absorbed power into energy to allow for the decreasing energy 'pulse' per modulation period with increasing modulation frequency. If the absorption coefficient is sufficiently large the total absorption of radiation occurs in a very small depth and Equation 4.13 reduces to

$$F_o = \frac{a \cdot I_o}{w} \cdot \cos w t \quad \ldots 4.14$$

and F_o is now the heat flux generated at the sample surface following the absorption of modulated radiation.

The heat flux in a material is related to the temperature distribution by

$$F = -k\left(\frac{\partial T}{\partial x}\right) \quad \ldots 4.15$$

Thus, for a temperature distribution given by Equation 4.6, the heat flux can be represented as (104)

$$F = -k\, b\, T_o \cdot \exp(-b\, x) \cdot \cos(w\, t - b\, x + \pi/4) \quad \ldots 4.16$$

i.e., the heat flow leads the temperature wave by 45°. Conversely, for a sample heated at one surface by a heat flux, F_o, the temperature distribution is given by

$$T = \frac{F_o}{k\, w\, b} \cdot \exp(-b\, x) \cdot \cos(w\, t - b\, x - \pi/4) \quad \ldots 4.17$$

and substituting from Equation 4.14

$$T = \frac{a\, .I_o}{k\, w\, b} \cdot \exp(-b\, x) \cdot \cos(w\, t - b\, x - \pi/4) \quad \ldots 4.18$$

with the identity

$$b = \left(\frac{w}{2\alpha}\right)^{1/2}$$

It can be seen from Equation 4.18 that the phase difference between the temperature in the sample and the incident modulated radiation increases with increasing modulation frequency and depth of sample and decreasing thermal diffusivity.

Although this theoretical treatment is dependent upon a sinusoidally modulated source of radiation, it can still be applied to a square-wave modulated source as is the case in this work. It can be seen from Equation 4.18 that the amplitude of the temperature wave decreases with increasing modulation frequency. Thus, on considering a square-wave to be a superposition of sinusoidal components, it can be seen that the higher harmonics, which are initially attenuated with respect to the fundamental frequency, will be further attenuated as the thermal wave

is propagated.

The solid-gas interface.

In the apparatus employed in this work, the sample and diaphragm form part of the internal cell wall and measurement of the optoacoustic signal requires a pressure change in the atmosphere within the cell. The alternating gas pressure in the cell is achieved by the periodic temperature change of the sample surface in contact with the gas. The gas column in the cell can be considered, therefore, to be an extension of the sample, and the temperature wave produced in the solid sample will be propagated into the gas and can be described by Equation 4.6. Thus, the temperature distribution from the sample surface into the atmosphere is of the form of a damped sinusoidal wave and its propagation depth (thermal depth) will be a function of the frequency of the wave and the thermal diffusivity of the gas. Rosencwaig (107) has defined the thermal depth, l_1, as

$$l_1 = \left(\frac{2\alpha}{w}\right)^{1/2}$$

Within the range of modulation frequencies usually used for optoacoustic studies, l_1, is very much smaller than the gas column length, l_2, in the cell and complete attenuation of the temperature wave will be achieved in a shallow 'active-gas' layer close to the surface of the sample. This 'active-gas' layer undergoes an alternating rise and fall in temperature and can be considered as a gas piston, causing the pressure of the atmosphere within the cell to follow a similar periodic motion.

Phase shifts in this region can be neglected; the phase lag due to the propagation of a temperature is given by the dimensionless function $x(w/2\alpha)^{1/2}$ and provided $l_2 \gg l_1$, the thermal depth, l_1, can be equated with x (the distance into the gas) and zero phase shift

is produced.

Although Equation 4.18 has been developed from a relatively simple model, the general solution agrees well with a more rigorous mathematical treatment for a similar system studied by Cowan (108). Cowan was concerned with the determination of the thermal diffusivity of materials at high temperatures, using a modulated electron beam to provide the periodic heating of the sample surface at $x = 0$, and emitted radiation to monitor the temperature at the surface at $x = d$.

The dependence of T on the thermal diffusivity of the sample material, α, predicted from Equation 4.18, has been examined by Adams (109,110) by using two samples with widely different thermal characteristics and an optoacoustic apparatus employing undispersed source radiation. The samples, a thin glass plate (0.16mm thickness) and a thin copper disc (0.17mm thickness), were each studied in an optoacoustic cell by rear-surface illumination, i.e., the arrangement in Fig. 4.1(b). The samples were each coated on one face with a very thin layer of matt black enamel, which was of high absorptivity and was considered to have a negligible effect on the thermal characteristics of the samples. Each sample was mounted in the optoacoustic cell with the aid of double-sided adhesive tape in order to reduce heat loss into the silica sample plate and reduce sample edge effects. The magnitudes of the in-phase and quadrature components of the optoacoustic signal relative to a reference signal generated by the light chopper were determined at various modulation frequencies between 30 and 200Hz. From these measurements the phase angles of the resultant optoacoustic signals were computed for different values of modulation frequency. The phase angle, θ, of the resultant signal relative to the reference signal is given by

$$\mathrm{Tan}^{-1}\,\theta = \frac{A_1}{A_2}$$

where the amplitude of the quadrature component is denoted by A_1 and that of the in-phase component by A_2. From Equation 4.7, the phase angle, Θ, is given by

$$\Theta = x\left(\frac{w}{2\alpha}\right)^{1/2} \quad \ldots 4.19$$

Thus a plot of Θ versus $w^{1/2}$ should be linear with a gradient of $x(1/2\alpha)^{1/2}$. Adams (110) has experimentally verified this for copper and glass samples and obtained values for the thermal diffusivity of these materials in reasonable agreement with the literature values.

4.3. Thermal Effects in Optoacoustic Spectrometry.

In order to investigate the results obtained with the spinach leaf samples presented in Chapter Three, a simple two-layer leaf model was constructed (Fig. 4.4) consisting of an optically transparent layer of low thermal conductivity covering a radiation absorbing substrate. The results obtained from both this model and actual leaf samples are presented and discussed with reference to the above theoretical treatment.

4.3.1. Results and Discussion.

The optoacoustic spectrum obtained from the model is shown in Fig. 4.5A and is comparable with that observed from a whole spinach leaf specimen. The ultraviolet absorbing layer (Uvinol 400; I.C.I. Ltd., Welwyn Garden City) on the surface of the model, like the cuticle layer of the leaf, is transparent to visible region radiation. By removing the silica cover slip from the model the green paper surface is directly exposed to the incident radiation; no thermal barrier then exists between the absorbing paper and the surrounding atmosphere and the spectrum shown in Fig. 4.5B is observed.

The difference between the spectra shown in Figs. 4.5A and 4.5B

Fig. 4.4

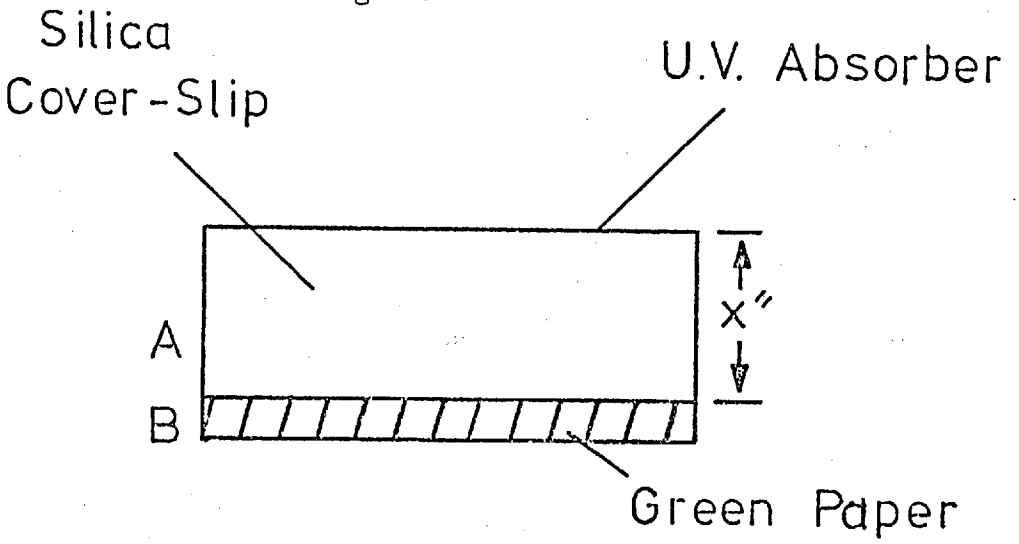
Silica
Cover-Slip
U.V. Absorber
A
B
X"
Green Paper

Fig. 4.5

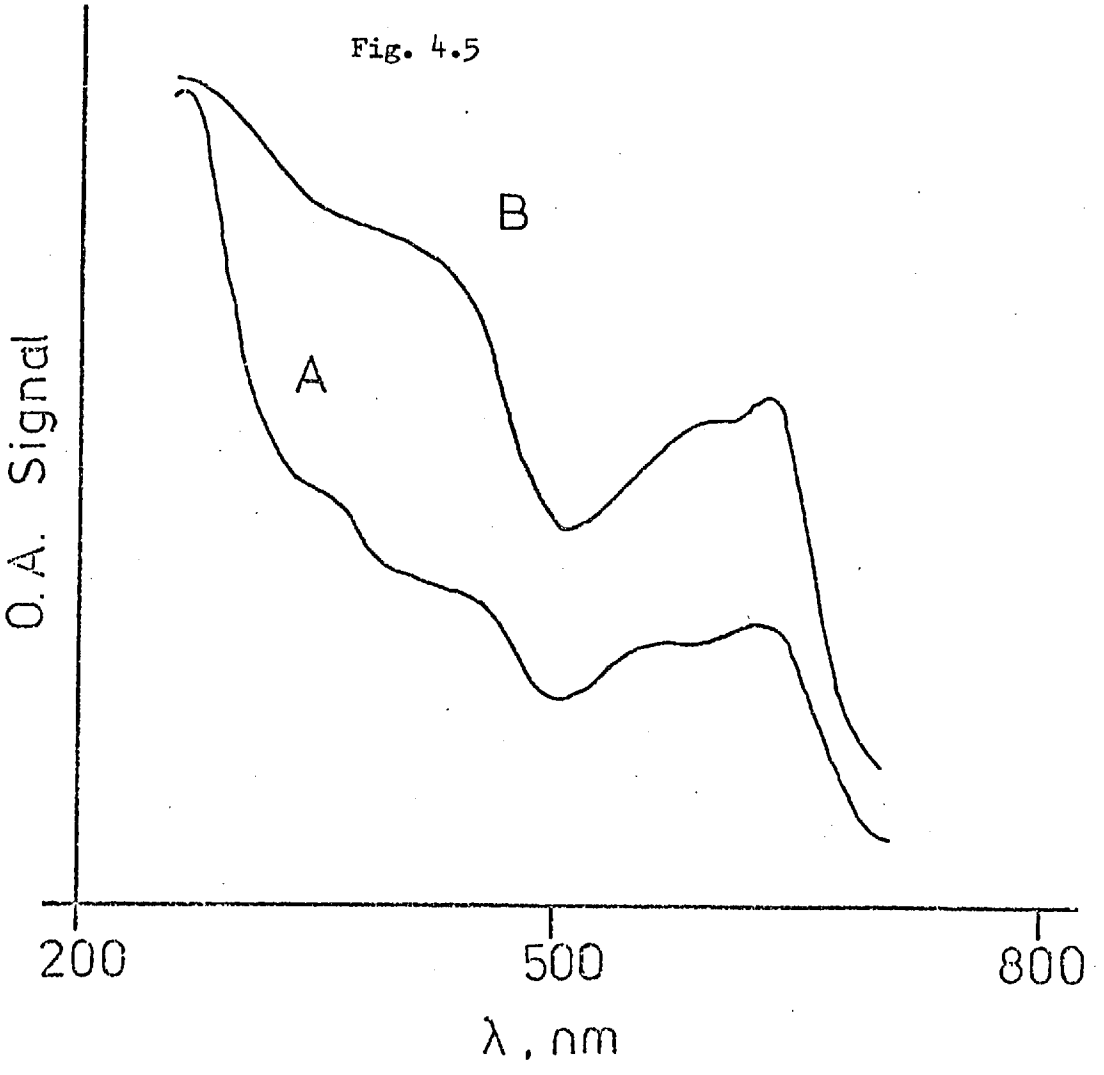
O.A. Signal
B
A
200
500
800
λ , nm

provides a qualitative insight into the above theoretical treatment. Optoacoustic spectrometry of solid samples relies on the transfer of heat through the sample, following the absorption of radiation and subsequent de-excitation, and a heat transfer at the solid-gas interface. The heat flow through the material is dependent on the thermal diffusivity, α, of the sample; α being defined as the ratio of the thermal conductivity and the thermal capacity of the sample. The larger the value of α, the faster heat will diffuse through the sample. A high value of α may result from a high value for thermal conductivity, i.e., a rapid rate of energy transfer, or from a low value for thermal capacity. The latter condition implies that less of the energy passing through the medium is required to raise its internal energy. If,however, the thermal capacity is large, the amount of energy available for diffusion through the sample is decreased and an optoacoustic signal of reduced magnitude is recorded. A dependence on time of the optoacoustic signal is therefore anticipated, as indicated by Equation 4.18, because thermal diffusivity controls the rate of energy transfer through a medium. This time dependence of the signal is observed and can be monitored by phase analysis of the optoacoustic signal.

With the exception of samples capable of triplet-state formation by intersystem crossing (5), the absorption and resultant emission of the energy of excitation, whether as light or heat, occurs on a time scale that is negligible (about 10^{-8} s) compared with the period of the signal modulation (about 10^{-2} s). Thus, by use of conventional absorption, fluorescence or reflectance techniques a phase difference between the absorbed or emitted signal and the reference signal is not detected. However, as is shown above, optoacoustic spectrometry of solid samples relies on heat transfer through the sample; this process is time-dependent and is responsible for any phase shift that may occur.

For an homogeneous sample, a phase shift observed between the optoacoustic signal and the reference signal only decreases the magnitude of the in-phase component of the optoacoustic signal and has no effect on the recorded spectral absorption characteristics of the sample, which are merely absorptivity dependent. This has been demonstrated by King (86) for particulate carbon black. For non-homogeneous systems, however, especially those exhibiting a well defined layer structure, such as leaf tissue, different layers may exhibit different absorption spectra and, therefore, might be expected to present the spectra at different phase angles, i.e., for a two-layer system the two spectra from the substrate and the top-layer can be separated in time and selected by choice of different phase angles between the incident radiation and the signal channel of the detector amplifier.

All of the spectra discussed above, and in Chapter Three, were determined by monitoring the signal from the optoacoustic cell in-phase with the reference signal from the rotating sector that is used to modulate the incident radiation. Fig. 4.6A shows the uncorrected optoacoustic spectrum obtained from a section of spinach leaf that has had the outer cuticle removed, and the phase angle (Θ) of the measured signal set to maximise the signal at 650nm. The spectrum was then recorded again with the phase angle set at ($\Theta - 90^{o}$), i.e., exactly out of phase so that no signal would be expected, and the result is shown in Fig. 4.6B; for the leaf sample without a transparent top layer no contribution to the signal was observed out of phase and the system can be considered to be a single layer. The same procedure was undertaken on a fresh leaf sample with the cuticle intact and the spectra obtained are shown in Fig. 4.7. In this instance, a different spectrum is obtained at ($\Theta - 90^{o}$), which closely resembles that in Fig. 4.6A in that it exhibits features of the chlorophyll spectrum; the results serve

Fig. 4.6

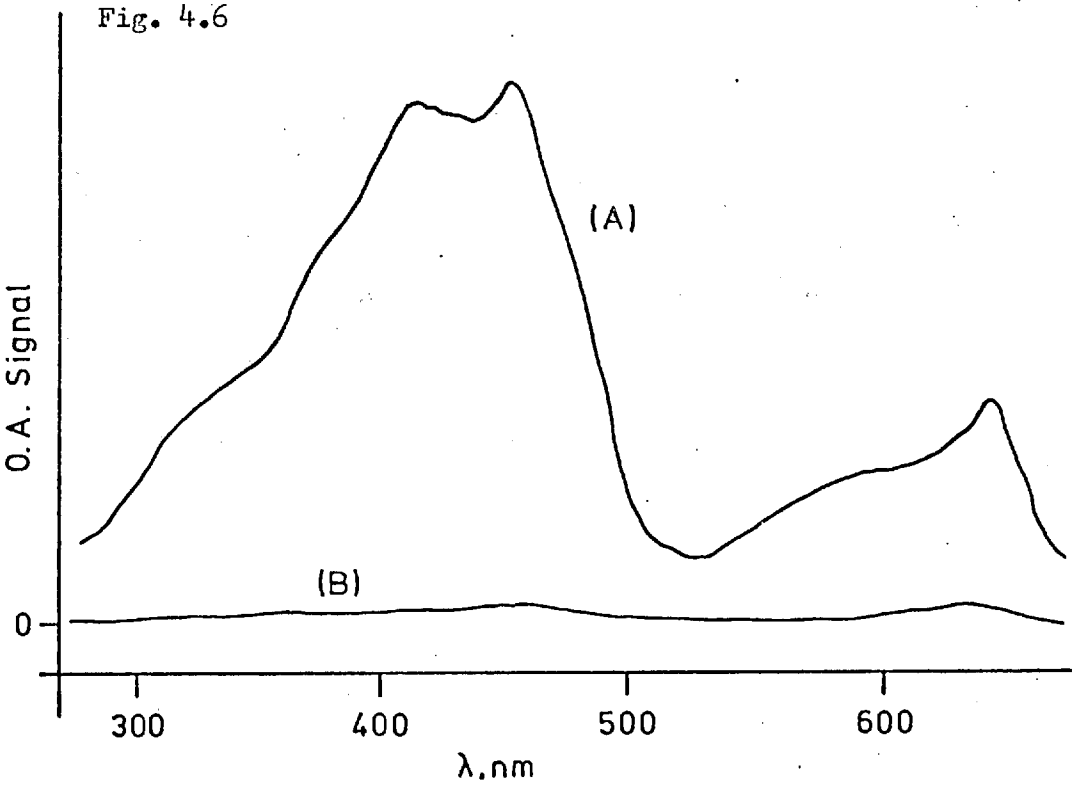
O.A. Signal
(A)
(B)
0
300
400
500
600
λ,nm

Fig. 4.7

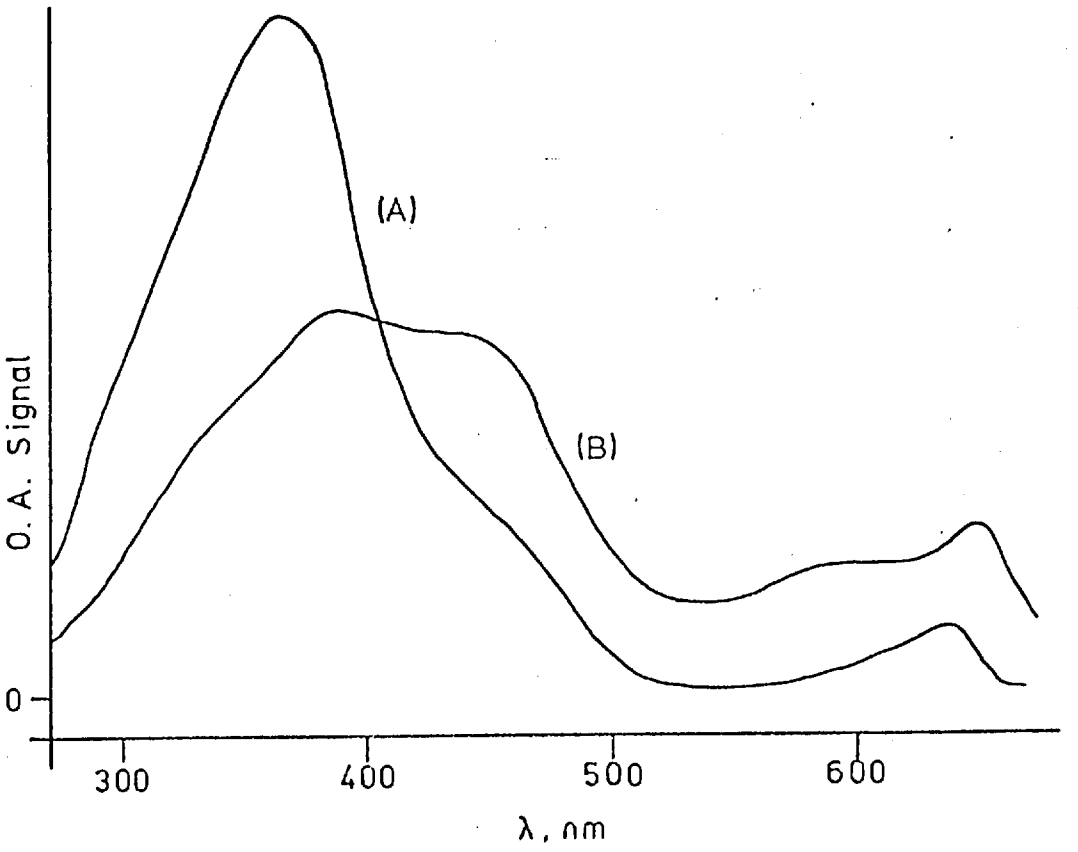
O.A. Signal
(A)
(B)
0
300
400
500
600
λ, nm

to produce evidence for the two-layer effect.

4.3.2. The Two-Layer Effect ; Theoretical Treatment.

The above theoretical treatment of the optoacoustic effect for homogeneous, solid samples can be extended to the case of non-homogeneous systems with a well defined layer structure; in this particular case, two layers.

The two-layer model described above can be considered to consist of a top layer, A , transparent to incident radiation and the substrate, B , which is highly absorbing and of negligible thickness (Fig. 4.4). Therefore, the thermal characteristics of layer B can be ignored and Equation 4.18 is applied as follows:

$$T_{(x = d)} = \frac{a' I_o}{w k b} \cdot \exp(-b x'') \cdot \cos(w t - b x'' - \pi/4) \quad \ldots 4.20$$

where the single prime refers to the lower, absorbing layer and the double prime to the upper, transparent layer. The two-layer system consisted of a silica cover slip coated with a dried smear of a dilute solution of Uvinol 400, an ultraviolet absorbing material, to form the upper layer. The lower layer was formed by green paper in close thermal contact with the cover slip.

With this sample arrangement the top, ultraviolet absorbing layer has negligible thickness and the optoacoustic signal (as a function of the temperature of the sample) is given by Beer's law as

$$T'' = \frac{a'' I_o}{w} \cdot \cos(w t - \pi/4) \quad \ldots 4.21$$

and for the lower layer, Equation 4.20 can be applied:

$$T' = \frac{a' I_o}{w k b} \cdot \exp(-b x'') \cdot \cos(w t - b x'' - \pi/4) \quad \ldots 4.22$$

where again, the single prime refers to the characteristics of the lower layer and the double prime to those of the upper ultraviolet absorber-silica layer. As is discussed above, the temperature wave generated by the lower absorbing layer will suffer an attenuation and phase lag, or time delay, in passing through the silica layer. This effect is well demonstrated by the whole-leaf sample. Each of the spectra shown in Fig. 4.7 can be considered as quadrature vector components of a resultant alternating pressure signal in the optoacoustic cell. Neglecting the attenuation of the signal from the bottom layer, and taking the ratio T'/T'' , then

$$\frac{T'}{T''} = \frac{a'}{a''} \circ \frac{\cos (w\,t - b\,x - \pi/4)}{\cos (w\,t - \pi/4)} \qquad \ldots 4.23$$

and the phase lag between the spectra, Θ , is given by

$$\mathrm{Tan}^{-1}\Theta = \frac{T'}{T''} \qquad \ldots 4.24$$

Thus, by the choice of suitable modulation frequencies, a more complete separation between the individual spectra of the two layers should be observed for the quadrature and in-phase spectra, rather than the partial spectral separation shown in Fig. 4.7. This can be better seen by considering the term b in Equation 4.20. The value of the phase lag between the spectra, $\Delta\Theta$, is a function of $b\,x''$, and from Equation 4.9

$$\Delta\Theta = -b\,x''$$

i.e.,

$$\Delta\Theta = -x'' \left(\frac{w}{2\alpha}\right)^{1/2} \qquad \ldots 4.25$$

The degree of separation, i.e., depth resolution, between the bottom-layer spectrum and top-layer spectrum can be controlled by controlling the modulation frequency, w , of the incident radiation.

4.4. Recent Advances.

Although the theoretical treatment of the production of optoacoustic signals by the absorption of radiant energy by gases has been well developed (32,55,111), the theory for solids has been of more recent origin, following the recent advances in optoacoustic spectrometry for the examination of condensed phase materials. Whilst performing gas-phase studies, Parker (49) observed that optoacoustic signals were generated upon illumination of a cell even though it contained a non-absorbing gas. The origin of this signal was attributed to a thin absorbing layer on the entrance window of the cell; this could not be explained in terms of surface water absorption. Kerr (50) produced a theoretical model which better described the results obtained with thin films. However, this model has to be regarded as a special case due to the low source modulation frequencies employed (< 1Hz) although it proved adequate for the 'Alphaphone' system employed to measure thin film absorption at laser wavelengths.

Aamodt et al (112,113) have extended Parker's theory to treat the diffusion processes that are considered to occur in both the solid and gas phase in a similar manner. The diffusion process in the gas is more complex than that in the solid as the temperature wave separates into a thermal, non-propagating, part and an acoustic propagating part. This separation means that the mechanism of signal production can be attributed to a piston effect utilising a boundary layer of gas at the solid-gas interface to generate the pressure waves in the cell. It was also shown that the theoretical model was still valid, when the cell dimensions were less than the length of this boundary layer, by use of the comprehensive theoretical treatment of Bennett and Forman (114). They were concerned with the application of the optoacoustic effect to determine the optical absorption coefficients of transparent materials

used in laser optical systems. The theoretical model and experimental system were developed to obtain the value of the surface and bulk absorption coefficients for laser optical materials (115 - 117); the surface absorption resulting in an inverse proportionality (w^{-1}) between the optoacoustic signal amplitude and the source modulation frequency (w), and the bulk absorption a $w^{-3/2}$ relationship. Hordvik (118) has reviewed the alternative techniques for measuring small absorption coefficients. Hordvik et al described a theoretical model (119) and an experimental system (120) for measuring the absorption coefficients of laser window materials. A piezoelectric strain transducer was employed to measure the stress set up in the window material due to the heat produced by absorbed incident radiation.

The most comprehensive theoretical treatment, of condensed phase optoacoustic spectrometry to date, has been that of Rosencwaig and Gersho (107,121). This treatment describes in particular the dependence of the magnitude of the optoacoustic signal on the absorption coefficient of the sample and the modulation frequency. The expression derived for the pressure variation with time is somewhat complicated, but may be considered in several stages, i.e.,

$$P = \frac{A \cdot B \cdot \beta}{k_s \cdot a_g (\beta^2 - \sigma_s^2)} \quad \ldots 4.26$$

where P is the pressure variation in the cell filler gas for sinusoidally modulated incident radiation, β is the optical absorption coefficient (cm^{-1}) of the sample and k_s is its thermal conductivity.

$$\sigma_s = (1 + j)\, a_s \quad \ldots 4.27$$

a_s and a_g are the thermal damping functions associated with an alternating temperature wave passing through the sample and gas respectively and are given by,

$$a_i = \left(\frac{w}{2\alpha_i}\right)^{1/2} \quad \ldots 4.28$$

where w is the modulation frequency and α_i is the thermal diffusivity of the material.

In Equation 4.26, A is a constant factor which is proportional to the incident radiant energy and the ambient pressure within the cell.

B is a complex function which may be expressed as

$$B = \frac{(r-1)(c+1)\exp(\sigma_s \cdot x) - (r+1)(c-1)\exp(-\sigma_s \cdot x) + 2(c-r)\exp(-\beta x)}{(g+1)(c+1)\exp(\sigma_s \cdot x) - (g-1)(c-1)\exp(-\sigma_s \cdot x)} \quad \ldots 4.29$$

where x is the thickness of the sample and the other functions are given by,

$$r = \frac{(1-j)\beta}{2a_s} \quad \ldots 4.30$$

$$c = \frac{k_b \cdot a_b}{k_s \cdot a_s} \quad \ldots 4.31$$

$$g = \frac{k_g \cdot a_g}{k_s \cdot a_s} \quad \ldots 4.32$$

The subscript b refers to the backing material of the sample, i.e., the sample support plate. The product $k_i \cdot a_i$ may be considered as a thermal flux coefficient for the material.

It is possible to gain physical insight into Equation 4.26 by examining the special cases where this expression becomes relatively simple. For solids of thickness, l, which are reasonably transparent to light ($\beta l < 1$), the amplitude of the pressure variation with time, i.e., optoacoustic signal amplitude, is proportional to βl unless the thermal diffusion length of the solid, $\mu_s = 1/a_s$, is less than l. In that case the signal amplitude is proportional to β/μ_s.

For optically opaque solids ($\beta l \gg 1$), the signal amplitude

is independent of β when the thermal diffusion length μ_s is greater than the light absorption length $1/\beta$. In this case the sample, as well as being optically opaque, is also 'optoacoustically opaque', i.e., when $\beta\mu_s \ll 1$, the signal amplitude is proportional to $\beta\mu_s$, irrespective of the magnitude of the optical absorptivity βl. Thus, even though the sample is optically opaque ($\beta l \gg 1$), it is not optoacoustically opaque, i.e., the signal amplitude is now dependent on the optical absorption coefficient β.

In this theoretical treatment, the effect of reflection losses by the incident radiation at the sample surface was not considered. However, this loss has been observed to be important for small optical absorption coefficients (122) and the diffuse reflectance theory of Melamed (123) has been employed to account for this. The theory has also been extended (124) to solids where the optical absorption coefficient is spatially varying, although the sample is thermally homogeneous, e.g., semiconductors where the doping varies with depth from the surface.

McClelland and Kniseley (125) have applied Rosencwaig and Gersho's theoretical treatment to the study of signal-saturation effects observed in optoacoustic spectrometry. Wetsel and McDonald (126) have applied the case for optically thick and thermally thick samples to measure absolute absorption coefficients. Wong (127) has found good agreement between the theory and the results obtained for different cell filler gases. In addition to the variation in signal amplitude with the thermal constants of the gases predicted by Rosencwaig and Gersho, he also observed that physical absorption of the gas by the sample solid increased the signal amplitude due to increased solid-gas coupling efficiency.

It should be noted that all of these theoretical treatments reported above are complementary to each other, i.e., they either give

an alternative description for the same physical process or are limiting cases.

4.5. Conclusion.

It has been demonstrated that with optoacoustic spectrometric studies on samples such as leaf tissue, it is possible for the surface layer to be examined with negligible interference from the substrate. This property, which is not possessed by conventional optical spectroscopy, is important in surface studies. In this particular instance the waxy cuticle layer affects the wettability of the foliage and its structure and development are of considerable importance in connection with research into the effects of agricultural sprays (128).

In addition, Rosencwaig has shown that the optoacoustic signal is ultimately governed by the magnitude of the thermal diffusion length of the sample. Since the thermal diffusion length can be changed by altering the modulation frequency (121), a solid that is completely opaque optically need not be optoacoustically opaque. It should be possible, therefore, to obtain the optical absorption spectra of materials that are difficult to measure by conventional optical spectrometric techniques.

CHAPTER FIVE

A DOUBLE-BEAM OPTOACOUSTIC SPECTROMETER FOR USE WITH SOLID AND LIQUID SAMPLES IN THE ULTRAVIOLET-VISIBLE REGION

5.1. Introduction.

The single-beam optoacoustic spectrometer described previously required manual correction of the spectra for the variation in source intensity with wavelength. This procedure is a tedious, time-consuming operation. The spectrometer described in this chapter provides for the automatic correction of optoacoustic spectra by means of a second, reference, channel. Two arrangments are commonly employed in conventional optical spectroscopy to achieve double-beam operation(9); double-beam in time, and double-beam in space.

In the arrangement denoted double-beam in time, a single beam of energy leaving the dispersing element is alternately switched between reference and sample paths to provide a double-beam system within the sample compartment. The two beams are then recombined, although separated in time, to fall on a single detector. The output of the detector is an alternating signal whose amplitude is proportional to the difference in intensities in the two channels. For a prism monochromator a slit servo continuously adjusts the slit openings to keep the energy through the reference cell constant at a 100 percent setting when the reference sample is in the light beam. The switching between reference and sample paths is usually done by either a rotating half-sector mirror system, e.g., Model DK-A, Beckman Instruments Ltd., or a vibrating mirror assembly, e.g., Model DB, Beckman Instruments Ltd. For grating instruments, e.g., Model SP.700, Pye Unicam Ltd., a variable cam in the reference beam adjusts the 100 percent setting; a sine-bar linkage is used to solve the grating equation and provide a linear wavelength scale.

Ratio recording eliminates inaccuracies due to such effects as source fluctuations, changes in amplifier gain, sensitivity or spectral response of the detector, and the presence of interfering absorption bands.

The double-beam in space arrangement employs two separate light paths which are created by a beam splitter and mirrors; separate detectors measure the radiant power of each beam. The readout is based on measurement of the ratio of intensities in the two channels. This system is used in double monochromator instruments, in which two dispersing systems are used in series with an intervening slit, to overcome stray light problems in precise measurements, e.g., in the Model 350 ultraviolet-visible spectrophotometer (Perkin-Elmer Corp.). It is not widely employed in conventional instruments due to the expense involved and the precise optical alignment required between each channel.

In addition to these true double-beam methods, a single-beam spectrometer may be employed with a digital storage system (52). In this case, the sample and reference spectra are stored sequentially and then the corrected spectrum is readout via a ratiometer unit. This technique requires the system to be temporally stable, i.e., the source should be highly stable with respect to time.

The actual arrangement employed in the double-beam optoacoustic spectrometer was double-beam in space. This was necessary since the optoacoustic sample constitutes the radiation detection device and, therefore, a separate optical channel is necessary for the sample and reference optoacoustic cells.

5.2. Instrumentation.

Although in general the instrument design was based upon the single-beam optoacoustic spectrometer, described previously, an evaluation was made of alternative sources of radiant energy. This was necessary due to the large physical size of the 1kW xenon arc previously employed, making this difficult to fit into the proposed instrument

design, and the poor radiation collection efficiency of the mirror and lens system.

The various sources were placed before the rotating sector in the experimental arrangement shown in Fig. 3.2. The sources evaluated were:-

i) A 1kW xenon arc (Type 6269, Oriel Corporation).

ii) A 300W short-arc, high-pressure xenon arc, with an integral aluminium parabolic reflector and 25mm diameter sapphire window (Type VIX 300UV, Varian Associates).

iii) A 150W mercury vapour lamp (Philips Electrical Ltd., Croydon).

iv) A 250W quartz-halogen tungsten filament bulb (Type A1/223, Wotan Lamps Ltd., London).

In addition a deuterium arc (removed from a Unicam SP 500 spectrophotometer) and a 150W sodium lamp (Philips Electrical Ltd.) were tested, but no appreciable signal was observed from an optoacoustic cell containing carbon black. The xenon arcs were operated within their appropriate housings which contained the focusing and collection optics. The mercury vapour lamp and tungsten bulb were used with a concave, front-surfaced mirror to focus the radiation through the rotating sector on to the entrance slit of the monochromator.

The spectrum of each source was recorded by the use of an optoacoustic cell containing carbon black, prepared by 'smoking' a thin glass microscope slide (19mm in diameter) and mounting it in the optoacoustic cell on the silica sample plate. The amplitude of the acoustic signal was measured with a lock-in amplifier (Model 186, Princeton Applied Research Corp.) and recorded, against the wavelength of the incident radiation during wavelength scanning, by means of a potentiometric chart recorder (Servoscribe, Model RE511). The signal amplitude axis on these spectra was then converted to a power reading by

comparing the signal amplitude obtained with the optoacoustic cell, at discrete wavelengths in the 1kW xenon arc spectrum, with the measurements obtained with a laser power meter (Model 142LR, Laser Instrumentation Ltd., Chertsey) placed at the exit slit of the monochromator.

The spectra obtained for these sources, shown in Figs. 5.1 and 5.2 , were measured at a spectral half-bandwidth of 10nm and a modulation frequency of 30Hz. The spectrum of the 300W xenon arc, however, is not shown, being similar to that of the 1kW arc. The sharp inflection in the spectra at 550nm corresponds to the insertion of a filter (Type 26-4317, Ealing Beck, Watford) employed to remove overlapping spectral orders of diffraction from the grating. The peak intensities of the sources examined are given in Table 5.I.

From these results, and the spectral distribution of this power, it can be seen that the xenon arcs are the obvious choice of source for optoacoustic spectrometry; the ideal light source having not only a highly intense emission but also a reasonably constant intensity with wavelength (to facilitate correction of sample spectra). The 300W xenon arc was employed for this work as it was physically smaller, and thus easier to mount in the instrument. It appears that much of the energy from the 1kW arc is not utilised due to the poor collection of this energy at the monochromator entrance slit.

5.2.1. Double-beam Spectrometer.

A schematic diagram of the double-beam spectrometer is shown in Fig. 5.3 together with a photograph of the system. The continuum source employed was a 300W, high-pressure, short arc xenon illuminator lamp with integral aluminium parabolic reflector and 25mm diameter sapphire window (Type VIX 300UV, Varian Associates). The lamp was mounted within a fan-cooled housing (Type R300-1, Varian Associates). Power for

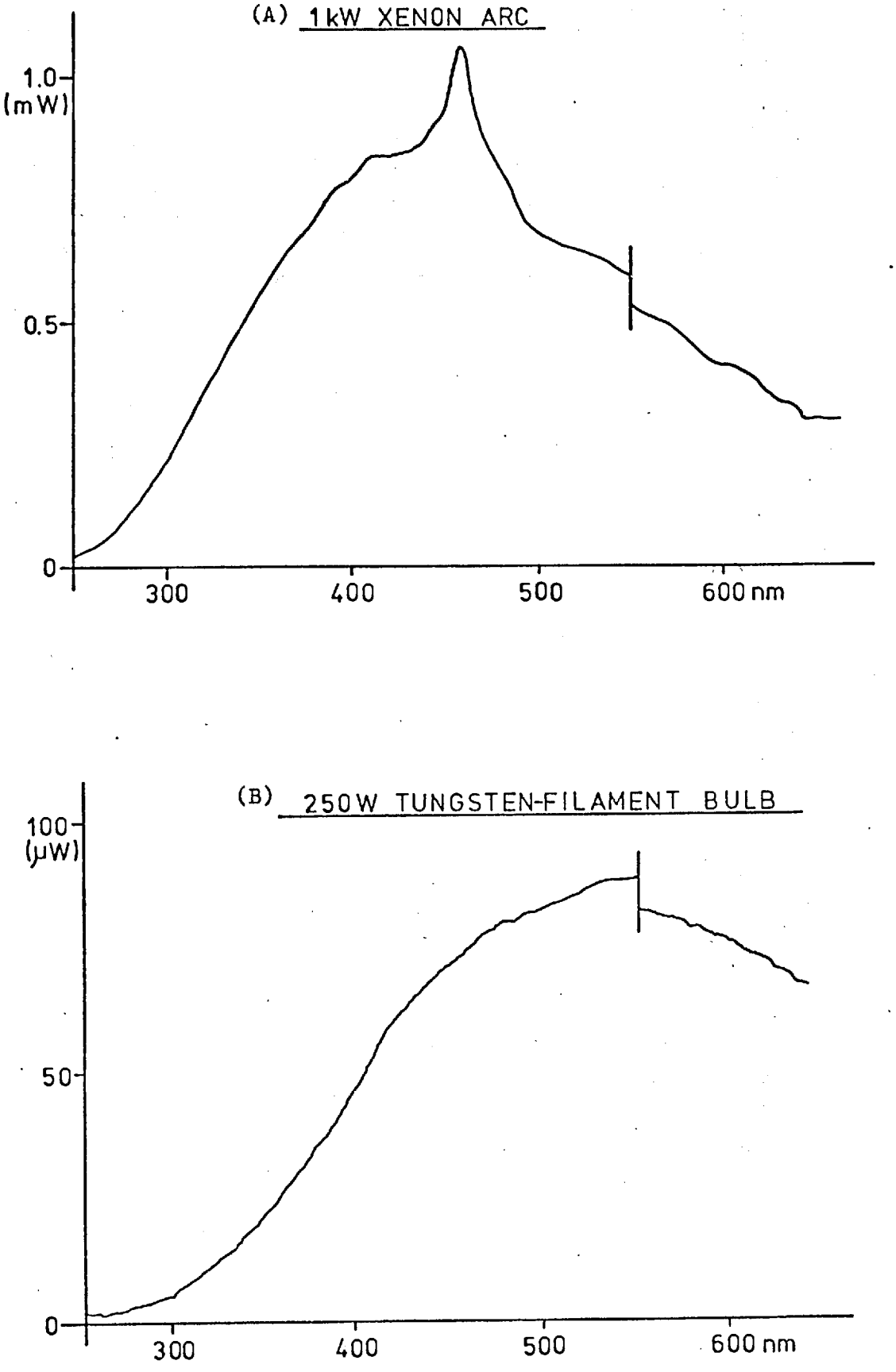

Fig. 5.1 Power spectra of potential sources for OAS.

Fig. 5.2 Power spectrum of:

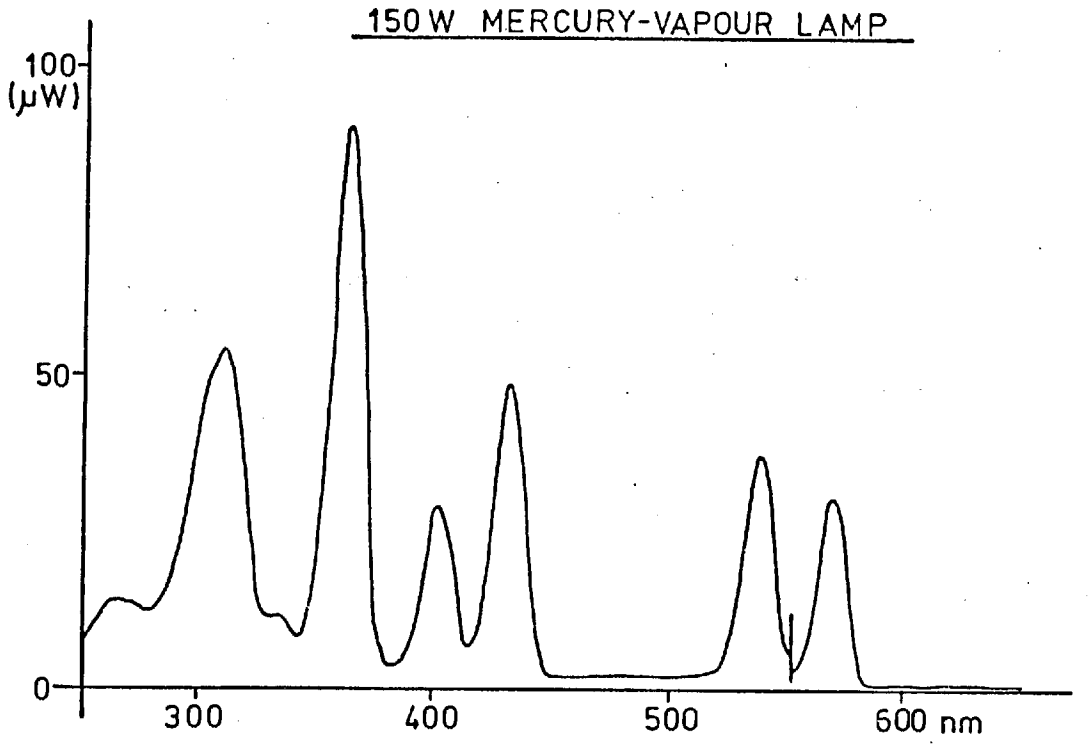

SOURCE	MAXIMUM INTENSITY (mW)
1kW Xenon arc	1.16
300W Xenon arc	1.11
250W Tungsten bulb	0.094
150W Mercury lamp	0.095

Table 5.I Source emission intensities in the ultraviolet-visible region.

this source and cooling system was provided at 15V and 20A by a Varian associates PS300-1 power supply unit. The radiation from the source was focused, by means of a silica lens (25mm in diameter, with a 70mm focal length), on to the plane of rotation of a variable-speed rotating sector (Model 9479, Brookdeal Electronics Ltd.) placed adjacent to the entrance slit of the f/4 grating monochromator (Metrospec DGO Ltd.) previously described in this thesis. The monochromator was fitted with a plane diffraction grating (50 x 50mm , 1200 lines mm^{-1}) blazed at 300nm for use in the ultraviolet-visible region. As is shown in Fig. 5.3 , the monochromator was fitted with two exit slit assemblies, in each of which fixed slits ruled on silica plates could be positioned to provide spectral half-band widths of 1, 2, 5, 10 and 20nm. In order to prevent the transmission of radiation at wavelengths less than 490nm from overlapping spectral orders of diffraction, yellow coloured glass filters (Type 26-4317, Ealing Beck) were used at each exit slit when measuring optoacoustic spectra in the visible region at wavelengths greater than this. Within the monochromator housing the dispersed radiation was split by a 50% plane mirror positioned so as to produce radiation of equal intensity at each exit slit. Radiation emerging from the exit slits was refocused by using front-surfaced concave mirrors (50mm in diameter, 200mm focal length) and directed into the optoacoustic cells as shown in Fig. 5.4. The mirrors were mounted on springs in housings positioned at the exit slits and their angle to the emerging radiation could be readily arranged for optimum illumination of the samples contained within the cells. The transducers employed were sensitive $\frac{1}{2}$ in capacitor microphones (Type 4166, Brüel and Kjaer Ltd.). Each of the microphone cartridges had a rated sensitivity of 50mV Pa^{-1} and was fitted with a Type 4169 preamplifier (Brüel and Kjaer Ltd.). The polarisation voltage to the microphones (200V) was supplied from a dry battery source mounted within the base of the

Fig. 5.3.A Schematic diagram of the double-beam optoacoustic spectrometer.

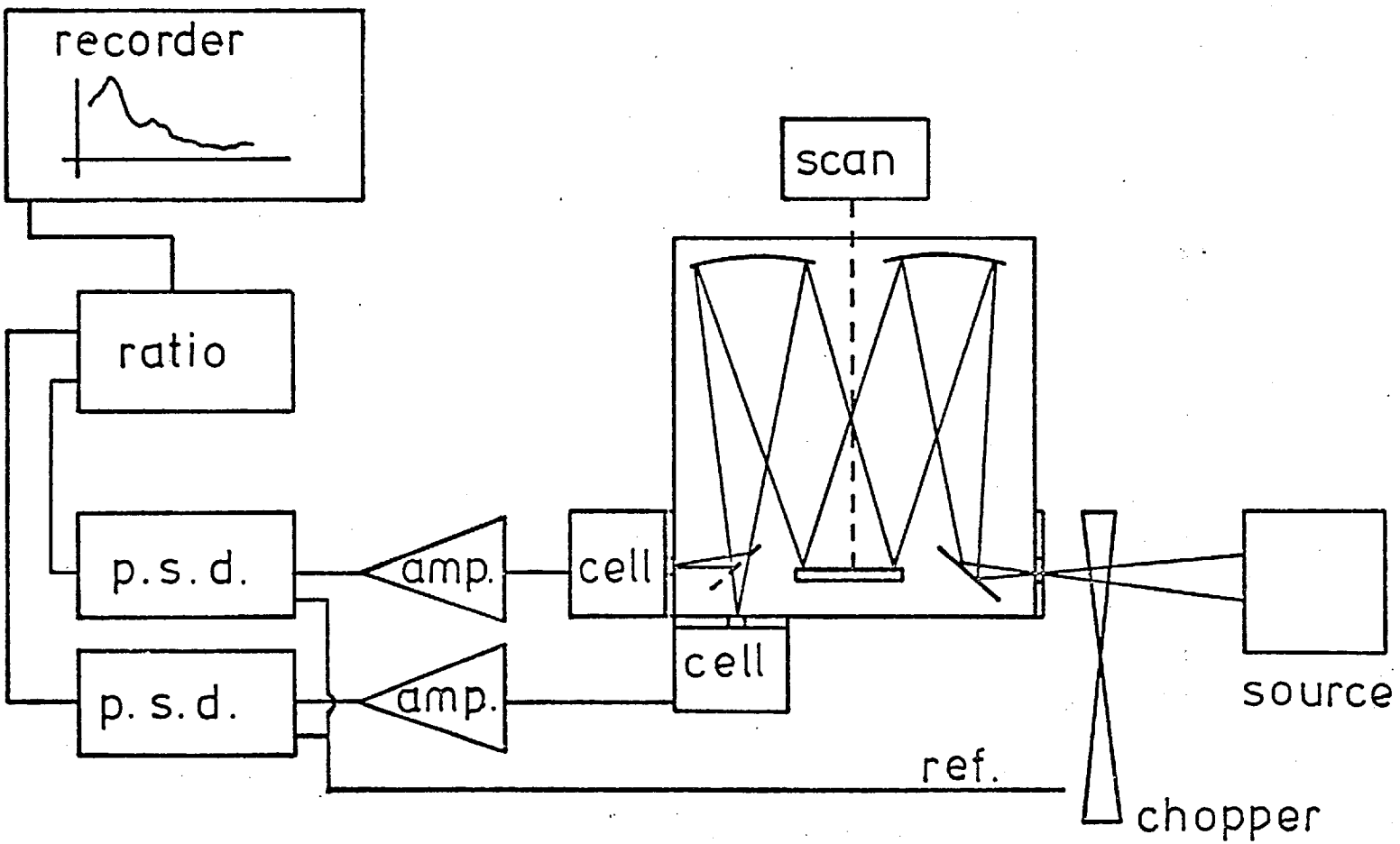

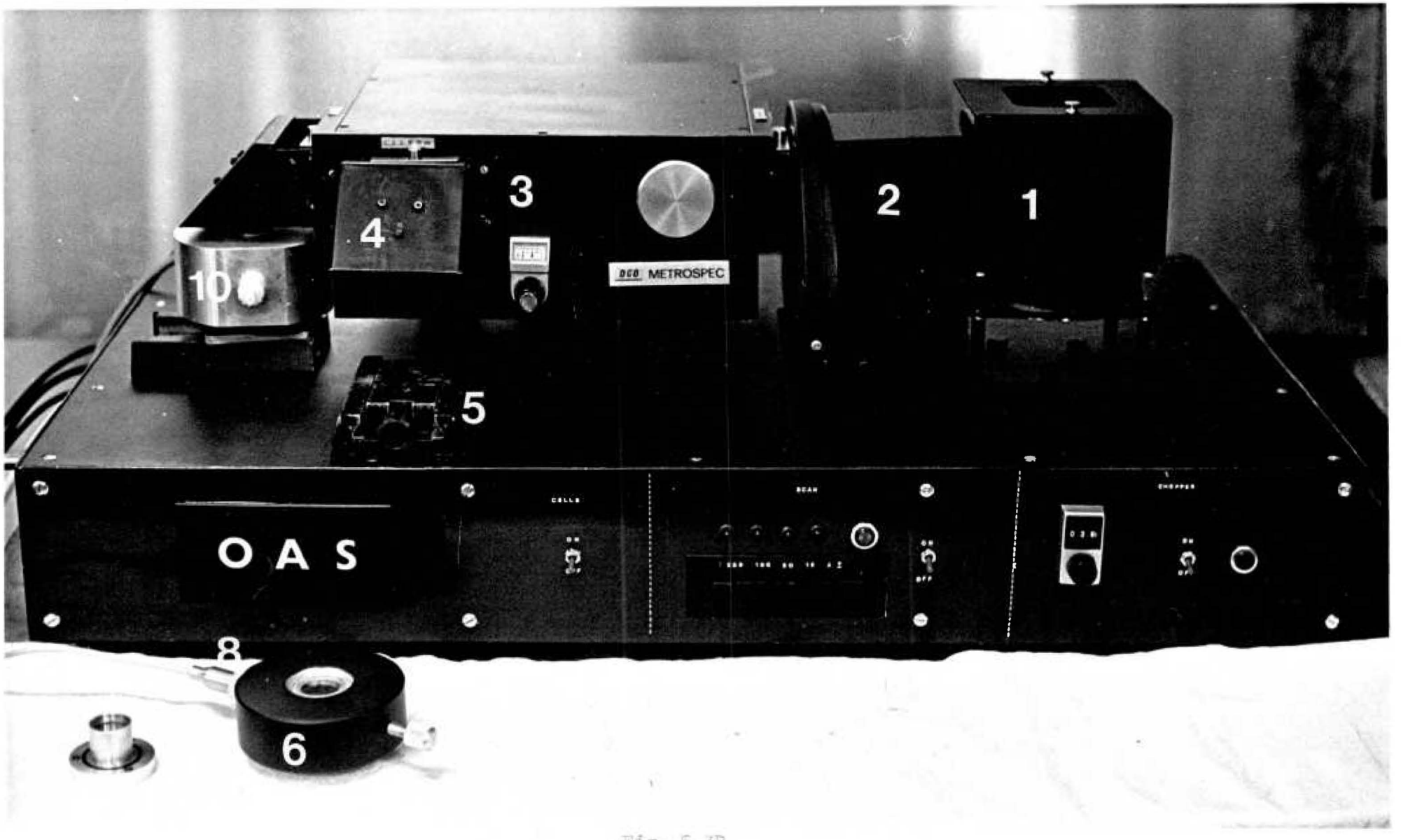

Fig. 5.3B

Key to Fig. 5.3B.

1. Xenon arc source.
2. Variable-speed rotating sector.
3. Monochromator.
4. 45° mirror.
5. Sliding sample cell mounting.
6. Sample optoacoustic cell.
7. Pressure release valve.
8. Microphone preamplifier.
9. Sample tray.
10. Reference optoacoustic cell.

Fig. 5.4 The Optoacoustic Cell.

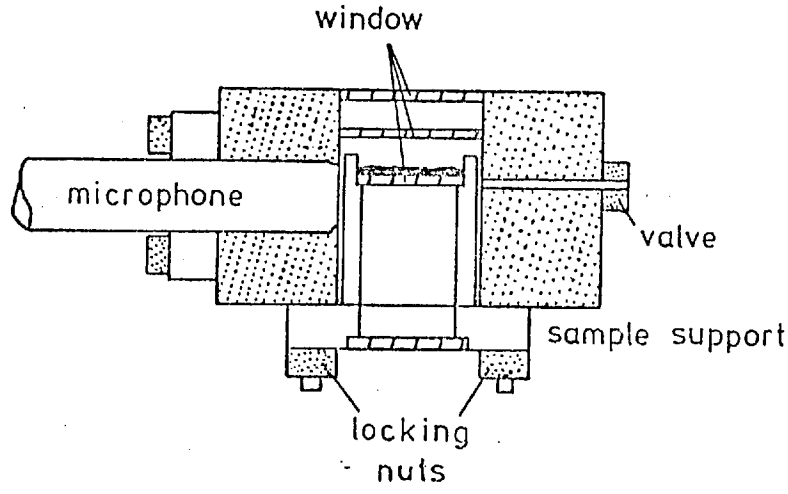

instrument.

Identical cells were positioned below each exit slit of the monochromator and the design employed is shown in Fig. 5.4. The cells were constructed from aluminium and were sealed by means of double silica windows to attenuate environmental acoustic noise; they were operated at atmospheric pressure, using air as the filler gas. Samples were positioned on a silica plate (20mm diameter) mounted in an aluminium tube, which was placed in the cell and sealed by means of three locking nuts. Front-surface illumination of the samples was used throughout.

Wavelength scanning of the continuum radiation was achieved by means of a stepping motor (Type 23PM-C003, Astrosyn Ltd., Strood, Kent) connected directly to the cam-drive mechanism of the grating mount within the monochromator. The source, rotating sector, monochromator and optoacoustic cells were mounted together on a single steel plate ($\frac{1}{4}$in thick, 30in long x 18in wide) and the chopper and stepping motor electronic systems, together with the dry cells providing the polarisation voltage for the microphones, were located inside a steel frame below the optical components. The circuit diagram for the stepping motor electronic system is shown in Fig. 5.5; the drive card (Type 001, Astrosyn Ltd.) contained an inbuilt oscillator to drive the motor at 400 steps per revolution. This system provided pre-selected scanning rates of 250, 100, 50 and 15nm min^{-1}. These were selected by the use of push-button controls which were mounted, along with the forward and reverse scan selection and modulation frequency controls, on the front panel of the spectrometer assembly.

The optoacoustic signals from the microphone transducers were led directly, via screened cables, to two lock-in amplifier systems (reference channel, Model 124A amplifier, Princeton Applied Research

Fig. 5.5

ASTROSYN STEPPING MOTOR

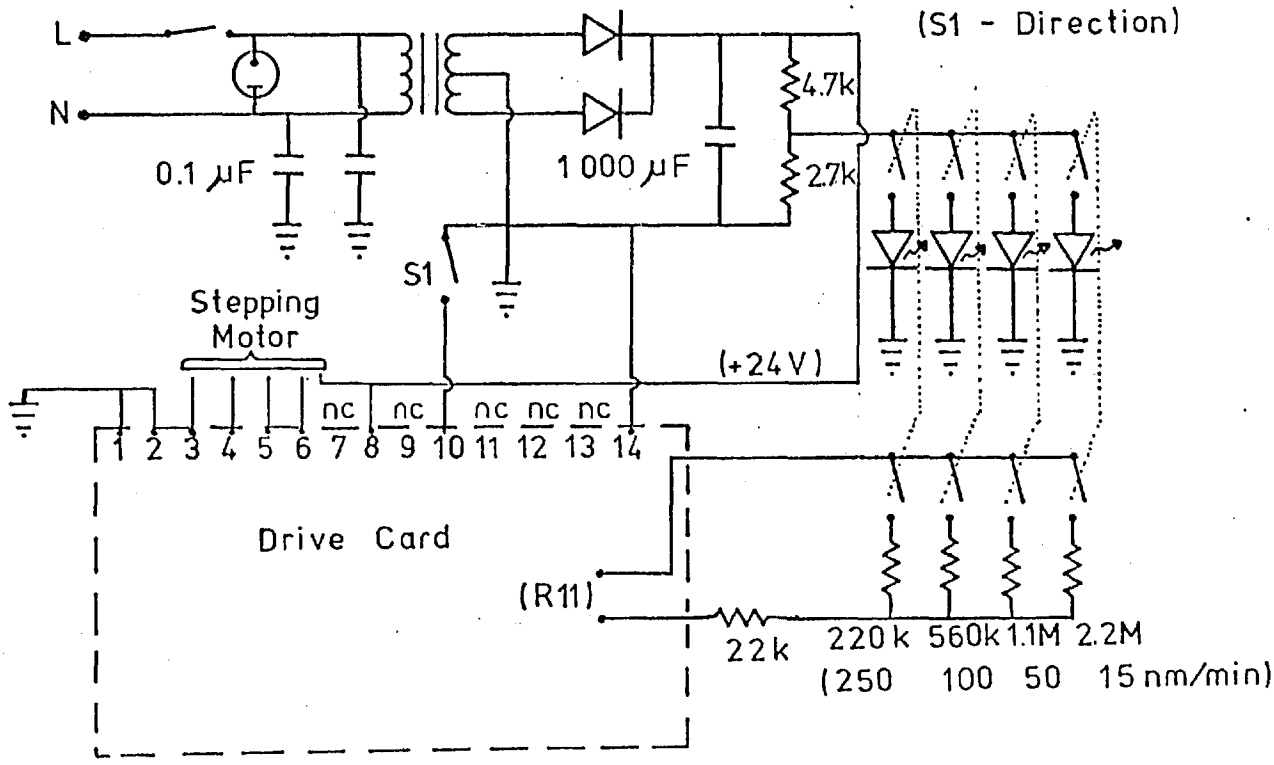

Fig. 5.6 Schematic diagram of a vector voltmeter. (82)

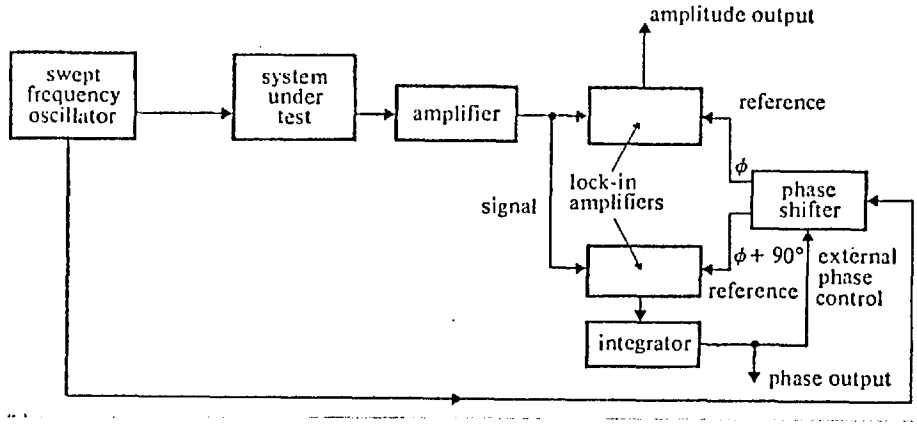

Corp.; sample channel, Model 9502, Brookdeal Electronics Ltd.). The reference signal for each amplifier was that generated by the variable-speed rotating sector. The lock-in amplifiers extracted the signal waveforms and presented these as DC potentials to a ratiometer unit (Brookdeal Electronics Ltd., Model 5047); the signal from the reference cell was presented directly to the denominator, while the sample signals were taken to the numerator input. The ratiometer output was shown as a DC potential and taken, via a simple resistance-capacitor time-constant circuit (2s) to a potentiometric chart recorder (Servoscribe, Model RE511 Smiths Industries Ltd.). Corrected optoacoustic spectra were then obtained by recording the output of the ratiometer against the wavelength of the incident radiation during wavelength scanning at the monochromator.

The Model 9502 (Brookdeal Electronics Ltd.) lock-in amplifier was capable of either making two-phase p.s.d. measurements or of acting as a phase-insensitive detection system, i.e., an automatic vector voltmeter (82). In the two-phase arrangement measurements could be made of the in-phase and quadrature components of the optoacoustic signal simultaneously. In the vector voltmeter configuration, direct measurement could be made of signal amplitude without the need to optimise the phase of this signal relative to that of the reference signal which was previously the case for the Model 186 (Princeton Applied Research Corp.) lock-in amplifier. In addition, a direct readout of the phase of the optoacoustic signal relative to the reference signal is provided by this system. In the schematic diagram (Fig. 5.6) of a vector voltmeter it can be seen that the lower lock-in amplifier is used to control the phase shift in the phase shifter. When the phase angle of the phase shifter is sufficiently close to the phase of the incoming signal, the phase-shifter locks with the signal phase and tracks it over the full 360°

phase angle range. The output of the lower lock-in amplifier is the error point of the feedback loop. The integrator sums the phase errors and provides the required DC voltage to drive the phase-shifter. This voltage is proportional to the phase shift through the experimental system, while the DC output from the top lock-in amplifier is proportional to the signal amplitude from the experimental system.

5.3. Results and Discussion.

The optoacoustic spectra of solid and liquid samples were recorded by using carbon black (a smoked glass microscope slide) as a reference absorber. The use of the smoked glass sample gave an order of magnitude increase in signal amplitude over that obtained with particulate (<76μm) carbon black, due to the very much smaller particle size; typical signal levels at the xenon peak emission wavelength (ca. 473nm) being 20 - 50mV.

Solid samples were examined by placing a few milligrams of the material in the sample tray of the optoacoustic cell and recording the spectra in the conventional manner against a carbon black reference cell or, if differential spectra were required, against the necessary reference sample placed in the reference optoacoustic cell. Liquid materials and solutions were examined by pipetting about 100μl of the solution into the sample tray.

In order to record solution transmission spectra a silica cuvette (20mm in diameter, 10mm in depth) was positioned between the sample optoacoustic cell and the exit slit on the monochromator. Both sample and reference cells were loaded with carbon black samples for these measurements. The instrument was then operated conventionally, i.e., energy transmitted through the sample solution in the cuvette was received at the sample cell and gave an optoacoustic signal for

carbon black, the magnitude of which varied depending on the transmittance of the incident radiation at different wavelengths.

Unless otherwise stated, the spectra reported in this chapter were obtained with a spectral half-band width of 10nm, a scan rate of 50nm min^{-1} and an instrumental time constant of 3s.

5.3.1. Instrument Performance.

Corrected optoacoustic spectra in the wavelength range 250 - 800nm were determined with the double-beam spectrometer by taking the ratio of the amplitude of the optoacoustic spectrum at different wavelengths to the power emitted by the xenon arc continuum source at these wavelengths. The power spectrum of the source was obtained by measuring the optoacoustic spectrum of carbon black, assuming this to approximate to a black-body absorber.

The emitted power spectrum of the lamp in the ultraviolet-visible region obtained by single-beam operation of the instrument is shown in Fig. 5.7a. The efficiency of the beam splitting arrangement, used with the spectrometer in order to produce a uniform response with respect to wavelength for identical sample and reference cells, was determined by mounting carbon black samples in both cells and examining the ratio of the output from each when obtained by double-beam operation as described above. The flatness response for the ultraviolet-visible and near-infrared regions is shown in Fig. 5.7b. The result obtained, typically $\pm$ 4% flatness, was considered satisfactory for double-beam spectrometric examination of samples.

Fig. 5.8(a) and (b) shows the ultraviolet-visible spectra of two rare earth oxides, holmium oxide and erbium oxide, respectively, which were obtained as fine powders (Johnson Matthey Ltd., London). Because the f orbitals in lanthanides are so well shielded from their

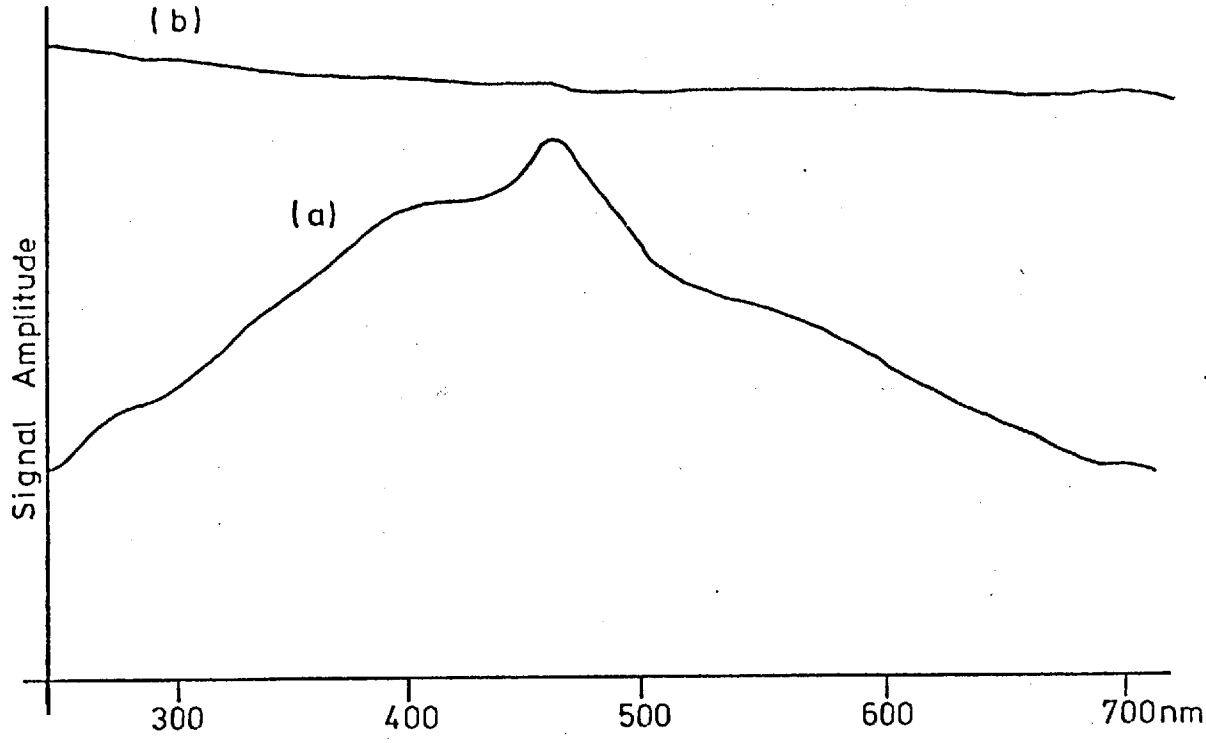

Fig. 5.7

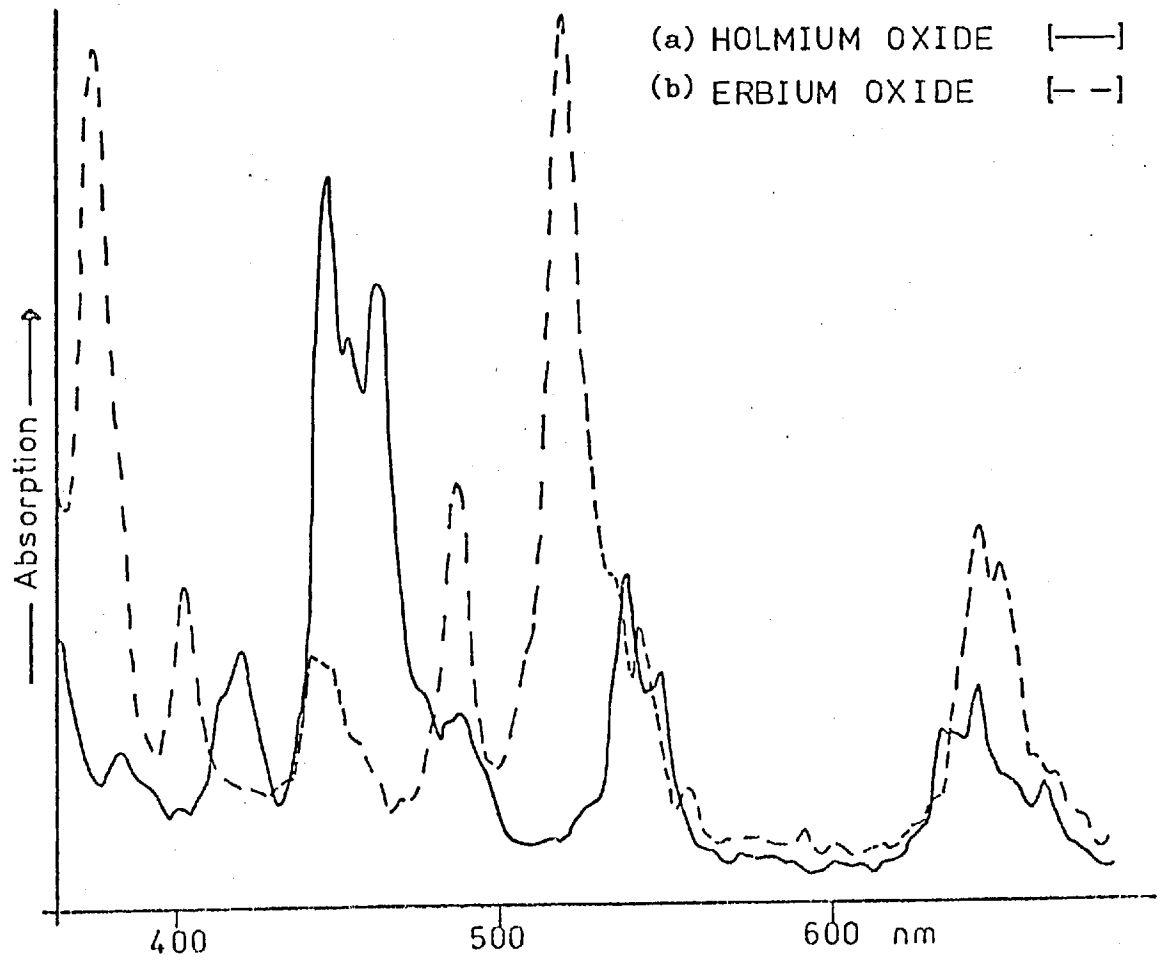

Fig. 5.8 Instrument settings: half-band width 2nm; scan rate 15nm min^{-1}; time constant 3s.

surrounding lattice, the various states arising from the f^n configurations are split by external fields only to the extent of ca. 100cm^{-1}(129). Thus when the f - f electronic transitions occur from one J (total angular momentum) state of an f^n configuration to another J state of this configuration, the absorption bands are extremely sharp. They are similar to those for free atoms and are quite unlike the broad bands observed for d - d transitions. Virtually all the absorption bands found in the ultraviolet, visible and near-infrared spectra of the lanthanide +3 ions have this line-like spectral characteristic. Thus these materials provide good test samples with which to evaluate the spectral resolution and signal-to-noise ratios obtainable with the optoacoustic spectrometer and small solid samples. Since the absorption bands always appear at about the same energy regardless of the host crystal due to the slight influence of the crystal field on the J - level multiplets of rare earth spectra, these compounds may be usefully employed for wavelength calibration of the spectrometer. White (130) has reported the diffuse reflectance spectra of eleven rare earth oxides of various structural types within the spectral range 225 - 2,700nm. The optoacoustic spectra obtained with a range of rare earth oxides were in agreement with these spectra.

Both solid samples and solutions can be examined directly by optoacoustic spectrometry, as is illustrated in Fig. 5.9(a) and (b). Fig. 5.9(a) shows the corrected optoacoustic spectrum obtained from a few milligrams of purified catalase powder and the characteristic absorption bands at about 400 and 500nm of a haemoprotein (92) are evident. Fig. 5.9(b) shows a similar optoacoustic spectrum of a suspension of catalase, obtained by pipetting 100µl of the solution into the sample tray of the optoacoustic cell. The solid catalase sample was a purified extract from bovine liver, and the solution sample was a

crude, sterile solution from bovine liver (Sigma Chemicals Co., St. Loius, Mo.,USA). The corrected optoacoustic spectrum obtained from a 2μl sample of whole human blood is shown in Fig. 5.10. The clear spectrum obtained from this liquid sample serves to further illustrate the freedom from scattering of the incident radiation by the sample matrix (high molecular mass protein material) that is obtained by the use of optoacoustic spectrometry. The spectrum shown in Fig. 5.10 is characteristic of the oxyhaemoglobin contained in the blood sample (93).

An important advantage of a two-cell double-beam spectrometer is that difference spectra (9) can be studied with relative ease. This technique is illustrated in Fig. 5.11, where the optoacoustic spectrometer was used to record the spectra of the rutile and anatase forms of titanium(IV)oxide. The samples were powders of sub-micrometer particle size (Tioxide International Ltd., Stockton-on-Tees). The reference cell sample tray was filled with the powdered rutile sample and the sample cell with the anatase powder. Uncorrected difference spectra can be recorded by employing an (A - B) technique at the input of one of the lock-in amplifiers or, as with Fig. 5.11(c), the ratio of the amplitudes of the optoacoustic signals for each sample and the variation of this ratio with the wavelength of the incident radiation can be monitored; while the latter does not provide a true difference spectrum it does enable corrected spectra to be obtained. The difference in the location of the edge of the absorption peak of the two samples is clear in Fig. 5.11(c). King (86) constructed a calibration graph for the opto-acoustic signal at 384nm versus the percentage composition of rutile titanium(IV)oxide in rutile-anatase mixtures. This graph was only linear for low percentage rutile compositions, curving towards the concentration axis at higher concentrations, probably due to the relative particle sizes of the mixture components as discussed in Chapter Three. Reflectance

Fig. 5.9

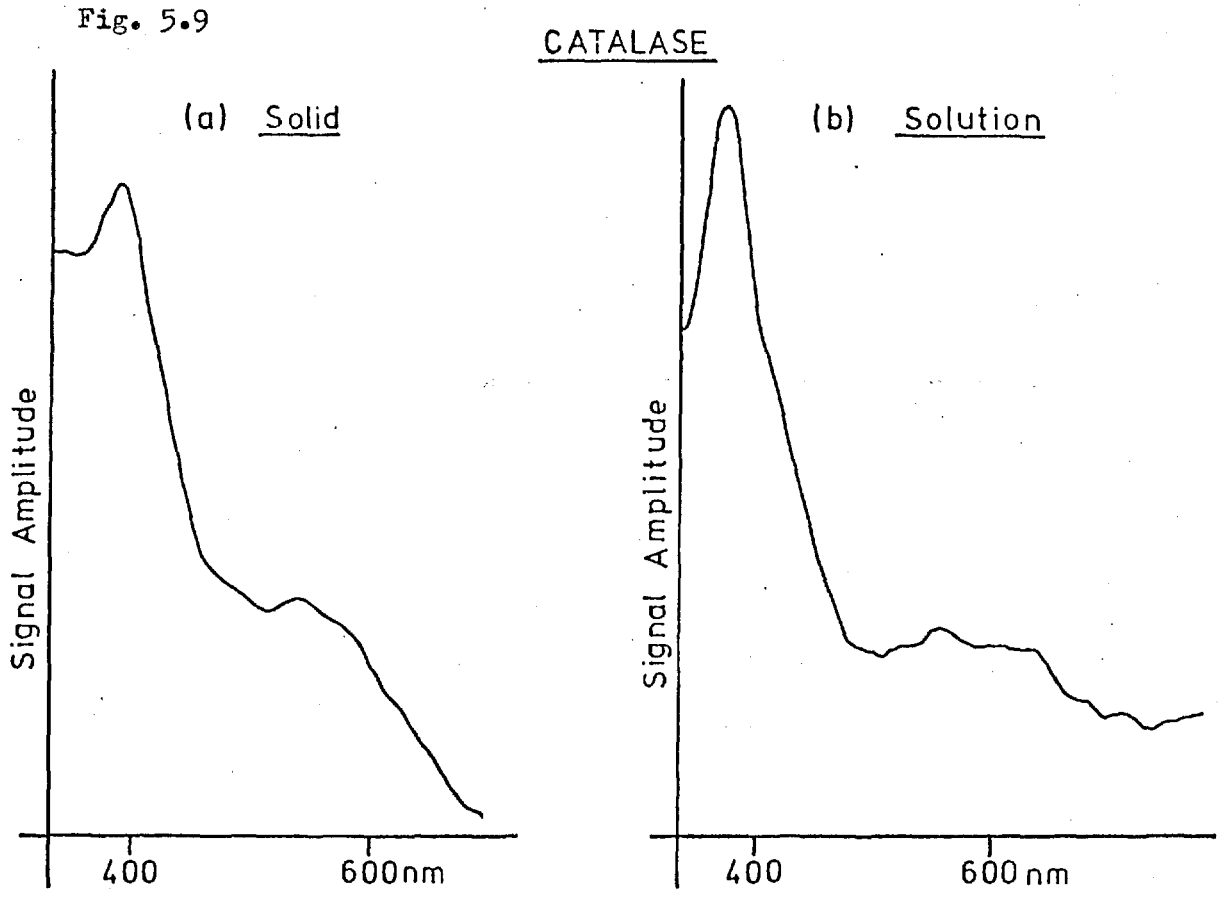

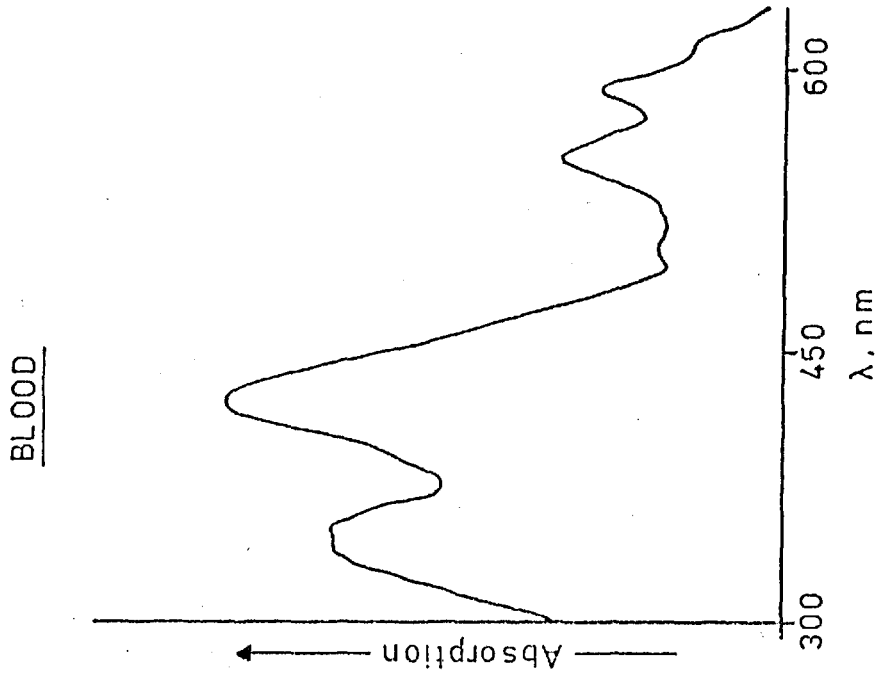

Fig. 5.10

spectroscopy has been employed for a similar, quantitative, compositional analysis of such mixtures and Kortüm has reported a mean deviation of $\pm 2\%$ of one component by this method (131). This analysis is of interest since it affects the quality of the titanium(IV) pigment used as a white colouring. It is evident that this difference spectrum optoacoustic technique can be applied to any multi-component mixture if sufficient difference in the absorptivities is apparent at a suitable wavelength. An advantage of the use of optoacoustic spectrometry rather than reflectance spectroscopy for this type of work lies in the small sample requirement and the need for a minimum of sample preparation.

The double-beam optoacoustic spectrometer can also be used for solution transmission studies. The optoacoustic sample cell fitted with a carbon black sample served as the detector of the transmitted radiation and an example in which the instrument was operated in this mode is shown in Fig. 5.12. Oxygenated whole blood was diluted (1 + 199) with distilled water and placed in a silica cuvette; the transmission spectrum obtained was characteristic of oxyhaemoglobin (93). This technique of examining transmission data was initially employed for spectrometer wavelength calibration in the ultraviolet-visible region.

5.4. Applications.

The examination of a large number of sample types was undertaken with the double-beam optoacoustic spectrometer. In a large number of cases the required information was differentiation of samples by colour, e.g., the food dyes, ponceau 4R, amaranth and erythrosine (supplied by the Laboratory of the Government Chemist), paint chips (Forensic Science Service, Aldermaston) and human hair (Palaeontology Section, Natural History Museum). In Fig. 5.13 can be seen representative spectra obtained from this type of sample; in this case red ballpoint

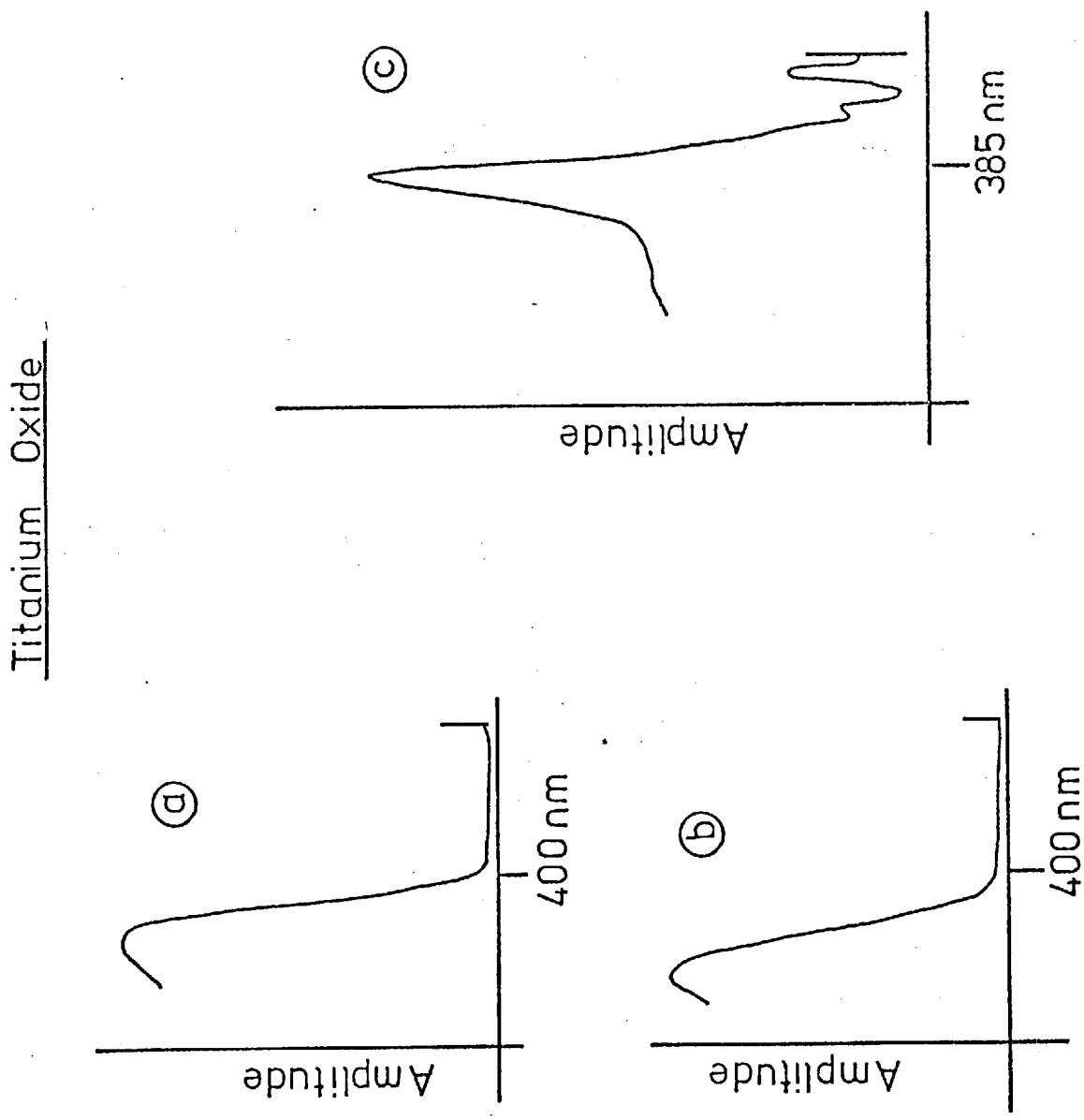

Fig. 5.11 Uncorrected optoacoustic spectra of (a) rutile and (b) anatase titanium(IV)oxide, and (c) their difference spectrum.

pen ink samples. These were examined as part of a general evaluation for the Laboratory of the Government Chemist (L.G.C.) of the applications of optoacoustic spectrometry. The samples consisted of five ink lines drawn on a piece of writing paper (10 x 10mm). Although a clear difference can be seen between these samples, the lack of structure in the spectra is evident. This broadening effect that was observed for solid samples could be overcome by the use of suitable 'white' (non-absorbing) diluents, i.e., the lack of spectral structure appears to be an absorption saturation effect. This effect is well demonstrated in the spectra obtained from spots of coloured materials on thin-layer chromatography (TLC) plates where the diluent was the substrate, silica gel. An additional problem encountered with the materials presented for investigation with the spectrometer was the lack of suitable standards for quantitative analysis. Although attempts were made to produce a range of concentrations of different materials in magnesium oxide, it was not possible to produce an homogeneous mixture such that successive loadings of the mixtures gave a uniform surface concentration, i.e., poor reproducibility was obtained. However as part of the study for L.G.C. a series of TLC plates containing spots of different materials were supplied. Well-resolved optoacoustic spectra (Figs. 5.14, 5.15) were obtained from spots that contained less than 200ng of material. These samples thus suggested a method of obtaining a series of measurements at different concentrations with relatively small quantities of material. The spectra in Figs 5.14 and 5.15 were obtained by scraping all of the TLC substrate containing the sample spot off the plate and placing this on the silica sample plate in the optoacoustic cell. It was also established, by running a 'blank' of the substrate containing no sample material, that this had a negligible absorption in the region 400 - 700nm but did show increasing absorption in the ultraviolet

Fig. 5.12 Transmission spectrum of diluted whole blood.

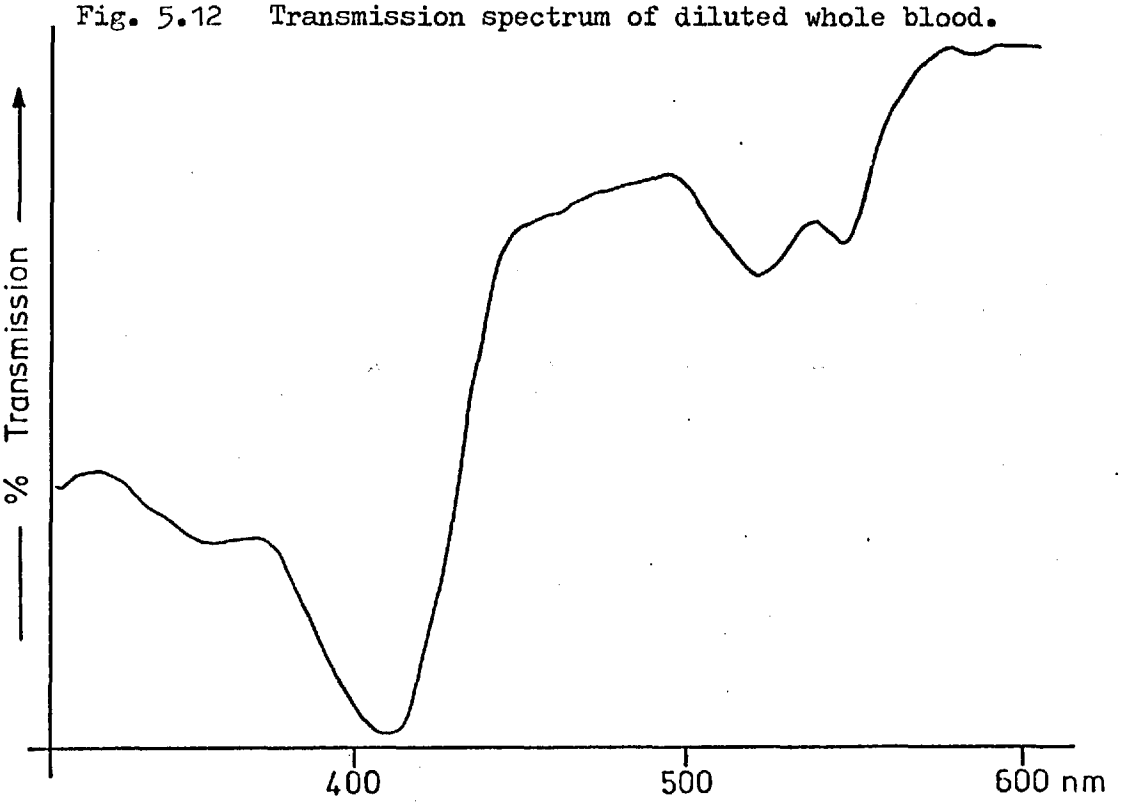

Fig. 5.13

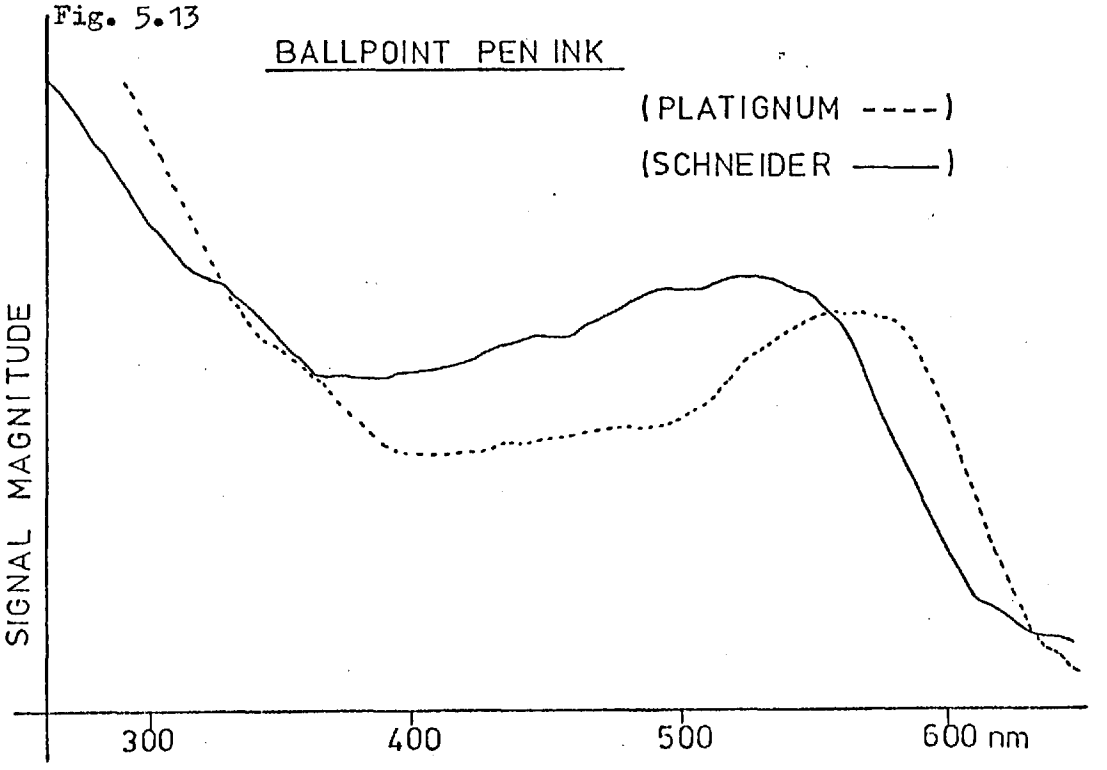

Fig. 5.14 Corrected optoacoustic spectra of TLC spots containing:

(a) ROSE BENGAL

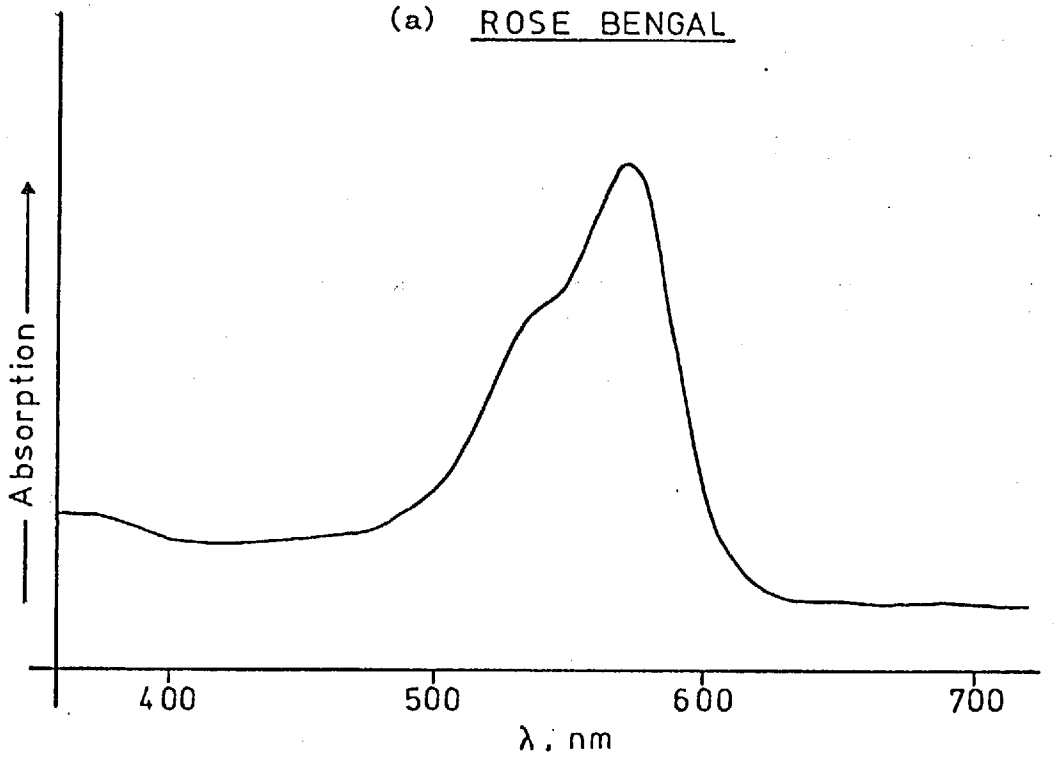

(b) 2,7 - DIIODOFLUORESCEIN

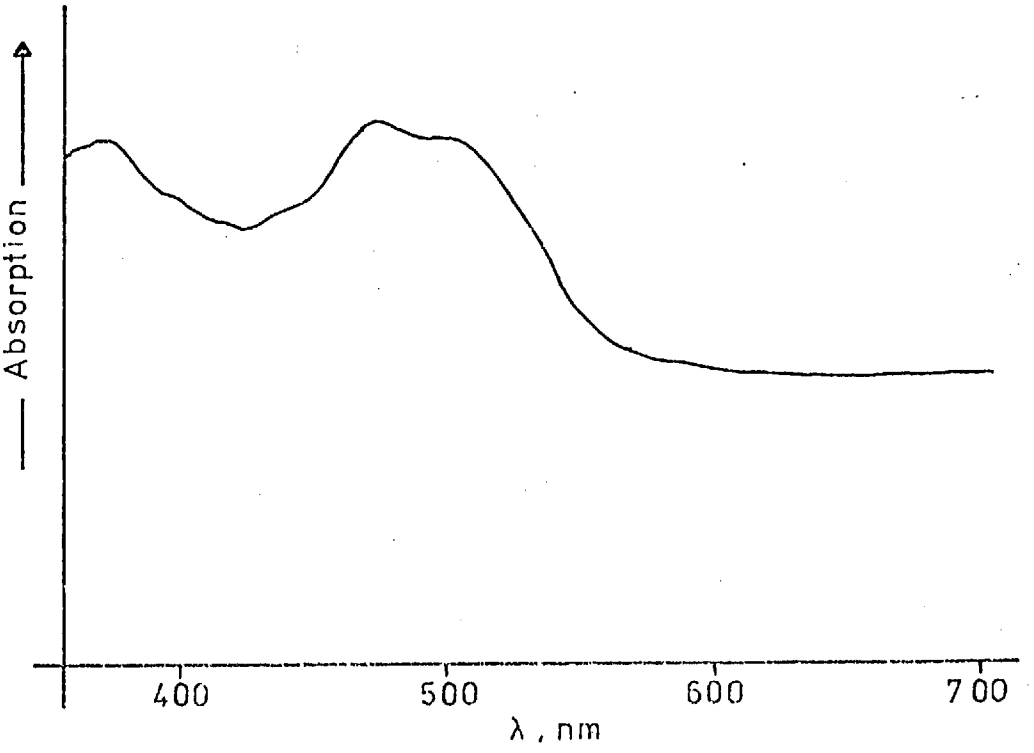

Fig. 5.15 Corrected optoacoustic spectrum of a TLC spot containing:
FLUORESCEIN

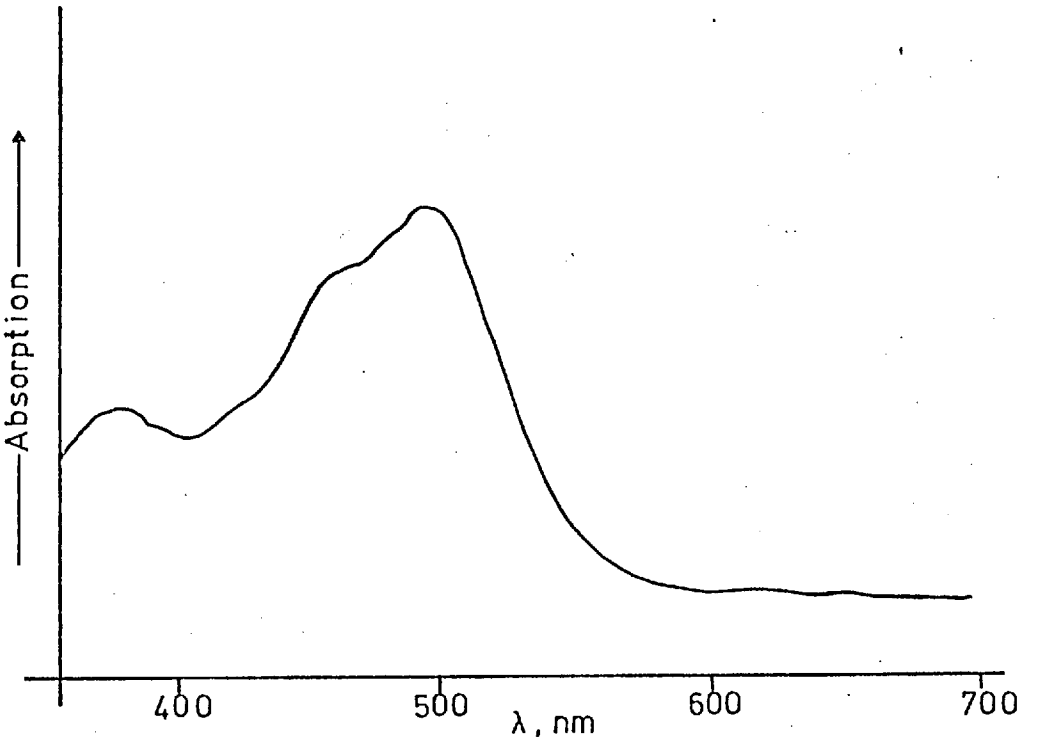

Fig. 5.16

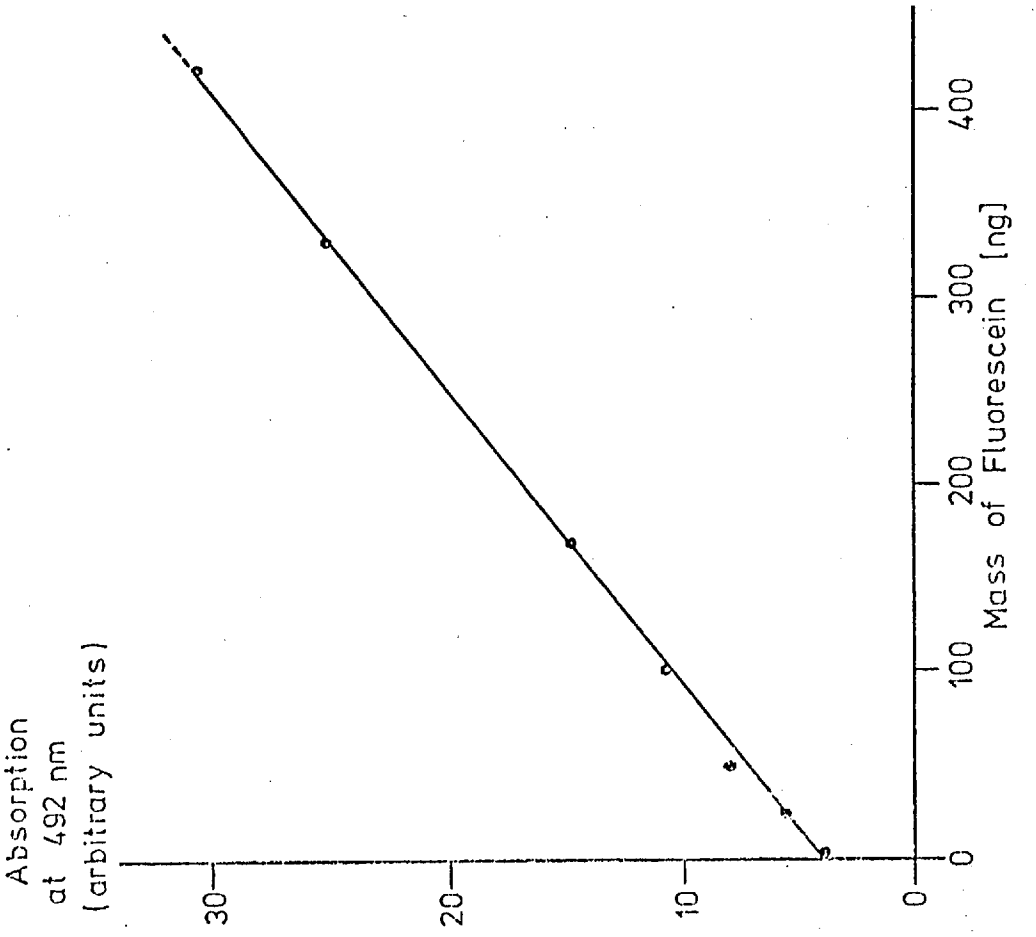

region below 400nm.

5.4.1. Thin-Layer Chromatography.

The quantitative evaluation of thin-layer chromatograms has traditionally used the techniques of reflectance or transmission spectrometry (13,132). The TLC spots are either scraped off, eluted and determined photometrically, or are evaluated in situ. In the latter technique the spot is scanned by a slit whose width can be adapted to the diameter of the spot. The area enclosed by the absorption versus location curve and the baseline is used as a measure of concentration. A comparison of reflectance versus transmittance measurements in situ on thin-layer chromatograms has been made by several workers (133-136). In general, these researchers have concluded that reflectance offers advantages over transmittance when the absorbent is strongly scattering and has high transmission losses. Reflectance spectroscopy has also been shown to be less sensitive to layer variations than transmittance (137). In order to quantify the data obtained by reflectance spectroscopy, using the Kubelka-Munk equation, it is necessary for an infinite layer optical thickness to exist for the sample (13). Although Kortüm (15) reported that a layer at least 1mm thick of powder with a particle diameter of about 1μm is needed to achieve infinite layer thickness, it was found (138) that the portion of visible light that can penetrate a compressed layer of silica gel of 0.4mm thickness is negligibly small for analytical purposes. Therefore, there is minimal interference from the sample support. However, for filter paper chromatograms (138) or silica gel layers (139) of 160μm (a realistic plate-layer thickness) the effect of the backing material is appreciable. The use of white backing paper inserted behind the plate as a reflecting background has, therefore, been recommended if spectra are to be recorded directly from

the plate and in the visible region of the spectrum (140). The light that would otherwise be absorbed by the background is now reflected back through the plate, which results in an enhancement of the signal. The Kubelka-Munk theory will not be valid under these conditions, and this has resulted in semi-empirical approaches to the direct evaluation of chromatograms (141).

Rosencwaig (142) reported that optoacoustic spectra could be obtained from TLC spots in the ultraviolet-visible region. A detection limit of approximately 100ng was reported for benzylidene acetone. The high sensitivity obtained with these samples may be attributed to the large surface area of the sample spot when coated on to the TLC substrate.

The TLC plates used in this investigation consisted of glass microscope slides coated with a silica substrate (Type GF254, Merck, Germany) using a calcium sulphate binder. The absorbing species spotted on to the plates was fluorescein (Acid, Hopkin & Williams, Chadwell Heath, Essex). A series of solutions of fluorescein in ethanol were pipetted (1µl) on to the TLC plate such that a range of sample spot weights between 10 and 450ng were obtained. The spots were developed with an ethyl acetate/acetone mixture (2:1 V/V) and the plates were then air-dried at room temperature. The developed spots were located with the aid of an ultraviolet source (a mercury vapour lamp) and then scraped off into the optoacoustic cell. The optoacoustic spectrum was measured for each spot. A graph of the optoacoustic signal amplitude at the absorption maximum (492nm) for fluorescein versus the mass of material expected in the developed spot was plotted (Fig. 5.16). It can be seen that a linear plot was obtained. The minimum detectable mass of fluorescein was found to be ca. 20ng; this limitation being due to the signal-to-noise ratio of the equipment. It was established, by comparing the signal amplitudes from both the initial and the developed spots that all of the

material was recovered on developing the chromatogram and scraping off the spot, within the limits of the experiment. However, on running a number of calibration plots using different TLC plates, it was noted that poor reproducibility was obtained for a measurement at a given sample mass; typically $\pm 8\%$. The variation in signal amplitude obtained for spots of the same initial sample mass was found to correlate with the variation in the thickness of the TLC substrate (about 0.1 - 0.5mm). Thus, for a 'thick' TLC plate a lower signal amplitude was recorded, than would be the case for a 'thin' plate, due to the smaller surface area of substrate containing the sample.

5.4.2. One-dimensional Polymer.

The optical properties of partially and fully polymerised crystals of the bis (p-toluene sulphonate) ester of 2,4-hexadiene-1,6-diol (TSHD) have been examined and discussed by Bloor et al (143 - 145). TSHD exists in a liquid crystal form at room temperatures, forming graded droplets having a terracelike surface. This material is not isotropic and spurious absorption lines are observed at low temperatures due to the intense 'Brewster's brush' associated with the dispersed optic axes of the pleochroic, partially polymerised crystals. The TSHD studies were conducted using either transmittance or reflectance spectroscopy; however, the latter required a Kramers-Konig analysis (16) with all the consequent approximations.

The optoacoustic studies were conducted on samples of the TSHD crystal and polymer (supplied by C.Hubble, Physics Dept., Queen Mary College). The optical properties of these materials result in pseudo-absorption occuring due to optical interference as well as the true absorption of radiation due to the TSHD molecule. Optoacoustic spectrometry permits the absorption spectrum of TSHD to be measured with freedom

Fig. 5.17 Corrected optoacoustic spectrum of bis (p-toluene sulphonate) ester of 2,4-hexadiene-1,6-diol as the (a) polymer and (b) crystal.

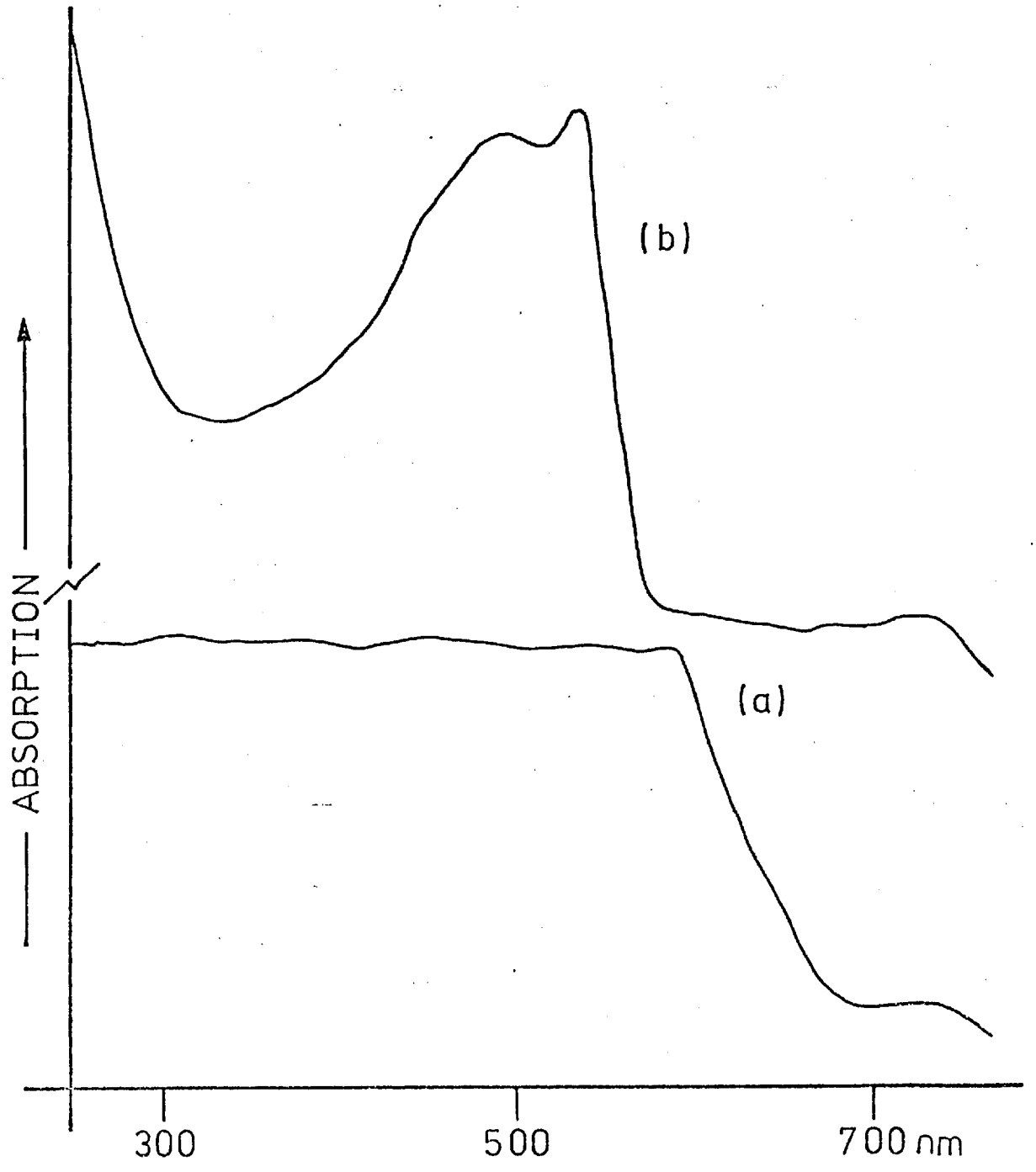

from these effects as only the absorbed component of the incident radiant energy is measured (Fig. 5.17). In the polymer spectrum (Fig. 5.17a), the absorption is due to the polydiacetylene chains. In the crystal spectrum (Fig. 5.17b), the absorption bands are better defined and were found to be optically active. Using the natural polarisation of radiation by the spectrometer optics, e.g., by reflection at the grating, it was found that the relative intensities of the bands at ca. 500 and 540nm were altered upon rotation of the crystal sample relative to the monochromator slit image. Results employing polarising filters at the exit slit of the monochromator confirmed these initial findings.

5.4.3. Thin-film Studies.

The optoacoustic effect has been employed as a calorimetric technique for the determination of the absorption characteristics of the coatings applied to optical components employed in laser technology (114,117). Several workers have employed this technique for the determination of low absorption coefficients of optical materials, using laser sources.

The samples investigated in this work consisted of infrared quality silica discs coated with a zinc sulphide layer of 1.1 and 1.2μm thickness (Standard Telephones and Cables Ltd., Harlow, Essex). The optoacoustic spectra were obtained directly from the samples with the coated surface uppermost (Fig. 5.18). It can be seen that upon comparison of these spectra with that obtained by transmission spectroscopy (Fig. 5.19) employing a Perkin-Elmer Model 124 spectrophotometer for the 1.2μm thickness sample, that although both types of spectrum contain the same essential absorption characteristics the transmission spectrum has interference fringes superimposed. These result from the constructive

Fig. 5.18 Corrected optoacoustic spectra of silica coated with ZnS:
(a) 1.1μm thick (b) 1.2μm thick

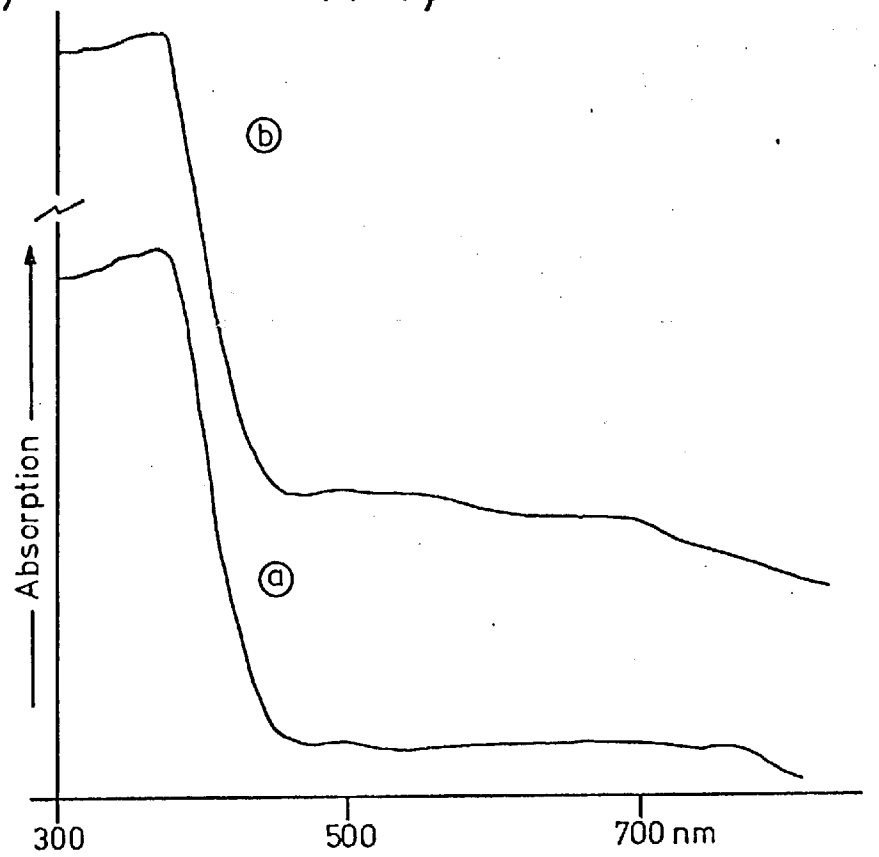

Fig. 5.19 Transmission spectrum of sample (b).

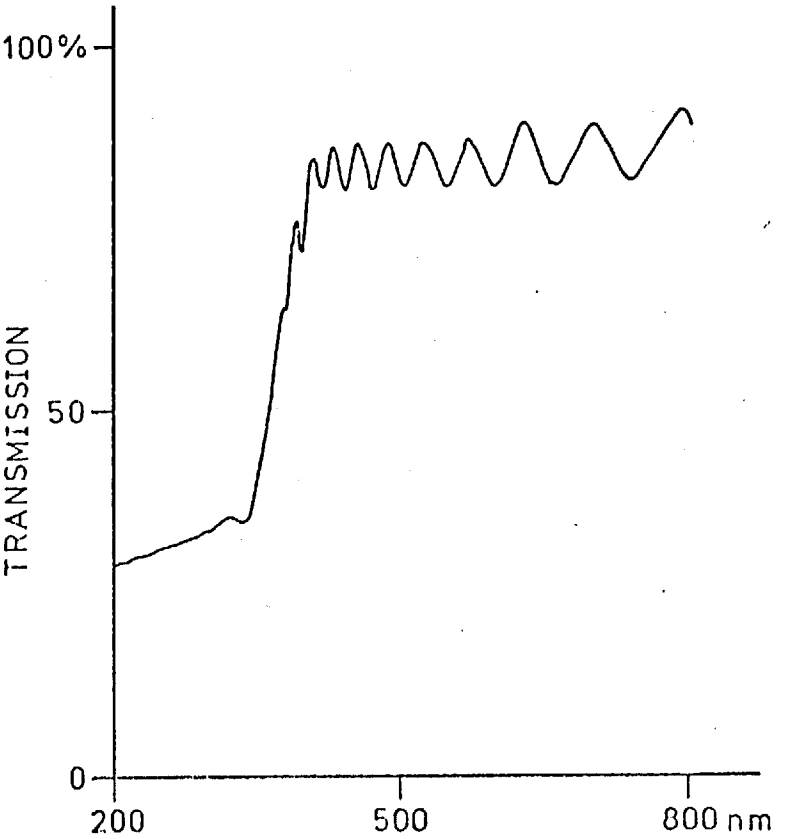

and destructive combination of radiation (1) reflected from the air/film and film/silica substrate interfaces. The freedom of the opto-acoustic spectra from this effect is again due to the fact that only absorbed radiation can give rise to a signal; the interference phenomena results from non-absorbed radiation.

The absorption band edge observed in Fig. 5.18 is characteristic of a semiconductor material. The spectral position of this band edge can be used to determine the energy necessary to transfer an electron from the top of a filled valence band to the bottom of a higher conduction band (146). The extremely high absorption coefficients encountered with solid semiconductors in the ultraviolet-visible region make transmission measurements impractical in many cases, thus much of the work on the determination of band gaps involves the analysis of normal incidence reflectance data (147) using the Kramers-Konig relations. It was found that the optoacoustic spectra of semiconductors, such as a powder sample of zinc sulphide which gave an identical spectrum to that in Fig. 5.18, gave band edge values which were in good agreement with the values obtained by reflectance techniques. Rosencwaig (52) has determined the optoacoustic spectra of several semiconductors which also gave band edge values in agreement with those published in the literature.

5.5. Improvements in Instrumentation.

In much of the work discussed above, the signal-to-noise ratio present in the corrected optoacoustic spectra was a limiting factor upon the sensitivity of the technique. The possibility of improvement in the signal-to-noise ratio was examined by both decreasing the noise level and increasing the signal amplitude.

The noise level was reduced by mounting the spectrometer on vibration isolators (Type S.A.25, S.A.V.E. (Acoustics) Ltd., Weybridge,

Surrey), which were mechanical spring mountings placed under each corner of the spectrometer. This had little effect upon the continuous background noise, but did reduce the noise 'spikes' observed at the low modulation frequencies employed in this work. These 'spikes' were due to the microphone transducer detecting building vibrations, e.g., from slamming doors, that were conducted through the spectrometer housing and optoacoustic cell material.

The signal amplitudes measured for weakly absorbing samples were improved by altering the ratio of the beam-splitting arrangement such that a higher intensity of radiation was focused on to the sample. A pyroelectric detector was employed as the reference channel. The pyroelectric detector (Eltec type 404CM, Rofin Ltd., Egham, Surrey) had an active detector element of lithium tantalate (2mm diameter) which was black coated. The small detector area and high sensitivity of the device (see Appendix I) allowed a beam split of approximately 5:1 (sample:reference channel) to be achieved. The pyroelectric detector, which had a sapphire window, was mounted inside a stainless steel housing which had a silica entrance window (20mm diameter, 1.5mm thickness). This housing protected the detector both from microphonic pick-up and changes in the ambient temperature which affect the sensitivity of the device. In addition, the silica window was coated with a black paint apart from a central hole of approximate diameter 1mm. This limiting aperture was necessary as not all of the lithium tantalate was coated black, only the central region. Thus, any radiation incident upon the unblackened detection element would result in a wavelength dependent response for the detector. The circuit diagram of the power supply and the connections for the pyroelectric detector are shown in Fig. 5.20.

The double-beam optoacoustic spectrometer employing the pyroelectric detector was observed to have a similar flatness response

Fig. 5.20 Pyroelectric detector.

(A) Power supply unit.

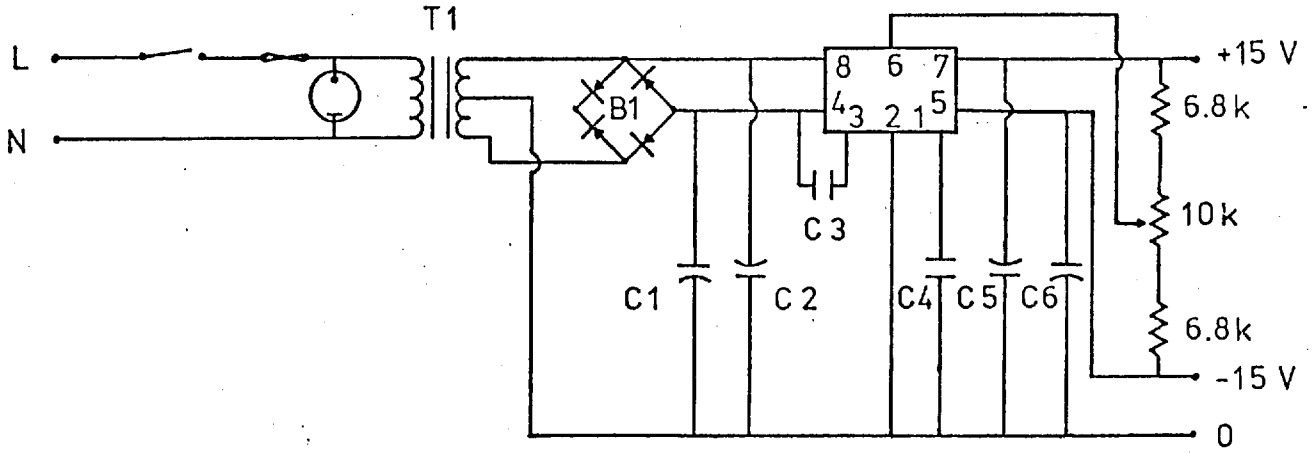

T1 6VA Transformer (15-0-15)

B1 Diode bridge rectifier (1A, V_{RRM} 400V)

C1, C2 1000uF, 25V

C3, C4 0.1uF

C5, C6 10uF, 25V

(B) Connections.

Pin connection numbers refer to the standard TO-99 housing employed for the detector. Pins 7 & 8 were both connected to the 0-line of the power supply.

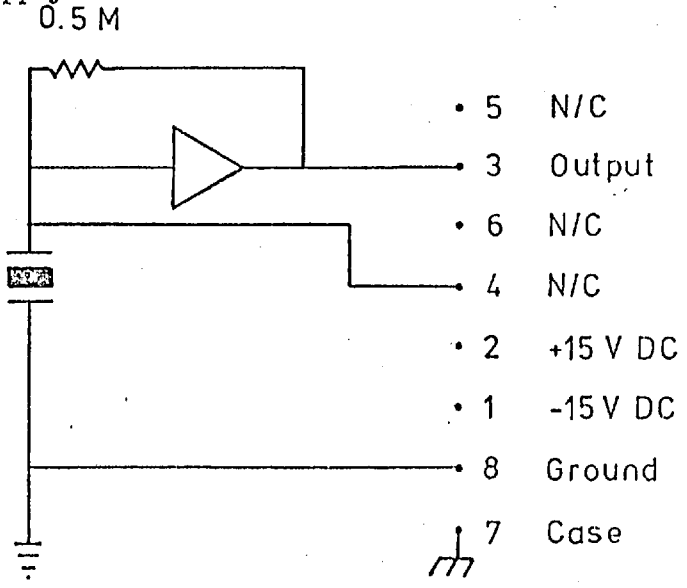

curve when the signal obtained from an optoacoustic cell containing carbon black was ratioed against that from the pyroelectric detector, i.e., a similar black-body response was observed for each detector.

5.6. Application to the Study of Dielectric Coatings for Laser Mirrors.

Employing the experimental system described above, the initial study of thin films of zinc sulphide was extended to multilayer, dielectric coated laser mirrors. The laser mirror samples were supplied as 50mm square, 1mm thickness, flat plates (Leybold-Heraeus Gmbh, Hanau, W. Germany); 16mm diameter discs were cut from these for analysis. Four samples were examined. Two of these samples were of a multilayer composition consisting of alternate layers of titanium dioxide and silicon oxide on a glass substrate, the third sample comprised a single coating of titanium dioxide and the fourth sample examined was the uncoated glass substrate.

The optoacoustic spectra, transmission spectra and reflectance spectra of the samples were obtained with the double-beam optoacoustic spectrometer. The optoacoustic spectra were obtained by placing the sample discs on the silica tray and sealing the cell. The transmission spectra were obtained by using the optoacoustic cell, containing a carbon black sample prepared by smoking a glass plate, to detect the radiation transmitted by the samples which were positioned above the cell. The entrance windows to the optoacoustic cell were masked to ensure that only radiation transmitted by the sample entered the cell and produced a signal. The zero and 100% transmission levels were set by blanking off the sample-beam and having no sample present, respectively. The reflectance spectra of the samples were obtained in a similar manner, employing the optoacoustic cell as a radiometric detector. The samples were mounted on to a black, non-reflecting cloth and positioned over the

mirror employed to direct the radiation from the exit slit of the monochromator down into the optoacoustic cell. Thus, only radiation reflected by the sample entered the optoacoustic cell containing a carbon black sample.

The spectra of the four samples examined (Figs. 5.21, 5.22) were obtained with a spectral half band-width of 10nm within the wavelength range 300nm to 650nm. A scan-rate of 50nm min^{-1} was employed with an instrumental time-constant of 3 seconds. The rare-earth oxide, holmium oxide, was employed for wavelength calibration of the optoacoustic spectrometer. The optoacoustic (——), transmission (- - -), and reflectance (. . .) spectra of the four samples (Figs. 5.21, 5.22) may be considered for comparison purposes in three wavelength regions; the ultraviolet (300nm - 400nm), the blue (400nm - 550nm) and the red (550nm - 650nm) regions.

Fig. 5.21A shows the spectra obtained from the uncoated glass substrate. The reflectance spectrum exhibits a high specular component because of the optically-flat nature of the sample and little spectral detail is available. Both the optoacoustic spectrum and transmission spectrum show similar ultraviolet absorption by the glass. The optoacoustic spectra obtained from the glass blank were found to be identical irrespective of which surface was examined.

The spectra from the titanium dioxide coated glass is shown in Fig. 5.21B. An ultraviolet absorption band is shown in both the transmission spectrum and the reflectance spectrum. At longer wavelengths the spectrum is complicated by the apparent absorption maxima produced by the appearance of an interference pattern. The optoacoustic spectra are more simple. In the ultraviolet region the absorption band edge characteristic of titanium dioxide (a semiconductor) is observed, with a cut-off at ca. 380nm, upon examining the top, coated surface of the

Fig. 5.21 Laser mirror samples.

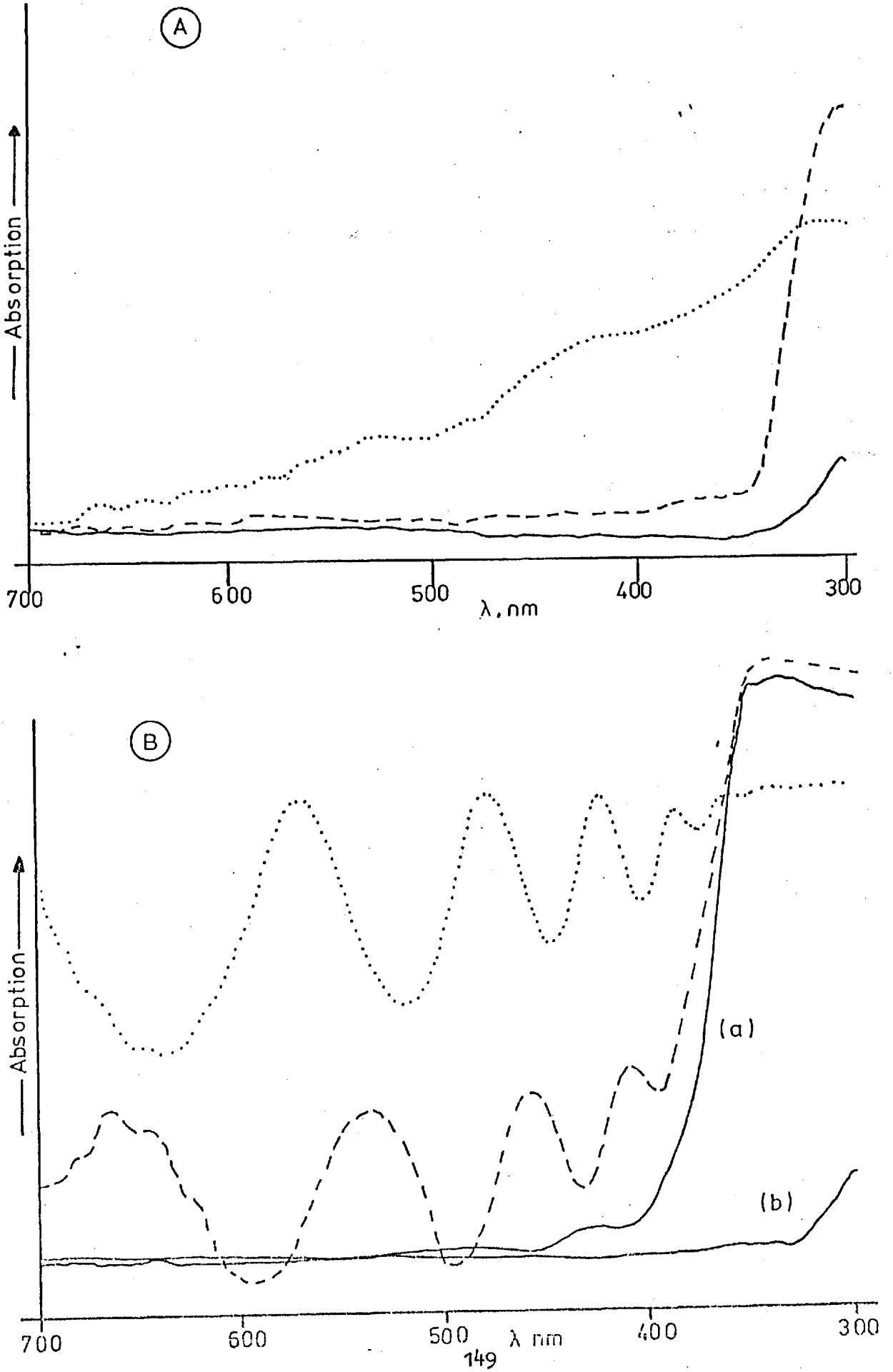

Fig. 5.22 Laser mirror samples.

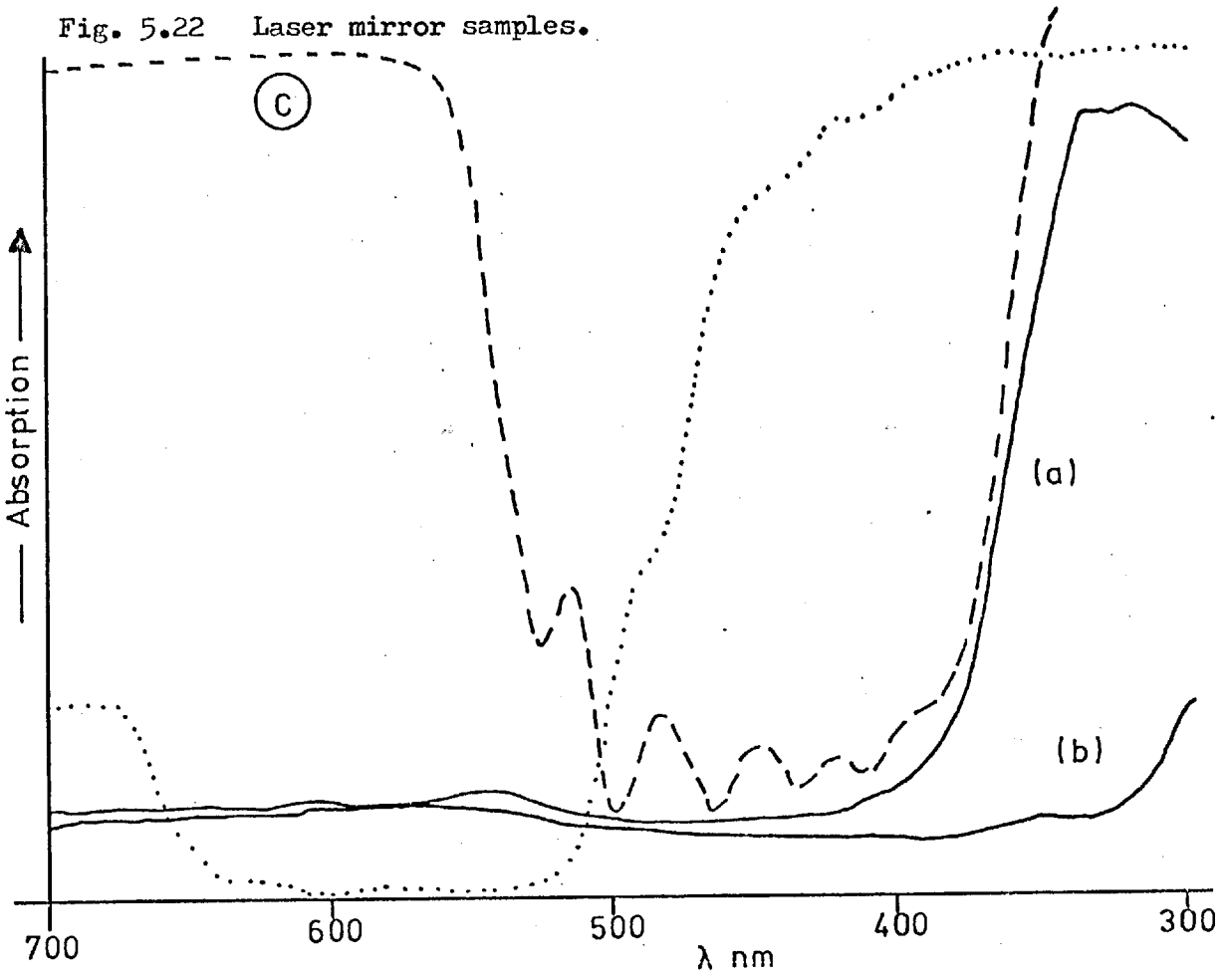

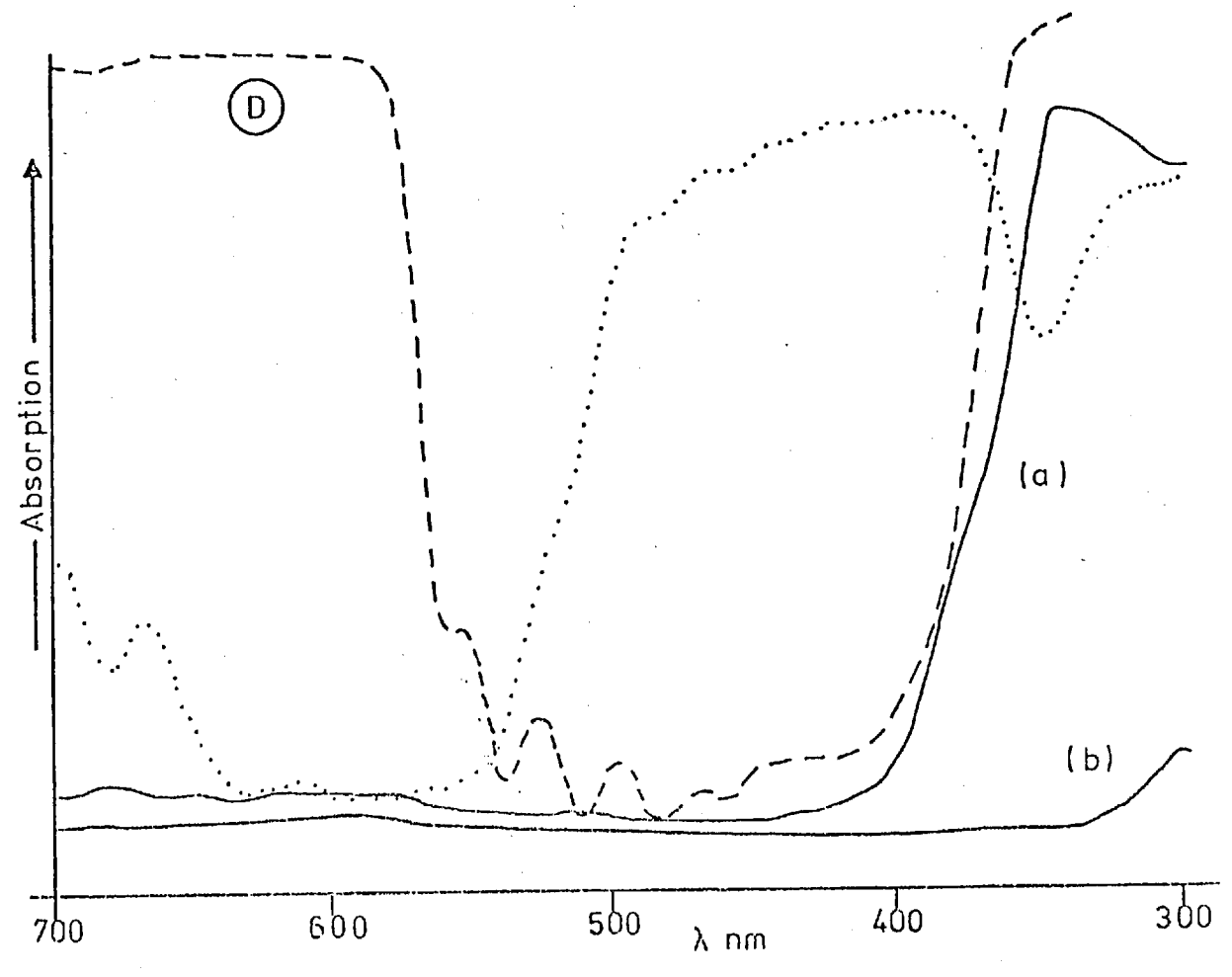

glass (spectrum a). When the uncoated glass surface is examined (spectrum b) only the glass substrate absorption spectrum is obtained.

Fig. 5.22A shows the spectra obtained from a dielectric-coated laser mirror. The sample is shown to be highly reflecting in the red region but to have apparently high absorption characteristics in the blue and ultraviolet spectral regions in the reflectance spectrum. The alternate coatings of the dielectric layers are responsible for the interference pattern. The transmission spectrum exhibits apparent absorption bands in the red and ultraviolet regions. The interference pattern caused by the multilayer coating is evident. The optoacoustic spectrum of the coated glass surface illustrates that strong absorption, characteristic of titanium dioxide, occurs only in the ultraviolet region. At wavelengths greater than 400nm there is relatively little absorption. The optoacoustic spectrum obtained when the rear uncoated surface is illuminated directly (b) shows again the weak ultraviolet absorption by the glass substrate.

The spectra of a second laser mirror (Fig. 5.22B) shows the complementary nature of the reflectance, transmission and optoacoustic spectra and is similar to Fig. 5.22A. As before, the optoacoustic spectrum of the coating or substrate may be obtained by simply reversing the sample to illuminate the appropriate surface. The interference effects of the multilayer coatings are not observed in the optoacoustic spectrum as the apparent absorption produced is not actually responsible for the absorption of any radiant energy.

Although the transmission and reflectance spectra differ for samples 5.22A and 5.22B, it is apparent from the optoacoustic spectra that this difference is a function of the thickness and separation of the dielectric layers and is not due to the nature of the absorbing titanium dioxide.

5.7. Conclusion.

In this chapter the construction of a double-beam optoacoustic spectrometer is described. This instrument enables the spectra of solid and liquid samples to be studied in the ultraviolet- visible region of the spectrum. The initial evaluation of sources that was made led to the choice of a 300W xenon arc continuum source. This unit is of much lower power than those reported by other workers (5, 91) and that employed in earlier work. Because of the integral parabolic reflector of the source, however, the collected radiation output from the source is as great as that available from the 1kW source previously employed. Gelbwachs (148) has recently presented a comparison of sources in the ultraviolet-visible spectral region for optoacoustic spectrometry. The xenon arc is shown to be an intense source of continuum radiation in this spectral region.

The twin-cell arrangement, initially employed with this spectrometer, provides the opportunity of recording difference spectra; this is an important function for a great deal of quantitative work. The use of a pyroelectric reference detector does not allow difference spectra to be recorded but does improve the sensitivity obtained due to the increased power incident upon the sample. Other workers have obtained corrected optoacoustic spectra by the use of a pyroelectric detector (149) or by digital recording of a reference spectrum prior to examination of the sample material (52, 150).

From the spectra presented above, it is evident that optoacoustic spectrometry is a complementary technique to the conventional techniques utilising transmission and reflectance spectra. As only radiant energy absorbed by the sample may produce an optoacoustic signal the technique may be employed as a rapid calorimetric method of analysis.

Unlike the more conventional calorimetric methods involving

the use of temperature transducers (120) to monitor directly the variations in temperature of a sample following the absorption of radiant energy, optoacoustic spectrometry employs a microphone to monitor the pressure changes in the cell caused by the changes in the temperature of the sample. As direct contact between the transducer and sample is not necessary, a wide variety of sample types may be examined with little difficulty. The use of an indirect method for temperature also provides the technique with the capability for the examination of surfaces, as shown above. The sample depth examined is a function of the optical absorption coefficient of the material under study and its thermal characteristics. This depth may be selected and controlled as was described in Chapter Four. The spectra of the laser mirrors discussed above demonstrates how by reversing the sample the spectrum of either the dielectric coating or the substrate may be obtained.

CHAPTER SIX

OPTOACOUSTIC SPECTROMETRIC STUDIES IN THE NEAR-INFRARED REGION

6.1. Introduction.

The near-infrared spectral region is usually considered to lie between 0.7μm and about 3μm. However, from the theoretical viewpoint, the upper wavelength limit may be set near 2.5μm and near-infrared spectroscopy may be defined then as the study of low-energy electronic transitions and overtones and combinations of hydrogenic (principally C-H, N-H and O-H) stretching and bending vibrations (151).

Near-infrared spectroscopy is primarily a quantitative rather than a qualitative technique (10). However, it is employed for the characterisation of rare-earth (130) and transition metal (152) ions. Quantitative applications include the determination of water, alcohols, phenols, amines, unsaturated hydrocarbons, and other classes of compounds containing hydrogenic groups (153,154).

6.1.1. Theory.

In Chapter One, it was stated that the frequency of an infrared absorption band is dependent upon the masses of the atoms involved in the vibration and the force constant of the interatomic bond (Equation 1.3). To a first approximation, a molecular vibration is analogous to a linear harmonic oscillator in which the restoring force acting upon the vibrating masses is proportional to the displacement of the masses from the equilibrium positions. Quantum mechanical treatment of a strict harmonic oscillator yields the equation

$$E = (v + 1/2)h\,c\,\nu \qquad \ldots 6.1$$

where E is the vibrational energy; v is the vibrational quantum number which can assume integer values of 0, 1, 2, 3, ...; ν is the fundamental vibration (cm^{-1}); h is Planck's constant; and c is the velocity of light (151). The oscillator can reside only in energy levels that are equally spaced and separated by $h\,c\,\nu$. Transitions between

nonadjacent energy levels and interaction between different oscillators are forbidden by selection rules. Thus, if molecular vibrations were strictly harmonic, the vibrational spectrum of a compound would consist only of those bands corresponding to the fundamental modes of vibration.

Actual molecular vibrations are not strict harmonic oscillators. As a result, their energy levels are not equally spaced, transitions between nonadjacent energy levels are allowed, and interaction between vibrations are possible. The energy levels are given by

$$E = h c \nu \left[(v + 1/2) - x(v + 1/2)^2\right] \quad \ldots 6.2$$

where x is the anharmonicity constant (11). The energy difference between states v and v - 1 is then $h c \nu (1 - 2v x)$. Transitions between the ground state (v = 0) and the first, second or higher excited states (v = 1, 2, 3, ...) give rise to first, second or higher overtone bands at wave numbers slightly less than two, three, or more times the wave number of the fundamental vibration. Interaction between vibrations gives rise to combination bands, which result from the absorption of radiation having a wave number slightly lower than the sum of the wave numbers of two fundamental vibrations.

The accurate determination of anharmonicities requires that higher-order terms be added to Equation 6.2. A detailed discussion of this subject has been given by Herzberg (155).

The probability of a transition between two energy levels becomes progressively less for Δv values of 1, 2, 3, ..., etc. (151). Consequently, a first overtone band is generally an order of magnitude less intense than a fundamental band. Second and higher overtone bands are correspondingly less intense than the preceeding overtone band. The intensities of simple binary combination bands are of the same order of magnitude as those of first overtone bands. Higher-order combination

bands have intensities comparable to those of second and higher overtone bands.

6.1.2. Applications.

Although applications based upon low-energy electronic transitions in the near-infrared region to aid characterisation of inorganic species are well documented in the literature (156 - 158) the work presented in this thesis is concerned mainly with those compounds giving rise to hydrogenic vibrational absorption bands.

The approximate theoretical wavelengths of some vibrational overtone bands are given in Table 6.I. Goddu et al (159) have compiled an extensive list of spectra-structure correlations and molar absorptivity data in the near-infrared region.

In a diatomic molecule there is only one possible mode of vibration, namely a stretching vibration along the axis of a bond. However, in polyatomic molecules, a second mode of vibration is possible, involving a bending or rocking of a bond between a pair of atoms about the axis joining them to a third atom. Stretching vibrations give rise to absorption between 2 and 10μm (except for heavy halogen atoms), and bending vibrations between 10 and 25μm (11). The overtones of the bending vibrations will occur as very weak bands in the 2 to 10μm region, and will generally be hidden by the much stronger vibrational stretching bands. However, most of the overtones of the fundamental stretching frequencies will occur below 2μm, in a region which is otherwise free from absorption bands. Thus groups having strong fundamental bands in the region 3 to 5μm will give easily detectable overtones in the near-infrared region (10). The most commonly occuring are the carbon - hydrogen group which has its fundamental stretching vibration in the range 3.0 to 3.6μm, and the oxygen - hydrogen group with its fundamental in the

Table 6.I. Approximate theoretical wavelengths of overtones (11).

Group	Overtone	λ	Intensity*	Group	Overtone	λ	Intensity*
		μ				μ	
C—H.....	1	1.7	s	C—C.....	3	1.75	vw
	2	1.1	m		4	1.4	n
	3	0.85	w	C—O.....	3	1.85	w
	4	0.7	vw		4	1.5	vw
O—H.....	1	1.4	s	C=C.....	3	1.5	vw
	2	0.95	m		4	1.2	n
	3	0.7	w	C=O.....	2	1.9	m
	4	0.55	vw		3	1.45	w
N—H.....	1	1.4	m		4	1.15	vw
	2	0.95	w	C≡C.....	2	1.6	n
	3	0.7	vw		3	1.15	vw
	4	0.55	n	C≡N.....	2	1.5	w
S—H.....	1	1.95	w		3	1.1	vw
	2	1.3	vw	C—F.....	4	1.6	vw
C—D.....	2	1.55	s	C—Cl.....	6	1.9	n
	3	1.15	m	Si—H.....	2	1.5	s
O—D.....	2	1.45	m		3	1.15	m
	3	1.1	w	P—H.....	2	1.4	w
N—H.....	2	1.35	w		3	1.05	vw
	3	1.0	vw				

* Relative intensities: s, strong; m, medium; w, weak; vw, very weak; n, not detectable or extremely difficult to detect.

range 2.7 to 2.9μm. Both of these groups give relatively strong overtones below 2μm (see Table 6.I). A nitrogen - hydrogen group with its fundamental at 2.7 to 2.9μm, and a sulphur - hydrogen group with its fundamental at about 3.9μm will give weaker overtones, since the intensities of the fundamentals are less.

The single-bond carbon - carbon and the carbon - oxygen stretching vibrations give bands at 6.9 to 7.3μm and 7.1 to 7.9μm respectively, and the band of the former is less intense. Thus, only the third and higher overtones will occur below 2μm and such overtones are quite weak (11). A carbon - carbon double bond absorbs at 5.95 to 6.15μm with low intensity, so that its third overtone will occur as a very weak band below 2μm. However, the carbon - oxygen bond, with an intense fundamental at about 5.8μm, will have its second overtone just below 2μm and thus be more easily detectable. Carbon - carbon triple bonds or carbon - nitrogen triple bonds absorb very weakly at about 4.5μm, and although their second overtones will occur below 2μm, they will not be of appreciable intensity.

The heavy halogen atoms have very intense fundamental stretching vibration intensities with carbon which occur at 8.0 and 14.0μm for fluorine and chlorine respectively, so the bands that would be observed in the near-infrared region would be those due to the fourth and sixth overtones respectively, and hence very weak. Silicon - hydrogen and phosphorus - hydrogen bands have fundamentals at 4.35 to 4.75μm and 4.1 to 4.25μm respectively, and their second overtones should be found below 2μm.

As previously mentioned, the C-H group is characterised by fundamental stretching bands in the range of 3.0 to 3.6μm, combination bands between 2.0 and 2.4μm, first overtone stretching bands between 1.6 and 1.8μm and second overtone stretching bands in the region of

1.1 to 1.2μm (11). Higher order combinations give rise to other weak bands throughout the near-infrared region. Miller and Willis (160,161) have discussed the determination of the terminal methylene group as an estimation of monomer in polymers using the 1.6μm band. Holman and Edmondson (162) have reported a technique for distinguishing between cis- and trans- isomers of olefins. The cis-olefins exhibit characteristic absorption bands near 1.18, 2.14 and 2.19μm, whereas the trans-olefins do not have any characteristic bands in the near-infrared region. The spectra of hydrocarbons and their application to analyses in the near-infrared region have been reviewed by Lauer and Rosenbaum (163).

The O-H group exhibits a fundamental stretching band near 2.8μm, first and second overtone bands near 1.4μm and 1.0μm respectively and a combination band near 2.0μm. These bands have been employed in the study of water, alcohols and phenols. In water, the combination band occurs at about 1.9μm and has been widely used for its determination (151,164,165). Hydroxide groups produce a combination band at about 2.2μm, which is particularly useful when the concentration of these groups is such that the fundamental band is too intense for accurate measurement (166). The hydroxyl overtone band at about 1.4μm has been employed for the determination of alcohols (167) and phenols (168).

The fundamental N-H stretching bands of amines, amides and related compounds fall in the region 2.8 to 3.0μm. The first overtone stretching bands occur near 1.5μm and the second overtone stretching bands near 1.0μm; both of these have been employed quantitatively. Whetsel et al (169) have reported the determination of primary, secondary and tertiary aromatic amines using the first overtone and combination bands. Aliphatic N-H stretching vibrations are unique in that the intensities of the first overtone bands are of the same order of magnitude as those of the fundamental bands (169). As the fundamental

bands are comparatively weak compared to those of aromatic amines, the first overtone region is particularly useful for the quantitative analysis of aliphatic amines (170). The single, intense N-H band between 1.44 and 1.47μm of heterocyclic amines, such as pyrroles, indoles and carbazoles, has been used for both their quantitative and qualitative determination (171). The spectra of amides, arising from their N-H vibrations, are similar to those of amines though they may be more complex because of the possibility of an enol- as well as a keto-form (172).

Although the above studies in the near-infrared region were conducted using transmission spectroscopy, recent work has used reflectance techniques. This work has been concerned with the analysis of agricultural products (72,173), especially the determination of the protein content of wheat (174). Ahmed and Goldstein (175) have applied reflectance techniques to the determination of fat in dried milk powders using the first overtone of the C-H stretching vibration, of the methylene groups in fats, at 1.742μm.

It was decided to extend the optoacoustic studies undertaken with the double-beam spectrometer into the near-infrared region due to the relative accessibility of this region (74); i.e., sources and optical materials employed in the ultraviolet and visible regions are also useful in the near-infrared region. The analytical selectivity, and utility, of the technique may also be extended in the near-infrared region due to the relatively narrow, vibrational absorption bands observed compared to the broad, rather featureless, electronic transitions in the ultraviolet-visible region.

6.2. Double-beam Optoacoustic Spectrometer Operation in the Near-Infrared Region.

The only modifications initially made to the double-beam optoacoustic spectrometer described in the previous Chapter were the replacement of the ultraviolet-visible diffraction grating, with a similar grating (50 x 50mm, 300 lines mm^{-1}) blazed at 2.0μm, and different wavelength cut-off filters being positioned at the exit slits of the monochromator. The spectral transmission range of the two filters employed was 0.8μm - 1.4μm (Chance OX5 filter, Ealing Beck Ltd.) and 1.4μm - 2.7μm (Type E9521F filter, Davin Optical Ltd., Barnet, Herts.). The linear reciprocal dispersion at the monochromator exit slits was 12nm mm^{-1} (0.012μm mm^{-1}). In the work described in this section a spectral half-bandpass of 30nm, a scan rate of 150nm min^{-1} and an instrument time constant of 3s were employed with the twin-cell arrangement; a smoked glass plate being used as the reference absorber. The black-body absorption characteristics of this sample were confirmed by comparison of the spectrum with the source emission spectrum obtained with a calorimeter detector, a laser power meter (Model 142 LR, Laser Instrumentation Ltd.) as described by King (86).

The emitted power spectrum of the xenon arc source in the near-infrared region, obtained by single-beam operation of the instrument is shown in Fig. 6.1A. The flatness response, determined by mounting carbon black samples in both cells and measuring the ratio of the output from each when obtained by double-beam operation, is shown in Fig. 6.1A. The efficiency of the beam splitting arrangement, used with the spectrometer in order to produce a uniform response with respect to wavelength, appeared to be satisfactory for double-beam operation in the near-infrared region; typically ±7%. However, it was found that the alignment of the two optical paths in the spectrometer was so critical

Fig. 6.1 (A) Single-beam near-infrared optoacoustic spectrum of carbon black.

(B) Typical flatness response curve for double-beam, carbon-carbon, operation in the near-infrared region.

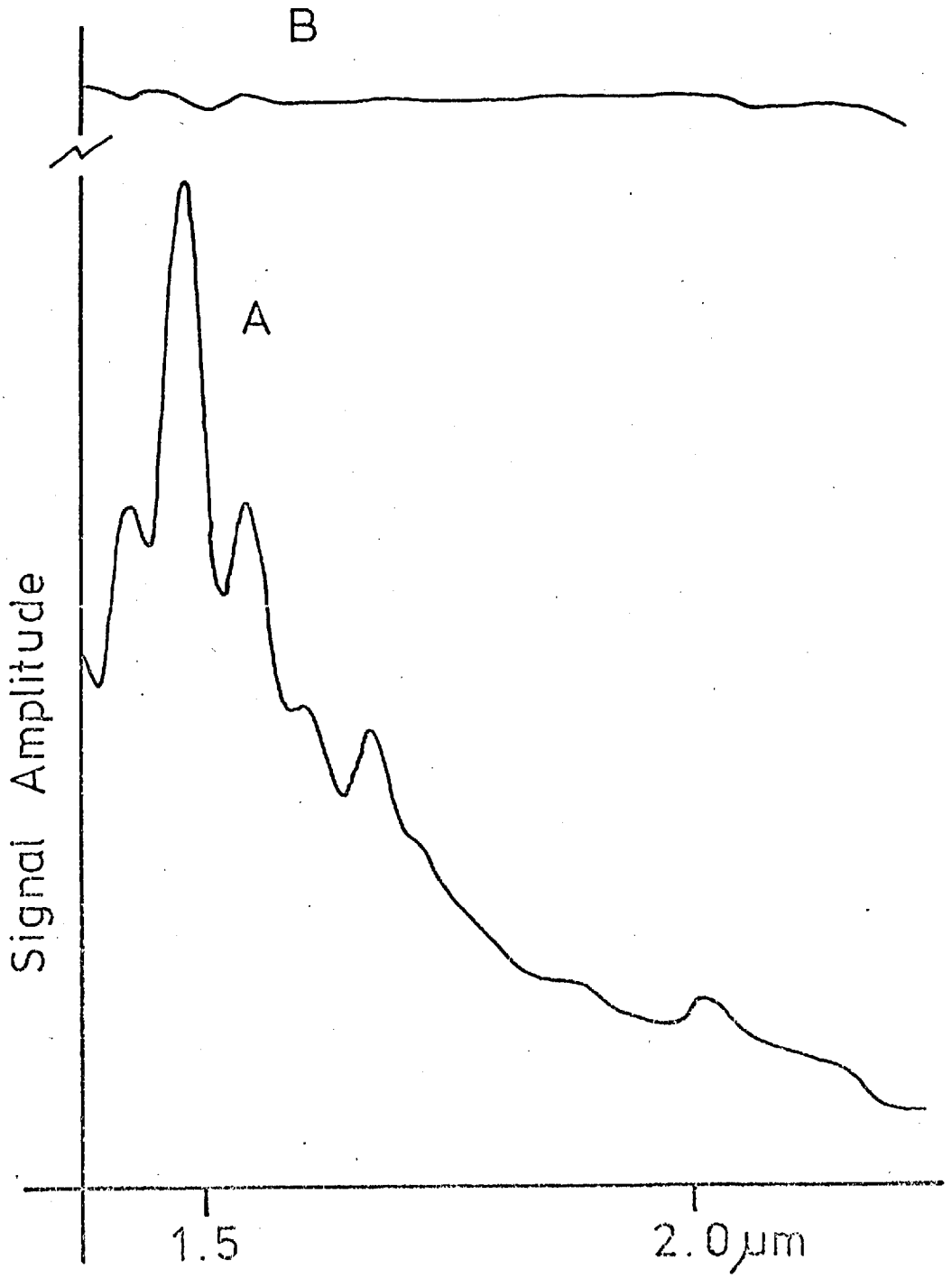

that it was necessary to adjust this each day for satisfactory operation. This variation in the flatness response with time was due to the poor stability of the optical components in the separate radiation paths, principally the monochromator exit slits. This is a well known disadvantage of the double-beam in space arrangement; commercial instruments employ a very rigid base and optical mountings. Since this situation did not arise for double-beam operation in the ultraviolet-visible region, it is likely that the greater spectral detail observed for the xenon arc source in the near-infrared region (Fig. 6.1A) compared to that observed previously (Fig. 5.7A) is responsible.

An additional difficulty encountered in this work arose from the optoacoustic cell employed (Fig. 5.4). It was observed that strong absorption bands were observed in the corrected optoacoustic spectrum of the empty cell near 1.4μm and 1.9μm corresponding to the first overtone and combination bands of water. These bands were also observed when non-absorbing materials, e.g., dried magnesium oxide, were placed in the cell, and in the spectra of absorbing species. In order to determine the origin of this cell 'background' signal, several experiments were tried. The cell was left with the desiccant, silica gel, in the sample tray overnight; the cell background was initially attenuated but soon regained its former value. The interior of the cell was coated with magnesium oxide by burning magnesium ribbon; this did not affect the background signal. A coating of paraffin wax was then applied to the cell walls in case the magnesium oxide contained absorbed water; this did not affect the cell background, but C-H overtone and combination bands were observed. Thus, although the background signal appeared to be due to water in the cell, it was not possible to physically remove this.

This problem was overcome to some degree by the use of the phase-techniques described in Chapter Four. It was observed that upon

Fig. 6.2 Corrected optoacoustic spectrum, in-phase (θ) and out-of-phase ($\theta + 90^{\circ}$) with the reference signal, of:

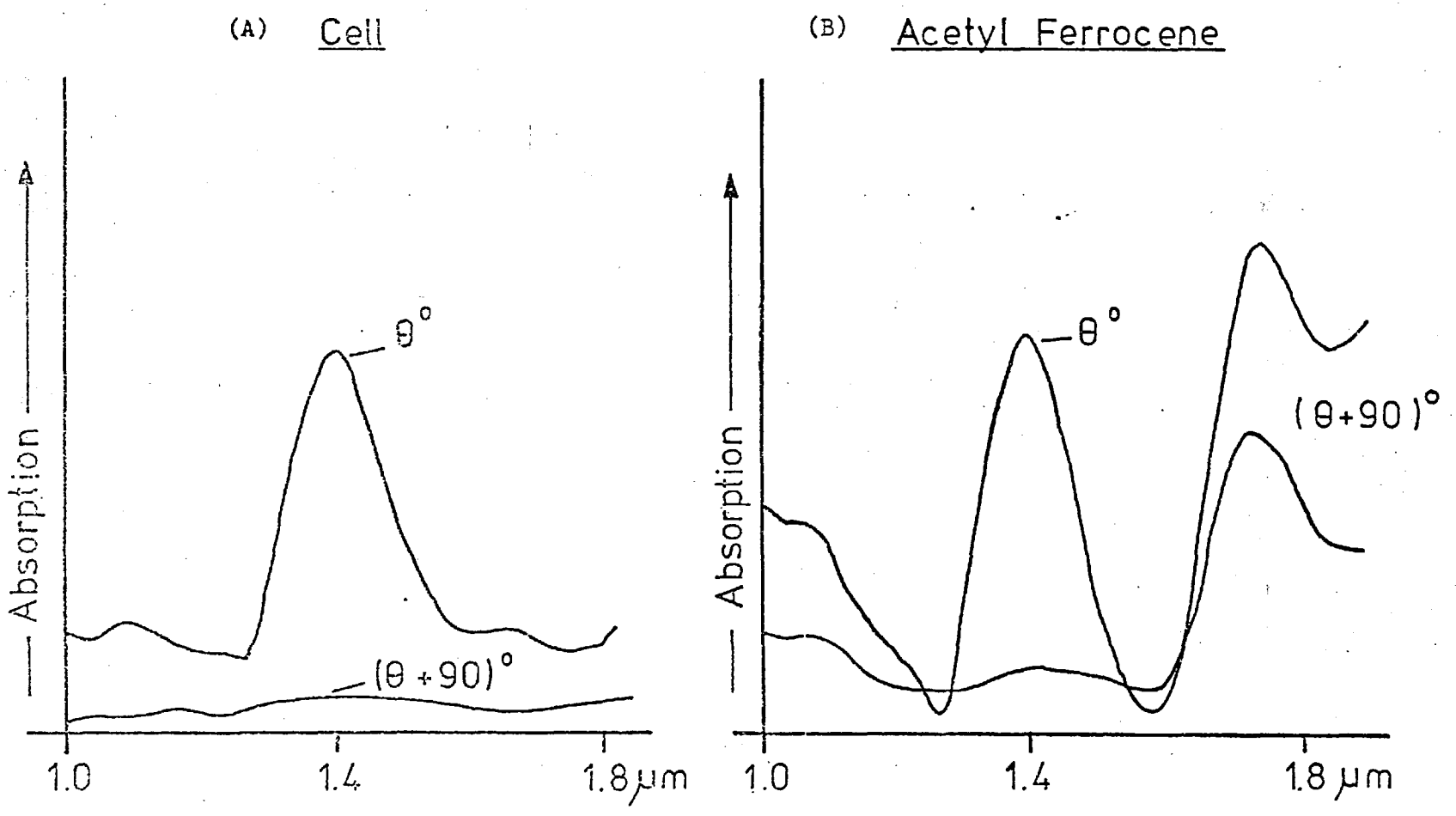

maximising the signal, by altering the phase angle relative to that of the reference signal from the rotating sector, for the cell background absorption maximum and then a sample absorption maximum a small phase angle difference was observed (ca. 10^{o}). The corrected optoacoustic spectrum of the cell 'blank' can be seen in Fig. 6.2A with the phase angle set (Θ) to maximise the signal at about 1.4μm and exactly out of phase ($\Theta + 90^{o}$) so that no signal would be expected. However, when this procedure was repeated with a sample present in the cell (Fig. 6.2B), e.g., acetyl ferrocene, the effect was to remove the cell background signal from the sample spectrum. The absorption band that remains in the spectrum of acetyl ferrocene is the first stretching overtone of the C-H bonds in the cyclopentadienyl ring (176).

Although this 'phasing-off' of the cell background signal was successful it degraded the signal-to-noise ratio of the signal from weakly absorbing samples considerably as the sample signal was not maximised for phase, and magnitude. The acetyl ferrocene spectrum corrected for the cell background shown in Fig. 6.2B was actually an order of magnitude less than the in-phase, uncorrected, spectrum. Thus, a reappraisal of the equipment used to measure optoacoustic spectra in the near-infrared was undertaken.

6.3. Instrumental Modifications.

An evaluation of sources similar to that described in Chapter Five was necessary to find a source that would facilitate the spectrometric analysis of samples in the near-infrared region.

The various sources were placed before the rotating sector in the experimental arrangement shown in Fig. 3.2; the monochromator having been fitted with the near-infrared diffraction grating and appropriate transmission filters. The sources evaluated were:-

i) a 1kW xenon arc (Type 6269, Oriel Corporation).

ii) a 300W short-arc, high pressure xenon arc (Type VIX 300UV, Varian Associates).

iii) a 150W mercury vapour lamp (Philips Electrical Ltd.).

iv) a 250W quartz-halogen tungsten-filament bulb (Type A1/223, Wotan Lamps Ltd.).

v) a Nernst-type filament (removed from an Infracord infrared spectrometer, Perkin-Elmer Ltd.).

The xenon arcs were operated within their appropriate housings which contained the focusing and collection optics. The mercury vapour lamp, tungsten bulb and Nernst filament were used with a concave, front-surfaced mirror to focus the radiation through the rotating sector on to the entrance slit of the monochromator. The spectrum of each source was measured by using an optoacoustic cell containing a smoked-glass carbon black sample. The optoacoustic signal was measured by a lock-in amplifier (Model 186, Princeton Applied Research Corp.) and recorded, against the wavelength of the incident radiation during wavelength scanning, by means of a potentiometric chart recorder (Servoscribe, Model RE511). The signal amplitudes were again converted to power readings by comparing them with the measurements obtained with a laser power meter (Model 142LR, Laser Instrumentation Ltd.).

The spectra obtained for these sources, shown in Figs. 6.3 and 6.4., were measured at a spectral half-bandwidth of 30nm and a modulation frequency of 30Hz. The spectrum of the 300W xenon arc was again similar to that of the 1kW arc, and is not shown. The sharp inflection in the spectra at about 1.4μm corresponds to the change of filters employed to remove overlapping spectral orders of diffraction from the grating. The peak intensities of the sources examined are given in Table 6.II.

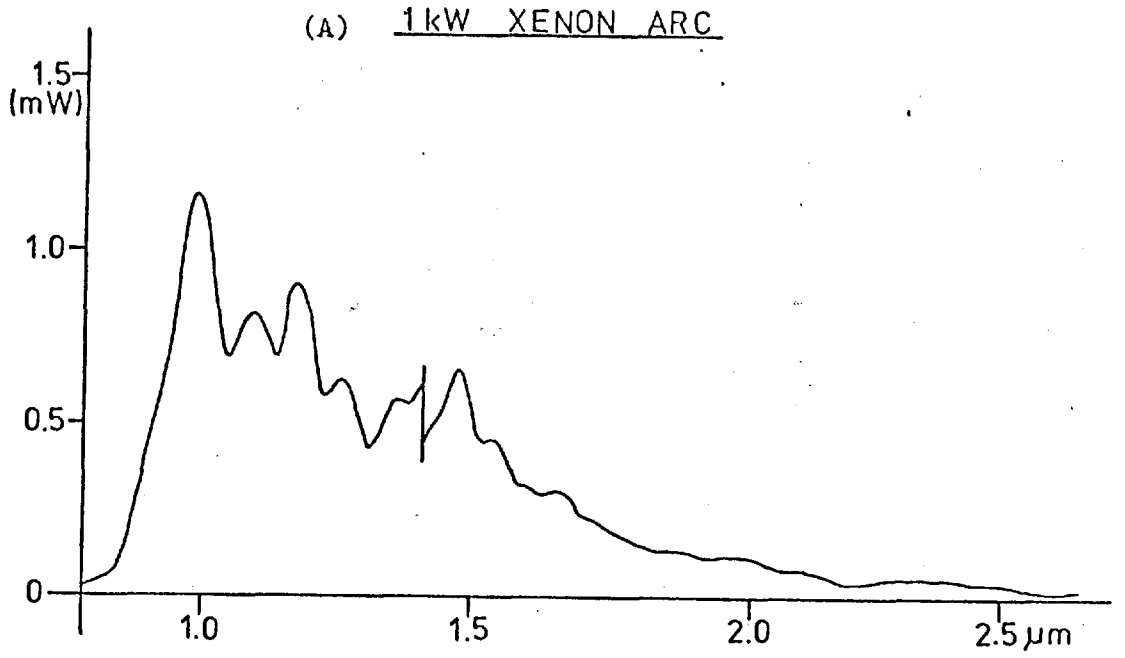

Fig. 6.3 Power spectra of potential sources for OAS.

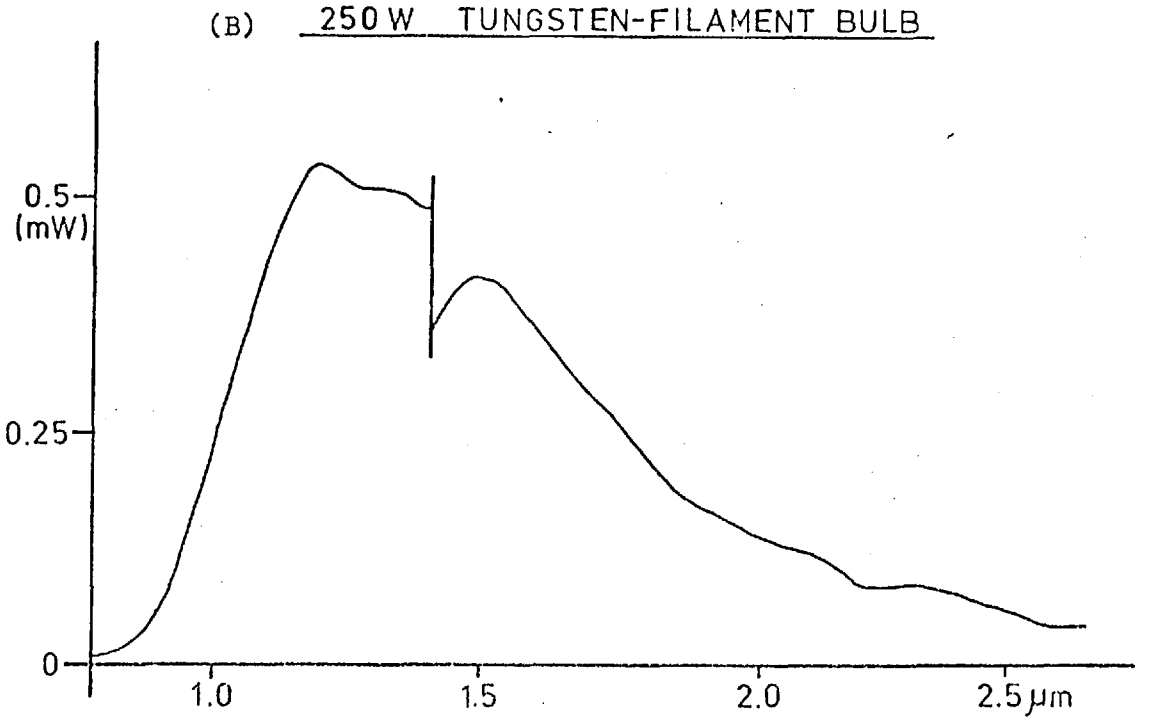

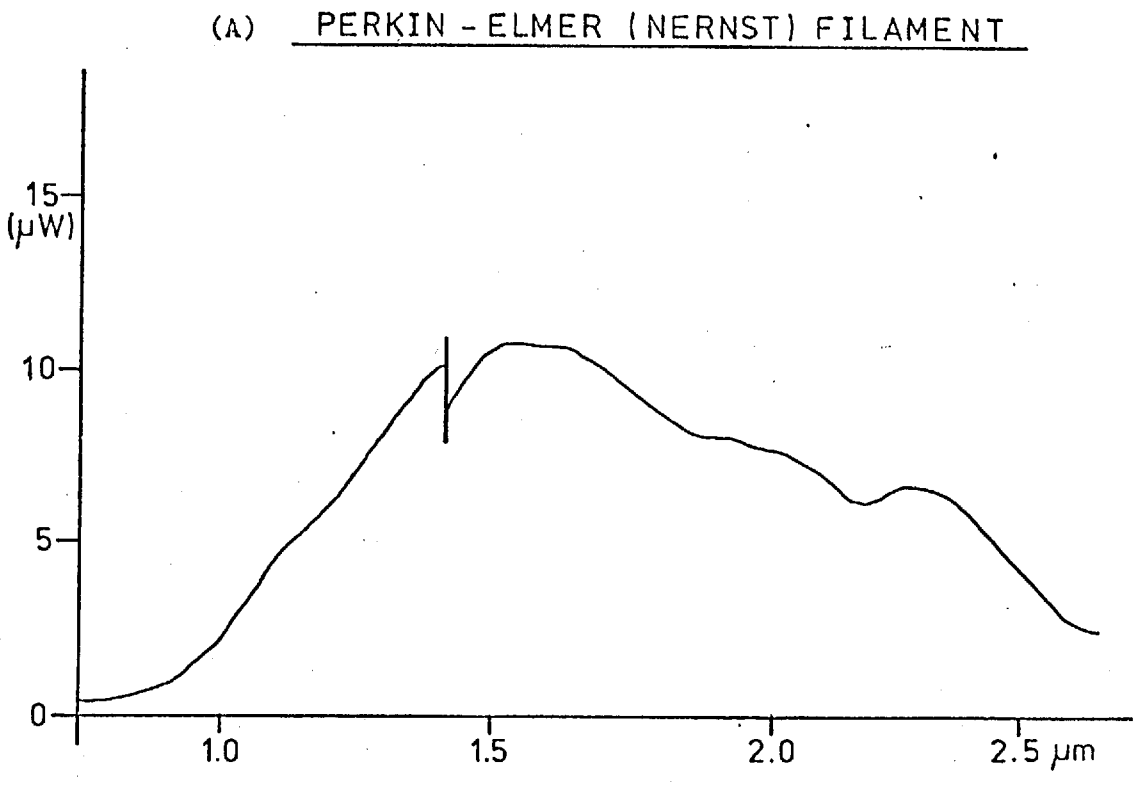

Fig. 6.4 Power spectra of potential sources for OAS.

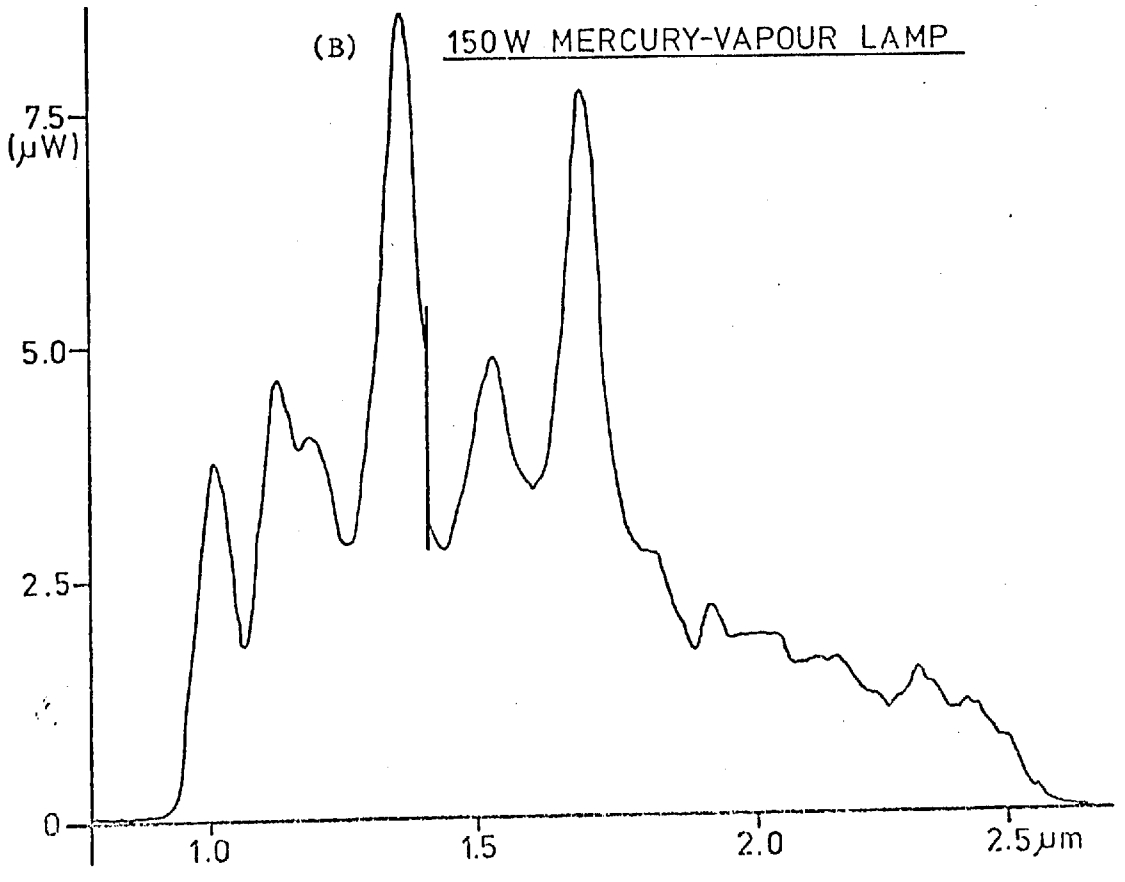

SOURCE	MAXIMUM INTENSITY (mW)
1kW xenon arc	1.28
300W xenon arc	1.22
250W tungsten-filament bulb	0.603
150W mercury vapour lamp	0.054
Nernst filament	0.113

Table 6.II. Source emission intensities in the near-infrared region.

From these results, and the spectral distribution of this power, it can be seen that the tungsten-filament bulb is the most suitable source for this region. The lower intensity of this source relative to the xenon arcs should be compensated for by the much smaller variation in emission intensity with wavelength. In fact, this loss of source power was overcome by removing the beam-splitting arrangement and using a digital scan recorder to sequentially correct for variations in source emission intensity with wavelength.

A schematic diagram of the spectrometer assembly for studies in the near-infrared region, is shown in Fig. 6.5. The source employed was the 250W quartz-halogen, tungsten-filament bulb described above, operated at 25V/DC. The radiation from the source was focused, using a concave, front-surfaced mirror, through a variable speed rotating sector (Model 9479, Brookdeal Electronics Ltd.) mounted at the entrance slit of a f/4 monochromator (Metrospec DGO Ltd.). A plane diffraction grating (300 lines mm^{-1} , 50 x 50mm) blazed at 2.0μm with fixed, 2.5mm wide, entrance and exit slits was employed in this work. This arrangement provided for a half-spectral bandwidth of 30nm (0.030μm) at the exit slit of the monochromator. To prevent overlapping spectral orders of diffraction being transmitted to the optoacoustic cell, low-wavelength cut-off filters were positioned at the exit slit of the monochromator.

The radiation from the exit slit of the monochromator was focused into the optoacoustic cell by means of a concave mirror.

The optoacoustic cell employed is shown in Fig. 6.6 and is similar to that described by McClelland and Kniseley (177). The cell was constructed from aluminium with a 20mm diameter silica entrance window. A type 4166 capacitor microphone (Brüel and Kjaer Ltd.) was employed as the pressure transducer. The polarisation voltage (240V) and preamplifier voltage (28V) for the microphone were supplied from a dry-battery source. Samples were placed in highly polished aluminium cups (16mm internal diameter, 3-5mm deep) and sealed within the cell by means of four locking nuts.

The optoacoustic signal at the microphone transducer was led directly to a lock-in amplifier (Model 186, Princeton Applied Research Corp.); the reference signal was derived from the rotating sector. The output from the lock-in amplifier was led to a digital scan-recorder system (Model 4101, Princeton Applied Research Corp.). This recorder was employed in the two-channel mode to store the reference (lamp emission) spectrum and a sample spectrum. Spectral correction was achieved with the aid of the internal ratiometer unit. The corrected optoacoustic spectra were displayed on a potentiometric chart recorder (Model 3000, Oxford Instrument Co., Oxford; input module, Type P).

All the optoacoustic spectra described in this chapter were obtained with a wavelength scan-rate of 300nm min^{-1} and an instrumental time constant of 1sec.

6.4. Results and Discussion.

The source emission spectrum (reference) was obtained by recording the optoacoustic spectrum of a silica plate coated with carbon black. The flatness response curve for carbon-carbon was as good as that

Fig. 6.5 Schematic diagram of the single-beam optoacoustic spectrometer employing a scan recorder for correction of spectra.

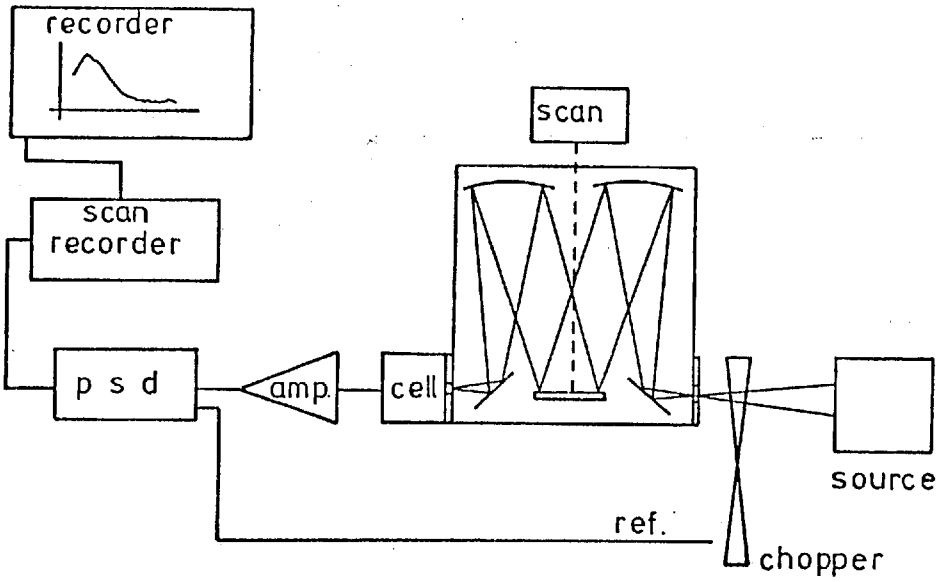

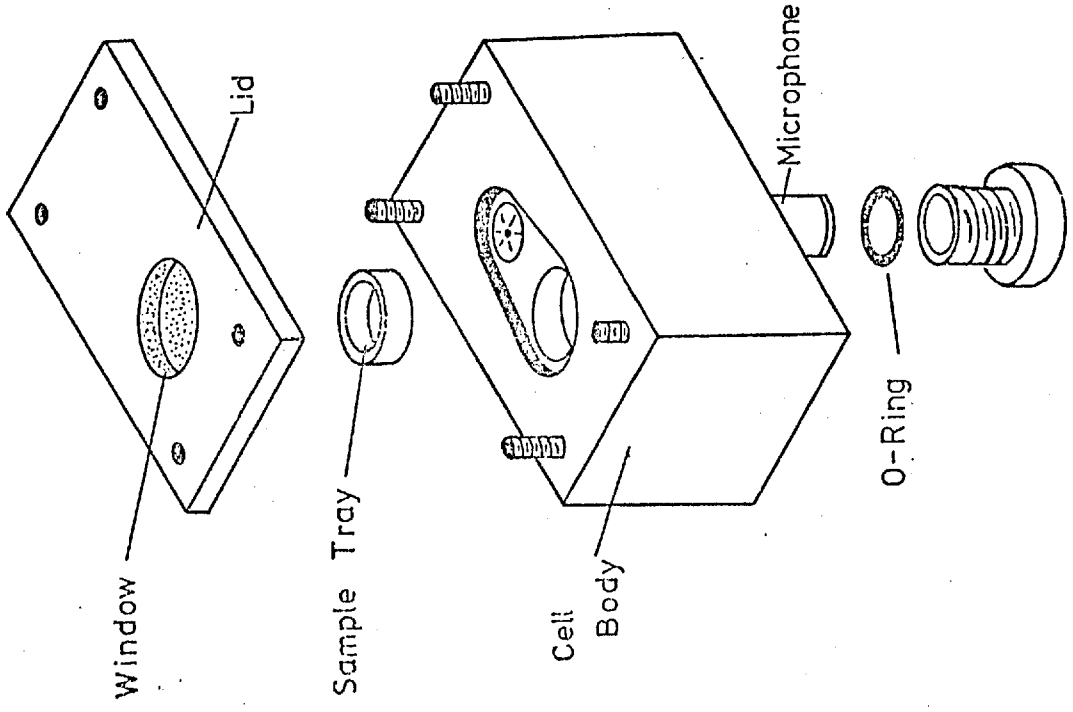

Fig. 6.6 The Optoacoustic Cell.

obtained previously, without the need for constant realignment of the optical system.

Samples were examined by placing the powder (ca. 100mg) or solution (ca. 100µl) into the aluminium sample cup and sealing this into the optoacoustic cell

It was observed that the amplitude of the signal from the empty cell at the wavelengths characteristic of water was more than an order of magnitude less than that obtained with the previous cell construction. When the internal cell surfaces exposed to incident radiation were highly polished, the background signal from the cell was less than the detection limit imposed by the signal-to-noise ratio at the microphone transducer.

6.4.1. Low Energy Electronic Transitions.

Electronic transitions in molecular species characteristically occur in the ultraviolet-visible region of the spectrum. However, many inorganic compounds exhibit low-energy transitions which may be examined by their near-infrared absorption spectra (151). Fig. 6.7 shows the absorption spectra of two rare-earth oxides in the 1µm to 2.7µm spectral region. The rare-earth oxides were obtained as high purity, fine powders (Johnson Matthey Ltd., London). As with the ultraviolet-visible spectra of these materials the electronic transitions are observed as intense, narrow absorption bands due to the shielding of the 4f electrons (129). The spectra shown in Fig. 6.7 agree well with those obtained by reflectance studies (130). The rare-earth oxide absorption bands were employed for wavelength calibration of the spectrometer as they are so well defined.

6.4.2. O-H Absorption Bands.

The fundamental oxygen-hydrogen vibrations of a non-bonded hydroxyl group (water) occur at ca. 2.7µm to 2.8µm and the first overtone

Fig. 6.8

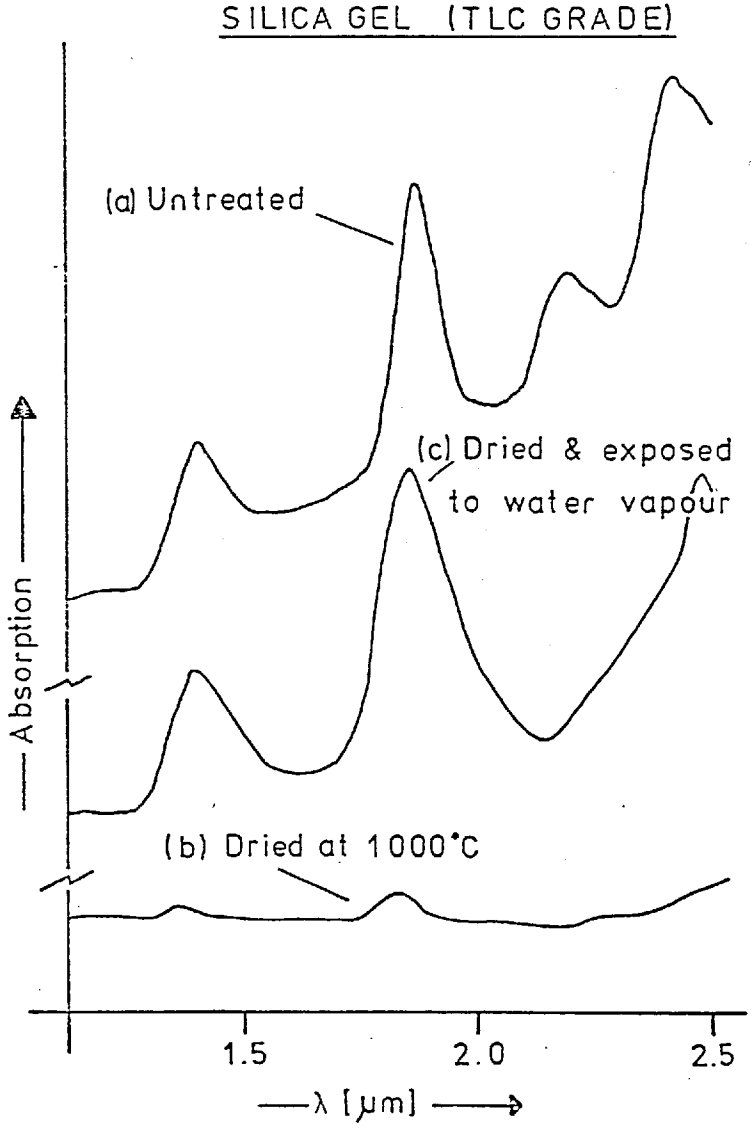
SILICA GEL (TLC GRADE)
(a) Untreated
(c) Dried & exposed to water vapour
(b) Dried at 1000°C
Absorption
1.5
2.0
2.5
λ [μm]

Fig. 6.7

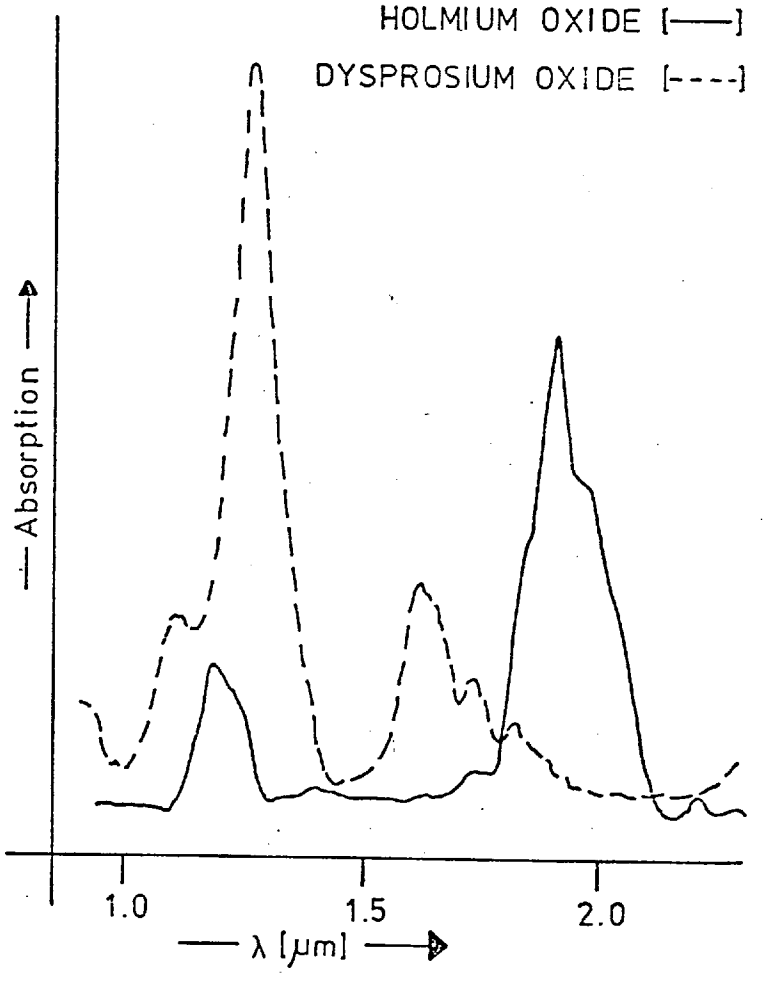
HOLMIUM OXIDE [——]
DYSPROSIUM OXIDE [- - - -]
Absorption
1.0
1.5
2.0
λ [μm]

at ca. 1.4μm; the combination band is observed at 1.9μm. For bonded hydroxyl groups, the first overtone is apparent also at 1.4μm but the combination band occurs at 2.2μm. Thus, near-infrared absorption studies may be employed to characterise the nature of -OH groups present in a sample (151).

Fig. 6.8 shows several optoacoustic spectra obtained from samples of TLC grade silica gel (Type 60, Merck, Germany). The activity of this material for thin-layer chromatography depends on the surface hydroxyl groups bound to the silica. It is evident from the spectrum of the untreated sample (Fig. 6.8a) that both bound hydroxyl groups (1.4μm and 2.2μm) are present as well as surface water (1.4μm and 1.9μm). After drying this sample at about 1000°C, the activity of the silica gel is destroyed and, as shown in Fig. 6.8b, this is accompanied by a loss in -OH absorption bands. Fig. 6.8c demonstrates how, upon exposure to water vapour, the preheated silica gel may adsorb water (1.4μm and 1.9μm) but does not regain the bonded hydroxyl groups necessary for TLC activity.

In an extensive survey of the visible and near-infrared diffuse reflectance spectra of minerals and rocks, Hunt (178 - 184) has discussed the -OH absorption bands in detail with numerous examples. Water has three fundamental vibrational modes, all of which are infrared active. These vibrational modes are the symmetric OH stretch (v_1), the H-O-H bend (v_2) and the asymmetric OH stretch (v_3). In the vapour transmission spectrum, the absorption bands due to these modes occur at 2.73μm, 6.27μm and 2.66μm respectively. Rotational fine structure distinguishes water from all other forms of OH and H_2O present. In the liquid phase, these bands shift to 3.11μm, 6.08μm and 2.90μm respectively; there is not a resolvable fine structure. In ice, the bands occur at 3.11μm, 6.06μm and 2.94μm, again with no resolvable fine structure. In the liquid and solid states, shifts in v_1 and v_3 to lower values are characteristic of hydrogen

bonding. The absorption bands may also be split or shifted for adsorbed water due to the types of site available. In minerals the overtones or combinations of these fundamental vibrational absorption bands occur at 1.88μm ($v_2 + v_3$), 1.45μm ($2v_2 + v_3$), 1.38μm ($v_1 + v_3$), 1.14μm ($v_1 + v_2 + v_3$) and 0.942μm ($2v_1 + v_3$).

The absorption spectra of the silicate minerals Kaolinite ($Al_4Si_4O_{10}(OH)_5$), Bentonite ($Al_2Si_4O_{10}(OH)_2 . x\ H_2O$) and Talc ($Mg_3Si_4O_{10}(OH)_2$) are shown in Figs. 6.9 and 6.10. It can be seen that compared to the silica gel spectra, the absorption bands are broadened in these materials, probably due to the factors indicated above. However, the distinction between the combination bands due to 'free' water at ca. 1.9μm and the -OH forming part of the silicate lattice at ca. 2.2μm is evident. Although these spectra were obtained from relatively impure, crude samples of these minerals (Geology Department, Imperial College), a similar spectrum was obtained for Talc from a commercial prepartion ('Warm Springs', Boots Co. Ltd.).

6.4.3. N-H Absorption Bands.

Secondary N-H groups are charactarised by fundamental stretching bands near 2.9μm, first overtone stretching bands near 1.5μm, and second overtone stretching bands near 1.0μm (151). The comparable bands for the $-NH_2$ group exhibit symmetric and antisymmetric components, but the antisymmetric components of the overtone bands are relatively weak. The $-NH_2$ group also exhibits a highly characteristic band near 2.0μm.

However, the only compounds likely to show these absorption characteristics clearly are inorganic complexes containing N-H groups or ammonia itself. In organic compounds, complex vibrational bands will occur as well as those absorption bands due to the other groups present (11). Thus, the optoacoustic spectrum (Fig. 6.11) of a low protein wheat

Fig. 6.9

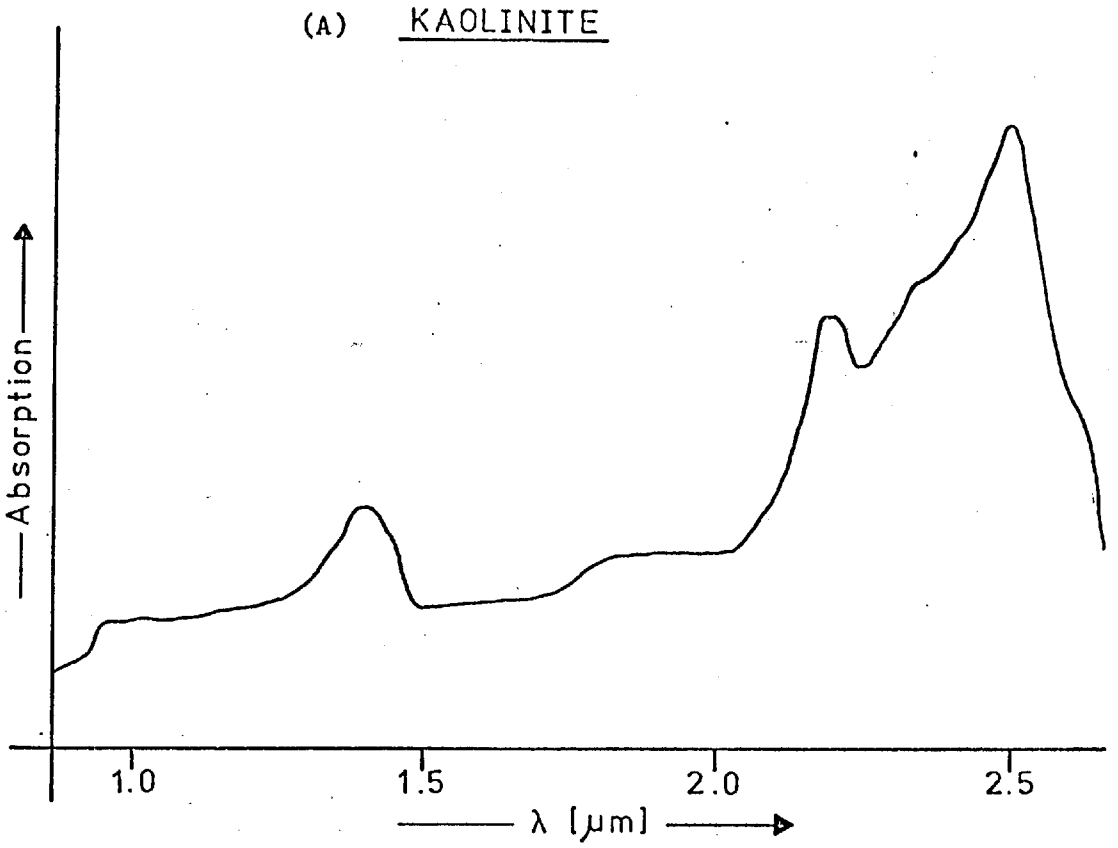
(A) KAOLINITE
Absorption
1.0
1.5
2.0
2.5
λ [μm]

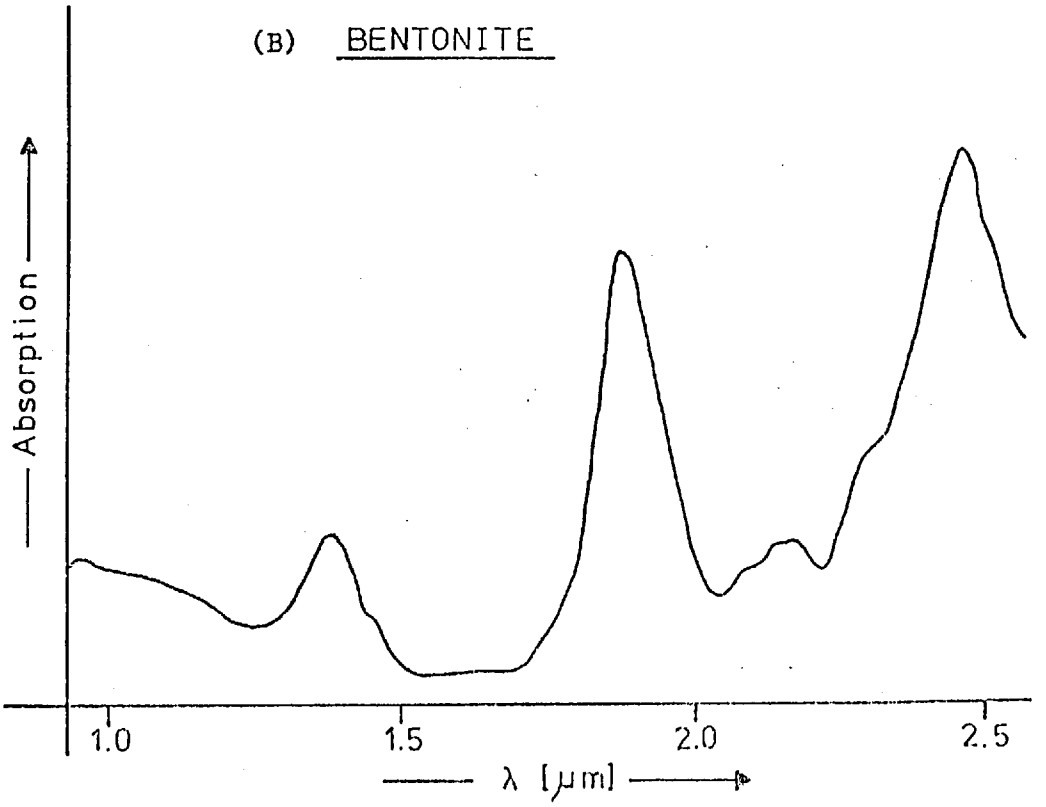
(B) BENTONITE
Absorption
1.0
1.5
2.0
2.5
λ [μm]

Fig. 6.10

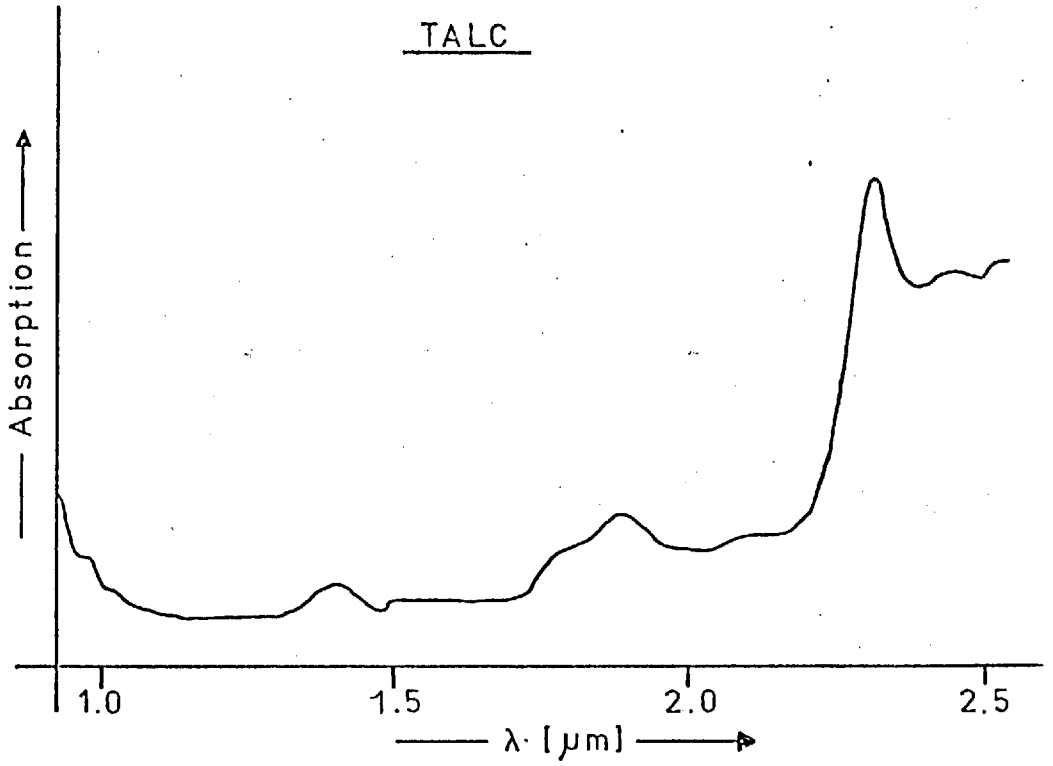

Fig. 6.11

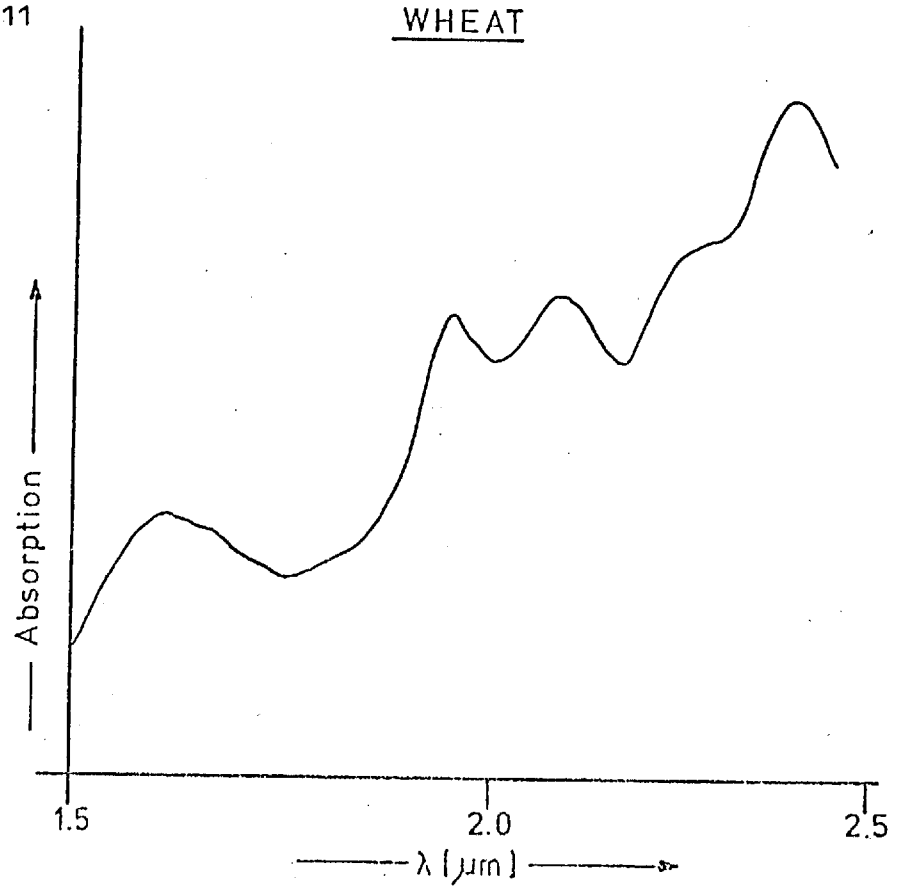

sample (Foss Electric, Norway) shows little spectral character other than an absorption band at 1.94μm from water. The broad absorption band at ca. 2.1μm was typical of a low protein sample with the high protein samples exhibiting almost a straight line in this region. The results were in agreement with those obtained by Norris et al (174) using diffuse reflectance spectroscopy. The lack of detail in the absorption spectra was overcome by these workers using reflectance data at eight wavelengths with a multiple-linear-regression analysis to construct calibration graphs for the crude protein content of dry forage samples. This approach to the poor characterisation of near-infrared spectra obtained from in-vivo samples is the basis of the 'InfraAlyzer' near-infrared reflectance instrument (Technicon Industrial Systems, Tarrytown, N.Y., U.S.A.).

However, it can be seen from Fig. 6.12 that better characterisation of near-infrared absorption spectra may be obtained by using pure compounds; in this case the sulphonamide drugs, sulphonamide and sulphamerazine (Laboratory of the Government Chemist, London). Although the spectra of these compounds are seen to differ their identification from band assignments is a complex and difficult matter, especially as similar molecular structures may not be clearly identified. When the analyte does have clearly identifiable spectral bands, then quantitative analyses are possible. Unfortunately commercial preparations of such pharmaceutical products are not available in any significantly different concentrations and so a quantitative study of these compounds was not possible.

It was found that similar spectra were obtained from either whole tablets or powdered pharmaceutical samples. The only difference between them was that absorption bands occured at about 1.4μm and 1.9μm in the whole tablet samples. These bands are characteristic of free, undissociated water and indicate surface adsorption of atmospheric water

Fig. 6.12

(a) SULPHANILAMIDE

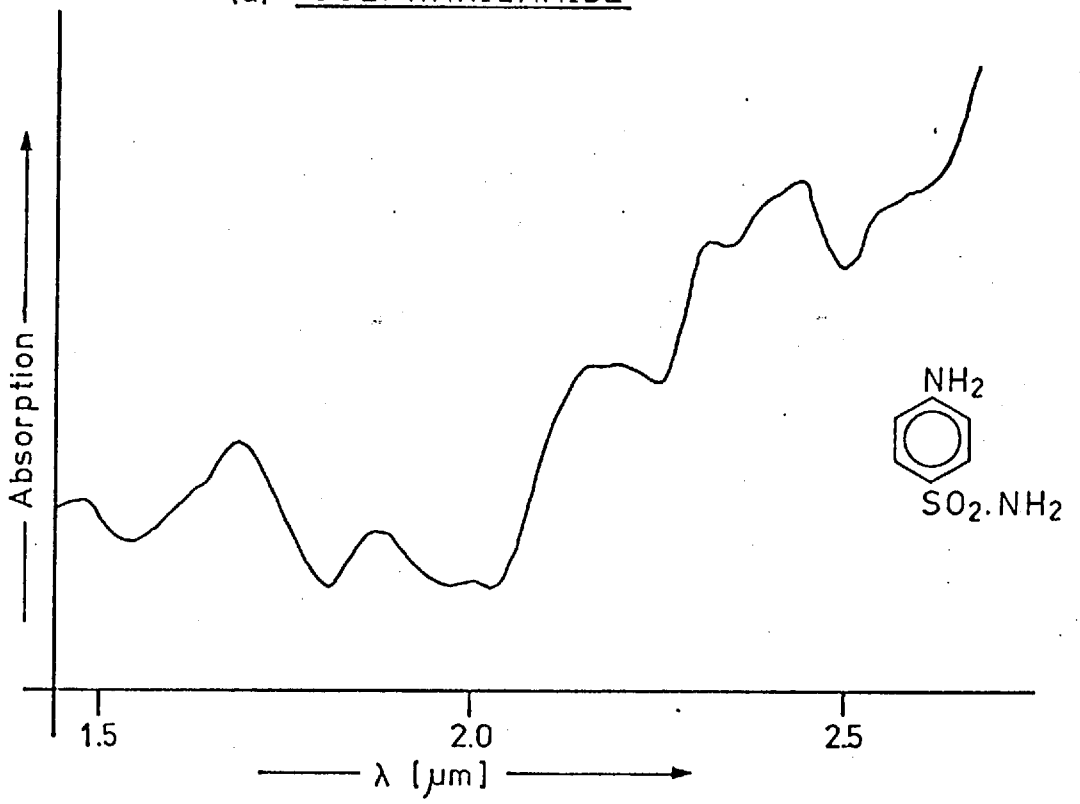

(b) SULPHAMERAZINE

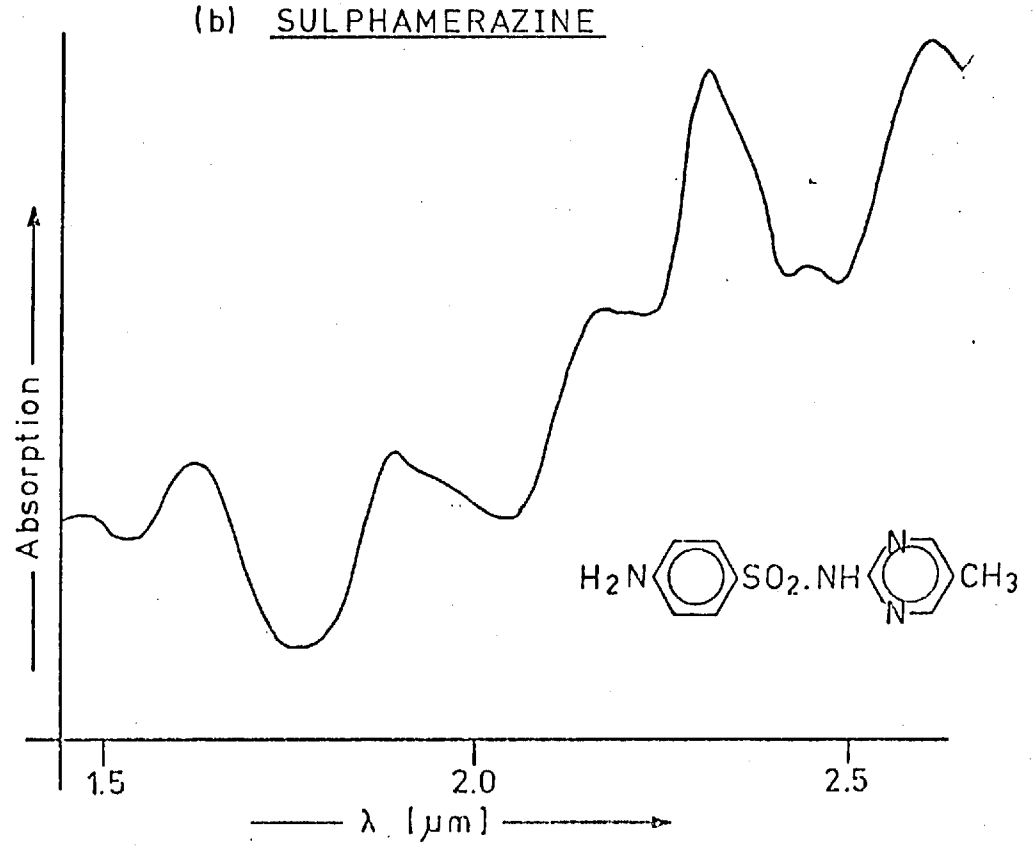

by the tablet.

6.4.4. C-H Absorption Bands.

The fundamental carbon-hydrogen stretching vibration absorption is observed normally at ca. 3.3μm to 3.5μm and the first overtone at ca. 1.7μm (151). In practice, however, numerous absorption bands are observed in the near-infrared region due to C-H bending overtones and the many combination bands possible. As the separation of C-H overtones is greater than that between the fundamentals from which they arise, the near-infrared region may be employed for their identification and characterisation.

The optoacoustic spectra of a series of polyaromatic hydrocarbons (PAH's) were measured; two of which, benzanthracene and anthracene, are shown in Fig. 6.13. It can be seen that the spectral features are similar for these compounds, i.e., it is not possible to distinguish between members of a homologous series of compounds at this spectral resolution. However, for a group (X-H) which has a near-infrared overtone band where the intensity of absorption is nearly constant regardless of the position of the group in the molecular species under study then,

$$K = \sum n\,a \qquad \ldots 6.3$$

where K is the total absorption intensity, n is the number of absorbing groups and a is the molar absorption intensity per group (11).

For a series of PAH's, a graph of the aromatic absorption band near 2.2μm, a combination band, versus the number (n) of aromatic nuclei in the PAH gave a linear plot except for n=1 and n=7, i.e., benzene and coronene respectively. In these cases a change in the physical appearance of the samples was evident, resulting in a change of surface area and, therefore, the amplitude of the acoustic signal.

Combination C-H bands have been used extensively in the analysis of polymers. Miller and Willis (160) analysed styrene-butadiene

Fig. 6.13 Near-infrared optoacoustic spectra of a) benzanthracene b) anthracene

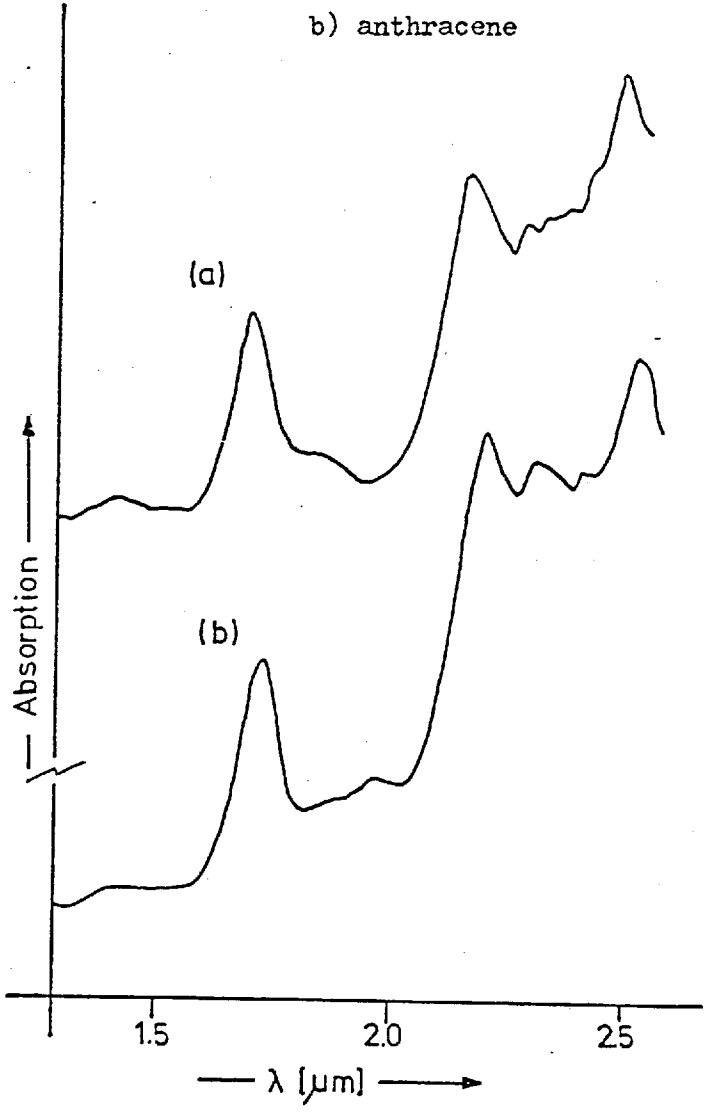

Fig. 6.14

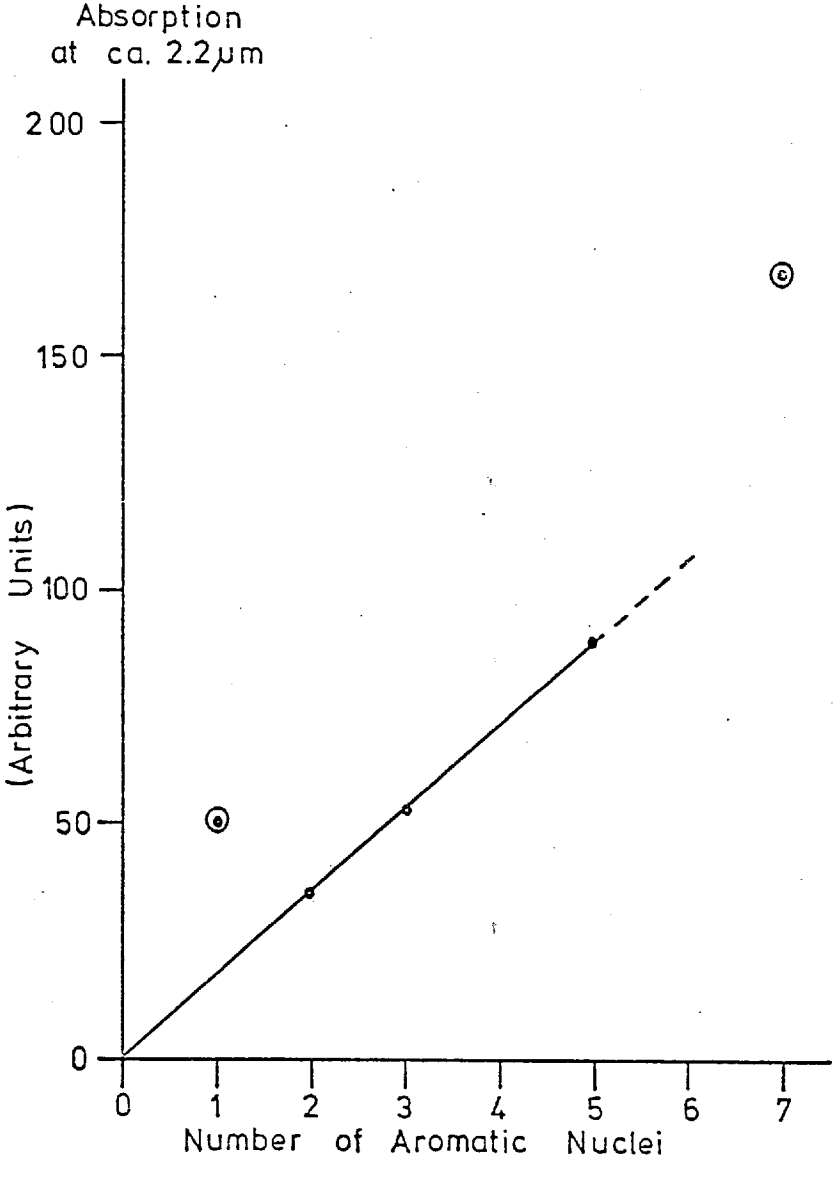

copolymers by determining the ratio of aromatic and aliphatic absorption near 2.2μm and 2.4μm, respectively. The near-infrared optoacoustic spectra of a number of polymer films were measured, but were extremely noisy due to the low signal amplitudes obtained from the low-surface area samples. The only spectral feature that could be clearly seen in these spectra was the C-H overtone band at ca. 1.7μm.

However, the clear differences between the optoacoustic spectra of aromatic and aliphatic systems (Fig. 6.15) in the C-H combination region above ca. 2.0μm prompted the quantitative investigation of these systems. The aromatic C-H band at 2.2μm was observed not to occur in aliphatic systems and was employed as a means of quantitative analysis for aromaticity in organic mixtures. As stated above, the absorption band intensities have been shown to be additive, according to the number of absorption centres in a molecule. Mixtures of benzene in n-hexane (both laboratory grade reagents) were prepared and 100μl aliquots of these were examined by optoacoustic spectrometry. A linear relationship was observed between peak height, at ca. 2.2μm, and benzene concentration between zero and 100% benzene in the samples (Fig. 6.16). A similar result was obtained by plotting the peak height at ca. 2.4μm versus n-hexane concentration in benzene. Neither of these graphs passed through the origin, some absorption due to the diluent being present at the measured peak absorption wavelength.

These graphs were repeated using a complex matrix, an Iranian crude oil sample (Shell Research Ltd., Thornton). Fig. 6.17 shows the optoacoustic spectra of undiluted Iranian crude oil samples to which standard additions of benzene have been made. A graph of peak height, at 2.2μm, versus benzene concentration in the sample was linear (Fig. 6.18). Again, similar results were obtained for standard additions of n-hexane using the aliphatic C-H combination band at 2.4μm. Unfortunately,

Fig. 6.15 Near-infrared optoacoustic spectra of (a) benzene (b) n-hexane

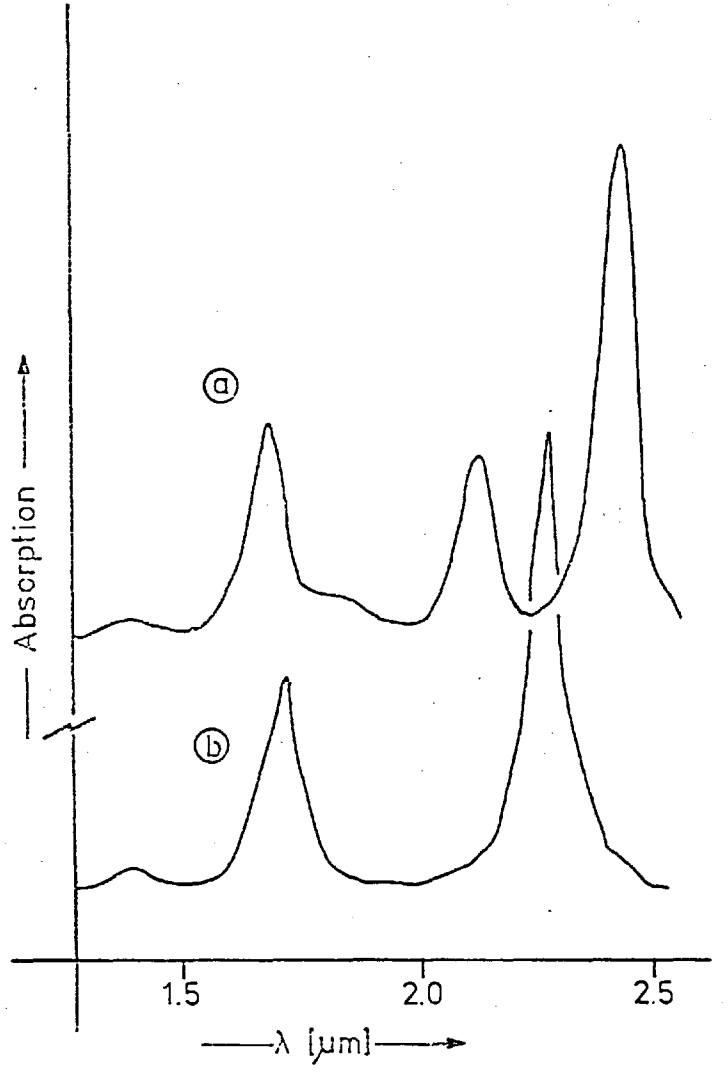

Fig. 6.16

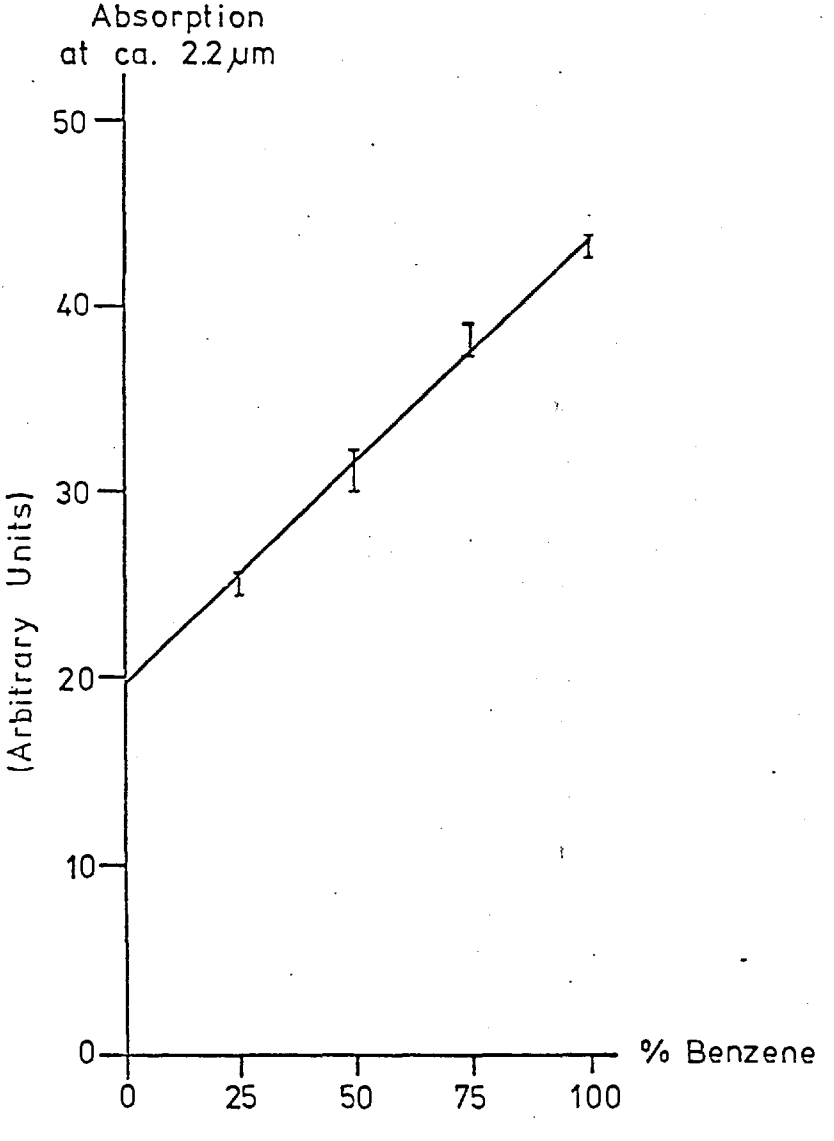

Fig. 6.17 Near-infrared optoacoustic spectra of Iranian crude oil with standard additions of (a) 10% benzene (b) 30% benzene

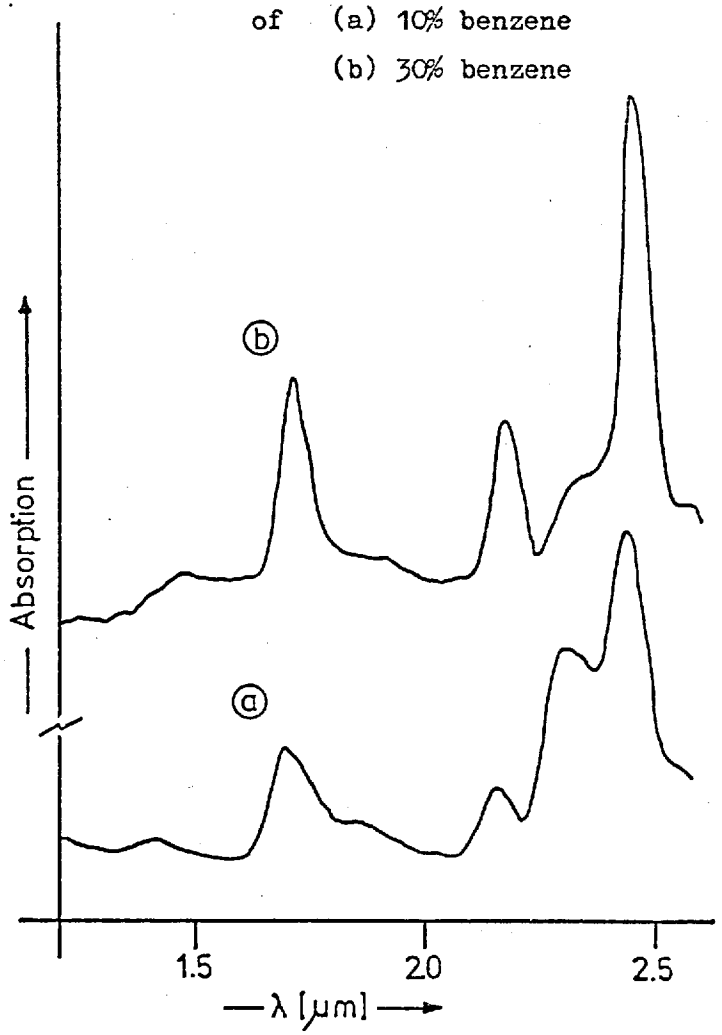

Fig. 6.18

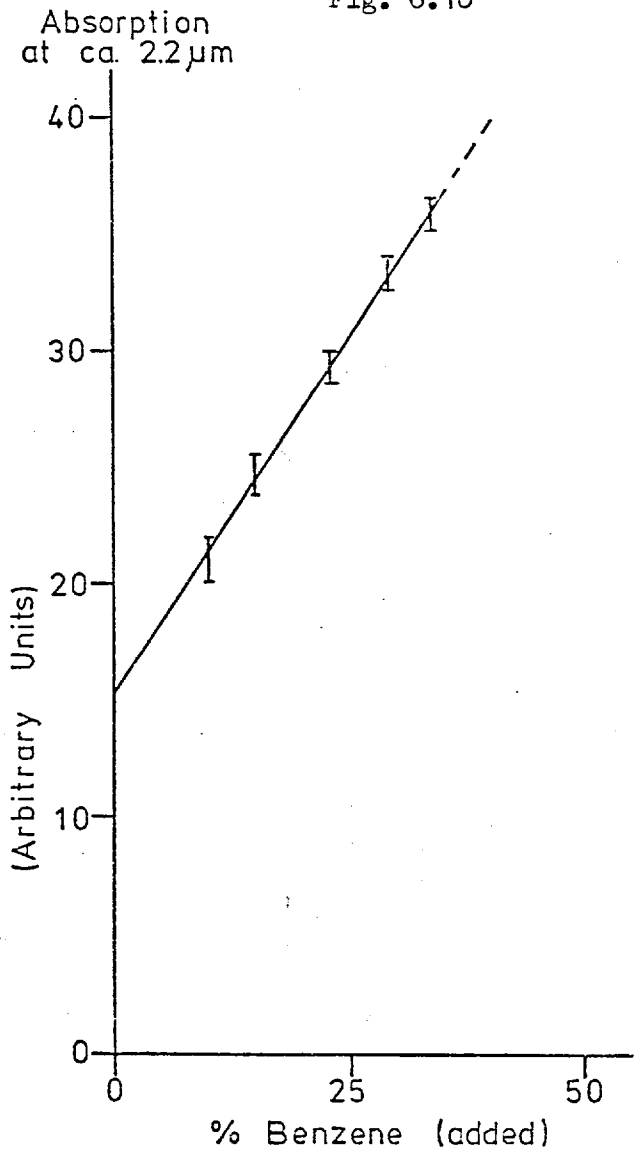

this work could not be extended to an actual determination of the aromaticity in the crude oil since the actual composition of the oil sample was not known. However, it has demonstrated the potential of optoacoustic spectrometry for the study of impure, viscous samples such as crude oils.

It is interesting to note that the ratio of the extinction coefficient of the aromatic C-H band to the corresponding coefficient of the aliphatic C-H band ("Varal" index) has been proposed (186) as a measure of the aromatic content of a hydrocarbon. The absorption bands employed in this measurement were the second overtones of the C-H stretching vibration in the region 1.1μm to 1.2μm.

6.5. Conclusion.

The single-beam optoacoustic spectrometer described enables the study of absorption spectra in the near-infrared region. Unlike the majority of spectrometers described in the literature the system discussed employs a relatively low power tungsten-filament continuum source. Whilst rare-gas filled arc-lamps have a greater radiant flux and are suitable for use in the ultraviolet- visible regions, their use is limited in the near-infrared because of the intense narrow line emission superimposed on the continuum background, thus making double-beam operation difficult to achieve. The tungsten-filament source described above provides a near black-body emission with an emission wavelength maximum, with the above spectrometer, at ca. 1.2μm.

The use of the spectrometer to examine a variety of sample types has been described and clear spectra have been obtained from solid powder, solution and thixatropic oil samples. The near-infrared spectral region may be employed for the examination and characterisation of inorganic and organic materials by the absorption bands in this region

due to low energy electronic transitions, overtone bands and combination bands. With the advantages already proposed for optoacoustic spectrometry, the extension of the working spectral range to include the near-infrared as described above should provide for many further applications of the technique in the examination of materials which are normally difficult to study. Quantitative analysis is possible in the near-infrared region and may be employed, as described, for the determination of aromaticity in organic mixtures.

CHAPTER SEVEN

CONCLUSIONS

7.1. Conclusion.

This thesis has been concerned with the investigation of the optoacoustic effect and its development for use as an analytical tool for the study of solid and liquid/solution samples. This effect was observed almost a century ago by Bell (23) and whilst its applications to the study of gaseous reactions and gas analysis have been numerous, the use of the effect to examine condensed phase materials by optoacoustic spectrometry is of relatively recent origin.

The optoacoustic effect is only observed when modulated (typically 20 Hz to 20 kHz) electromagnetic radiation incident upon a sample, contained in a constant-volume cell, is absorbed. The signal magnitude at the microphone transducer enclosed in the cell is proportional to the energy of the incident radiation and the absorption coefficient of the sample at the wavelength of irradiation. Hence, by employing a wavelength-dispersive element between the source and the cell and monitoring the magnitude of the microphone signal as a function of the wavelength of the incident radiation, an absorption spectrum of the sample is obtained, usually similar to that observed with conventional spectrophotometric techniques.

7.1.1. Instrumentation.

Much of the research of this thesis has been concerned with the design and construction of instrumentation to study the optoacoustic effect. Single-beam and double-beam spectrometers have been assembled and both are capable of operation in the wavelength region 250nm to 2,500nm (40,000cm^{-1} to 4,000cm^{-1}). With the single-beam instrument, uncorrected spectra are obtained, i.e., the spectra are functions of not only the absorption characteristics of the sample but also the emission spectrum of the source employed. Manual normalisation is tedious and so

two methods of automatic correction of spectra have been examined. The first, discussed in Chapter Five, comprises a "true" double-beam instrument and provides for simultaneous spectra-correction whilst scanning. This is acheived by the use of two optoacoustic cells, one of which contains the sample of interest and the other a black absorber (usually a heavily smoked black silica or glass plate). A second, sequential, means of normalisation has been studied also (Chapter Six). This system utilised a digital scan recorder to sequentially store the reference and sample spectra and then readout the corrected sample spectra via an internal ratiometer unit.

Whilst both methods of achieving normalisation are successful, each has its own inherent advantages and limitations. With a double-beam spectrometer there is no delay period before the corrected spectrum is obtained and by employing a reference sample other than carbon-black in the reference beam, difference spectra can be recorded. Sequential correction of single-beam spectra has this delay period but has the advantage that no optical beam-splitter arrangement is required and all the dispersed radiation can be focused into the single sample cell; thus enhancing the signal-to-noise ratio.

Normalisation with the double-beam instrument has been achieved also by means of a reference channel employing a pyroelectric detector. The highly sensitive, flat spectral response of this detector to modulated radiation, and its low response to changes in DC light, means that only a small fraction of the dispersed radiation is required as a reference channel. Signal-to-noise figures for the sample optoacoustic cell are thus improved, although the ability to perform simultaneous difference spectroscopy is lost.

It is of interest to note that of the three commercial optoacoustic spectrometers capable of studying solid samples to have

appeared recently, one (Gilford Instrument Labs., U.S.A.) has double-beam operation with two optoacoustic cells, whilst two (EDT Research, London; and Princeton Applied Research, U.S.A.) employ a pyroelectric detector as the reference channel.

Instrument design for analytical systems is frequently concerned with achieving the best signal-to-noise ratio. Optoacoustic spectrometry is no exception to this and the single unit of such a spectrometer which controls this ratio is the optoacoustic cell. A variety of cell types were designed and studied in this work. The general requirements for such a cell for use with solid or liquid samples have been discussed by many other workers in the field (112, 125, 187-195). Although concerned primarily with gaseous studies the report by Rosengren (187) is the most comprehensive to date. In general, acoustically resonant detectors have received little attention for solid sample work (196) due to the low modulation frequencies employed. Also, optically resonant detectors and multiple-pass detectors, often used for gaseous research, have received little attention. McClelland and Kniseley (125, 188,189) have discussed a variety of sample cell designs for solid and solution studies and have examined the problems of scattered and stray-light (in particular the efficient acoustic coupling of incident radiation with the microphone diaphragm) and the effect of the sample backing material on the signal magnitude. Aamodt et al (112,113) have reported the effects of size considerations (gas volume) in the design of cells for optoacoustic spectrometry. These workers have also made a preliminary study of the effects of cell material on signal magnitude. Munroe and Reichard (189) have described a preamplifier, suitable for use with Brüel and Kjaer condenser microphones, that should overcome the inherent noise problems in cell designs which employ commercial preamplifier systems of larger physical dimensions than the cell itself.

It is difficult to draw absolute conclusions from the literature. Many workers examined the effect of varying a single parameter and provide no reference to other important considerations. From this work, and with reference to the literature, the following cell parameters may be considered as determining the final cell design.

1. The material from which the cell is constructed plays a minor role in determining the signal magnitude. However, to prevent environmental acoustic noise from interfering it appears that the cell should be firmly mounted and well sealed.

2. To minimise any background signal, scattered light should be directed from the cell and coupling between incident radiation and the microphone diaphragm should be avoided. Silica cell liners or cells constructed from transparent materials appear to assist with reducing this interference.

3. The sample should be contained within a silica tray. This not only reduces loss of signal caused by the heat-sink effect of the substrate, but also allows any radiation transmitted by the sample to leave the cell and not be scattered on to the cell walls.

4. The gas volume coupling the sample surface to the pressure transducer should be kept small (typically about $1cm^3$). Care needs to be taken, however, that the coupling efficiency is not impaired by minimising this volume too much.

5. Finally, the ease with which the sample can be changed should be considered; preferably this should be possible without disturbing the cell and its optical alignment.

The pressure transducer employed in the optoacoustic cell is a major consideration. Throughout this work highly sensitive capacitor microphones were employed. This appears to be the choice also, of the majority of workers for optoacoustic spectrometric studies of solid samples. However, the study of liquid samples has been conducted in many

cases with a piezoelectric tube acting as both cell and detector (197, 198).

In general, however, the microphone transducer appears to be the most satisfactory when a variety of sample types are to be examined. But the microphone is used only as an indirect means of monitoring the alternating temperature at the surface of the sample and other means of accomplishing this are sure to be advanced in future work.

7.1.2. Theoretical Parameters.

The optoacoustic effect is an energy conversion process; electromagnetic radiation absorbed by the sample leads to an increase in the internal energy of the system and subsequent de-excitation provides an increase in temperature at the sample/gas interface which may be monitored by the pressure change in the gas by the microphone.

These three parameters, which govern the observed magnitude of the optoacoustic signal, S , may be summarised in the following general expression:

$$S = P_{abs} \cdot T_E \cdot R_E \qquad \ldots 7.1$$

where: (1) P_{abs} is the radiant power absorbed by the sample and is related to the incident DC power, P_o , and the absorption coefficient, a , by:

$$P_{abs} \propto \frac{P_o \cdot a}{w} \qquad \ldots 7.2$$

where w is the modulation frequency.

(2) T_E is the thermal transfer efficiency within the sample to the sample/gas interface and is a function of the thermal diffusivity, α , and surface area, A , of the sample, i.e.,

$$T_E \propto \alpha \cdot A \quad \text{or} \quad T_E \propto \frac{k}{c_v} \cdot A \qquad \ldots 7.3$$

where k is the thermal conductivity of the sample and c_v its molar heat capacity at constant-volume.

(3) R_E is the efficiency of radiationless conversion following the absorption of electromagnetic radiation, i.e., the complement to luminescence emission or photochemical rearrangement/reaction mechanisms.

This work has been concerned with the study of the first two of these three general functions and their interrelation in producing a measurable optoacoustic signal.

7.1.3. Applications.

1. For any given sample, which does not luminesce or react photochemically, Equation 7.1 predicts a proportionality between the magnitude of the optoacoustic signal and the absorption coefficient. This relationship has been confirmed by a study of the optoacoustic absorption spectra of many inorganic, organic and biochemical samples.

Unlike conventional optical spectrometric techniques, only photons absorbed by the sample produce an optoacoustic signal. Thus spectra of biological fluids containing high molecular weight protein or fat molecules, e.g., blood, suspensions, colloids, etc., may be obtained free of scattering effects. It has also been possible to obtain the absorption spectra of thin-film samples free from "pseudo-absorption" bands due to optical interference effects.

2. It is the combination of the optical and thermal characteristics of the sample which provide optoacoustic spectrometry with its unique capabilities and potential as a spectroradiometric method of analysis. The heat transfer mechanism within the sample may take several milliseconds, i.e., it is of the same order of magnitude as the period of modulation of the incident radiation. In more detail, this time-delay, or phase-lag ($\Delta\Theta$), in the signal observed with reference to the time

of radiation absorption is a function of the thermal properties of the material and the modulation frequency employed, viz.

$$\Delta\theta = x \cdot \left(\frac{w}{2\alpha}\right)^{1/2} \quad \ldots 7.4$$

where x is the depth within the sample in which the absorption process occurs, w is the modulation frequency and α the thermal diffusivity of the sample.

For a given sample, α is constant and x is a function of the absorption coefficient of the material at the wavelength of incident radiation. The modulation frequency, however, is an instrumental parameter that may be selected and controlled by the operator. Thus, the two-layer leaf study described in Chapter Four has recently been repeated by A.Rosencwaig at Gilford Instrument Labs. in the U.S.A., employing variable modulation frequencies to control the thermal penetration depth rather than the signal phase. The reported results are similar to those in Chapter Four. The thermal effect has been shown to be of particular importance in the examination of non-homogeneous and layered materials.

7.2. Trends.

Much of the work recently reported in the literature has utilised the fact that radiationless processes are responsible for the optoacoustic effect to measure fluorescence quantum efficiencies and radiationless transition lifetimes.

Adams et al (199) have reported the use of a microphone to measure the optoacoustic signals produced by irradiation of quinine bisulphate solutions. The fluorescence quantum efficiency of quinine bisulphate in aqueous acid solution was determined by measuring the increase in acoustic signal at an excitation wavelength of 366nm upon

quenching the fluoresence with halide ions. The working equation for these studies was:

$$Q = \frac{\lambda_F}{\lambda_o}\left(1 - \frac{P(OAS)_F}{P(OAS)_{NF}}\right) \quad \ldots 7.5$$

where Q is the absolute quantum efficiency of fluorescence, λ_F is the mean wavelength of fluorescence, λ_o is the wavelength of excitation, and $P(OAS)_F$ and $P(OAS)_{NF}$ are the magnitudes of the optoacoustic signals at λ_F and λ_o respectively. It is assumed that no optical or thermal saturation occurs, the absorptivity of both the fluorescent and nonfluorescent compounds are identical, and the thermal characteristics of the solutions are equal. The value obtained for the absolute quantum efficiency of quinine bisulphate was in good agreement with the literature.

Other studies concerning the determination of absolute quantum efficiencies of fluorescent materials utilising the optoacoustic effect have employed pressure transducers immersed in the analyte and non-fluorescent materials as reference solutions (200,201). This is achieved by ensuring that the reference material and the fluorescent compound to be examined have comparable absorption coefficients and equating the difference in magnitude of the optoacoustic signals from the two solutions to the efficiency of fluorescence of the sample. Rockley and Waugh (202) have used an internal standard rather than a reference solution for measuring the fluorescence quantum efficiencies of dye solutions. The internal standard employed was the absorption intensity of the dye solution at a non-excitation wavelength.

Aamodt and Murphy (203,204) have applied optoacoustic spectrometry to the study of both fluorescence and non-radiative processes in ruby powder samples, where concentration dependent metastable-level quenching rates are observed. Merkle and Powell (205) have investigated the

radiationless transitions in Eu^{2+} ions in potassium chloride crystals with an optoacoustic spectrometer. The spectra obtained at different phase angles relative to the time of radiation absorption by the sample revealed an anomalously long relaxation rate from the higher $4f^6 5d$ state of Eu^{2+}. A model was proposed to explain this result based on the excited states of the $4f^7$ configuration acting as a "bottleneck" in the relaxation mechanism. The lifetime of the state from which the radiationless decay occured was determined by making phase measurements relative to a band assumed to directly deactivate.

Measurements of radiationless transitions in solids at low temperatures have been made by several workers, (204,206,207). Robin (206) studied the decay of the excited states of ruby at 2K using a lead-film, bolometric detector. Parker et al (207) examined the photophysical processes occuring in biacetyl using a thin-film, germanium semiconductor detector. However, Murphy and Aamodt (204) employed a more conventional arrangement to study further the concentration-dependent metastable-level quenching rates in ruby. The optoacoustic cell was immersed in liquid nitrogen; the microphone transducer being connected by a capillary tube to the sample cell.

Several reviews on condensed-phase optoacoustic spectrometry have appeared in the literature recently (208 - 210) together with a text on "Optoacoustic Spectroscopy and Detection" (211) discussing the technique in both the gaseous and condensed phases. Most of the applications reported have been discussed in principle already in this thesis; many of them being concerned with determining the absorption spectrum of a highly-light scattering species, e.g., an iridium carbonyl halide linear-chain conductor (212) or the stratum corneum of a newborn rat (213).

A novel application has been the use of a laser source to

obtain the single- and two-photon spectra of liquid media using the optoacoustic effect (214). Rockley and Devlin (215) have reported the observation of a nonlinear optoacoustic signal with potential application to a nanosecond time resolution. Using rose bengal as the sample, it was demonstrated that the absorption spectra of transient excited states (and time-resolved spectra) can be measured by employing two lasers and varying the wavelength of one laser, or by incorporating time delays between each laser pulse.

The application of the technique to non-spectroscopic measurements has been reported by Adams et al (216). Rear-surface illumination was employed with a copper sample which had a polymer bonded to it on the opposite side to the incident radiation. The time delay for propagation of the thermal wave through the polymer was measured as the phase angle between the absorption of the radiation and the detection of the acoustic signal. Thus, it was possible from a series of measurements at different modulating frequencies to determine the thickness, or thermal diffusivity, of the polymer layer. Rosencwaig (217) has suggested that it may be possible to determine the thickness of films or layers on substrates with different optical properties, in particular for substrates that do not absorb the incident radiation.

7.3. Suggestions for Further Work.

The future development of the optoacoustic effect as an analytical technique will depend greatly upon advances in the instrumentation employed. Much of the limitation of the utility of the technique is due to the poor signal-to-noise(S/N)ratio at the cell. The construction of a cell containing an integral microphone preamplifier (193) would probably do much to improve this. An alternative method of improving the signal-to-noise ratio at the cell would be to increase the intensity

of incident radiation. It has already been shown that more intense continuum radiation sources do not perform this function with the present optical system, due to the increased physical size of the source. An alternative method of increasing the radiation flux at the cell would be the use of an interferometer (62) to permit "white-light" irradiation. However, this would require on-line computing facilities to process the Fourier transform of the sample spectrum, which would be obtained with a Michelson interferometer system.

An improvement in the S/N figure of merit for the cell would enable the technique to be employed in conditions of lower optoacoustic signal magnitudes, i.e., at high modulation frequencies or in the fundamental infrared region. The use of higher modulation frequencies would enable the technique to be applied to true surface analyses. At present, sample depths of typically 30μm are examined with a modulation frequency of 30 - 100Hz. To decrease this depth by an order of magnitude would require an increase in the modulation frequency to ca. 10kHz. However, the f^{-1} relationship between acoustic signal and modulation frequency (f), or indeed $f^{-3/2}$ for weak absorbers (121), means that very small signal amplitudes will be observed at these frequencies, hence the need for improved S/N figures.

The extension of the technique to the mid-infrared region would permit the better characterisation of samples, but again an improvement in the cell S/N ratio is required. This is necessary due to the source power limitations imposed in this region by their blackbody response. A combination of operation at high modulation frequencies and infrared illumination of the sample would be extremely useful since it would permit the characterisation of surface species, e.g., absorbed organic materials, particularly on catalyst surfaces.

APPENDIX I

PERFORMANCE FIGURES FOR THE OPTOACOUSTIC CELLS AND THE PYROELECTRIC DETECTOR

1. Introduction.

A technique for measuring the efficiency of production of an optoacoustic signal is described. This is of particular importance when establishing the relative merits of different cell designs.

A comparison of the pyroelectric detector and optoacoustic cell is also made with application to their use in the reference channel of the double-beam optoacoustic spectrometer.

2. Cell Calibration.

The major practical difference between optoacoustic spectrometry and the more conventional optical techniques of transmission and reflectance spectrometry is in the use of a microphone transducer to monitor indirectly the absorption of incident electromagnetic radiation by the sample under study. The design of the optoacoustic cell and the transducer is, therefore, a critical feature of any optoacoustic system. At present, two methods have been proposed for the calibration of optoacoustic cells (193,218). Murphy and Aamodt (218) have described the use of a "photothermophone", which is a metal "black", vacuum deposited on to a glass substrate, with electrical connections to the metal. Thus, this can act as both a blackbody-absorber and as an electrical heating element. The power input can either be electrical or optical, a comparison of the two being made. The method of calibrating the optoacoustic cells described here is that of Munroe and Reichard (193).

A low-power neon laser (Metrologic Inc., Bellmawr, N.J., U.S.A.) was employed. The radiation from this source was modulated by using the variable-speed chopper employed throughout this work, and de-focused by using a biconcave lens to fill the sample tray of the optoacoustic cell containing a smoked-plate, carbon black sample. The output power of the laser was determined using a laser power meter (Model 142LR, Laser Instrumentation Ltd., Chertsey), and integration of the output energy for

a 5s irradiation period.

The output power of the laser employed for calibration purposes was found to be 0.23mW by radiometric measurements. The cell efficiency measurements were made at a modulation frequency of 30Hz, a lock-in amplifier (Model 186, Princeton Applied Research Corp.) being employed to determine the rms value of the optoacoustic signal from a carbon black sample. The results obtained were for the cells described in Chapters Five and Six (denoted as A and B respectively); a comparison was also made with the pyroelectric detector (Eltec type 404CM, Rofin Ltd.) employed as an alternative reference channel in the double-beam spectrometer (Table I). Unfortunately, the original optoacoustic cell described in Chapter Three was no longer available when these measurements were made, having been modified whilst investigating the design of suitable cells. When using a type 4166 microphone cartridge (Brüel and Kjaer Ltd.), the rated sensitivity of which was 50mV Pa^{-1}, the cell efficiencies were, therefore, determined as 0.39 Pa W^{-1} and 0.43 Pa W^{-1} for cells A and B respectively.

DETECTOR	SIGNAL mV (rms)
Optoacoustic cell A	0.45
Optoacoustic cell B	0.49
Pyroelectric detector	6.8

Table I. Relative sensitivities of optoacoustic cells and pyroelectric detector.

It can be seen from Table I that the pyroelectric detector gave an output signal that was more than one order of magnitude greater than that obtained from the optoacoustic cells.

Fig. 1. Graph of signal-to-noise versus frequency for

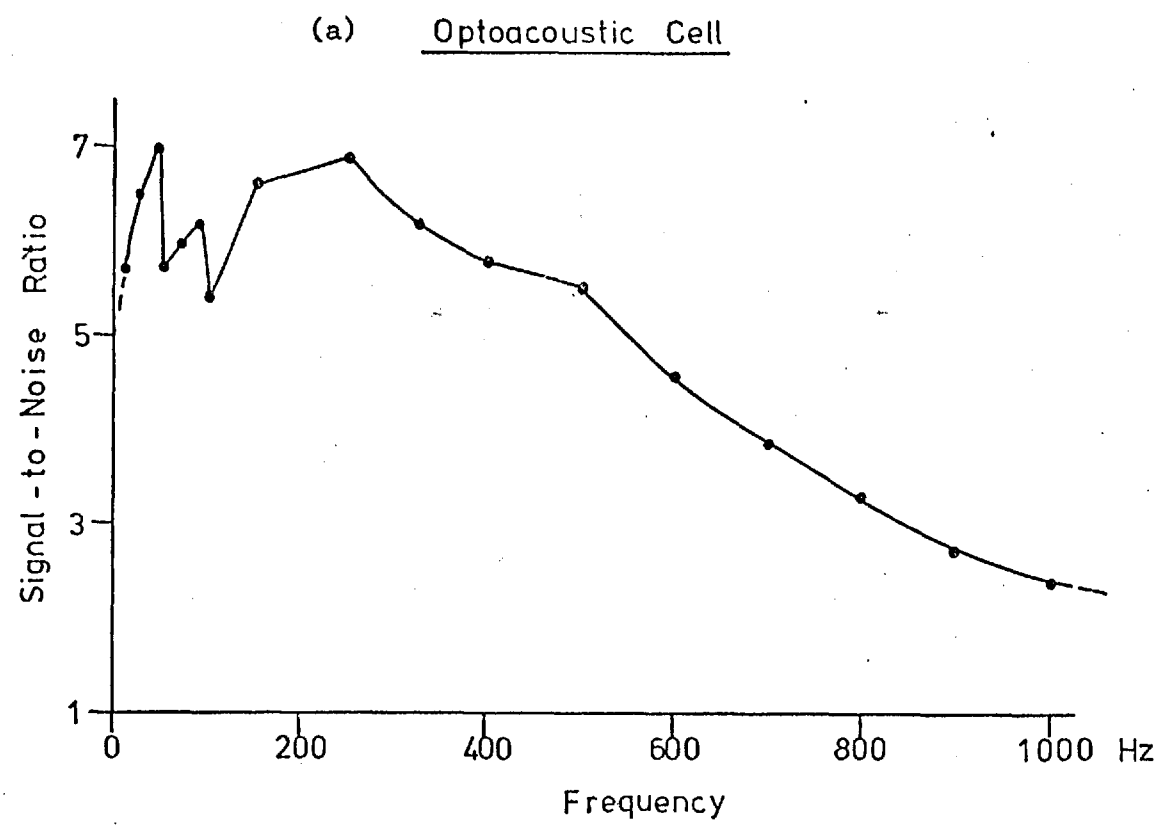

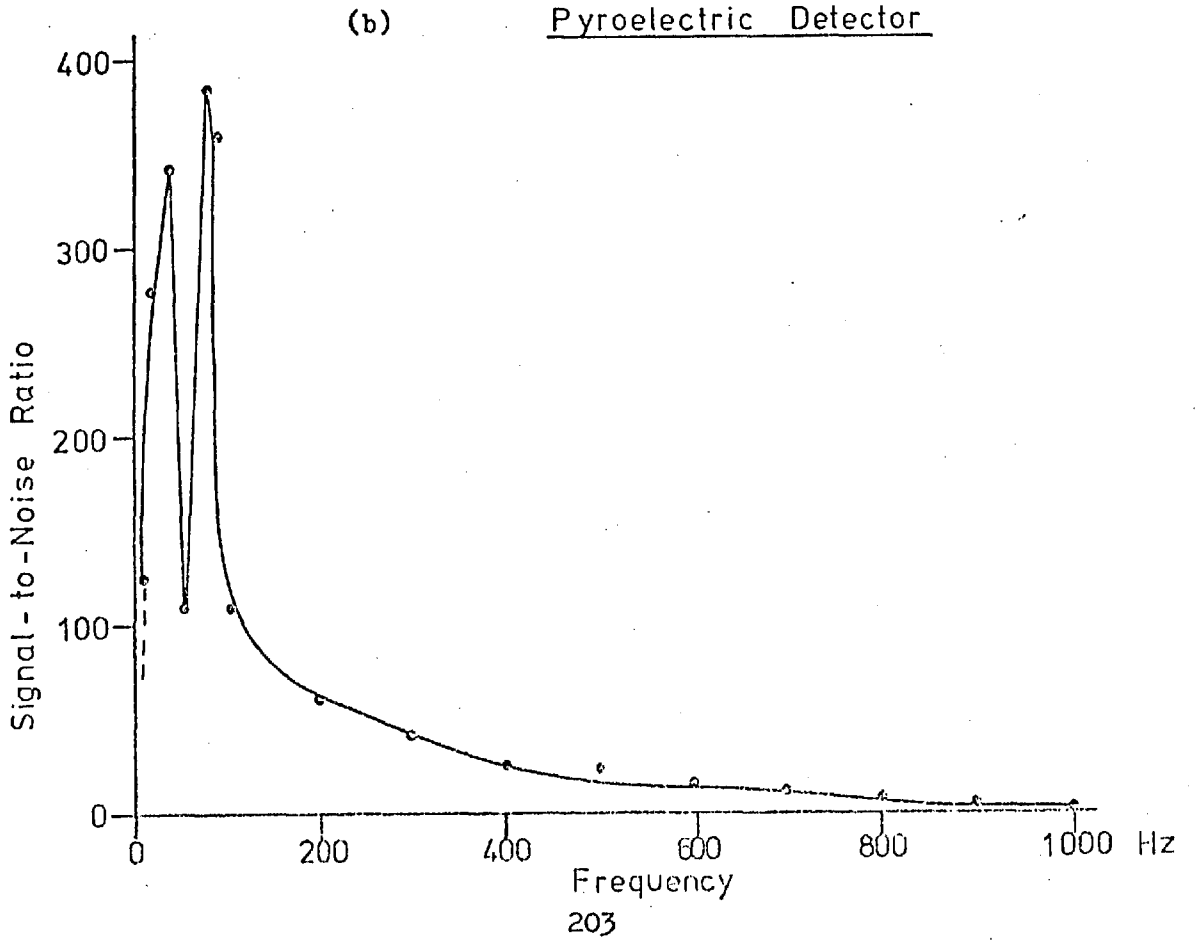

3. Signal-to-Noise Evaluation.

Employing a similar experimental arrangement to that above, the signal-to-noise figures at various modulation frequencies were determined. The output of the lock-in amplifier was displayed on a potentiometric chart recorder (Model 3000, Oxford Instrument Co.) and the noise content of the signal measured directly from this recording. The phase of the signals relative to that of the absorbed radiation was adjusted to maximise the signal at each chosen modulation frequency.

It can be seen (Fig. 1) that below ca. 200Hz the signal-to-noise figures for the pyroelectric detector are two orders of magnitude greater than that obtained from optoacoustic cell A. The inflections in these graphs at 50Hz and 100Hz originated from the corresponding frequency components of the mains power supply. It should be noted that the figures obtained were for the optoacoustic cell containing a carbon black sample. For a more weakly absorbing sample, lower signal-to-noise figures will be obtained at higher modulation frequencies due to the more rapid decrease in optoacoustic signal with modulation frequency (121).

It can be clearly seen that at low modulation frequencies, the pyroelectric detector possesses clear advantages over an optoacoustic cell for use as the reference channel in a double-beam optoacoustic spectrometer.

References.

1. Longhurst, R.S., "Geometrical and Physical Optics", Longmans (1967).
2. Howarth, O., "Theory of Spectroscopy", Nelson, London (1973).
3. Tassie, L.J., "The Physics of Elementary Particles", Longmans (1973).
4. Straughan, B.P. and Walker, S. (eds.), "Spectroscopy", Vol. 3, Chapman and Hall, London (1976).
5. Parker, C.A., "Photoluminescence of Solutions", Elsevier (1968).
6. Birks, J.B., J. Res. Nat. Bur. Stand. (U.S.), 80A, (Phys. and Chem.), No.3, 389 (May-June 1976).
7. St. John, P.A., "Fluorometric Methods for Traces of Elements" in "Trace Analysis", (ed. Winefordner, J.D.), Wiley (1976).
8. Herzberg, G., "Atomic Spectra and Atomic Structure", Dover, New York (1944).
9. Willard, H.H., Merritt, L.L. and Dean, J.A., "Instrumental Methods of Analysis", Van Nostrand (1965).
10. Kaye, W., Spectrochim. Acta, 6, 257 (1954).
11. Wheeler, O.H., Chem. Rev., 59, 629 (1959).
12. Bauer, H.J., J. Chem. Phys., 57, 3130 (1972).
13. Frei, R.W., "Diffuse Reflectance Spectroscopy in Environmental Problem-Solving", Chemical Rubber Co. (1973).
14. St. John, P.A., "Optical Molecular Spectroscopic Methods" in "Trace Analysis", (ed. Winefordner, J.D.), Wiley (1976).
15. Kortüm, G., "Reflectance Spectroscopy", Springer-Verlag, New York (1969).
16. Wendlandt, W.W. and Hecht, H.G., "Reflectance Spectroscopy", Wiley (1966).
17. Kortüm, G., Trans. Faraday Soc., 58, 1624 (1962).

18. Bell, A.G., Proc. Am. Assoc. Advan. Sci., 29, 115 (1880).

19. Röntgen, W.C., Phil. Mag., 11, 308 (1881).

20. Tyndall, J., Proc. Roy. Soc. (London), 31, 307 (1881).

21. Mercadier, M.E., Phil. Mag., 11, 78 (1881).

22. Preece, W.H., Proc. Roy. Soc. (London), 31, 506 (1881).

23. Bell, A.G., Phil. Mag., 11, 510 (1881).

24. Veingerov, M.L., Doklady. Akad. Nauk U.S.S.R., 19, 687 (1938).

25. Veingerov, M.L., Doklady. Akad. Nauk U.S.S.R., 46, 182 (1945).

26. Veingerov, M.L., Doklady. Akad. Nauk U.S.S.R., 51, 195 (1946).

27. Veingerov, M.L., Zavodskaya Laboratoriya, 13, 426 (1947).

28. Luft, K.F., Zeit. tech. Phys., 24, 97 (1943).

29. Verdin, A., "Gas Analysis Instrumentation", Macmillan, London (1973).

30. Veingerov, M.L., Compt. Rend. Acad. Sci. U.R.S.S., 46, 182 (1945).

31. Mori, K., J. Sci. Res. Inst., 49, 290 (1955).

32. Kaiser, R., Can. J. Phys., 37, 1499 (1959).

33. Pankratov, N.A., Opt. and Spect., 8, 53 (1959).

34. Gerbovin, Ya.I., Opt. and Spect., 7, 63 (1959).

35. Kreuzer, L.B., J. Appl. Phys., 42, 2934 (1971).

36. Kreuzer, L.B., Science, 173, 45 (1971).

37. Hayes, H.V. and Craw, E.R., U.S. Patent 654,630, filed June 7, 1897.

38. Hayes, H.V., Rev. Sci. Instrum., 7, 202 (1936).

39. Hall, W.M., Rev. Sci. Instrum., 7, 205 (1936).

40. Zahl, H.A. and Golay, M.J.E., Rev. Sci. Instrum., 17, 511 (1946).

41. Golay, M.J.E., Rev. Sci. Instrum., 18, 347 (1947).

42. Golay, M.J.E., Rev. Sci. Instrum., 18, 357 (1947).

43. Golay, M.J.E., Rev. Sci. Instrum., 20, 816 (1949).

44. Terenin, A.N. and Yaroslavkii, N.G., Izvest. Ak. Nauk S.S.S.R., 9, 203 (1945).

45. Luchin, S.M., Zhur. tech. Fiz., 16, 1115 (1946).

46. Weber, P.F., Optik, 152 (1950).

47. Pankratov, N.A. and Vasilev, E.F., Opt. and Spec., 10, 61 (1961).

48. Houghton, A.V. and Acton, R.V., AIAA, 2, 120 (1964).

49. Parker, J.G., Appl. Opt., 12, 2974 (1973).

50. Kerr, E.L., Appl. Opt., 12, 2520 (1973).

51. Harshbarger, W.R., and Robin, M.B., Acc. Chem. Res. 6, 329 (1973).

52. Rosencwaig, A., Phys. Today, 28, 23 (1975).

53. Gorelic, G., Dokl. Akad. Nauk S.S.S.R., 54, 779 (1946).

54. Slobodskaya, P.V., Izvest. Acad. Nauk U.S.S.R., 12, 656 (1948).

55. Cottrell, T.L., Macfarlane, I.M., Read, A.W. and Young, A.H., Trans. Faraday Soc., 62, 2655 (1966).

56. Read, A.W., Advan. Mol. Rel. Processes, 1, 257 (1967).

57. Kaya, K., Harshbarger, W.R. and Robin, M.B., J. Chem. Phys., 60, 4231 (1974).

58. Samson, J.A.R., "Techniques of Vacuum Ultraviolet Spectroscopy", Wiley (1967).

59. Martin, D.H. (ed.), "Spectroscopic Techniques for Far-Infrared, Sub-Millimetre and Millimetre Waves", North Holland (1967).

60. Sawyer, R.A., "Experimental Spectroscopy", Dover (1963).

61. Cann, M.W.P., Appl. Opt., 8, 1645 (1969).

62. Thorne, A.P., "Spectrophysics", Chapman and Hall, London (1974).

63. Martin, A.E., "Infrared Instrumentation and Techniques", Elsevier (1966).

64. Cann, G.K.T. and Avery, D.G., "Infrared Methods", Academic Press (1960).

65. Gaydon, A.G. and Wolfhard, H.G., "Flames", Chapman and Hall, London (1960).

66. Kirkbright, G.F. and Sargent, M., "Atomic Absorption and Fluorescence Spectroscopy", Academic Press (1974).

67. Veillon, C., "Optical Spectroscopic Methods" in "Trace Analysis", (ed. Winefordner, J.D.), Wiley (1976).

68. Brewer, R.G. and Mooradian, A. (eds.), "Laser Spectroscopy", Plenum, New York (1974).

69. Schäfer, F.P., "Principles of Dye Laser Operation" in "Topics in Applied Physics", Vol.I, Springer-Verlag (1973).

70. Mooradian, A., "High Resolution Tunable Infrared Lasers" in "Laser Spectroscopy", (eds. Brewer, R.G. and Mooradian, A.), Plenum, New York (1974).

71. Harrison, G.R., Lord, R.C. and Loofbourow, J.R.,"Practical Spectroscopy", Prentice-Hall (1948).

72. Watson, C.A., Anal. Chem., 49, 835A (1977).

73. James, J.F. and Sternberg, R.S., "The Design of Optical Spectrometers", Chapman and Hall, London (1969).

74. Kaye, W., Spectrochim. Acta, 7, 181 (1955).

75. Smith, R.A., Jones, F.E. and Chasmar, R.P., "Detection and Measurement of Infrared Radiation", Oxford (1968).

76. Tiffany, W.B., Opt. Spectra, 22 (Feb. 1975).

77. Brüel and Kjaer, Instruction Manual for Type 4166 Microphone Cartridge (1971).

78. Brüel and Kjaer, "Condenser Microphones and Microphone Preamplifiers", (1976).

79. Malmstadt, H.V., Enke, C.G., Crouch, S.R. and Horlich, G., "Electronic Measurements for Scientists", Benjamin (1974).

80. O'Haver, T.C., "Analytical Considerations" in "Trace Analysis", (ed. Winefordner, J.D.), Wiley (1976).

81. Kalvoda, R., "Operational Amplifiers in Chemical Instrumentation", Wiley (1975).

82. Jones, B.E., "Instrumentation, Measurement and Feedback",

McGraw-Hill (1977).

83. Blair, D.P. and Sydenham, P.H., J. Sci. Instrum., 8, 627 (1975).

84. Ortec/Brookdeal, "Your Guide to Lock-in Amplifiers", (1974).

85. Adams, M.J., King, A.A. and Kirkbright, G.F., Analyst, 101, 73 (1976).

86. King, A.A., Ph.D. Thesis, Univ. of London (1976).

87. Nemhauser, R.I., Alexander, G. and Duda, R., Opt. Spectra, 30 (April 1976).

88. Piller, H., "Microscope Photometry", Springer-Verlag (1977).

89. Weast, R.C. (ed.), "Handbook of Chemistry and Physics", Chemical Rubber Co. (1972).

90. Pankove, J.I., "Optical Process in Semiconductors",Prentice Hall, Englewood Cliffs, N.J. (1971).

91. Rosencwaig, A., Anal. Chem., 47, 592A (1975).

92. Saunders, B.C., Holmes-Siedle, A.G. and Stark, B.P., "Peroxidase", Butterworths, London (1974).

93. Rao, C.N.R., "Ultraviolet and Visible Spectroscopy", Butterworths, London (1967).

94. Rosencwaig, A., Science, 181, 657 (1973).

95. Scott, D.R. and Becker, R.S., J. Chem. Phys., 35, 516 (1961).

96. Brauer, G., "Handbook of Preparative Inorganic Chemistry", Vol.2, Academic Press, p.1391 (1965).

97. McGarvey, B.R., J. Chem. Phys., 37, 2001 (1962).

98. Swalen, J.D. and Ibers, J.I., J. Chem. Phys., 37, 17 (1962).

99. Anysas, J.A. and Companion, A.L., J. Chem. Phys., 40, 441 (1964).

100. Harborne, J.B., "Phytochemical Methods", Chapman and Hall, London (1973).

101. Rabinowitch, E. and Govindjee, "Photosynthesis", Wiley (1969).

102. Weier, T.E., Stocking, C.R. and Barbour, M.G., "Botany: An Introduction

to Plant Biology", Wiley (1974).

103. Touloukian, L.R., Powell, R.W., Ho , C.Y. and Nicolasu, M.C., "Thermal Diffusivity", IFI/Plenum, New York (1973).

104. Carslaw, H.S. and Jaeger, J.C., "Conduction of Heat in Solids", Second Edition, Oxford University Press (1959).

105. Ingersoll, L.R., Zobel, O.J. and Ingersoll, A.C., "Heat Conduction", University of Wisconsin Press (1954).

106. Moore, R.K., "Wave and Diffusion Anologies", McGraw-Hill (1964).

107. Rosencwaig, A. and Gersho, A., Science, 190, 556 (1975)

108. Cowan, R., J. Appl. Phys., 32, 1363 (1961).

109. Adams, M.J. and Kirkbright, G.F., Spec. Lett., 9, 255 (1976).

110. Adams, M.J. and Kirkbright, G.F., Analyst, 102, 281 (1977).

111. Rosengren, L.G., Infrared Phys., 13, 109 (1973).

112. Aamodt, L.C., Murphy, J.C. and Parker, J.G., J. Appl. Phys., 48, 927 (1977).

113. Aamodt, L.C. and Murphy, J.C., J. Appl. Phys., 49, 3036 (1978).

114. Bennett, H.S. and Forman, R.A., Appl. Opt., 15, 347 (1976).

115. Bennett, H.S. and Forman, R.A., Appl. Opt., 15, 2405 (1976).

116. Bennett, H.S. and Forman, R.A., Appl. Opt., 16, 2834 (1977).

117. Bennett, H.S. and Forman, R.A., J. Appl. Phys., 48, 1432 (1977).

118. Hordvik, A., Appl. Opt., 16, 282 (1977).

119. Hordvik, A. and Schlossberg, H., Appl. Opt., 16, 101 (1977).

120. Hordvik, A. and Skolnik, L., Appl. Opt., 16, 2919 (1977).

121. Rosencwaig, A. and Gersho, A., J. Appl. Phys., 47, 64 (1975).

122. Monahan, E.M. and Nolle, A.W., J. Appl. Phys., 48, 3519 (1977).

123. Melamed, N.T., J. Appl. Phys., 34, 560 (1963).

124. Afromowitz, M.A., Yeh, P. and Yee, S.J., J, Appl. Phys., 48, 209 (1977).

125. McClelland, J.F. and Kniseley, R.N., Appl. Phys. Lett., 28, 467 (1976).

126. Wetsel, G.C. and McDonald, F.A., Appl. Phys. Lett., 30, 252 (1977).

127. Wong, K.Y., J. Appl. Phys., 49, 3033 (1978).

128. Samuels, A., Shell Research Laboratories, Sittingbourne, Kent (Private Communication).

129. Cotton, F.A. and Wilkinson, G., "Advanced Inorganic Chemistry", Third Edition, Wiley-Interscience, p.1060 (1972).

130. White, W.B., Appl. Spec., 21, 167 (1967).

131. Kortüm, G., in West, P.W., Macdonald, A.M.G. and West, T.S. (eds.), "Analytical Chemistry 1962", Elsevier, New York, p.307 (1963).

132. Hezel, U., Int. Lab., 73 (May/June 1978).

133. Frei, R.W., J. Chromatogr., 64, 285 (1972).

134. Touchstone, J.C., Levin, S.S. and Murawec, T., Anal. Chem., 43, 858 (1971).

135. Goldman, J. and Goodall, R.R., J. Chromatogr., 47, 386 (1970).

136. Pollock, V. and Boulton, A.A., J. Chromatogr., 63, 87 (1971).

137. Jork, H., Z. Anal. Chem., 236, 310 (1968).

138. Frei, R.W. and Frodyma, M.M., Anal. Chim. Acta, 32, 501 (1965).

139. Jork, H., Z. Anal. Chem., 221, 17 (1966).

140. Klaus, R., J. Chromatogr., 16, 311 (1964).

141. Goldman, J. and Goodall, R.R., J. Chromatogr., 32, 24 (1968).

142. Rosencwaig, A. and Hall, S.S., Anal. Chem., 47, 548 (1975).

143. Bloor, D. and Preston, F.H., Phys. Stat. Sol. (a), 37, 427 (1976).

144. Bloor, D. and Preston, F.H., Phys. Stat. Sol. (a), 39, 607 (1977).

145. Bloor, D., Batchelder, D.N. and Preston, F.H., Phys. Stat. Sol. (a), 40, 279 (1977).

146. Greenaway, D.L. and Harbeke, G., "Optical Properties and Band Structure of Semiconductors", Pergamon (1968).

147. Tandon, S.P. and Gupta, J.P., Phys. Stat. Sol., 38, 363 (1970).

148. Gelbwachs, J.A., "Tunable Radiation Sources in the Ultraviolet and

Visible Spectral Regions" in "Optoacoustic Spectroscopy and Detection (ed. Pao, Y.H.), Academic Press (1977).

149. Munroe, D.M. and Reichard, H.S., Applications Note 147, Princeton Applied Research Corp., Princeton, N.J., U.S.A. (1976).

150. Eaton, H.E. and Stuart, J.D., Anal. Chem., 50, 587 (1978).

151. Whetsel, K.B., "Near-Infrared Spectrophotometry" in "Applied Spectroscopy Reviews", Vol.II (ed. Brame, E.G.), Marcel Dekker, New York (1969).

152. Goodgame, D.M. and Goodgame, M., Inorg. Chem., 4, 139 (1965).

153. Goddu, R.F., Advan. Anal. Chem. Instrum., 1, 347 (1960).

154. Goulden, J.D.S., J. Dairy Res., 24, 242 (1957).

155. Herzberg, G., "Molecular Spectra and Molecular Structure", Vol.II, Van Nostrand, Princeton, N.J., U.S.A. (1945).

156. Carnall, W.T., Anal. Chem., 34, 786 (1962).

157. Hagan, P.G. and Cleveland, J.M., J. Inorg. Nucl. Chem., 28, 2905 (1966).

158. Sacconi, L. and Ciampolini, J. Am. Chem. Soc., 85, 1750 (1963).

159. Goddu, R.F. and Delker, D.A., Anal. Chem., 32, 140 (1960).

160. Miller, R.J.G. and Willis, H.A., J. Appl. Chem. (London), 6, 385 (1956).

161. Willis, H.A. and Miller, R.J.G., Spectrochim. Acta, 14, 119 (1959).

162. Holmann, R.T. and Edmondson, P.R., Anal. Chem., 28, 1533 (1956).

163. Lauer, J.L. and Rosenbaum, E.J., J. Appl. Spec., 6, 29 (1952).

164. Cordes, H.F. and Tait, C.W., Anal. Chem., 29, 485 (1958).

165. Chapman, D. and Nacey, J.F., Analyst, 83, 377 (1958).

166. Dodd, D.M. and Fraser, D.B., J. Appl. Phys., 37, 3911 (1966).

167. Crisler, R.O. and Burrill, A.M., Anal. Chem., 31, 2055 (1959).

168. Blondheim, V. and Gramstad, T., Spectrochim. Acta, 17, 1073 (1965).

169. Whetsel, K.B., Robertson, W.E. and Krell, M.W., Anal. Chem., 30,

1598 (1958).

170. Durocher, G. and Sandorfy,C., J. Mol. Spectry., 22, 347 (1967).

171. Quentin, R.J., Anal. Chem., 34, 1170 (1962).

172. Russell, R.A. and Thompson, H.W., Proc. Roy. Soc. (London), A, 234, 318 (1956).

173. Norris, K.H., Agric. Eng., 45, 370 (1964).

174. Norris, K.H., Barnes, R.F., Moore, J.E. and Shenk, J.S., J. Animal Sci., 43, 889 (1976).

175. Ahmed, W. and Goldstein, M., Lab. Practice, 25, 385 (1976).

176. Reid, A.F., Scaife, D.E. and Wailes, P.C., Spectrochim. Acta, 20, 1257 (1964).

177. McClelland, J.F. and Kniseley,R.N., Appl. Opt., 15, 2967 (1976).

178. Hunt, G.R. and Salisbury, J.W., Mod. Geol., 1, 283 (1970).

179. Hunt, G.R. and Salisbury, J.W., Mod. Geol., 2, 22 (1971).

180. Hunt, G.R., Salisbury, J.W. and Lenhoff, C.J., Mod. Geol., 2, 192 (1971).

181. Hunt, G.R., Salisbury, J.W. and Lenhoff, C.J., Mod. Geol., 3, 1, (1971).

182. Hunt, G.R., Salisbury, J.W. and Lenhoff, C.J., Mod. Geol., 3, 121 (1972).

183. Hunt, G.R., Salisbury, J.W. and Lenhoff, C.J., Mod. Geol., 4, 217 (1973).

184. Hunt, G.R., Salisbury, J.W. and Lenhoff, C.J., Mod. Geol., 4, 237 (1974).

185. Ginsberg, A.P. and Koubek, E., Inorg. Chem., 4, 1186 (1965).

186. Groenwege, M.P. and Van Vucht, H.A., Mikrochim. Acta, 43, 471 (1955).

187. Rosengren, L.G., Appl. Opt., 14, 1960 (1975).

188. McClelland, J.F. and Kniseley, R.N., Appl. Opt., 15, 2658 (1976).

189. McClelland, J.F. and Kniseley, R.N., Appl. Opt., 15, 2967 (1976).

190. Gray, R.C., Fishman, V.A. and Bard, A.J., Anal. Chem., 49, 697 (1977).

191. Eaton, H.E. and Stuart, J.D., Analyst, 102, 531 (1977).

192. Ferrell, W. and Haven, Y., J. Appl. Phys., 48, 3984 (1977).

193. Munroe, D.M. and Reichard, H., Am. Lab., 9, 119 (1977).

194. Nordal, P. and Konstad, S.O., Optics Comm., 22, 185 (1977).

195. Nordal, P. and Konstad, S.O., Optics Comm., 24, 95 (1978).

196. Quimby, R.S., Selzer, P.M. and Yen, W.M., Appl. Opt., 16, 2630 (1977).

197. Lahmann, W., Ludewig, H.J. and Welling,H., Anal. Chem., 49, 549 (1977).

198. Oda, S., Sawada, T. and Kamoda, H., Anal. Chem., 50, 865 (1978).

199. Adams, M.J., Highfield, J.G. and Kirkbright, G.F., Anal. Chem., 49, 1850 (1977).

200. Lahmann, W. and Ludewig, H.J., Chem. Phys. Lett., 45, 177 (1977).

201. Starobogotov, I.O., Opt. Spectrosc., 42, 172 (1977).

202. Rockley, M.G. and Waugh, K.M., Chem. Phys. Lett., 54, 597 (1978).

203. Aamodt, L.C. and Murphy, J.C., Bull. Am. Phys. Soc., 21, 423 (1976).

204. Murphy, J.C. and Aamodt, L.C., J. Appl. Phys., 48, 3502 (1977).

205. Merkle, L.D. and Powell, R.C., Chem. Phys. Lett., 46, 303 (1977).

206. Robin, M.B., J. Lumin., 12/13, 131 (1976).

207. Parker, H., Hipps, K.W. and Francis, A.H., Chem. Phys., 23, 117 (1977).

208. Kirkbright, G.F. and Adams, M.J., European Spec. News, 14, 22 (1977).

209. Somaono, R.B., Angew. Chem. Int. Ed. Engl., 17, 238 (1978).

210. Rosencwaig, A., Rev. Sci. Instrum., 48, 1133 (1977).

211. Pao, Y.H. (ed.), "Optoacoustic Spectroscopy and Detection", Academic Press, New York (1977).

212. Rosencwaig, A., Ginsberg, A.P. and Koepke, J.W., Inorg. Chem., 15, 2540 (1976).

213. Rosencwaig, A. and Pines, E., Biochim. et Biophys. Acta, 493, 10 (1977).

214. Bruevich, A.M.B., Razummara, T.K. and Starobogotov, I.O., Opt. Spectrosc., 42, 45 (1977).

215. Rockley, M.G. and Devlin, J.P., Appl. Phys. Lett., 31, 24 (1977).

216. Adams, M.J. and Kirkbright, G.F., Analyst, 102, 678 (1977).

217. Rosencwaig, A., J. Appl. Phys., 49, 2905 (1978).

218. Murphy, J.C. and Aamodt, L.C., Appl. Phys. Lett., 31, 728 (1977).